Imperial College London
Department of Chemical Engineering

Flexible Operation of Electricity-Intensive Industrial Processes

Iván Ying Xuan

Submitted in part fulfilment of the requirements for the degree of
Doctor of Philosophy in Chemical Engineering
of Imperial College

Declaration of Originality

I hereby confirm that the work in this thesis is entirely my own, and has not been previously submitted, nor accepted for any assessed qualifications. I certify that any material obtained or derived from other sources has been appropriately referenced and fully acknowledged.

The copyright of this thesis rests with the author. Unless otherwise indicated, its contents are licensed under a Creative Commons Attribution-Non Commercial 4.0 International Licence (CC BY-NC). Under this licence, you may copy and redistribute the material in any medium or format. You may also create and distribute modified versions of the work. This is on the condition that: you credit the author and do not use it, or any derivative works, for a commercial purpose. When reusing or sharing this work, ensure you make the licence terms clear to others by naming the licence and linking to the licence text. Where a work has been adapted, you should indicate that the work has been changed and describe those changes. Please seek permission from the copyright holder for uses of this work that are not included in this licence or permitted under UK Copyright Law.

Abstract

The aim of this thesis is to study the flexibility of electricity-intensive industrial processes to adapt their electricity consumption to the available power.

Electricity-intensive processes may use hundreds of megawatts during normal operation. An industrial site typically generates electricity locally and distributes it to electrical loads comprising the processes and other equipment. However, if an electrical contingency occurs, the available power reduces and the power consumed by the electrical loads must also reduce. Currently, a process power management system handles an electrical contingency by disconnecting loads until the total consumption of the site is lower than the remaining available power. This operation is named load shedding. If the shed equipment was essential for the process, then the whole process shuts down.

The contribution of the thesis is to demonstrate that flexible process operation gives an alternative to load shedding. The concept is to reduce the power available to the process, so that the process can continue to operate but at a lower production rate. An electrical power outage occurs over a time scale of the order of 100ms. Therefore, in flexible operation, the power available to the process also reduces within 100ms. At the same time, the process control system must receive new set points so that the process moves to an operating point that is consistent with the available power.

The thesis studied flexible operation of liquefaction of natural gas and aluminium smelting to find the set points for the process controllers as a function of available electrical power. Results show that the reduction in production rate can be ameliorated by adjusting other secondary process variables. The results also show that a process with significant energy storage such as aluminium smelting can continue operating for short periods of power reduction even with a very significant loss of available power.

The final chapters of the thesis discuss how to generalize the study of flexible operation so that it can also be applied to other electricity-intensive processes.

Acknowledgements

The years I spent studying my PhD have become an important part of my life, and the journey was full of obstacles that, without the support and advice I received, I would not be able to overcome. Therefore, I would like to express my gratitude towards the people that helped me throughout these years.

I am truly grateful to my supervisor, Nina Thornhill, who has taught me more than what a PhD could teach me. She taught me the importance of hard work and perseverance, but more importantly, her guidance and patience made this thesis possible. Nina has helped me since I came to London to study my MSc and offered me the opportunity to extend my knowledge by studying this PhD, for which I am genuinely grateful.

This thesis would not be possible without the financial support of ABB under the ABB-Imperial College Strategic Alliance Framework. Therefore, I would like to express my sincere gratitude towards ABB for helping me take this journey. Special thanks go to Charlotte Skourup, Trond Haugen, and John Pretlove, who gave me fantastic advice that was helpful for both the PhD and my personal life. I would also like to thank Jørgen Jensen, Jan Wiik, and Stein Trostheim for their very useful feedback and input.

I would like to thank my partner, Nube, who has never stopped taking care of me and supporting me, particularly during the tough days. Many thanks to my friends, who have made this journey smoother, and special thanks to Rodrigo, who despite being kilometres away, has given me constant advice. Last but not least, I want to thank my family, who always have shown faith in me, and encouraged me to persuade my goals.

Contents

Abstract **2**

Acknowledgements **3**

List of Figures **15**

List of Tables **24**

I Introduction and Overview 35

1 Introduction to the Topic and Thesis 37

1.1 Introduction to Process Power Management 38

1.2 Introduction to Flexible Operation 39

1.3 Introduction to the Case Studies 40

1.3.1 LNG Process 41

1.3.2 Aluminium Smelter 42

1.4 Structure of the Thesis 44

2 Background and Motivation **47**

2.1 Electricity Supply for Large Industrial Sites 48

2.1.1 Energy Security 48

2.2 Process Power Management 51

2.2.1 Load Shedding 52

2.3 Flexible Operation for Process Power Management 55

2.3.1 Present PPM Operation vs Proposed PPM Operation 59

2.4 Background to the Processes 61

2.4.1 Liquefaction of Natural Gas 61

2.4.2 Aluminium Smelter 66

2.4.3 Comparison between the Processes 71

2.5 Summary of the Chapter 73

3 Literature Review **75**

3.1 Current Trends in Flexible Operation 75

3.1.1 Flexible Operation in Electricity-Intensive Processes 77

3.2 Liquefaction of Natural Gas 79

3.3 Aluminium Smelter 82

3.4 Summary of the Chapter 83

4 Methodology of the Study of Flexible Operation 85

4.1 Flexible Operation for Process Power Management 85

4.2 Flexible Operation Tasks 86

4.2.1 Finding the New Set Points 87

4.2.2 Assessing the Feasibility 89

4.3 Flexible Operation in the Case Studies 89

4.3.1 Liquefaction of Natural Gas 90

4.3.2 Aluminium Smelter 91

4.4 Summary of the Chapter 93

II Flexible Operation in Liquefaction of Natural Gas 95

5 Modelling of the LNG Process 97

5.1 Heat and Mass Balances 97

5.1.1 Overall Heat Balance 98

5.1.2 Heat Balance in the Precooling Heat Exchanger (HEX1) 100

5.1.3 Heat Balance in the Liquefying Heat Exchanger (HEX2) 100

5.1.4 Heat balance in the Subcooling Heat Exchanger (HEX3) 101

5.2 Redlich-Kwong Soave Equation of State 101

5.2.1 RKS for Mixtures 103

5.2.2 RKS for Enthalpy and Entropy Calculations 103

5.3 Vapour and Liquid Equilibrium 106

5.3.1 Rachford-Rice Algorithm 109

5.3.2 Bubble Point and Dew Point Calculations 110

5.4 Power Consumption of the Plant 115

5.4.1 Power Consumption of the Compressors 115

5.4.2 Model of the Compressors 115

5.5 Joule-Thomson Cycle 118

5.5.1 Joule-Thomson Cycle under Nominal Operation 120

5.5.2 Joule-Thomson Cycle in a Lower Pressure Operation 122

5.5.3 Joule-Thomson Cycle in an Optimal Pressure Operation 123

5.6 Solution Approaches in the Study of the LNG Process 124

5.6.1 Assumptions of the LNG model 125

5.6.2 Degrees of Freedom and Input Values 125

5.6.3 Fixed Variables 128

5.7 Summary of the Chapter 129

6 Optimization of the Pressures in the Refrigeration Systems 131

6.1 Effects of the Pressure on the Flow Rate of the Refrigerants 131

6.1.1 Effects of the Pressure on the Precooling Refrigerant 132

6.1.2 Effects of the Pressure on the Liquefying Refrigerant 134

6.1.3 Effects of the Pressure on the Subcooling Refrigerant 136

6.2 Effects of the Pressure on the Electrical Power Consumption 137

6.2.1 Electrical Consumption in a Compressor 137

6.2.2 Overall Consumption of the LNG 139

6.3 Discussion of the Effects of the Pressure 141

6.4 Summary of the Chapter 142

7 Results from the Study of Flexible Operation in the LNG Process 143

7.1 Effects of the Production Rate 143

7.2 Effects of the LNG Exit Temperature 146

7.2.1 Discussion of the Effects of the LNG Exit Temperature 147

7.3 Effects of the LNG Flash Drum Temperature 148

7.3.1 Discussion of the Effects of the LNG Flash Separator Temperature . . . 151

7.4 Effects of the Combined Variables 153

7.4.1 Flow rate and LNG Exit Temperature 154

7.4.2 Flow rate, LNG Exit Temperature, and Flash Temperature 155

7.5 Discussion of the Results 159

7.6 Summary of the Chapter 161

8 Summary of the Analysis of the LNG Process 163

III Flexible Operation in the Aluminium Smelter 167

9 Modelling of the Aluminium Smelting Process 169

9.1 Modelling Principles 170

9.1.1 Principles of the Mass Balance Model 170

9.1.2 Principles of the Electrical Model 173

9.1.3 Principles of the Heat Balance Model 175

9.1.4 Electrolyte Properties 176

9.2 Mass Balances 181

9.2.1 Reactions in the Bath 181

9.2.2 Material Feed 185

9.3 Electrical Model 187

9.3.1 Ohmic Voltage 188

9.3.2 Decomposition Voltage 193

9.3.3 Overvoltage 196

9.3.4 Overall Electrical Model 200

9.4 Heat Balances 201

9.4.1 Heat Entering the Cell 203

9.4.2 Heat Absorbed by the Compounds Entering 204

9.4.3 Heat Lost to the Surroundings 204

9.4.4 Heat Absorbed and Released by the Reactions 209

9.5 Solution Approaches in the Study of the Aluminium Smelter 212

9.5.1 Assumptions of the Aluminium Smelter 212

9.5.2 Degrees of Freedom and Fixed Variables 213

9.5.3 Solution Approaches 213

9.6 Control Systems in the Aluminium Smelter 215

9.6.1 Control Systems in Industrial Practice 216

9.6.2 Control Systems in the Model 217

9.7 Summary of the Chapter 218

10 Steady State Operation of the Aluminium Smelter 221

10.1 Calculations of the Steady State Operation 221

10.1.1 Effects of Varying the Alumina Concentration 222

10.1.2 Effects of Varying the Bath Ratio 224

10.1.3 Effects of Varying the Bath Temperature 227

10.2 Envelope of Feasible Operation in an Aluminium Smelter 228

10.3 Summary of the Chapter 232

11 Transient Behaviour of the Aluminium Smelter 235

11.1 Dynamic Behaviour 235

11.2 Simulations of a Power Reduction in the Aluminium Smelter 237

11.2.1 Power Reduced for One Hour 238

11.2.2 Power Reduced for Four Hours 241

11.2.3 Power Reduced for Six Hours 245

11.3 Relationship Between Duration and Magnitude of a Power Reduction 246

11.3.1 Maximum Power Reduction without Power Recovery 250

11.4 Summary of the Chapter 251

12 Discussion of the Results **253**

12.1 Discussion of the Steady State Results 254

12.2 Discussion of the Dynamic Behaviour Results 255

12.3 Summary of the Chapter 257

13 Summary of the Aluminium Smelter **259**

IV Discussions and Conclusion **263**

14 Discussion of Flexible Operation **265**

14.1 Comparison of the Results between LNG and Aluminium Smelter 266

14.1.1 Duration of the Power Reduction 266

14.1.2 Magnitude of the Power Reduction 267

14.1.3 Minimising the Reduction of Production Rate 268

14.1.4 Comparison of the Energy Transformations between LNG and Aluminium Smelter 272

14.2 Possible Implementation in Industrial Sites 282

14.2.1 Conclusions from Comparing the LNG and the Aluminium Smelter . . 282

14.2.2 Questions for Implementing Flexible Operation in Industrial Practice . 285

14.3 Further Work 286

14.3.1 Further Work in the Study of Flexible Operation 287

14.3.2 Further Work in the LNG and Aluminium Smelter Models 288

14.3.3 Potential Processes to be Researched 290

15 Conclusions **295**

Bibliography **298**

V Appendices **319**

A Thermodynamic Tables **321**

B Cleaner Energy Integration **327**

C Flexible Operation in an LNG plant **331**

C.1 Analysis of the Degrees of Freedom 331

C.2 Discussion of the Assumptions Made in the LNG Process 337

C.3 Assumption on the Dynamics of the LNG Process 339

C.4 Implementation of the Pumps 342

C.4.1 Effects of the Temperature on the Flow Rate of the Refrigerant 342

C.4.2 Effects of the Temperature on the Electrical Power Consumption 345

C.5 Use of the Envelope of Feasible Operation 349

List of Figures

1.1 LNG process seen as a heat pump, and scheme of the LNG process 41

2.1 Simplified representation of a power grid 49

2.2 Causes and allocation of the main power outages in the United Stated between 2000 and 2015 50

2.3 Simplified schematic of the electrical circuits in a microgrid 52

2.4 Example of a load shedding operation for restoring power balance in the microgrid after an incident 54

2.5 Power consumption in a process with high granularity 55

2.6 Flexible operation strategy for restoring power balance in the site after an incident 56

2.7 Points of view for adjusting the power generation 58

2.8 Representation of the Mixed Fluid Cascade Process by Linde 62

2.9 Cross-section representation of an electrolytic cell for aluminium production. . 66

2.10 Flow diagram of the energy transformations in the aluminium smelter 70

3.1 Breakdown of the cost of producing LNG 80

4.1 Example of operational points and feasible operational points 88

4.2 Aluminium smelter model divided into its three sub-models 92

5.1 LNG process used in this research. 98

5.2 Flow diagram for determining the bubble point. 112

5.3 Flow diagram for solving the RR algorithm 114

5.4 Example of a compressor map 116

5.5 Entropy-enthalpy diagram for an isentropic and a real compression 117

5.6 Algorithm for calculating the total electrical consumption of the plant 119

5.7 Subcooling cycle exploiting the Joule-Thomson effect 120

5.8 Pressure-Enthalpy diagram for a Joule-Thomson expansion using a nominal operation pressure. 121

5.9 Pressure-Enthalpy diagram for a Joule-Thomson expansion using a lower pressure. 122

5.10 Pressure-Enthalpy diagram for a Joule-Thomson expansion using an optimal pressure. 124

6.1 Effects of the discharge pressures of each refrigerant on the precooling refrigerant flow rate 133

6.2 Effects of the discharge pressures of the liquefying and the subcooling refrigerants on the liquefying refrigerant flow rate, and on their respective vapour fractions. 135

6.3 Effects of the discharge pressures of the subcooling refrigerants on the subcooling refrigerant flow rate and its vapour fraction 136

6.4 Relationship between the compressor specific electrical consumption and the discharge pressure. 138

6.5 Relationship between the compressor electrical consumption and the discharge pressure for each refrigerant 138

6.6 Consumption of the LNG process when the liquefying and the subcooling pressures vary, and the precooling pressure remains constant. 139

6.7 Consumption of the LNG process when the precooling and the subcooling pressures vary, and the liquefying pressure remains constant. 140

6.8 Consumption of the LNG process when the precooling and the liquefying pressures vary, and the subcooling pressure remains constant. 141

7.1 Relationship between the compressor efficiency and the natural gas production rate for each compressor 144

7.2 Relationship between the LNG production rate and the electrical power consumption 145

7.3 Relationship between the temperature of the natural gas at the end of the process and the overall consumption of the plant. 146

7.4 Effects of varying the LNG exit temperature on the flow rate of the refrigerants . 148

7.5 Relationships between the natural gas flow rates entering and exiting the flash drum and the temperature in in the flash drum 149

7.6 Relationship between the purity of the natural gas at the end of the process and the temperature of the flash drum 149

7.7 Relationship between the overall consumption of the plant and the temperature of the flash separator 150

7.8 Effects of varying the temperature in the flash drum on the flow rate of the refrigerants 151

7.9 Relationships between the enthalpies of each stream of the natural gas and the temperature of the flash separator. 152

7.10 Overall consumption of the whole LNG plant when the natural gas production rate and the temperature of the natural gas at the exit vary. 154

7.11 Effects of varying the flash drum temperature on the natural gas flow rates of the streams exiting the flash drum when the feed rate is kept constant, and on the composition of the LNG. 156

7.12 Effects of varying the LNG production rate and the temperature at the flash separator on the overall electrical power consumption of the plant. 157

7.13 Effects of varying the natural gas temperature at the end of process and the temperature at the flash separator on the overall electrical power consumption of the plant. 158

7.14 Effects of varying the natural gas temperature at the end of process and the LNG production rate on the overall electrical power consumption of the plant, when the temperature at the flash separator is constant. 159

9.1 Schematic representation of an electrolytic cell 170

9.2 Schematic representation of the IPD and the bubble layer thickness to calculate the voltage drop in the electrolyte bath 174

9.3 Schematic representation of the electrolyte cell, and its corresponding electrical circuit diagram 187

9.4 Conductivity of the electrolyte bath as a function of the alumina concentration and the bath temperature 190

9.5 Bubble layer thickness as a function of the electrical current. 191

9.6 Voltage drop in the electrolyte as a function of the alumina concentration, the bath temperature, the electrical current, and the IPD 192

9.7 Voltage drop in the bubble layer as a function of the alumina concentration, the bath temperature, the electrical current, and the bath ratio. 193

9.8 Decomposition voltage as a function of the alumina concentration and the bath temperature 196

9.9 Voltage drop caused by the anode concentration overvoltage as a function of the alumina concentration, and the bath ratio. 198

9.10 Voltage drop caused by the cathode concentration overvoltage in V as a function of the bath ratio. 199

9.11 Voltage drop caused by the reaction concentration overvoltage as a function of the alumina concentration, and the bath ratio. 200

9.12 Total voltage drop in electrolyte cell as a function of the alumina concentration, the bath temperature, the bath ratio, the IPD, and the electrical current. 202

9.13 Representation of the insulation of the aluminium cell 205

9.14 Schematic representation of the upper face of the insulation of the electrolytic cell. 206

9.15 Schematic representation of the lower face of the insulation of the electrolytic cell. 207

9.16 Schematic representation of one of the side faces of the insulation of the electrolytic cell. 208

9.17 Optimal operating window in an aluminium electrolytic cell. 215

9.18 Control loops of an aluminium smelter in the industry. 216

9.19 Control loops of an aluminium smelter in the model. 218

10.1 Effects on the aluminium production rate of varying the alumina concentration, for various levels of power consumption. 222

10.2 Effects on the voltage drop in the cell and the electrical current of varying the alumina concentration, for a constant power consumption 223

10.3 Effects on the current efficiency of varying the alumina concentration, for a constant power consumption 224

10.4 Effects on aluminium production rate of varying the bath ratio, for a constant power consumption. 225

10.5 Effects of changing the bath ratio on the electrical current and the voltage drop. 226

10.6 Effects on the contributions to the total voltage of varying the bath ratio, for a constant power consumption. 226

10.7 Effects on the current efficiency of varying the bath ratio, for a constant power consumption. 227

10.8 Effects on the aluminium production rate of varying the bath temperature, for various levels of power consumption. 228

10.9 Effects on the contributions to the total voltage of varying the bath temperature, for a constant power consumption. 229

10.10 Effects on the contributions to the total voltage of varying the bath temperature, for a constant power consumption. 230

10.11 Effects on the the distance between electrodes of varying the bath temperature, for a constant power. 230

10.12Relationship between the bath temperature and the power consumption. 231

10.13Variations of the, electrical current, current efficiency, and aluminium production rate when the power consumption changes 232

11.1 Dynamic behaviour of the temperature of the bath when the power supply is cut. 237

11.2 Evolution of the aluminium production rate and the temperature for a one-hour power reduction 239

11.3 Evolution of the IPD, voltage drop in the cell, and electric current for a one-hour power reduction. 240

11.4 Evolution of the contributions to the total voltage for a one-hour power reduction 241

11.5 Evolution of the aluminium production rate and the temperature for a four-hour power reduction 242

11.6 Evolution of the IPD, voltage drop in the cell, and electric current for a four-hour power reduction. 243

11.7 Evolution of the current efficiency for a four-hour power reduction 243

11.8 Evolution of the contributions to the total voltage for a four-hour power reduction244

11.9 Evolution of the aluminium production rate and the temperature for a six-hour power reduction 246

11.10Evolution of the IPD, voltage drop in the cell, and electric current for a six-hour power reduction. 247

11.11Relationship between the alumina feed and the power consumption 248

12.1 Maximum feasible duration of a power reduction as a function of the magnitude of the power reduction. 256

14.1 Sankey Diagram for the LNG process. 275

14.2 Sankey Diagram for the aluminium smelter. The diagram represents how electrical energy is transformed in the process in a nominal operation. 278

14.3 Time trends of the heat consumed in the cell, the Joule heat generated in the cell, and the difference between the heat generated and lost. 280

14.4 Sankey Diagram for the aluminium smelter when there is an imbalance between the heat generated and the heat consumed. 281

14.5 Simplified diagram of the chloralkali process. 293

B.1 Expected frequency and the respective magnitude of shortages in the UK during 1998 and 2003 328

C.1 Qualitative example of the natural gas valve controlling its flow rate and the subcooling compressor dynamic behaviour 340

C.2 Representation of the LNG process with flash drums and pumps after each heat exchanger. 341

C.3 Effects on the precooling flow rate and vapour fraction of varying the temperature of stream P4. 343

C.4 Effects on the liquefying flow rate and vapour fraction of varying the temperature of stream L5. 344

C.5 Effects on the subcooling flow rate and vapour fraction of varying the temperature of stream S6. 345

C.6 Effects on the specific consumption of the compressor, the specific consumption of the pump, the total consumption of the compressor, and the total consumption of the pump of the precooling cycle of varying the temperature of the stream exiting HEX1 346

C.7 Effects on the specific consumption of the compressor, the specific consumption of the pump, the total consumption of the compressor, and the total consumption of the pump of the liquefying cycle of varying the temperature of the stream exiting HEX2 347

C.8 Effects on the specific consumption of the compressor, the specific consumption of the pump, the total consumption of the compressor, and the total consumption of the pump of the subcooling cycle of varying the temperature of the stream exiting HEX3 348

C.9 Effects on the electrical power consumption of the plant of varying the temperatures of the refrigerants exiting their respective heat exchangers. 349

C.10 Example of using an envelope of feasible operation 350

C.11 Family of temperatures in the envelope of feasible operation. 351

List of Tables

2.1 Comparison between PPM and PPM+ 60

5.1 Input values for the temperatures in the LNG process 127

5.2 Input values for the pressures in the LNG process 127

5.3 Compositions of the natural gas and the refrigerants 127

7.1 Maximum production rate that can be achieved if one or more process variables are changed for a given power reduction. 160

9.1 Gibbs Free Energy of Formation in kJ mol^{-1} for the relevant compounds in the aluminium reduction 194

9.2 Enthalpy of Formation in kJ mol^{-1} for the relevant compounds in the aluminium reduction 210

A.1 Critical temperature, critical pressure, and acentric factor for the components present in the LNG process 322

A.2 Binary interaction parameters for the components present in the LNG process . 322

A.3 $WA_{i,j}$ parameters for calculating the Wilson interaction parameter for the components present in the LNG process 323

A.4 $WB_{i,j}$ parameters for calculating the Wilson interaction parameter for the components present in the LNG process 324

A.5 c_p vapour for the components present in the LNG process 325

A.6 c_p liquid parameters of the components present in the LNG process 326

C.1 Analysis of the Degrees of Freedom in the Precooling Heat Exchanger 332

C.2 Analysis of the Degrees of Freedom in the Natural Gas Flash Separator 332

C.3 Analysis of the Degrees of Freedom in the Liquefying Heat Exchanger 333

C.4 Analysis of the Degrees of Freedom in the Subcooling Heat Exchanger 334

C.5 Analysis of the Degrees of Freedom of the Refrigerant Expansion Valves (V1, V2, and V3) 334

C.6 Analysis of the Degrees of Freedom of the Precooling Compressor (Comp1) . . 335

C.7 Analysis of the Degrees of Freedom of the Liquefying Compressor (Comp2) . . 335

C.8 Analysis of the Degrees of Freedom of the Subcooling Compressor (Comp3) . 336

C.9 Analysis of the Degrees of Freedom of the Refrigerant Sea Coolers (C1, C2, and C3) 336

C.10 Analysis of the Degrees of Freedom of the LNG Process 336

Nomenclature

Physic Constants

F	Faraday's constant	96485 C mol^{-1}
R	Ideal Gas constant	8.314 J $\text{K}^{-1}\text{mol}^{-1}$

Process Variables in the LNG Process

A, B	RKS parameters for mixtures	
a, b	RKS parameters	
c_p	Specific heat capacity	J mol^{-1} K^{-1}
F	Flow rate of a stream	mol s^{-1}
f	Fugacity	Pa
g^E	Excess Gibbs energy	
H	Enthalpy of a stream	W
h	Specific enthalpy of a stream	J mol^{-1}
K	Vaporization equilibrium ratio	
$k_{i,j}$	Binary interaction parameter between components i and j	
P	Pressure	Pa

P_c	Critical pressure	Pa
S	Entropy of a stream	W K^{-1}
s	Specific entropy of a stream	J mol^{-1} K^{-1}
T	Temperature	K
T_c	Critical temperature	K
V_m	Molar volume	m^3 mol^{-1}
W	Electrical power consumption	W
x	Molar fraction in the liquid phase	
y	Molar fraction in the vapour phase	
Z	Compressibility factor	
z	Overall molar fraction	

Greek Letters in the LNG Process

α	RKS Parameter
η_{isen}	Isentropic efficiency
γ	Activity coefficient
Λ	Wilson interaction parameter
ω	Acentric factor
ϕ	Fugacity coefficient
Ψ	Vapour Fraction
Σ	Poynting factor

Process Variables in the Aluminium Smelter

A	Superficial area	m^2
A_{eff}	Effective area of the anode	A m^{-2}
c	Concentration	% wt
c_p	Heat capacity of the bath	J g^{-1} K^{-1}
$c^{max}_{Al_2O_3}$	Alumina solubility	% wt
c^{max}_{Al}	Maximum solubility of the aluminium	% wt
d_{bub}	Bubble layer thickness	cm
d_{IPD}	Distance between poles	cm
E^0	Standard electrode potential	V
E_0	Decomposition voltage	V
G	Gibbs energy	W
G_f	Gibbs energy of formation	W
H	Enthalpy	W
I	Electrical current	A
j	Current density	A m^{-2}
j_{crit}	Critical current density	A m^{-2}
m	Mass of the bath	kg
n	Moles generated from the electrolysis	mol
n_{e^-}	Number of electron flowing in the electrolysis	

OV_{AC}	Anode concentration overvoltage	V
OV_{CC}	Cathode concentration overvoltage	V
OV_{R}	Reaction concentration overvoltage	V
P	Power	W
P_b, P_m, P_d	Barometric, monomer, and dimer pressures	bar
R	Electrical resistance	Ω
R'	Thermal resistance	$\mathrm{K\ W^{-1}}$
R_b	Bath ratio	
T_b	Bath temperature	K
T_{Ext}	External temperature	K
V	Voltage drop in the cell	V

Greek Letters in the Aluminium Smelter

η	Current Efficiency	%
κ	Electrical conductivity of the bath	$\mathrm{S\ cm^{-1}}$
μ	Dynamic viscosity of the bath	$\mathrm{kg\ m\ s^{-1}}$
ρ	Density of the bath	$\mathrm{kg\ m^{-3}}$

Superscripts

Dep	Departure function
IG	Ideal Gas value of the function
mix	Mixture

sat	Value of the function at its saturation point
AE	Related to the Anode Effect
isen	Value of the function in an isentropic process
L	In the liquid phase
V	In the vapour phase

Subscripts

i, j	Components
Abs	Absorbed
Al_2O_3	Related to alumina
AlF_3	Related to aluminium fluoride
An	Related to the anodes in the electrolyte cell
Br+Rod	Related to the bridges and rods in the electrolyte cell
Bub	Related to the bubble layer in the electrolyte cell
CaF_2	Related to calcium fluoride
Cat	Related to the cathode in the electrolyte cell
CO	Related to carbon monoxide
CO_2	Related to carbon dioxide
Collector	Related to the collector in the electrolyte cell
Cr	Related to the crust layer in the electrolyte cell
disc	In the discharge stream of the compressor or pump

Ext	Related to the external parts of the electrolyte cell
Gen	Generated
In	Entering to the system
KF	Related to potassium fluoride
LiF	Related to lithium fluoride
Liq	Belongs to the liquefying refrigeration cycle
Liq x	Stream x in the liquefying refrigeration cycle
MgF_2	Related to magnesium fluoride
NaF	Related to sodium fluoride
NG	Belongs to the natural gas streams
Out	Leaving the system
Prec	Belongs to the precooling refrigeration cycle
Prec x	Stream x in the precooling refrigeration cycle
Sub	Belongs to the subcooling refrigeration cycle
Sub x	Stream x in the subcooling refrigeration cycle
suction	In the suction stream of the compressor or pump

List of Abbreviations

DoF	Degrees of Freedom
DSM	Demand Side Management
EoS	Equation of State
FLNG	Floating Liquefied Natural Gas
HEX	Heat Exchanger
IPD	Interpolar Distance
LNG	Liquefied Natural Gas
MFC	Mixed Fluid Cascade
NG	Natural Gas
PPM	Process Power Management
RES	Renewable Energy Source
RKS	Redlich-Kwong Soave
RR	Rachford-Rice
VLE	Vapour Liquid Equilibrium

Part I

Introduction and Overview

Chapter 1

Introduction to the Topic and Thesis

The flexibility of a process measures its ability to adapt to changes and disturbances in the process and its environment. For an electricity-intensive industrial process, a possible disturbance might be an electrical contingency in the power grid, which would decrease the available power. In that condition, the process has to reduce its power consumption to keep operative and produce, but it must assure that the new operating point is feasible and that the process variables are consistent with the power consumption.

Currently, a number of electricity-intensive industries operate flexibly during an electrical contingency by means of disconnecting loads in the process, so they reduce their power consumption. This operation is named load shedding and consists of shedding loads until the consumption of the plant is equal or lower than the available power. In microgrids arrangements, Process Power Management (PPM) systems coordinate this operation and decide what loads to shed.

Adjusting the consumption of the plant to the desired level is complicated, especially when the granularity of the plant is low. Thus, this project inspects the possibility of, instead of shedding the loads, turning them down. The result of the proposed method is a strategy whereby the process is prepared for a possible electrical contingency.

The challenge lies in determining the behaviour of the process when the available power reduces. Thus, this research evaluates the steady state values of the process variables as a function of the electrical power, so it can establish the corresponding set points when the electrical contingency takes place. The result is an envelope of feasible operating points that the PPM system can use for sending the set points for the process variables immediately after the available power decreases. The process will therefore settle to a steady state operation point that is consistent with the available electrical power

This PhD thesis has studied the flexibility of two electricity-intensive processes, namely the liquefaction of natural gas process and the aluminium smelting process, by determining the envelope of feasible operation for each process.

1.1 Introduction to Process Power Management

Electricity-intensive processes are often in microgrids that include power generation. Process Power Management (PPM) systems ensure that the generated and consumed power in the microgrid are balanced.

If an electrical contingency occurs, the available power reduces and the power consumed by the electrical loads must also reduce. In these conditions, the PPM system disconnects electrical loads until the electrical power consumption is equal or lower than the available power. This operation is named load shedding.

If the shed equipment was essential for the process, then the whole process shuts down. If the process stops, the loss of production and the costs of restarting the process cause significant economic impacts. Therefore, this thesis proposes an alternative to load shedding in which the PPM turns down the electrical loads rather than shutting them down. This mechanism is named flexible operation.

This thesis hypothesises that, during an electrical contingency, it is possible to operate a process flexibly to exploit the remaining available power. To do this requires knowledge of the envelope

of feasible operation of the electricity-intensive process. This will enable an advanced process power management system to specify an operating point for the process that is consistent with the available electrical power.

1.2 Introduction to Flexible Operation

Swaney and Grossmann (1985) defined flexibility as: "Flexibility is concerned with the problem of insuring feasible steady-state operation over a variety of operating conditions".

Flexible operation can be used for many purposes:

- Increasing the sustainability of the process by decreasing the emissions of CO_2 with carbon capture and storage strategies (Chalmers and Gibbins, 2007; van der Wijk et al., 2014)
- Increasing the economic revenues by considering the electricity prices (Caspari et al., 2019a) and the penalties for emitting CO_2 (Lambert et al., 2016; Luo and Wang, 2016).
- Increasing the flexibility of future power systems that integrate renewable energy sources (Holttinen et al., 2013; Lannoye et al., 2012).

Although the processes change their operating point due to a disturbance or a price change, the process variables are consistent amongst each other, and the operation is still feasible. This PhD thesis studies that flexibility in electricity-intensive processes when the disturbance is a reduction of the available electrical power and determines the operating range in which the process can work.

Thus, in this project, flexible operation ensures that the process can adequately respond against possible electrical contingencies by changing the process variables. These process variables

have to be consistent amongst each other, and they must be within some limits. Thus, to implement flexible operation in a process, this process has to be analysed and modelled, so the model can determine the behaviour of the plant when the electrical contingency occurs.

The calculations provide a series of operating points corresponding to to the available electrical power. The operating points have to be within limits established by the process and the equipment to ensure that they are feasible. Ultimately, the result is an envelope of feasible operation that relates the electrical power consumption with a series of operating points. PPM systems use these envelopes of operation to prepare the process for possible electrical contingencies by knowing, beforehand, what variables are to be changed and to what extent.

The power supplied to the process reduces almost instantly (within about 200ms). Simultaneously, the PPM system sends new set points to the process control system. The process then moves to its new operating point over a time scale determined by the process time constants. These time constants determine the time taken to dissipate the energy stored in the process.

This project has focused on modelling the processes to determine the envelope of feasible operation that provides the values for the process variables corresponding to the electrical power consumption. The case studies are the liquefaction of natural gas and the aluminium smelter.

1.3 Introduction to the Case Studies

This project chose two case studies to assess the potential of flexible operation of electricity-intensive processes. One is Liquefied Natural GasLiquefied Natural Gas (LNG), and the other is the aluminium smelting process. This section introduces the processes and their role in flexible operation.

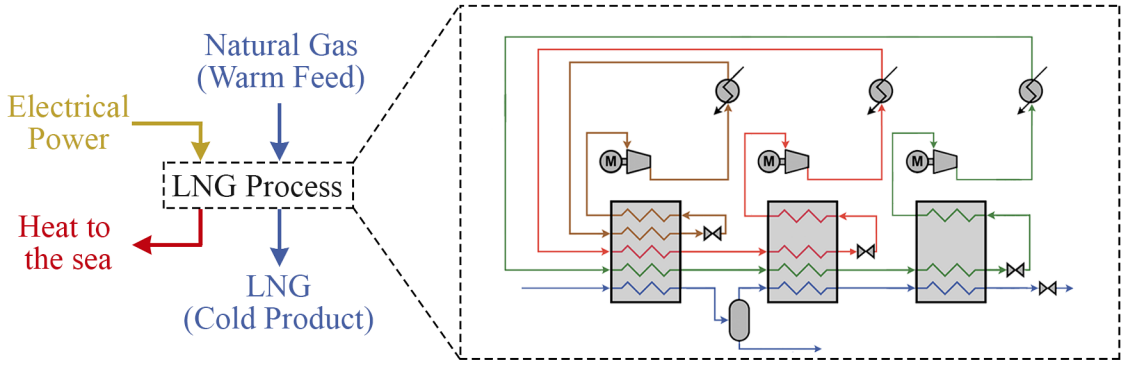


Figure 1.1: The LNG process can be seen as a heat pump, as represented in the left hand side of the picture, where the process receives electrical power (yellow) to convey the heat from the natural gas (blue), and release the heat to the sea (red). The right hand side of the picture represents a scheme of the MFC process by Linde (Linde AG, 2018)

1.3.1 LNG Process

This process liquefies natural gas by refrigeration. There are several processes for liquefaction, but during this project, the case study is broadly based on publicly available information about the LNG plant on the process carried out in the LNG plant in Hammerfest in the north of Norway. The process is the Mixed Fluid Cascade (MFC) developed by Linde (Linde AG, 2018). In this process, the natural gas passes through three stages, precooling, liquefying, and subcooling. Each stage involves a refrigerant cycle that undergoes a Joule-Thomson cycle whereby the refrigerant is compressed using compressors driven by electric motors. Thus, electrical consumption in the process comes mainly from the compressors used in the Joule-Thomson cycle.

Therefore, as a whole unit, the process can be observed as a heat pump that moves the thermal energy from the natural gas to the sea by using electrical energy. Figure 1.1 shows this simplification along with a more detailed scheme of the LNG process. In the scheme, the electric motors use electricity for powering the electric motors attached to the compressors of each refrigeration cycle.

In Figure 1.1, the study of flexible operation determines how much energy can be absorbed from the natural gas for a given level of electrical power consumption. The right-hand side of Figure 1.1 shows that obtaining the relationship between electrical power consumption and absorbed heat involves many inner energy transformations, for example from the motor to the compressor and from the compressor to the refrigerant. Thus, the process variables involved in the power transformations have an impact on the relationship between the absorbed heat and electrical power consumption.

The study of flexible operation finds the operating envelope of the LNG process. Part II of this thesis shows that, for a given power consumption, the parameters of the envelope are:

- The discharge pressures of the compressors
- The LNG production rate
- The LNG temperature at the exit of the process
- The LNG composition

The PPM system uses this envelope to regulate the power consumption, so when an electrical contingency takes place, the PPM can use these relationships to instantly send the set point signals to the controllers that adjust the production rate, exit temperature and composition, so that the process move towards an operating point that corresponds to the available power.

1.3.2 Aluminium Smelter

The aluminium production process involves several steps such as grinding the bauxite containing the alumina, and the furnace for preheating the alumina. The smelting step consists of the electrolysis of alumina for obtaining molten aluminium, and therefore, it is an electricity-intensive process. The following redox reaction takes place during the electrolysis:

$$2\,Al_2O_3 + 3\,C \longrightarrow 4\,Al + 3\,CO_2$$

The reaction takes place in a cell that contains an electrolyte bath with two purposes: it allows electricity to flow through it, and it dissolves the alumina. Typically, cryolite is used as the electrolyte, whose melting point is 1010 °C, but this temperature can be reduced to around 950 °C if additives (such as NaF or AlF_3) are fed to the electrolyte bath. Additionally, the concentration of these additives can change the performance of the smelter. Electricity is used for carrying out the redox reaction, and secondly, it is transformed into thermal energy for maintaining the high temperatures that keep the cryolite molten.

If the cryolite bath solidifies, the components of the cell would be damaged, so it is crucial to be always operating above the solidification point. Due to the high heat capacity, the bath stores thermal energy, so if the electrical input stops, the temperature will not instantly drop.

If no current is flowing, there is no production of aluminium. However, if the electrical current is reduced rather than stopped, the production rate would be reduced, but the process would still be operative. Moreover, if instead of cutting the electrical power consumption, it is reduced to a certain point, the temperature would decrease at a slower rate.

The study of flexible operation finds the envelope of feasible operation of the aluminium smelting process. Part III of this thesis shows that, for a given power consumption, the parameters of the envelope are:

- The bath temperature
- The alumina concentration
- The ratio between the concentrations of NaF or AlF_3

The study of flexible operation simulates the operation when the electrical power to the process reduces. The simulation varies the duration and magnitude of the power reductions to determine the transient behaviour of the aluminium smelter.

1.4 Structure of the Thesis

This thesis is structured in four parts, each one divided into chapters:

Part I. Introduction and Overview: The first part corresponds to the introductory matter. It is divided, counting this introduction as one of them, into four chapters:

1. **Introduction to the Topic and Thesis**
2. **Background and Motivation:** This chapter discusses the basics of the process power management system and the physical principles of the processes of the case studies
3. **Literature Review:** This chapter examines current research concerning flexible operation, and the applicability and potential of flexible operation in the LNG process and the aluminium smelter
4. **Methodology of the Study of Flexible Operation:** This chapter discusses the methodology for studying flexible operation in an electricity-intensive process

Part II. Flexible Operation in the LNG Process: The second part corresponds to the study of flexible operation in the LNG process

5. **Modelling of the LNG Process:** This chapter describes the mathematical model of the LNG process, and enumerated the assumptions made for solving the obtained model. This chapter obtains the degrees of freedom to determine the independent variables
6. **Optimization of the Pressures in the Refrigeration Systems:** This chapter studies the impact of the pressure on the power consumption of the process. The results show that, for a given production rate, there is an operating point that causes the LNG process to work at its minimum. This operating point is used as an input for studying flexible operation in the following chapter

7. **Results from the Study of Flexible Operation in the LNG Process:** This chapter shows the results of the calculations made with the LNG model to determine the relationships between the characteristics of the LNG and the power consumption to find the operating envelope of the process

8. **Summary of the Analysis of the LNG Process**

Part III. Flexible Operation in the Aluminium Smelter: The third part is focused on the aluminium smelter and it is divided into:

9. **Modelling of the Aluminium Smelting Process:** This chapter describes the relationships within the aluminium smelter and discusses the assumptions to solve the model. Additionally, this chapter describes the calculations and simulations used to generate results for steady state operation and for studying the dynamic behaviour of the process

10. **Steady State Operation of the Aluminium Smelter:** The calculations in this chapter change the set point of some process variables to determine their relationship with the electrical power consumption. The results in this chapter are used to obtain an envelope of feasible operation at steady state

11. **Transient Behaviour of the Aluminium Smelter:** This chapter shows the results of the dynamic simulations of the process, so it can determine the relationship between the magnitude of the power reduction and its duration

12. **Discussion of the Results:** This chapter discusses and compares the results shown in the two previous chapters to draw conclusions and differences in the application of flexible operation during a steady state and a transient operation

13. **Summary of the Aluminium Smelter**

Part IV. Discussions and Conclusions: This part discusses the results obtained from Parts II and III, comparing both processes, and giving guidelines for studying flexible operation in other industries. It is divided into two chapters:

14. **Discussion of Flexible Operation:** This chapter compares the study of flexible operation in both processes. This chapter also discusses the importance of energy transformations on the electrical flexibility of a process. Additionally, this chapter suggests future work in the study of flexible operation and proposes potential electricity-intensive processes for implementing flexible operation

15. **Conclusions:** The conclusions drawn from the whole study are gathered in this chapter. This chapter shows how the objectives established have been met

Chapter 2

Background and Motivation

This chapter gives the necessary information for understanding the project and the drivers that lead the author to study flexible operation of electricity-intensive processes. This chapter explains the concept of flexibility in a process, and how its study leads to obtain an envelope of feasible operation that helps the process to fully exploit the available power. The chapter is divided into five sections:

- **Electricity Supply for Large Industrial Sites:** This section briefly explain how large industrial sites can contribute to manage the power in a microgrid
- **Process Power Management:** This section introduces the current operation performed by power management systems, namely load shedding, and how it can be improved
- **Flexible Operation for Process Power Management:** This section introduces the solution proposed and compares the current operation with the proposed operation
- **Processes Background:** This section explains the basics of the case studies considered to study flexible operation, which are the liquefaction of natural gas, and an aluminium smelter
- **Summary of the Chapter**

2.1 Electricity Supply for Large Industrial Sites

For proper operation, a power grid has to be balanced, meaning that all the electric power produced has to be consumed by the end-users, and vice versa. To ensure that the power generated is equal to the power consumed, frequency is measured so it can be adjusted if it deviates from its set value, typically by changing the electricity generated in the power stations.

Figure 2.1 is a simplified representation of the power grid, where power plants generate electrical power, and after transmitting and distributing it, industrial processes consume it. In Figure 2.1, a dotted box surrounds an industrial plant and a generation power plant. This arrangement is named microgrid. The U.S. Department of Energy defines a microgrid as "*[...] a group of interconnected loads and distributed energy resources within clearly defined electrical boundaries that acts as a single controllable entity with respect to the grid. A microgrid can connect and disconnect from the grid to enable it to operate in both grid-connected or island-mode*" (Ton and Smith, 2012).

A microgrid provides higher flexibility to the power grid, e.g. if the power in the power grid has a surplus, the microgrid can consume more energy, and, on the other hand, if there is a power deficit, the microgrid can export power to the power grid. As stated by Hirsch et al. (2018), there are three main drivers for placing the generation plant in the same site as the industrial process: (i) Energy security, (ii) economic benefits, and (iii) cleaner energy integration. This section introduces energy security, whereas Appendix B gives a brief explanation of the integration of cleaner energies. Economic benefits are related to power markets, and this thesis does not discuss them because they are outside the scope of the project.

2.1.1 Energy Security

Working in a microgrid arrangement allows the local power plant to reduce or eliminate their dependency on the public electricity supply, bringing benefits when the power grid undergoes an electrical contingency. One of the main reasons for the power grid to go down is severe weather.

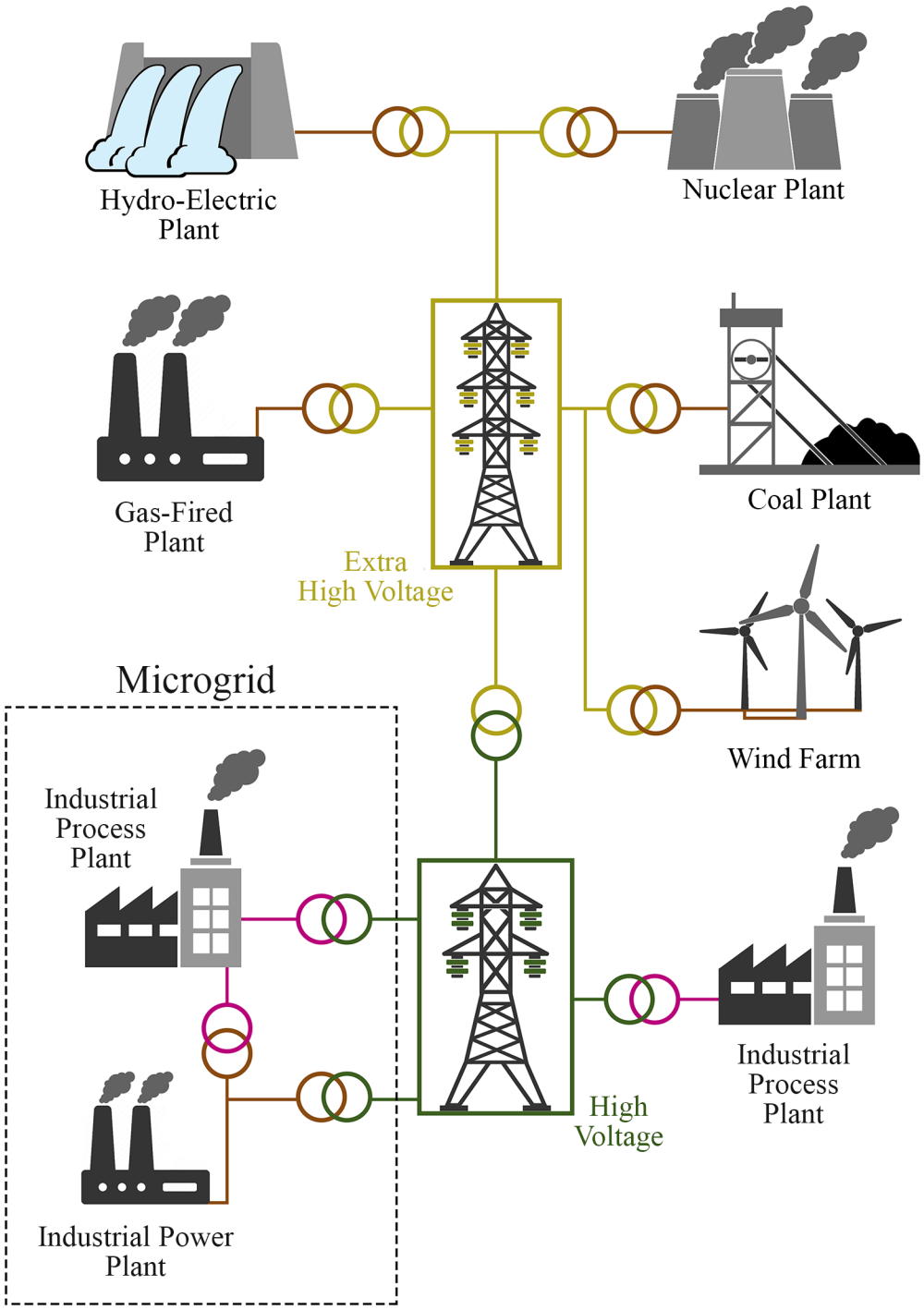


Figure 2.1: Simplified representation of a power grid. The power is produced (brown) in generation plant, and it is consumed (pink) by the process plants. The extra high voltage lines (yellow) go from the generation power plants to a transformer, so it can be transmitted to the high voltage lines (green). The dotted box surrounds a microgrid arrangement, in which the process and a power plant are in the same site.

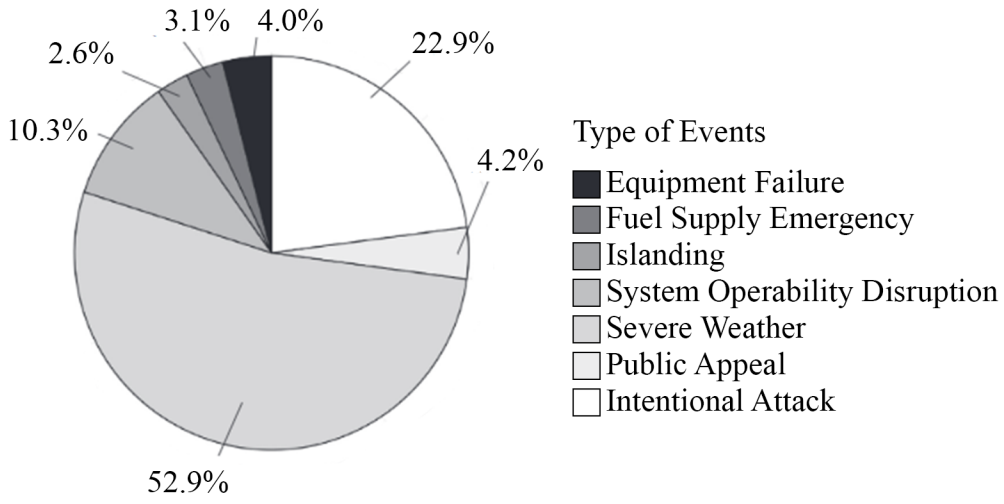


Figure 2.2: Causes and allocation of the main power outages in the United Stated between 2000 and 2015. This pictures is extracted from Mukherjee et al. (2018).

According to Mukherjee et al. (2018), between 2000 and 2015, the 52.9% of the power outages in the United States were caused by severe weather events, as seen in the graph provided by the same author (Figure 2.2). Figure 2.2 also shows that intentional attacks, including cyberattacks (Mrabet et al., 2018; Wang and Lu, 2013), caused 22.9% of the outages.

In both cases, the power outage causes the power grid to be inoperative, and therefore, having a local power generation plant whereby the process plant can still work is useful. Thus, working in a microgrid is advantageous if the electricity from the power grid is not very reliable. An example of connections with low reliability are the Floating Liquefied Natural Gas (FLNG) plants, in which natural gas is liquefied in a plant offshore (Jin et al., 2019; Lee et al., 2014; Zhao et al., 2011). The reason for constructing floating plants is the possibility of producing, liquefying, and offloading LNG in the same place. In these structures, the public connection might still be available, but, since it is an offshore facility, there are chances that the supply may fail.

The facility is still connected to the power grid, so, in case there is an issue in the generation plant in the FLNG, the facility can use public electricity as a backup power source. Additionally,

if the power produced is higher than the power consumed, the facility can export power to the grid as ancillary services and for economic revenues.

Facilities are still subjected to risk of an accident. For instance, Nam et al. (2011) mentioned that there are risks in the FLNG due to the hydrodynamics of the sea, and in severe conditions, the process might need to stop. If the process has to stop, it might take several days or weeks to restart the operation (Gloystein, 2016), causing significant monetary losses.

These disturbances may constrain the available power, so industrial processes can actively contribute to the power balance by adjusting their consumption. This contribution requires the processes to operate flexibly and the implementation of a Process Power Management (PPM) system that can react accurately to requests for power changes to avoid shutdowns.

2.2 Process Power Management

Process Power Management (PPM) systems in the market include ABB's Process Power Manager (ABB, 2016), and the SIMATIC Energy Management from Siemens (Siemens AG, 2018). As the information of the products states, and according to Pacheco et al. (2012) and Ravikumar et al. (2015), among other tasks, PPM systems allocate the available power on the microgrid and ensure that the generated and consumed power are balanced.

Figure 2.3 shows an example of the connections in a microgrid. The distribution bus has an interconnection with the electricity of the power grid, and thus, the microgrid can import or export electricity from or to the power grid. The PPM has control over the circuits and decides which circuit is open or closed, allocating the amount of power for each purpose. The circuit breaker in the bus connecting the site with the power grid allows the site to operate in island-mode, so if it is open, the site is isolated.

PPM system also balances the power in the microgrid by varying the power output from the generation plant. Nevertheless, electrical contingencies are not planned, and they imply a sudden

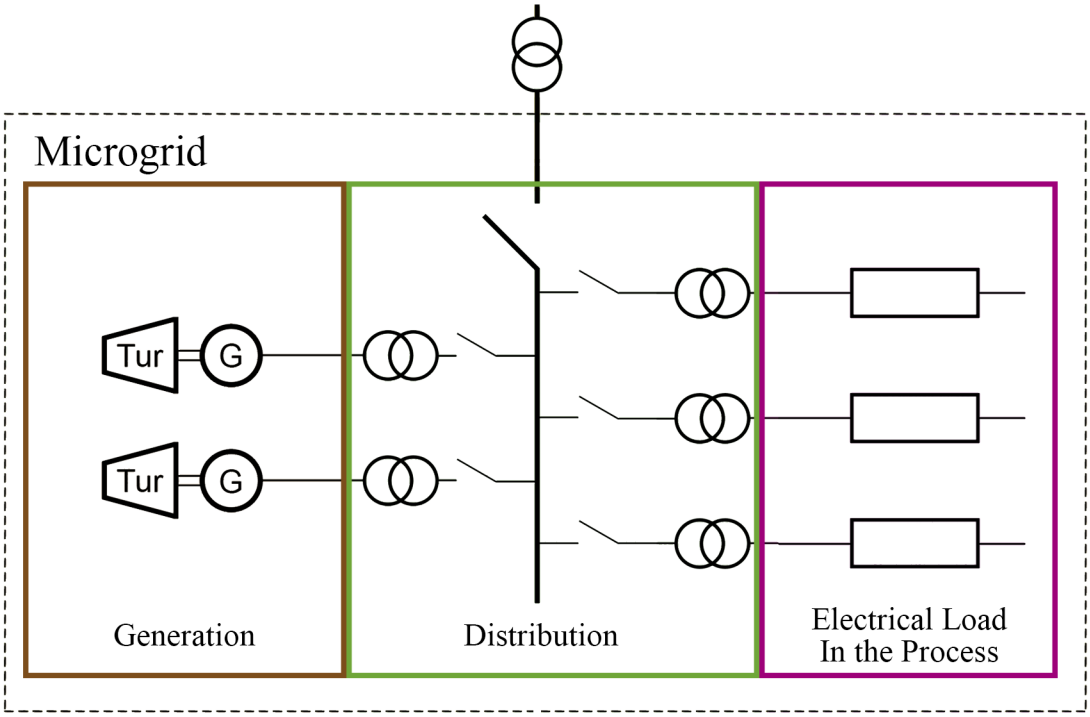


Figure 2.3: Simplified schematic of the electrical circuits in a microgrid, involving an industrial plant (pink) and a generation plant (brwon) connected by the distribution line (green). This Figure represents the dotted box in Figure 2.1.

change in the power balance. In these conditions, PPM can balance the power in the microgrid by disconnecting loads in the process. This strategy is called load shedding.

2.2.1 Load Shedding

Load shedding is a strategy in which the PPM system disconnects one or more electrical loads, so the power balance is restored when an electrical contingency, such as a generator trip, takes place. Figure 2.4 shows an example of load shedding, in which, after a failure, one of the gas turbine generators has to be disconnected. The graph in Figure 2.4 shows the evolution of the available and the consumed power in the microgrid. At t_1, the electrical contingency takes place, and the power from the turbine is no longer available, causing an imbalance in the grid. The process reduces its consumption by shedding one or more electrical loads to compensate this imbalance; thus, at t_2, the PPM system opens one of the circuits, but, since that is not enough for

recovering electrical balance, it opens a second circuit at t_3. The power consumption is lower than the power available, so the remaining generators are able to supply the reduced power consumption of the site.

Thus, PPM can adjust the power consumption to be equal or lower than the power available, but the challenge is to know which parts of the process can be shut down without having significant impacts on the operation. This is especially true when the process has a low granularity. In this context, granularity refers to the number and size of the load shedding increments, so if a process has a low granularity, it has a small number of large loads, and a high granularity implies a large number of small loads.

Granularity

In the example of Figure 2.4, there are only three loads using all the power supplied by the generators. If one load is to be disconnected, the electrical power consumption drops. In practice, PPM sheds the non essential loads first, and if it requires further reduction, it shuts down loads from the process until the consumption is equal or lower than the available power (van der Wal et al., 2005). Figure 2.5 shows the benefit of having a higher granularity. In this case, using a load shedding strategy gives more discrete states to the consumption, so it is more likely for the consumption to get closer to the available power. Therefore, the flexibility of an industrial site increases by increasing the granularity.

Figure 2.4 shows that there is a gap between the available and the consumed power, meaning that the process is not fully utilising the available power. This difference causes the process to have a lower outcome, or the operating conditions to not being optimal.

Granularity is higher in plants like refineries and petrochemical processes where there are numerous electrical loads. However, gas handling plants, like the LNG process, typically have a small number of large electricity-intensive loads and the granularity is low. Therefore, this project aims to overcome low granularity to achieve a better match between the available and the consumed power, so that the process makes the best use of all available power.

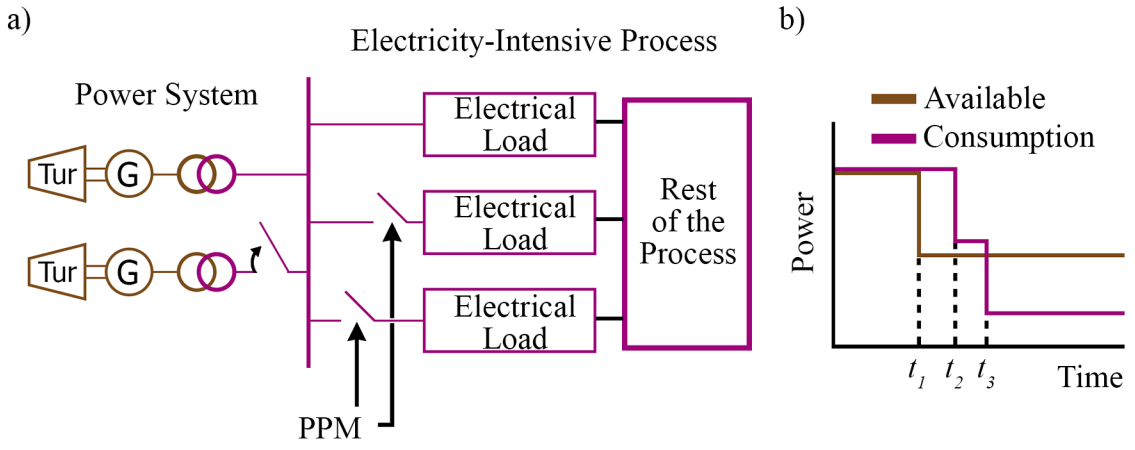


Figure 2.4: Example of a load shedding operation for restoring power balance in the microgrid. The graph shows the power consumed (pink), and the power available (brown) during an electrical contingency. The time axis has been magnified to explain the load shedding strategy. In practice, the elapsed time between t_1 and t_2 is no higher than 200ms.

Relevance of the Loads

If after shutting down the electrical loads, the consumed power is still higher than the available power, the next electrical load to be shut down might be crucial for the operation, and consequently, the whole plant would need to stop. A plant stop implies significant economic losses, due to the loss of production and the time necessary to restart the production.

Since PPM has to restore balance in the microgrid as fast as possible, there is no time for the operators to make decisions, and thus, PPM has preprogrammed load-shedding actions that the system takes according to the amount of electrical power to be reduced.

Thus, PPM needs an approach to control the consumption of the plant to the desired level, so that it is adapted precisely to the available power. Thereby, the available power will be exploited as much as possible, the crucial load is not shut down, and the process does not need to stop. The proposed solution is turning down the equipment rather than shutting it down. This approach is named flexible operation due to its ability to operate the process such that it can adapt to the available power.

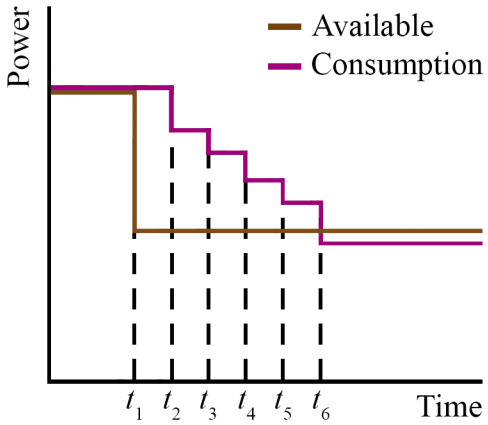


Figure 2.5: Effects of having a process with higher granularity than the one shown in Figure 2.4. In this example, the process has more loads that can be shed, and therefore, the consumption gap between the available and consumed power is smaller.

2.3 Flexible Operation for Process Power Management

Under a flexible operation strategy, the electrical loads reduce their consumption to a certain level rather than being disconnected as represented in Figure 2.6, so the consumption of the plant is not higher than the available power. In the picture, one of the generators trips, forcing the circuit to open, and decreasing the available power. The PPM turns down the electrical load at time t_2, so the consumption matches the available power at t_3. The power reduction takes place in no more than 200 ms, but the process variables might need more time to adapt to the new operating point.

If the consumed power is adjusted to the same level of the available power, the PPM can avoid shutdowns, and it will exploit all the available power, obtaining the optimal production outcome for the given available power.

The problem with decreasing the power to the desired level is the response of the rest of the process. For instance, for a compressor, it is possible to know the pressure, temperature and flow rate of the discharge stream of the compressor as a function of the power consumed. How-

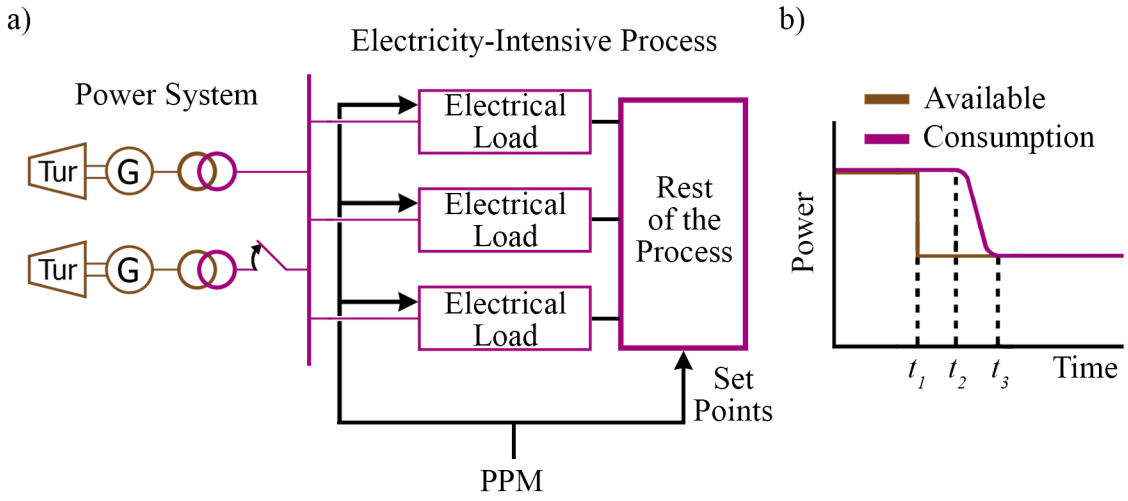


Figure 2.6: Example of a flexible operation strategy for restoring power balance in the site during an electrical contingency. The figure shows the available power (brown) and the consumption of the plant (pink) when the plant works under a flexible operation strategy.

ever, it is necessary to see the impacts of changing those process variables on the rest of the process. This project predicts the behaviour of the whole process when the consumption of the plant changes by determining relationships between the process variables and the power consumed. The obtained relationships provide an envelope of operation that tells the PPM the corresponding operating point corresponding to the available power. Thus, in case of an electrical contingency, the PPM can establish the corresponding set points to the process variables.

The equipment and the process determine limits for the calculated family of set points. Examples for these limits can be a maximum or minimum flow rate delivered by the compressor, or a specific temperature delimiting the valid range for a stream. The envelope of operation integrates these limits to form an envelope of feasible operation in which the process can work without jeopardizing the process.

For a single value of electrical power consumption, there could be many combinations of set points for the process variables. Thus, the values to be established for each electrical equipment also vary according to certain preferences, such as production rate, quality, or economic rev-

enues. If the PPM system implements flexible operation strategies, it needs to establish a series of preprogrammed actions for electrical contingencies. Because there could be several combinations of operating points for a single power consumption, PPM also needs preprogrammed preferences.

Traditionally in a microgrid, the generated power adapts to the power consumed by the process. Nevertheless, one of the objectives of flexible operation is to prepare the process for possible electrical contingencies. Figure 2.7.a) shows the progress of a process variable and the consequent power generated. This progress corresponds to the traditional operation in a microgrid.

Figure 2.7.b) reflects the approach by flexible operation, in which the process is prepared for an electrical contingency. When the power drops, the PPM decreases the consumption of the loads, and sends the set points to the process variables so the process moves towards the new set point that is consistent with the available power.

The envelope of operation tells the PPM the power consumption for a given family of operating points, and the other way around, it tells the PPM the corresponding operating points for given power consumption. Thus, the study of flexible operation has benefits both for adjusting the process variables to the generated power.

Additionally, flexible process operation will enable more precise PPM systems, and this in turn could enable future grid services by electricity-intensive industries to the power grid. For instance, with suitable financial incentives, an industrial microgrid might export power to the public grid rather than using it for the process. Less power would be available for the process, and flexible operation would enable the process to reduce its consumption by the required amount. Conversely, the process might even increase its production and electricity consumption if extra power is available from the public grid, for instance, because of an increased amount of renewable generation on a sunny windy day.

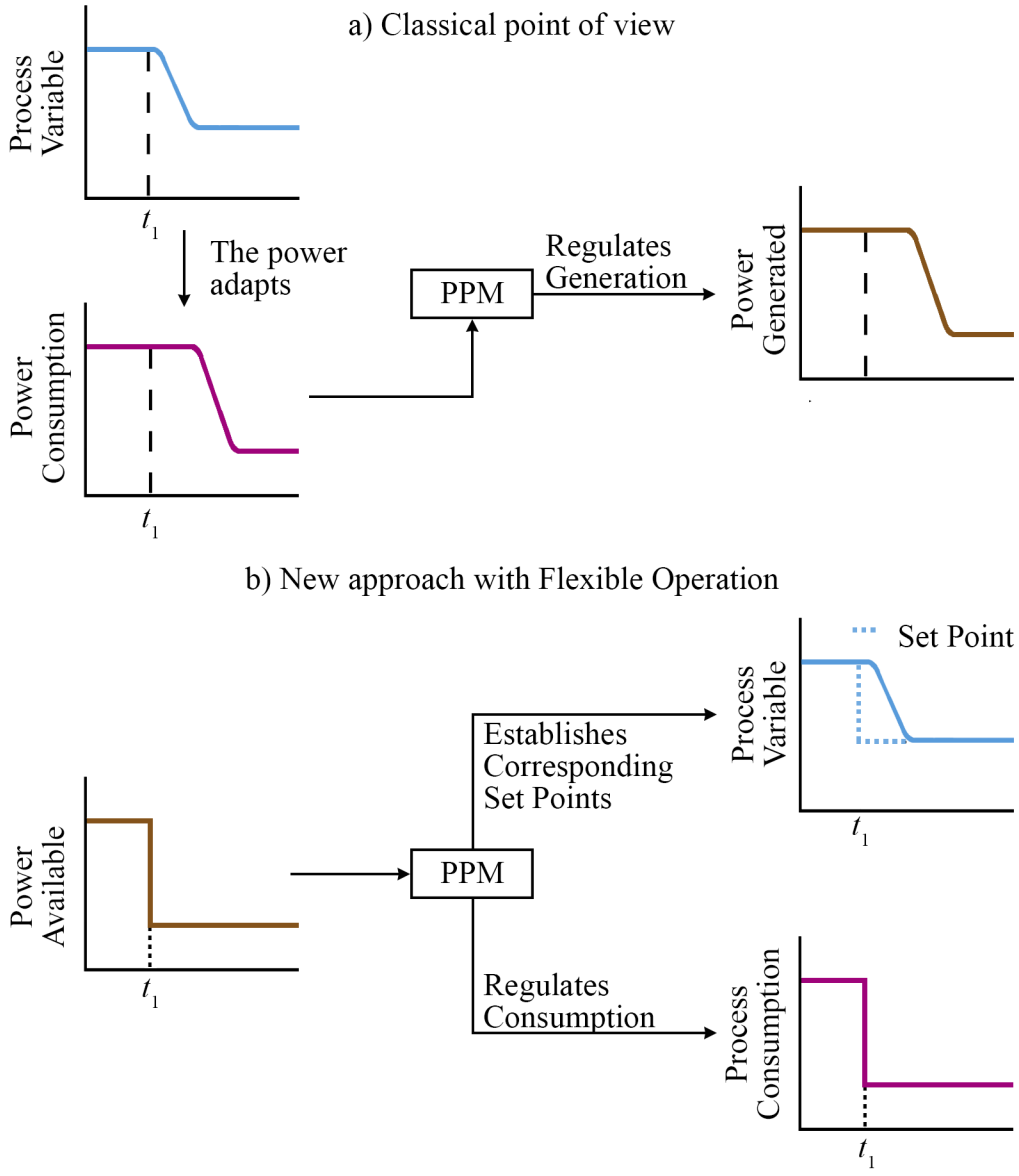


Figure 2.7: a) Representation of the classical point of view that adapts the power generated (brown) to the consumed power (pink) corresponding to the operating point (blue). b) Representation of the new approach by flexible operation, in which the PPM reduces the power consumption of the plant (pink) to match the available power (brown) and sends the set points (dotted blue) of the variables that corresponds to the available power (solid blue) .

2.3.1 Present PPM Operation vs Proposed PPM Operation

This subsection compares both operations for the PPM: the current PPM operation, and the proposed PPM, which in this section, for convenience is named PPM+. The comparison corresponds to an electrical contingency event.

PPM sheds non-essential loads in the process for adapting the consumption of the process to the available power. If the reduction is not enough for reaching the available power, the PPM sheds loads that might be crucial for the process, and the process may need to stop. Stopping the process leads to monetary losses due to the total loss of production and the costs of restarting the process.

PPM+ turns down the loads rather than shutting them down. Thus, the crucial load does not turn off, and the process keeps operating. The process continues the operation with a different level of consumed power, and consequently, the production is probably lower. Nevertheless, PPM+ reduces monetary losses because the production is not entirely lost, and it avoids the costs of shutdown and startup and lost production during the shutdown.

PPM uses circuit breakers for shedding loads, whereas PPM+ reduces the electrical power to the electrical loads and changes the set points of the variables so the process reaches a new operating point that is consistent with the available power. An electrical power outage occurs over a time scale of the order of 100ms, and therefore, PPM+ reduces the power consumption within 100ms. However, the process moves to the operating point over a time scale that depends on the process time constants.

PPM and PPM+ have to act as fast as possible, and therefore, they have preprogrammed actions. For shedding loads, PPM needs the available power as an input, and the system starts to shut down equipment until the consumption is equal or lower than the available power. On the other hand, for flexible operation, PPM+ needs additional information, such as the preprogrammed preferences.

Table 2.1: Comparison between the current Process Power Management (PPM) system operation and the proposed Process Power Management (PPM+) system operation.

	PPM	**PPM+**
Method	**Load Shedding** • Sheds electrical loads • Process might need to stop • Monetary losses due to loss of production and restarting	**Flexible Operation** • Turns down electrical loads • Process does not stop when reducing the consumption of the crucial equipment • Reduces monetary losses
Technology	**Circuit Breakers** Open or close a circuit to shed or connect loads	**Controllers** Reduces the power to the loads and send new set points, so the process moves to a new operating point corresponding to the available power
Inputs	Available Power	Available Power Preprogrammed preferences
Outcome	Load is shed in excess of what is required	The process fully exploits the available power

Apart from decreasing the consumption of the loads, PPM+ uses an envelope of feasible operation to send the set point to the controllers of the process variables that correspond to the consumption of the loads. Table 2.1 shows a summary of the differences between the PPM and the PPM+.

This PhD thesis concerns the assessment of the envelope of feasible operation for two electricity-intensive processes, namely LNG production and the aluminium smelter. It proceeds using first-principles process modelling to:

- Determine the steady power consumption at various operating points (envelope of operation)
- Determine the duration of a power reduction, in the case of aluminium smelter
- Define the limits of flexible operation considering the equipment and the process constraints (envelope of feasible operation)

2.4 Background to the Processes

This project chose two processes for studying flexible operation in electricity-intensive plants. The reason for choosing them is that they consume large amounts of electricity, and they are often in locations where the electricity of the public power grid is not reliable. Moreover, the difference of natures between both processes allows drawing more conclusions and heuristics on the implementation of flexible operation. The chosen processes are the liquefaction of natural gas and the aluminium smelting through reduction of alumina.

This chapter gives an introduction to the processes, while Parts II and III cover a more in-depth insight. This chapter provides a more general view of the process and describes the energy transforms.

2.4.1 Liquefaction of Natural Gas

Natural gas is a mixture of hydrocarbons, primarily constituted by methane, and its main uses are as a source of energy, or as feedstock for hydrogen production. As natural gas meets around 23% of the global energy needs, the procesing of this gas has increasingly become more important over the last two decades (BP p.l.c. (2019); Enerdata (2018)). Its liquid form needs 600 times less volume than its gaseous form, so liquefied natural gas (LNG) is more economically beneficial to store and to transport. Before being liquefied, natural gas has to be pretreated to

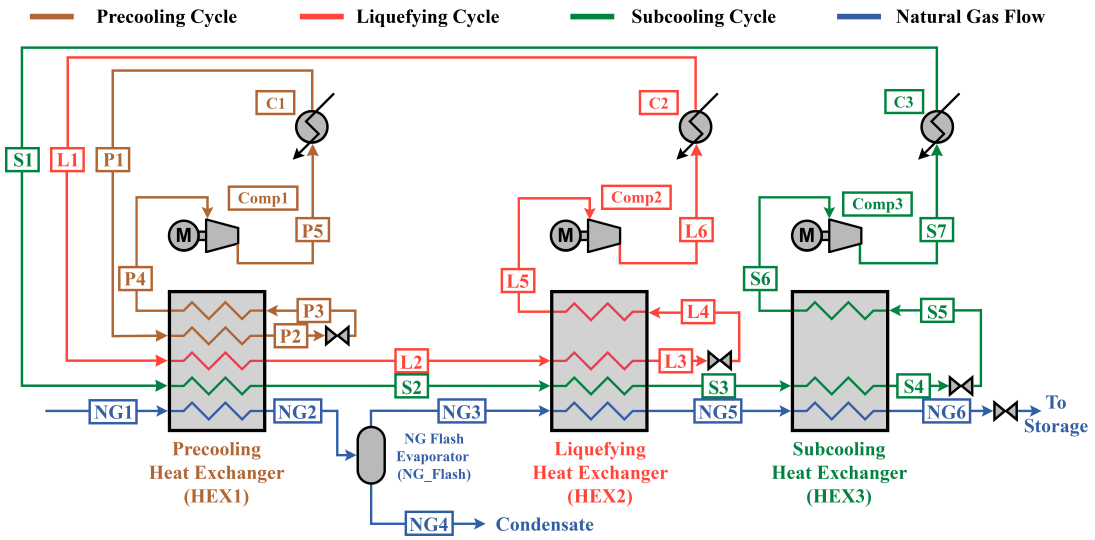


Figure 2.8: Schematic representation of the LNG process. This process corresponds to the Mixed Fluid Cascade, developed by Linde, and the picture is extracted from Linde AG (2018).

get rid of mercury, sulfides and carbon dioxide, before being dehydrated. After that, the purified dry natural gas is liquefied and stored.

This project focuses on the liquefying section because it is one of the most power-consuming parts of the plant. In the liquefaction process, natural gas enters the process at around 298K and 30 bar, and it is cooled down to -162°C using refrigeration cycles to remove the heat from the natural gas and release it to the environment. Upon liquefying the natural gas, the process decompresses and stores the LNG into vessels for transportation. Depending on the capacity of the plant, typical power consumption ranges from 30MW to 200MW (Linde AG, 2018). Its electrical power consumption makes the LNG process a suitable process for studying flexible operation.

LNG Process

There are several liquefaction processes, depending on the heat exchangers distribution, or the refrigerant used. Figure 2.8 shows the LNG process that this project studies, which is the Mixed Fluid Cascade (MFC) process.

Figure 2.8 has streams of four colours, with the blue colour assigned to the natural gas streams, and the three remaining colours associated with the refrigerants. Each of these three refrigerants has a role in the liquefaction of natural gas:

- **Precooling:** This refrigerant is represented in brown in Figure 2.8. Its composition is typically 80% mol propane and 20% mol ethane. Its role is to absorb heat from the natural gas, and from the liquefying and the subcooling refrigerants. At the exit of the heat exchangers, the natural gas and the refrigerants have a temperature of around 238K.
- **Liquefying:** This refrigerant is represented in red in Figure 2.8. Its composition is typically 85% mol ethane, 10% mol propane and 5% mol methane. This refrigerant absorbs heat from the natural gas and the subcooling refrigerant. The natural gas and the subcooling refrigerant exit the heat exchanger at around 173K. At that temperature and pressure, the natural gas is completely liquefied.
- **Subcooling:** This refrigerant is represented in green in Figure 2.8. Its composition is typically 40% mol methane, 30% mol ethane, and 30% mol ethylene. The subcooling refrigerant absorbs heat from the already liquefied natural gas until it cools down to around 110K. After the exit of the process, there is a decompression operation (not shown), that reduces the pressure from 30 bar to 1 bar. Subcooling is needed to decrease the LNG temperature below its saturation point at 1 bar, so after decompressing the LNG, it does not present any vapour phase.

Each refrigerant undergoes a Joule-Thomson cycle, which is a compression and expansion cycle whereby refrigerants can absorb large amounts of heat. Essentially, in the cycle, the refrigerant absorbs heat from the natural gas and releases this heat to the sea through a sea-water cooler. Section 5.5 provides further details regarding this cycle.

The cycle uses a compressor driven by an electric motor. Hence, the electrical power is consumed mainly for compressing the refrigerants. The discharge pressure of the compressors determines the performance of the refrigeration cycles for absorbing heat from the natural gas.

Chapter 6 gives physical insights about the consequences of adjusting the electricity used by a motor on the performance of the refrigeration cycles.

The refrigerant and the natural gas streams present many interactions, so it is crucial to consider all interactions when modelling the process. The mathematical model has to include the energy and mass balances, and the thermodynamic equations.

Energy and Mass Balances

Balances ensure that there is a steady state during the process, and that all variables are consistent. Figure 2.8 shows that there is no mass exchange amongst the refrigerants, or between the refrigerants and the natural gas. Thus, balances focus on the heat balances.

Thermodynamic Models

The enthalpy of a stream measures the energy carried by the stream. Calculating the enthalpy requires the proper thermodynamic equations and to know the process variables, namely the temperature, the pressure, the compositions, and in the case of having a Vapour Liquid Equilibrium (VLE), the vapour fraction, which is the fraction of the stream that presents a vapour phase.

Natural gas and the refrigerants are mixtures of hydrocarbons. Mathematical models of hydrocarbons require models more complex than the ideal gas law, and the adequate Equation of State (EoS) depends on the characteristics of the process and the components. Moreover, the appearance of VLE during the process causes the model to need additional equations to determine the vapour fraction.

The chosen EoS is the Redlich-Kwong Soave (RKS) EoS, and the algorithm for calculating the vapour fraction is the Rachford-Rice (RR) algorithm. The RKS is an two-parameter EoS that uses values characteristic to each component, including the critical pressure, the critical tem-

perature, and the acentric factor. This EoS can also model mixtures of fluids by implementing classical mixing rules in the main equations.

The RR algorithm considers the compositions of the vapour and liquid phases, and the RKS EoS calculates the composition for each phase. Thus, the model implements the RKS EoS and the RR algorithm together, so the RKS gives the necessary input to the RR algorithm, and the latter one gives the vapour fraction in the stream, which is necessary for obtaining all the thermodynamic properties, such as the enthalpy.

Ikeda and Schaefer (2011) supported the use of the RKS EoS, stating that, the Peng Robinson or the RKS EoS could be used to model a mixture of hydrocarbons. One of the objectives for assessing the potential of flexible operation in the industry is determining the impact of the process variables on the electrical consumption. To that end, an analysis changing the pressures of the refrigerants is carried out. Therefore, the broader range of pressures linked to the RKS EoS makes these equations appropriate for modelling the streams of the process. Chapter 5 gives a more detailed explanation of the RKS EoS and the RR algorithm, including their mathematical models, and how they are combined to obtain the enthalpy of a stream.

The model used in this PhD thesis is an adaptation of the Mixed Fluid Cascade process by Linde (Linde AG, 2018). The model in this thesis considers the VLE to broaden the envelope of feasible operation. To that end, the model implements flash separators for: (i) including a condensate stream for the natural gas after the precooling stage, so the heaviest compounds are separated earlier in the process; and (ii) including a liquid phase to the refrigerants after exiting the heat exchanger, which so far, the literature has not considered [1]. Both reasons give a wider range of possibilities, increasing the number of combinations of operating points. The main body of the thesis does not include the analysis of the presence of liquid phases in the refrigerants, leaving the analysis to the appendices (Appendix C.4).

[1] To the knowledge of the author

2.4.2 Aluminium Smelter

Aluminium is one of the most common metals, but it is not present in nature in its pure form. Aluminium smelters grind bauxite to obtain alumina, which is the oxide compound of aluminium, and adds it to an electrolyte bath, in which alumina undergoes an electrolysis to obtain the aluminium.

The electrolysis takes place in an electrolytic cell, which is equipment that uses electricity to drive redox reactions. The electrolyte cell is the focus of this case study. The power consumed in these cells can vary from kW to MW depending on the production rate (Altenpohl, 1998; Jiang et al., 2013; Molina-García et al., 2011). Moreover, due to the nature and size of the process, the plants may be placed in locations where the electricity of the power grid is not very reliable (UC Rusal, 2016). These reasons make the aluminium smelter an appropriate candidate for studying flexible operation.

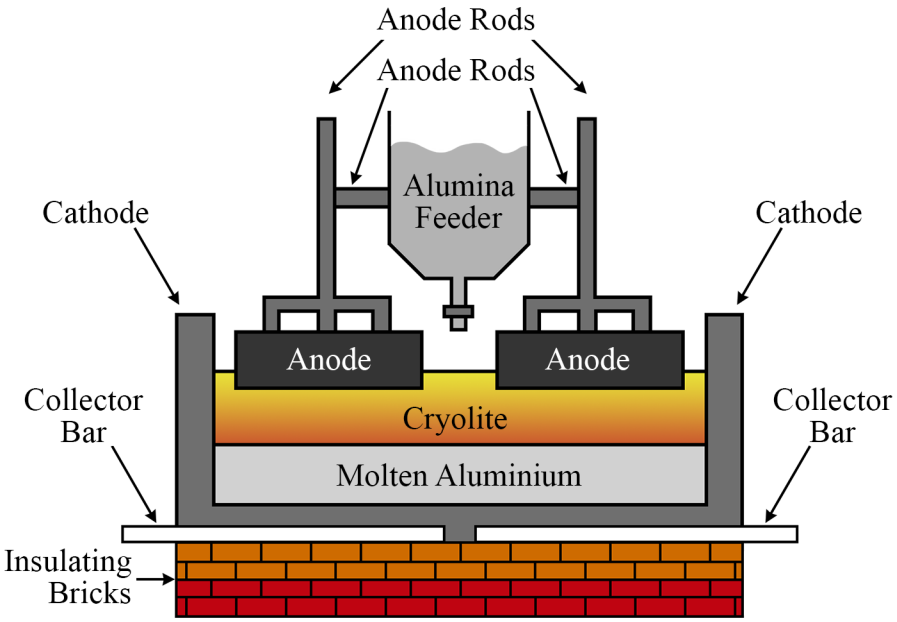


Figure 2.9: Cross-section representation of an electrolytic cell for aluminium production.

Figure 2.9 shows a simplification of the parts in an electrolytic cell. A direct electrical current flows from the anode bridges to the cathodes passing through the electrolyte bath, which presents a solution that dissolves the alumina and can conduct the electrical current.

In the aluminium smelter, the composition of the electrolyte bath is primarily cryolite (Na_3AlF_6). The melting point of alumina lies around 1050°C, which causes the electrical power consumption to increase to heat the bath to higher temperatures, and to offset the heat losses to the surroundings. Cryolite decreases the melting point to 900-1000°C. The melting point of the cryolite is 1010°C, but it can be lowered by introducing additives, including CaF_2, AlF_3, MgF_2, and NaF, to a melting point of 950 °C. LiF can also be added to increase the conductivity of the bath (Haupin, 2001). Therefore, ultimately the bath is composed by cryolite, additives, and the alumina itself, whose concentration also affects the melting point and the conductivity. It is preferable to maintain its concentration between 2 and 8% wt for correct operation (Chapter 9).

The electrolytic cell is the vessel in which the alumina reduction happens. It contains the electrolyte bath, and it has to withstand high temperatures, so the cryolite is molten during the operation. Thus, the electrolytic cell has an arrangement of layers that provide thermal insulation to the electrolyte bath. The layer in direct contact with the electrolyte bath is the cathode needed for the reduction reaction.

Additionally, the cell has anodes formed by carbon blocks placed on the surface of the electrolyte bath, and whose height can be adjusted. The distance between the anode blocks and the cathode is called Interpolar Distance (IPD), and it is manipulated to control the temperature of the bath.

Alumina is added to the bath using a feeder placed on top of the cell. After the reduction, aluminium settles at the bottom of the cell, and it exits the cell through the collector bars and special vacuum buckets. Depending on the capacity of the plant, additional cells can be arranged in parallel to include more anodes and more electrolyte.

The main reaction taking place in the cell is the reduction of alumina, in which aluminium is separated from the oxygen:

$$2\,Al_2O_3 + 3\,C \longrightarrow 4\,Al + 3\,CO_2 \tag{2.1}$$

The electrical potential of the products is larger than the potential of the reactants, and therefore, it is necessary to provide electrical energy to the reaction. Additionally, the chemical energy of the products is higher than the energy from the reactants, so the reaction absorbs thermal energy. Apart from the reduction reactions, other endothermic reactions take place in the bath, but they do not require a voltage drop and do not need as much as thermal energy.

The AC current from the generation plant is converted to direct current by passing it through a rectifier. For the aluminium smelter, the electrical input is a constant current supply, so the amperage is constant, and the voltage drop varies depending on the electrolyte bath properties, such as the IPD and the conductivity of the bath.

Energy transformations in an aluminium smelter

The temperature in the bath has to be around 950°C, and considering that the cell is not perfectly insulated, there has to be a power source to offset the heat losses to the surroundings. The initial form of this source is the electrical power, which transforms into heat via the Joule heating effect (or Ohmic heating), in which the electrical current flowing through a conductor produces heat.

The electrical current is constant, but the voltage drop depends on the electrical current and on the properties of the bath, especially on its conductivity. Additionally, the difference of potentials between the products and the reactants in the reduction reaction affects the overall voltage drop in the cell.

Outside the bath, there are parts of the cell that offer an ohmic resistance. Consequently, a fraction of the electrical power is lost due to the current flowing through these external parts.

Hence, it can be considered that the power allocated for heating the bath is the total input minus the ohmic losses due to the outer parts of the cell.

The heat derived from the Joule heating effect is used for:

- **Endothermic Reactions:** The alumina reduction needs a large amount of chemical energy for overcoming the difference of chemical potential between the products and the reactants (See Section 9.4.4). Additionally, most of the reactions occurring in the cell are endothermic. Consequently, part of the thermal energy in the bath is transformed into chemical energy. There are also exothermic reactions in the bath, which use chemical energy, and transform it into thermal energy.
- **Heating Feeds:** Alumina is added to the cell so there is enough raw material for producing aluminium. Moreover, other additives are added to the bath in order to maintain desirable properties The fed materials enter the cell at a lower temperature than the bath, so they absorb the thermal energy present in the bath to heat up. Ultimately, the thermal energy is not transformed, but rather transferred to another body .
- **Offsetting heat losses:** Thermal energy is constantly flowing, and one of the paths it follows is to the outside due to the lower temperature of the surroundings. The new added thermal energy produced with the Joule heating effect compensates those losses, so, once again, the thermal energy is not transformed, but instead, it is transferred.

Figure 2.10 shows the mechanisms for increasing or decreasing the thermal energy of the electrolyte bath. If the input energy flow rate (green arrows) is greater than the output energy flow rate (red arrows + black arrow), the temperature of the bath increases, and the other way around. At steady state, the rates of energy inflow and outflow are equal, and the temperature remains constant.

In Figure 2.10, the amount of electrical energy converted into thermal energy through the Joule heating effect depends on the voltage drop and the electrical current. The electrical power lost

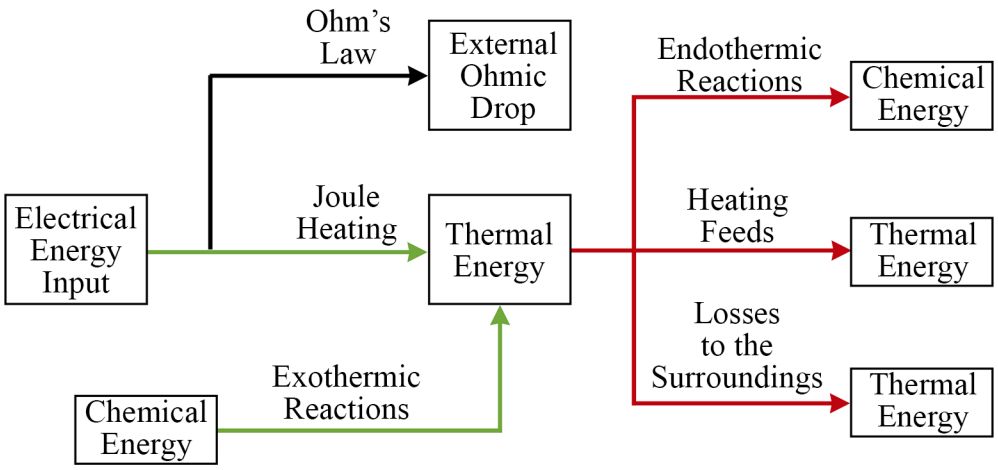


Figure 2.10: Energy transformations in the aluminium smelter. Each box represents a form of energy, and each arrow represents the mechanism for transforming the energies. The figure shows the mechanisms that increase the thermal energy (green), and the mechanisms that absorb thermal energy from the cell (red), as well as the energy lost due to the external ohmic resistances (black).

due to the external ohmic drops depends on this current, so when the electrical current is large, the cell produces more heat, but it also generates more losses. Parts III and IV discuss these mechanisms more in detail.

The overall model can be divided into three sub-models. The first one is a mass balance that considers the material entering and exiting the cell, and the produced material as a result of the reactions. This sub-model takes the concentration of each compound into account because they determine various properties of the electrolyte bath, such as the heat capacity or the conductivity. Additionally, the model calculates the heat absorbed or generated due to the reactions in the cell.

The second model is the electrical model, which determines the voltage drop considering the bath properties calculated in the mass balance. Knowledge of the voltage drop is crucial for calculating the amount of electrical power that is used for heating up the cell.

The third sub-model is the heat balance. This sub-model considers the heat lost to the surroundings and the heats determined in the mass balance and the electrical models to calculate the temperature of the bath. The bath temperature, in turn, is used by the mass balance model and the electrical model.

2.4.3 Comparison between the Processes

This thesis compares the LNG process and the aluminium smelting process to draw conclusions and extract heuristics for studying flexible operation in other potential processes. The comparison considers the operation mode of the process, the electrical equipment in the process, and the presence of chemical reactions.

Operation Mode

The LNG process is a continuous process, meaning that all the streams flow continuously, and therefore, there is no storage of material or energy. On the other hand, the electrolyte cell in the aluminium smelter works in a semi-batch operation, which means that either the feeding or the product extraction is periodic. Thus, the electrolyte bath can act as energy storage, and therefore, during an electrical contingency, the change of temperature is dampened by the energy stored in the bath.

Because of the continuous nature of the LNG, it is more challenging to implement flexible operation in this process. Because there is no energy stored, adjusting a single variable has immediate effects on the rest of the variables. This can be alleviated considering that flexible operation determines an envelope of feasible operation, so the process is prepared if the available power changes.

Electrical Equipment

In both processes, the energy-intensive electrical equipment significantly differs. In the LNG process, the motors transform the electrical energy into mechanical energy, and the compressors use that mechanical energy to provide the refrigerant with enthalpy (or internal energy). The electrolyte cell of the aluminium smelter, on the other hand, transforms the electrical energy into thermal energy, acting as an electric arc furnace. The chemical reaction in the cell transforms the thermal energy into chemical energy. Having such unlike equipment enables the analysis to observe what equipment can exploit the electrical input better.

Chemical Reactions

Due to the lack of chemical reactions, the LNG process does not transform the electrical energy into chemical energy, and the mass balances focus on what is entering and what is exiting the process. This can simplify some calculations, especially when concentrations are crucial for determining the properties of the process, which is the case of the aluminium smelter, in which the compound concentrations defines essential properties in the bath.

Having chemical reactions in a process implies they absorb or release energy, which interacts with the amount of electrical power consumed by the process. Hence, having a process with chemical reactions, like the aluminium smelter, helps develop the overview of investigating flexible operation for other processes with reactions in them.

Both processes are different in terms of energy transformations, which makes it favourable for drawing more conclusions in the flexible operation implementation.

2.5 Summary of the Chapter

This chapter has established the necessary knowledge for understanding the research results and the motivations for investigating this topic. It also gives a brief description of the processes that are studied, as well as the reasons for choosing them.

This chapter introduced the concept of a microgrid. In these structures, the industrial process and the power plant generation can operate in island-mode, isolating both elements from the power grid and still having the generated and consumed power balanced in the microgrid.

During an electrical contingency, Process Power Management (PPM) systems decide how to allocate the available power amongst the electrical loads in the process. In these conditions, the PPM system sheds loads until the consumption of the plant is equal or lower than the available power; this operation is known as load shedding.

For processes with low granularity, i.e. a small number of large loads, adapting the consumption to the same level as the available power might not be possible, and therefore, the process does not fully exploit all the available power. Moreover, if after shedding the non essential loads, the consumption is still higher than the available power, the PPM system needs to disconnect equipment whose function might be crucial for the rest of the operation, and therefore, the process would need to stop. This leads to monetary losses due to loss of production and restarting the process.

This project proposes flexible operation an alternative to load shedding. If working flexibly, during an electrical contingency, the PPM reduces the consumption of the loads and establishing set points for the process variables consistent with the desired power consumption. Consequently, the process does not need to stop.

To that end, the study observes the consequences of reducing the power on the process variables. This results in an envelope of feasible operation that relates the process variables and the electrical power consumption.

This research has chosen two processes to study flexible operation, namely the liquefaction of natural gas, and the aluminium smelter. The models of the processes use first-principles for determining the steady power consumption at various operating points, obtaining an envelope of feasible operation, and, for the case of the aluminium smelter, the duration of the power reduction.

Comparing both processes can lead to conclusions and heuristics that can be applied for other potential processes, so this chapter has compared the LNG process and the aluminium smelter.

Chapter 3

Literature Review

There are multiple applications of flexible operation in the industry, such as flexible generation, or running a carbon capture plant flexibly for matching the CO_2 generated by power stations. As processes are increasingly being powered by electricity, flexible consumption of electrical power is becoming more relevant in the industry.

This chapter discusses the current uses of flexible operation in the industry and the reasons for operating a process in this way. It also studies the trends and the potential applications of flexible operation in electrically driven processes.

Additionally, this chapter discusses the current trends of flexibly operating the liquefaction of natural gas process and the aluminium smelter. The analysis also includes studies on how these processes exploit the energy so that the mathematical model used for this research is as accurate as possible.

3.1 Current Trends in Flexible Operation

This section addresses the current uses of flexible operation and the methodology for implementing it in industries according to the literature.

The continuous variations present in a process and its environment, such as changes in the available power, the ambient temperature, or product requirements, might cause uncertainties on how the process has to operate. Thus, implementing flexible operation strategies helps the process to accommodate these variations and to keep the process running (Swaney and Grossmann, 1985; Floudas et al., 2001; Mitra et al., 2012). Dotzauer et al. (2019) studied the level of flexibility of different plants according to its equipment. As a conclusion, the authors highlighted that flexibility could be measured by three factors, (i) the amount of power curtailment, (ii) its speed, and (iii) its duration. Another conclusion is that flexibility is achieved as long as there is a trade-off, not only in the output of the process, but also in the operation conditions, for example, a by-product.

Many authors have studied the application of flexible operation for carbon capture in power plants Chalmers and Gibbins (2007); Chalmers et al. (2009); Kang et al. (2012); Mechleri et al. (2017); Qadir et al. (2015). They studied the carbon capture and storage technologies for reducing the CO_2 emissions in a power plant. The papers considered the operation from an economic point of view, taking into account the variable costs of venting the CO_2, and the costs of its storage.

These papers focused more on economic optimisation rather than on the technical advantages that flexible operation brings. From a technical point of view, Lin et al. (2012); Wetenhall et al. (2017) observed the impacts of the process conditions, such as the solvent flow or the temperature of the columns in the capture plant, on the CO_2 capture rate. Koytsoumpa et al. (2018) studied the integration of power to methanol process in a thermal plant to add flexibility to the power plant. The power to methanol process imports and exports heat to and from the power plant, so the whole facility integrates flexible operation strategies for optimising the use of heat.

An additional use of flexible operation is discussed by Eilers and Schaub (2016), who studied the flexibility of a synthesis reactor, observing the consequences of varying a number of process variables, such as the temperature, the composition, or the flow rate, on the yield of the reaction.

Therefore, flexible operation brings many benefits to the processes by defining an envelope of operability for it, so if a disturbance takes place, the process knows how to keep the operation running. In electrical driven processes, one of the possible disturbances is the available power.

3.1.1 Flexible Operation in Electricity-Intensive Processes

As processes are moving towards being powered by electricity, they also need to accommodate possible variations of the available electrical power. Many authors (Gutowski et al., 2009; Saidur, 2010; Trianni et al., 2019; Zhou et al., 2016) studied the tendency of processes being driven by electrical power. The report by Devold et al. (2006) discussed the advantages of using electrical drives over gas turbines drives in LNG processes.

Electricity-intensive process plants are often in microgrids structures so that they have a power plant. Therefore, they require the implementation of Process Power Management (PPM) systems to assure that the electrical power generated matches the electrical power consumed. Almada et al. (2016); Iovine et al. (2019); Guerrero et al. (2013) examined the use of these systems for balancing the power in the microgrids, for both AC and DC microgrids, focusing on the economic and reliability aspects of the operation.

Having a flexible load in the microgrid structure brings important benefits to the PPM systems (Sen and Kumar, 2018), so flexible operation in electricity-intensive processes has potential uses for helping PPM systems to control the power in the microgrid.

Another potential use of flexible operation of electricity-intensive processes would be for Demand Side Management (DSM). DSM are strategies to reschedule the electrical consumption of a plant for managing the production and demand of electricity in the power grid (Strbac, 2008). Various articles discussed the application of DSM in electricity-intensive processes (Hanrahan et al., 2014; Harjunkoski et al., 2014; Child et al., 2019), exploring the manner of optimising the costs of electrical power consumption according to the fluctuating electricity prices. By

assessing the flexibility of these processes, they can accommodate the schedule imposed by the electricity price.

Authors such as Chang-Chien et al. (2012), Golmohamadi et al. (2019), and Shoreh et al. (2016) studied the use of DSM to adjust the power to a certain level. In these documents, flexibility is analysed from an electrical perspective, observing solely how many watts industries can deploy, but it does not mention the consequences of this variation within the process.

There has also been much research on flexible operation of power generation. The articles by Cupertino et al. (2019) and Pavić et al. (2016) studied how to increase the flexibility of a photovoltaic field and wind power plants respectively for voltage and frequency dips. Other generation plants can also work flexibly; for instance, Martínez-Rodríguez et al. (2019) studied the flexibility of a network of the solar collector field. The authors discussed the impact of the operational conditions on the electrical power and heat generated to determine an envelope of operation. Jenkins et al. (2018) presented a paper concerning flexible generation focused on a nuclear plant stating that the plant can work flexibly by controlling the output of the nuclear reactor or the input to the steam generator. The paper analyses the possibilities of operational conditions that correspond to different energy outputs, creating, as the present work, an envelope of feasible operation. The issue of this methodology is that the plant has to schedule the change of process variables.

However, there has not been much research on flexible operation of electricity-intensive processes for PPM. Shi et al. (2017); Zhu et al. (2017) studied flexible operation of multiple loads in a microgrid for managing the power, but the study only considered the watts needed by the loads. Authors still miss analyses of how an electricity-intensive process is affected by a change in electrical power consumption. On the other hand, Caspari et al. (2019a,b) analysed flexible operation of an air separation process for producing liquid nitrogen and liquid oxygen, determining the impact of the production rate of the liquid nitrogen on the electrical power consumption. The authors also studied the operating point corresponding to the various values of the production rate. Nevertheless, the study only contemplated varying the production rate of one product rather than a set of operational variables.

Thus, this research explores flexible operation of electricity-intensive using the PPM technology considering multiple process variables that might affect the electrical power consumption. The findings of the thesis have the potential to be extended to provide load balancing and frequency control in the public power grid. Papaefthymiou et al. (2018) studied flexibility in the power grid as the contribution of various agents, including the flexibility of the loads as one of the agents. Several authors studied flexibility in the power grid to accommodate the penetration of renewable energy sources (Koytsoumpa et al., 2018; Li et al., 2016; Iovine et al., 2019; Wang et al., 2015; Zhao et al., 2015), so the findings of this thesis are potentially useful for the integration of cleaner energies.

3.2 Liquefaction of Natural Gas

To the author's knowledge, no studies analyse flexible operation in the process of liquefaction of natural gas. This section comprises reviews regarding the energy consumption of different LNG plants and other articles that help develop the model to be used during this thesis to show the potential of operating the LNG process flexibly.

Bosma and Nagelvoort (2009) and Lee et al. (2018) stated that the natural gas liquefaction is growing in interest because of the elevated cost compared to the rest of processes involving the natural gas. Figure 3.1 shows these processes along with their relative costs. According to Figure 3.1, the liquefaction process takes 42% of the total costs.

He et al. (2018), Nguyen and Elmegaard (2016), and Qyyum et al. (2018b) compared the energy efficiency of various liquefaction processes, concluding that the studied liquefaction processes are currently optimised, and the way for increasing the efficiency of the process would be re-designing the process or increasing the capacity of the equipment, more specifically, the heat exchangers. Since the studied process is already chosen (MFC by Linde AG (2018)), this research has focused on the operational part of the process, assessing its flexibility, and determining the trade-offs that help to meet the electrical power requirements.

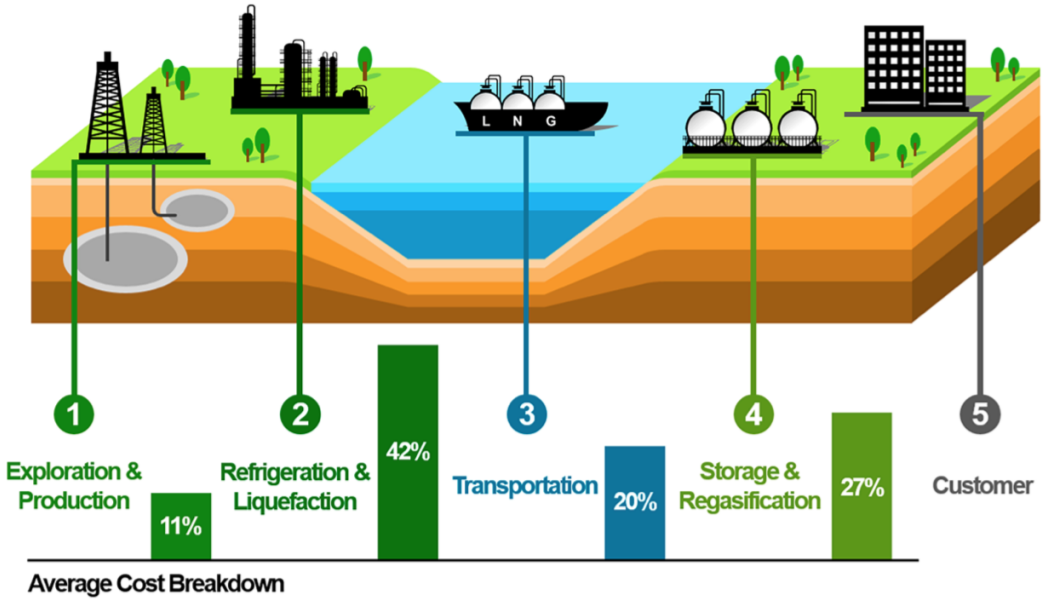


Figure 3.1: Breakdown of the cost of producing LNG, from the extraction of crude oil to the utilization of the LNG. The picture is extracted from Lee et al. (2018)

Nguyen and Elmegaard (2016) compared the performance of various equations of state for modelling the behaviour of the mixture of hydrocarbons by comparing the calculated results with empirical data. The authors only took into account the vapour-liquid equilibrium for intermediate calculations such as saturation points, or fugacity coefficients. Thus, the streams in the process contained just one phase, and therefore, the range of possible operational points significantly reduces. This thesis explores a broader range of process variables that causes the streams to present two phases to study the consequences on the power consumption.

In the liquefaction process, materials are continually flowing, so there is barely any energy storage. Thus, flexibility is limited to changing the process variables, instead of storing energy, as stated by de Sisternes et al. (2016),Wang et al. (2015), or Zhao et al. (2015). One method for storing energy in continuous processes is by producing in excess by consuming more electrical power during times where the electricity is cheapest. In the liquefaction process, this can be done by producing more LNG, storing it, and regasifying it when needed. Many authors studied the electrical power obtained during the regasifying stage (Łaciak et al., 2019; Kanbur et al., 2017; Jeong, 2017), but these studies focused on the LNG end-users. Mehrpooya and

Sharifzadeh (2017); Pospíšil et al. (2019) examined the possibility of storing energy in the liquefaction process by storing the LNG in the same plant that it is liquefied, but this would imply the redesign of the plant.

The LNG process adjusts the flow rates of the refrigerants according to the production rate by changing the speed of the compressors, so if the available power decreases, the flow rates of the refrigerants decrease. Thus, if the process operates flexibly when the available electrical power drops, the PPM reduces the electrical power consumption of the compressors and establishes set point for the LNG production rate corresponding to the reduced power consumption. The main issue during the transient behaviour from the nominal to the reduced power states is that the refrigerants might not be able to absorb as much heat as needed from the natural gas due to the differences of flow rates. If that occurs, the temperature of the natural gas can rise until it reaches the saturation point, presenting a vapour phase, which is undesirable due to the essential purpose of the process. Fazlollahi et al. (2015) and He and Ju (2016) studied the dynamic behaviour of different LNG processes when a disturbance in the plant takes place. The results show that the difference in flow rates between the refrigerants and the natural gas is not enough to make the LNG to reach the saturation temperature. Thus, the LNG model in this project obtains the process variables for the steady states corresponding to the nominal and reduced power states, so when an electrical contingency occurs, the PPM can send the new set points to the process immediately after the available power is known. Appendix C.3 discusses the dynamic behaviour more in detail.

Capacity of the process is also an important factor to consider to verify that the model is accurate. The model used in this project is based on the Linde process (Linde AG, 2018) used in the liquefaction plant in Hammerfest. This plant has a nominal production rate of 4.3 MTPA (Million Tonnes Per Annum), but it can produce up to 10 MTPA (Linde AG, 2019). This research established the nominal production rate to 7 MTPA. According to Devold et al. (2006), the electrical consumption of an LNG plant is between 30 MW and 35 MW for a production of 1 MTPA. The results obtained with the modelled plant agree to these numbers.

3.3 Aluminium Smelter

Several authors have studied the implication of aluminium smelters as active members in the regulation of the power grid. Authors such as Jiang et al. (2013), Molina-García et al. (2011), Yao et al. (2015a), and Zhang and Hug (2014) proposed the use of aluminium smelter for restoring balance to the power grid. However, these articles focused the study from a power system perspective, and they did not take into account the consequences that decreasing the power has on the process variables in the smelter.

Aluminium smelters are electricity-intensive processes that use electrical power for obtaining aluminium from alumina, and for heating the electrolyte bath. Due to its high temperatures and large volume, the electrolyte bath can store significant amounts of energy. Thus, if they are disconnected from the power supply, the temperature will slowly decrease, and they can remain disconnected as long as the bath temperature does not reach the cryolite solidification point. Dorreen et al. (2017) and Yao et al. (2015b) studied how this load shedding strategy affects the electrolyte cell, observing the temperature of the bath, and establishing a time limit before the cryolite solidifies. They, however, only applied this methodology for the case when the power supply is cut completely, without considering the time limit if the power is reduced instead.

According to Landry et al. (2018) and Liu et al. (2016), the heat balance in the bath severely affects the thickness of the cryolite ledge which is frozen cryolite formed in the borders of the bath due to the temperature distribution. The results have shown that this thickness does not affect the temperature of the bath significantly. Thus, due to simplicity reasons, this thesis assumes that the thickness of the ledge remains constant.

The objective of flexible operation is to obtain a new steady state for the process to keep producing after a power reduction. Naixiang et al. (2016) and Peyneau et al. (2016) studied how to operate the aluminium cell when it is working at lower electrical consumption. Additionally, they determined the maximum power reduction feasible. However, they only considered the steady state, neglecting the transient behaviour of the variables.

The presented studies have not contemplated the possibility of reducing electrical power consumption during a certain period. Thus, this thesis studies the transient behaviour when the power is reduced to a certain level rather than just being disconnected. Studying flexible operation during transient behaviour determines not only the level of power reduction but also the duration of the reduction. For instance, the power can be reduced beyond the feasible steady power consumption, as long as it is restored before the temperature of the bath decreases to the cryolite solidification point. Knowledge of the power reduction and its duration is useful to determine the total energy corresponding to the loss of production.

Data validation is crucial for ensuring that the plant is properly modelled. Input values, such as the electrical power consumption and electrical current, are extracted from the work by Jessen (2008), who took measurements from the Norðurál reduction plant in Iceland (Norðurál, 2019). The results have also been compared to the production rate from the Trimet aluminium smelter in Germany (Trimet Aluminium SE, 2019), which, according to Deign (2017), is about 13.5 MWh per tonne of produced aluminium.

3.4 Summary of the Chapter

This chapter has analysed the current uses of flexible operation in the industry. The literature showed that there is much research on flexible operation in carbon capture plants. Also, microgrids use Process Power Management (PPM) systems to control the power balance through flexible generation. Nevertheless, there is no much research regarding flexible operation of electricity-intensive processes for PPM. Thus, this thesis focuses on the assessment of the flexibility of two electricity-intensive processes, namely the liquefaction of natural gas and the aluminium smelter. The findings of this thesis might be extended to the public power grid, so industrial loads can actively participate in balancing the power in the grid.

This thesis studies flexible operation in the Liquefied Natural Gas (LNG) process to assess its range of operability examining the presence of vapour and liquid equilibrium. As suggested by

many authors, when the power consumption decreases, the LNG production rate has to decrease to adapt the process to the available power. Thus, this thesis aims to minimise the decrease of production rate by adjusting different variables in the process. The dynamic behaviour of the process is a variable to consider when studying power reduction, but as seen in the literature, the flow rate of the refrigerant varies according to the change of production rate without consequences on the process feasibility.

There are numerous articles investigating aluminium smelters as active members in the regulation of the power grid. Nevertheless, the articles studied the process from the perspective of the power system, ignoring the impacts on the process variables, observing only the power consumption of the plant. Reports regarding the process operation discussed the behaviour of the cell when it is disconnected or when it is working at a lower level of power consumption. This thesis examines the transient response of the process when the power is turned down. Even if a power reduction is not feasible in steady-state, the reduction can take place during a period as long as the power is restored before the bath temperature exceeds any limit.

Chapter 4

Methodology of the Study of Flexible Operation

This chapter discusses the methodology for studying flexible operation in the Liquefied Natural Gas (LNG) process and for the aluminium smelting process. The first section discusses the applications of flexible operation of electricity-intensive processes with a general overview of the job carried out by flexible operation, so the second subsection applies the general point of view to more specific examples, which are the two mentioned case studies.

4.1 Flexible Operation for Process Power Management

In an electrical contingency event, the available power suddenly decreases, so the PPM reduces the power consumption accordingly. To avoid shutdowns, the PPM reduces the power consumption within 200ms [1], and this change has consequences on the rest of the process variables. In steady state, the process must operate at a new operating point that is consistent with the available power. Therefore, the PPM must also send new set points to the process controllers to ensure the process operates at the new operating point.

[1] Data provided by an engineer in ABB

In order to predict the new steady state, this thesis models the processes, observing all the consequences that changing the power consumption has on all process variables. The models identify the potential variables that can be adjusted and have an impact on electrical power consumption. The study of flexible operation assesses the effects of these variables and to what extent they can be adjusted to create an envelope of feasible operation.

This thesis focuses the study on the process operation and assumes that the electrical power drops instantly. However, the action of reducing the electrical power could produce undesirable transients in the electrical system. To check that there are no electrical transient effects during a power reduction, the author received help from the ABB Sponsor. An engineer in ABB conducted an electrical simulation using a dynamic model of an electrical distribution system within a large LNG facility. He could determine the reduction in available power due to a generator trip, and also to simulate the simultaneous power reduction to the process as is proposed in this thesis. Thus, the ABB engineer showed that, during a power reduction due to the loss of a generator, there were no dangerous transient effects in the electrical system such as low voltage or frequency excursions.

Therefore, the objective of this project is to help PPM systems to operate electricity-intensive processes in a flexible manner. To that end, this thesis analyses two case studies by determining their envelope of feasible operation. This project compares both cases to draw conclusions and heuristics that can be extended to other processes.

4.2 Flexible Operation Tasks

This section discusses a general methodology for studying flexible operation in electricity-intensive processes. The methodology is later applied to the case studies in Section 4.3.

When an electrical contingency takes place, PPM operates the plant flexibly by:

- Rapidly reducing the power available to the load, as shown by the step change in the brown curve on the left side of Figure 2.7
- Looking up pre-programmed set points for the process variables and sending them to the process automation system

4.2.1 Finding the New Set Points

During the process modelling, the analysis studies the energy transformations in the process. For instance, in the LNG process, the motors attached to the compressors of the refrigeration cycles consume electrical power to transform it into mechanical power. The electrical consumption affects the flow rate of the refrigerants, which in turn affects the LNG production rate or its temperature at the exit of the process. An initial connection can be made between the electrical consumption and the production rate of the LNG. The study determines all the intermediate steps between the electrical power and the LNG characteristics.

Obtaining insights into the thermodynamic behaviour of each stream or element is necessary for determining how the different forms of power are transformed. Hence, the equations describing the energy of any element have to be as accurate as possible. For instance, for the LNG process, these equations are governed by the Redlich-Kwong Soave equations of state.

This thesis calculates the model observing the consequences that various levels of power reduction has on the process variables. The model looks for potential variables whose variation has an impact on the power consumption and does not put the process at risk. For instance, in the LNG process, increasing the LNG temperature at the exit of the process decreases the consumption of the plant keeping the same production rate, or allows the production rate to be higher with the same power consumption.

The mathematical model provides the envelope of feasible operation that relates the process variables and the electrical power consumption. The envelope would be used in the real-time PPM when an electrical contingency happens. A single value of power consumption can corre-

spond to various families of set points. The decision of choosing a group of set points depends on the preferences and needs at the given moment. For example, the LNG temperature at the exit of the process could be increased to achieve a higher production rate. The disadvantage of that strategy would be a higher risk of obtaining a vapour natural gas. This thesis defers decisions about the trade-off to the production manager.

Finding the operational points conforms an envelope of operation that the PPM can use look up set points for the variables that correspond to the available power. Figure 4.1.a) shows an example of this envelope of operation for the LNG temperature at the exit of the liquefaction. The picture shows three variables, the LNG temperature, the production rate, and the electrical power consumption. If the power is to be reduced, the production rate or the temperature have to vary. Also, for a fixed power consumption, the production rate can be increased if the temperature is increased.

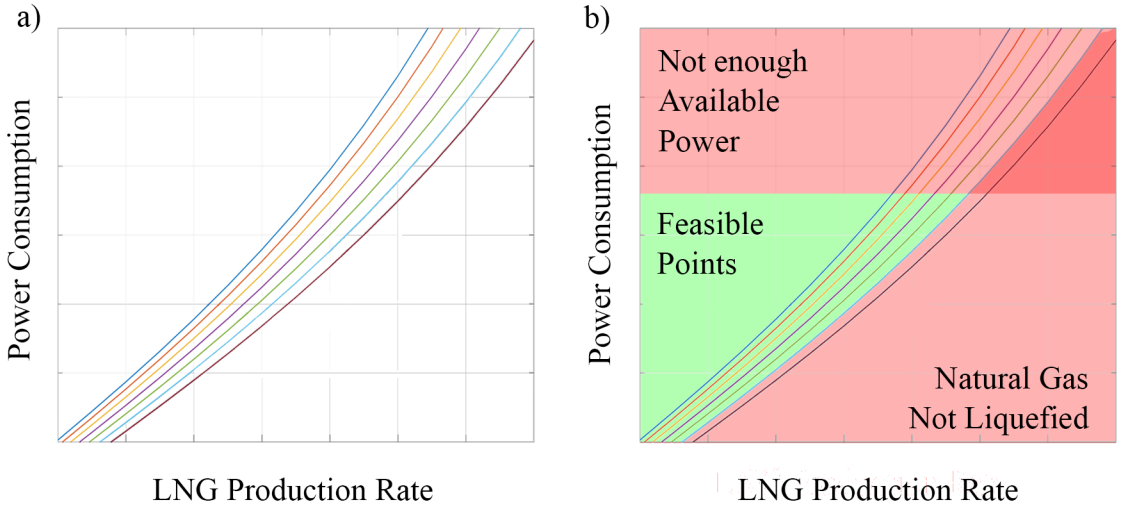


Figure 4.1: Example of the a) envelope of operation and the b) envelope of feasible operation for the LNG temperature at the exit of the process. Each curve represents a different LNG exit temperature. The envelope of feasible operation represents the areas in which the process is infeasible (red area), and the area in which the process can operate (green area).

Electrical emergencies are not scheduled, so all operations for reducing the power consumption must be preprogrammed. These decisions includes establishing the set points and operational values that correspond to the available power.

4.2.2 Assessing the Feasibility

The model must ensure that the operating point is feasible. The limits in the process are usually related to the temperature or pressure of the streams and by the operating limits of the process equipment such as compressors. In the LNG example, this can refer to the maximum temperature of the LNG at the exit of the process, or the minimum pressure delivered by the refrigerant compressors.

Figure 4.1.b) shows the envelope of feasible operation including the limits for both the electrical consumption and the upper limit of the LNG temperature, both represented by the red shaded area. The green area is the envelope of feasible operation, and it shows the points in which the process is operative.

Part II develops the envelope of feasible operation for the LNG process, and Part III develops envelopes for the aluminium smelter that account, apart from the amount of power reduction, its duration.

4.3 Flexible Operation in the Case Studies

The processes have been modelled in Matlab and Simulink Matlab (2010). The mathematical models are presented in Parts II and III, corresponding to the LNG process and the aluminium smelter respectively. This section discusses the study of flexible operation for both processes.

4.3.1 Liquefaction of Natural Gas

When the electrical power consumption decreases, the motors attached to the compressors slow down, and therefore, the flow rate or the pressure of the refrigerants decreases. The amount of heat from the natural gas absorbed by the refrigerants is a function of their pressures and flow rates, so ultimately, when the electrical power consumption varies, the LNG production rate changes as well. Therefore, the model has to include:

- How the motor speed is affected by the power consumed
- How the production rate is affected by the refrigerant characteristics
- Intermediate steps from the motor to the production rate. These include the compressors, the heat exchangers, and the valves
- Process limits
- Thermodynamic equations that determine the energy of each stream in the process
- Potential process variables with impact on the power consumption that can be varied without jeopardizing the process

The model calculates the production rate for various values of power consumption and process variables. Hence, the operating points can be determined for minimizing the necessary reduction of production rate for achieving the power consumption after reduction.

Chapter 5 shows the model of the LNG process, including the heat and mass balances of the process, the thermodynamic equations that explain the behaviour of the streams, and the limits of the process. Chapter 5.6 explains the assumptions taken for solving the model.

4.3.2 Aluminium Smelter

In the aluminium smelter, the production rate of aluminium is proportional to the electrical current. The electrical current controls the electrical power consumption, so both electrical power consumption and production rate are related directly to the electrical current.

Nevertheless, the properties of the bath, such as the concentration of the components, or the bath temperature, have effects on the relationship between electric current and power consumption. Additionally, the electrical current and the properties of the bath affect the voltage between the electrodes of the smelter. Similarly, the same variables affect the relationship between the electrical current and the aluminium production rate.

Figure 4.2 shows a scheme of the model of the whole process. The model is divided into three submodels, the electrical model, the mass balance, and the heat balance. Each sub-model sends and receives information from the other sub-models. Therefore, the whole model has to include:

- The relationship between power consumption and electrical current
- The relationship between electrical current and the aluminium production rate
- The relationship between voltage drop and bath properties
- Process limits
- Thermodynamic equations of each component and reaction. These can be determined by empirical tables found in the literature. (Chase, 1998; Perry and Green, 2008)
- Heat transfer equations. These include equations of conduction and convection, and the cell heat parameters can be found in Incropera et al. (2011)
- Potential process variables with impact on the power consumption that can be varied without jeopardizing the process

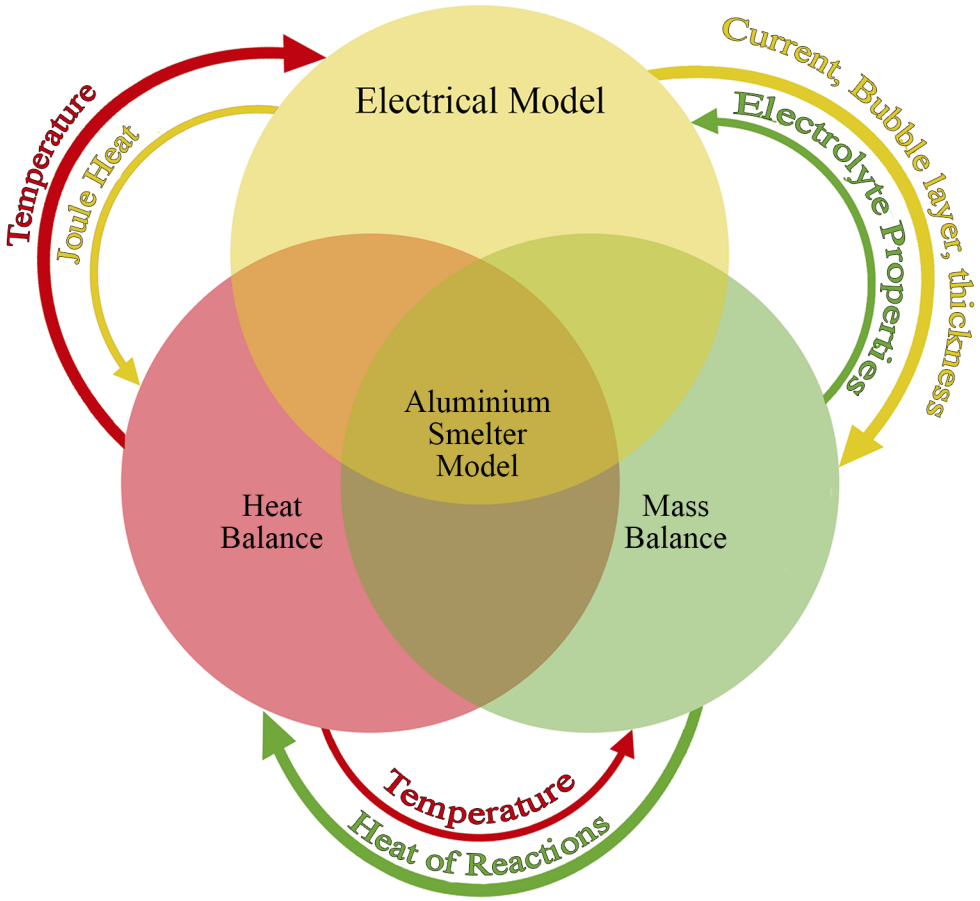


Figure 4.2: Aluminium smelter model. Each circle represents a sub-model providing to and receiving inputs from the others.

Chapter 9 presents the mathematical model of the aluminium smelter, including the three sub-models, and the assumption made for modelling the process. It is desirable to know for how long the power reduction is feasible without violating any limit, so this study models the dynamic behaviour of the smelter.

Steady State and Transient State

When the electrical power is reduced, the electrical current and the heat generated due to the Joule heating effect decrease. Consequently, the temperature of the bath starts decreasing, and

the cooling rate depends on the magnitude of the power reduced, the heat transfer properties of the cell, and the characteristics of the bath. The power consumption must return to its former state before the temperature of the bath reaches the cryolite solidification temperature. Therefore, the simulations will determine the lapse of time between the power contingency and the cryolite solidification.

Thus, the model is solved in two ways. The steady state values are determined from calculating the model for various values of production rate, bath temperature, bath ratio, and power consumption. For determining the transient behaviour, the model runs the simulations changing the level of power reduction and its duration to determine for how long the cell can withstand each level of power reduction.

4.4 Summary of the Chapter

This chapter has discussed the reasons for studying flexible operation in electricity-intensive processes, and the methodology for studying it, first from a general perspective, and then for the case studies.

The aim of the project is to help Process Power Management (PPM) systems to operate electricity-intensive processes flexibly by determining an envelope of feasible operation that relates the process variables with the available power. During an electrical contingency, the PPM reduces the power consumption of the process according to the available power. The PPM also can use the envelope of feasible operation to send the set points consistent with the available power. The PPM sends the signals immediately after knowing the available power to avoid significant power imbalances during the transient response.

This study divided the methodology into two parts, one for finding the set points corresponding to the available power, and the second one for assessing the feasibility of the set point. The model finds the relationship to form an envelope of operation, which, along with the process limits, provides the envelope of feasible operation.

Part II

Flexible Operation in Liquefaction of Natural Gas

Chapter 5

Modelling of the LNG Process

This chapter discusses the steady state heat and mass balances in the Liquefied Natural Gas (LNG) process and the thermodynamic principles for obtaining the enthalpies of each stream necessary to perform the heat balance. The Equation of State (EoS) used is the Redlich-Kwong Soave (RKS), and the algorithm for obtaining the vapour fraction is the Rachford-Rice (RR) algorithm (Section 2.4.1).

5.1 Heat and Mass Balances

Determining the enthalpies is essential for ensuring that the temperature in NG6 is below its saturation point, so the natural gas exits as a liquid. Thus, the model carries out an heat balance to ensure that NG6 is at an adequate temperature. The variables names in the following equations are referred to Figure 5.1. The balances consider assumptions and fixed variables that are presented in Chapter 5.6.

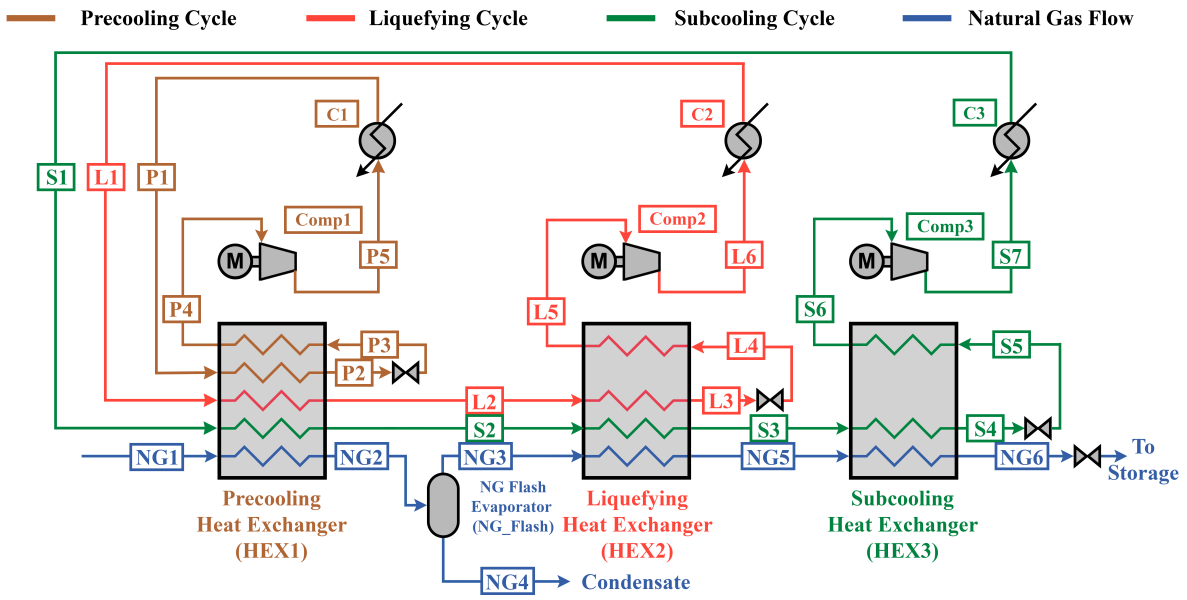


Figure 5.1: Liquefied Natural Gas process. The picture is a representation of the process introduced in the patent by Stockmann et al. (2001), and it is based on the MFC process by Linde (Linde AG, 2018).

5.1.1 Overall Heat Balance

The heat balance of the whole process accounts for all the heats entering and leaving the process. Figure 5.1 shows the Liquefied Natural Gas (LNG) process that this project has modelled. Figure 5.1 shows that the process receives heat from the fed natural gas and the compressors consuming electrical power, and the heat comes out of the process in the form of the natural gas leaving the process, the heat released by the refrigerants to the sea, and the losses in the compressors.

$$H_{\text{In}} = H_{\text{Out}}$$

$$H_{\text{NG1}} + W_{\text{Prec}} + W_{\text{Liq}} + W_{\text{Sub}} = H_{\text{NG4}} + H_{\text{NG6}} + (H_{\text{P5}} - H_{\text{P1}}) + W_{\text{Loss,Prec}} + \tag{5.1}$$

$$(H_{L6} - H_{L1}) + W_{\text{Loss,Liq}} + (H_{S7} - H_{S1}) + W_{\text{Loss,Sub}}$$

where H_x is the total enthalpy of stream x in kW, W_{Prec}, W_{Liq}, W_{Sub} are, respectively, the power consumed by the compressor in the precooling, liquefying, and subcooling refrigerant cycles in kW , and $W_{\text{Loss,Prec}}$, $W_{\text{Loss,Liq}}$,$W_{\text{Loss,Sub}}$ are the power losses in the compressor of the respective

cycles in kW. In the equation, $H_{P5} - H_{P1}$, $H_{L6} - H_{L1}$, and $H_{S7} - H_{S1}$ are the heat released to the sea in the sea coolers C1, C2, and C3 respectively. Eq. 5.1 then can be written as:

$$W_{\text{Total}} = H_{\text{NG4}} + H_{\text{NG6}} - H_{\text{NG1}} + H_{\text{Sea}} + W_{\text{Loss}_{\text{Total}}} \quad \text{kW} \tag{5.2}$$

where W_{Total} and $W_{\text{Loss}_{\text{Total}}}$ are, respectively, the total power consumption and the total losses of the compressors in kW, and H_{Sea} is the total heat released to the sea in kW:

$$W_{\text{Total}} = W_{\text{Prec}} + W_{\text{Liq}} + W_{\text{Sub}}$$

$$W_{\text{Loss,Total}} = W_{\text{Loss,Prec}} + W_{\text{Loss,Liq}} + W_{\text{Loss,Sub}}$$

$$H_{\text{Sea}} = (H_{\text{P5}} - H_{\text{P1}}) + (H_{\text{L6}} - H_{\text{L1}}) + (H_{\text{S7}} - H_{\text{S1}})$$

The thermodynamic properties are expressed in their extensive form. In their specific form, they are expressed as $w = \frac{W}{F}$ and $h = \frac{H}{F}$, where w is the specific energy consumed by a compressor in kJ kmol^{-1}, h is the specific enthalpy in kJ kmol^{-1}, and F is the flow rate in kmol s^{-1}.

The vapour flow rate after the flash drum (NG_Flash in Figure 5.1) is the same as the LNG production rate of LNG production, and considering that $F_{\text{NG3}} = \psi F_{\text{NG1}}$ and $F_{\text{NG4}} = (1-\psi)F_{\text{NG1}}$, Eq. 5.2 can be rearranged as:

$$\begin{gathered} W_{\text{Total}} = F_{\text{NG1}}((1 - \psi_{\text{NG2}}\, h_{\text{NG4}} + \psi_{\text{NG2}} h_{\text{NG6}} - h_{\text{NG1}}) + \\ F_{\text{Prec}}(h_{\text{P5}} - h_{\text{P1}}) + F_{\text{Liq}}\,(h_{\text{L6}} - h_{\text{L1}}) + F_{\text{Sub}}\,(h_{\text{S7}} - h_{\text{S1}}) + W_{\text{Loss,Total}} \end{gathered} \tag{5.3}$$

where ψ_x is the vapour fraction in stream x, and F_{Prec}, F_{Liq}, and F_{Sub}, are the flow rates of the refrigerants in kmol s^{-1}. From Eq. 5.3, the model has to solve four flow rates. Enthalpies and vapour fractions are calculated providing the temperature, pressure, and composition of the stream. The feed flow rate of natural gas (F_{NG1}) is fixed, so there are three remaining unknown flow rates. The model performs a heat balance to each heat exchanger (HEX1, HEX2, and HEX3) for obtaining the unknown flow rates.

5.1.2 Heat Balance in the Precooling Heat Exchanger (HEX1)

The heat balance in the precooling heat exchangers relates the heat entering and leaving HEX1 (Figure 5.1) to determine the necessary flow rate of the precooling refrigerant.

$$H_{\mathrm{NG1}} + H_{\mathrm{S1}} + H_{\mathrm{L1}} + H_{\mathrm{P1}} + H_{\mathrm{P3}} = H_{\mathrm{NG2}} + H_{\mathrm{S2}} + H_{\mathrm{L2}} + H_{\mathrm{P2}} + H_{\mathrm{P4}}$$

The valves in the process are isenthalpic, so H_{P2} has the same value as H_{P3}.

$$\begin{aligned} F_{\mathrm{Prec}}(h_{\mathrm{P1}} - h_{\mathrm{P4}}) &= F_{\mathrm{NG1}}(h_{\mathrm{NG2}} - h_{\mathrm{NG1}}) + F_{\mathrm{Sub}}(h_{\mathrm{S2}} - h_{\mathrm{S1}}) + F_{\mathrm{Liq}}(h_{\mathrm{L2}} - h_{\mathrm{L1}}) \\ F_{\mathrm{Prec}} &= \frac{F_{\mathrm{NG1}}(h_{\mathrm{NG2}} - h_{\mathrm{NG1}}) + F_{Sub}(h_{\mathrm{S2}} - h_{\mathrm{S1}}) + F_{\mathrm{Liq}}(h_{\mathrm{L2}} - h_{\mathrm{L1}})}{h_{\mathrm{P1}} - h_{\mathrm{P4}}} \end{aligned} \tag{5.4}$$

5.1.3 Heat Balance in the Liquefying Heat Exchanger (HEX2)

The heat balance in the liquefying heat exchangers (HEX2) determines the necessary flow rate of the liquefying refrigerant.

$$H_{\mathrm{NG5}} + H_{\mathrm{S2}} + H_{\mathrm{L2}} + H_{\mathrm{L4}} = H_{\mathrm{NG3}} + H_{\mathrm{S3}} + H_{\mathrm{L3}} + H_{\mathrm{L5}}$$

The flow rate of the natural gas after the flash drum (NG_ Flash in Figure 5.1) is the vapour generated after the separating the condensate. Therefore, the flow rate at these streams is $\psi_{\mathrm{NG2}}\, F_{\mathrm{NG1}}$, where ψ_{NG2} is the vapour fraction in the flash drum. The valve (V2) is isenthalpic, so $H_{\mathrm{L3}} = H_{\mathrm{L4}}$.

$$\begin{aligned} F_{\mathrm{Liq}}(h_{\mathrm{L2}} - h_{\mathrm{L5}}) &= \psi_{\mathrm{NG2}}\, F_{\mathrm{NG1}}(h_{\mathrm{NG5}} - h_{\mathrm{NG3}}) + F_{\mathrm{Sub}}(h_{\mathrm{S3}} - h_{\mathrm{S2}}) \\ F_{\mathrm{Liq}} &= \frac{\psi_{\mathrm{NG2}}\, F_{\mathrm{NG1}}(h_{\mathrm{NG5}} - h_{\mathrm{NG3}}) + F_{\mathrm{Sub}}(h_{\mathrm{S3}} - h_{\mathrm{S2}})}{h_{\mathrm{L2}} - h_{\mathrm{L5}}} \end{aligned} \tag{5.5}$$

5.1.4 Heat balance in the Subcooling Heat Exchanger (HEX3)

The heat balance in the subcooling heat exchangers (HEX2) determines the necessary flow rate of the subcooling refrigerant.

$$H_{NG5} + H_{S3} + H_{S5} = H_{NG6} + H_{S4} + H_{S6}$$

H_{S4} and H_{S5} have the same value.

$$\begin{gathered} H_{NG5} + H_{S3} = H_{NG6} + H_{S6} \rightarrow F_{Sub}(h_{S3} - h_{S6}) = \psi_{NG2} F_{NG1}(h_{NG6} - h_{NG5}) \\ F_{Sub} = \frac{\psi_{NG2} F_{NG1}(h_{NG6} - h_{NG5})}{h_{S3} - h_{S6}} \end{gathered} \tag{5.6}$$

Eqs. 5.4-5.6 are functions of the enthalpies of the streams. The model uses the Redlich-Kwong Soave equation and the Rachford-Rice algorithm to determine the value of these enthalpies.

5.2 Redlich-Kwong Soave Equation of State

The Redlich-Kwong Soave (RKS) equation needs the three parameters that are characteristic of each component, namely critical temperature (T_c), critical pressure (P_c), and acentric factor (ω). The RKS main equation is:

$$P = \frac{RT}{V_m - b} - \frac{a\alpha}{V_m(V_m + b)} \tag{5.7}$$

where P is the pressure in Pa, V_m is the molar volume in $m^3 mol^{-1}$, T is the temperature in K, R is the ideal gas constant, whose value is 8.314 J $mol^{-1}K^{-1}$. a, b, and α are parameters

characteristic of the RKS equation:

$$\begin{aligned} a &= 0.427\frac{(RT_c)^2}{P_c} \\ b &= 0.0866\frac{RT_c}{P_c} \\ \alpha &= \left(1+s\left(1-\sqrt{\frac{T}{T_c}}\right)\right)^2 \end{aligned} \tag{5.8}$$

where T_c is the critical temperature in K, P_c is the critical pressure in Pa, and s is:

$$s = (0.48508 + 1.552\omega - 0.15613\omega^2) \tag{5.9}$$

where ω is the acentric factor (dimensionless). The variables a and α can appear as a single parameter. The RKS EoS can be written in a cubic form by rearranging the a and b terms:

$$\begin{aligned} A &= \frac{a\alpha P}{R^2T^2} \\ B &= \frac{bP}{RT} \end{aligned} \tag{5.10}$$

and considering the compressibility factor:

$$Z = \frac{PV_m}{RT} \tag{5.11}$$

where Z is the compressibility factor (dimensionless). Combining Eqs. 5.7, 5.10, and 5.11, the cubic form of the RKS results in:

$$Z^3 - Z^2 + Z(A - B - B^2) - AB = 0 \tag{5.12}$$

The introduced equations are the main equations for the RKS, but when a mixture is modelled, the EoS has to implement mixing rules.

5.2.1 RKS for Mixtures

The mixing rules for the RKS EoS consider not only the molar fraction of each component, but also the interaction amongst components. The mixing rules are governed by the following equations:

$$\begin{aligned} \hat{a} &= \sum_{i}^{C}\sum_{j}^{C} y_i y_j a_{ij} \\ a_{ij} &= \sqrt{a_i a_j} \\ \hat{a\alpha} &= \sum_{i}^{C}\sum_{j}^{C} y_i y_j (a\alpha)_{ij} \\ \hat{b} &= \sum_{i}^{C} y_i b_i \end{aligned} \tag{5.13}$$

where C is the number of components in the mixture. The $\hat{}$ indicates that the variable corresponds to the mixture. $(a\alpha)_{ij}$ is:

$$(a\alpha)_{ij} = (1 - k_{ij})\sqrt{(a\alpha)_i (a\alpha)_j} \tag{5.14}$$

where y_i is the molar fraction of component i, $(a\alpha)_i$ is the $a\alpha$ term for component i, and k_{ij} is the binary interaction parameter for components i and j with $k_{ij} = k_{ji}$, and $k_{ii} = k_{jj} = 0$. Eqs. 5.13 and 5.14 can be used in the RKS equations by substituting their respective variables.

5.2.2 RKS for Enthalpy and Entropy Calculations

To model real fluids, the calculations use the departure function of the fluid. The departure function of a thermodynamic property is defined as the difference between the value of the property of ideal gas and the value of the same property in a real gas:

$$func^{\mathrm{Dep}} = func - func^{\mathrm{IG}}$$

where $func$ is the thermodynamic property function, $func^{\mathrm{Dep}}$ is the departure function of the thermodynamic property, and $func^{\mathrm{IG}}$ is thermodynamic property function if the fluid is treated as an ideal gas. The general expression for the enthalpy is:

$$h^{\mathrm{Dep}} = RT(Z-1) + \int_{\infty}^{V_m} \left(T \left(\frac{\partial P}{\partial T} \right)_v - P \right) dv \tag{5.15}$$

h^{Dep} is the specific departure enthalpy in J mol^{-1}. Applying the properties of the partial derivatives to the RKS EoS, the enthalpy results in:

$$\begin{gathered} h^{\mathrm{Dep}} = PV - RT - \left(\frac{a\alpha - T\frac{\partial(a\alpha)}{\partial T}}{b} \right) \ln\left(\frac{V_m + b}{V_m} \right) \\ \frac{\partial a\alpha}{\partial T} = \sum_i^C \sum_j^C y_i y_j (1-k_{ij}) \sqrt{a_i a_j} \\ \left(-\frac{s_i}{2T_{c,i}T_{r,i}^{0.5}} - \frac{s_j}{2T_{c,j}T_{r,j}^{0.5}} + s_i s_j \left(\frac{T_{r,j}^{0.5}-1}{2T_{c,i}T_{r,i}^{0.5}} + \frac{T_{r,i}^{0.5}-1}{2T_{c,j}T_{r,j}^{0.5}} \right) \right) \end{gathered} \tag{5.16}$$

where T_r is the reduced temperature and it is equal to T/T_c.

For the entropy, the departure function is:

$$\begin{aligned} s^{\mathrm{Dep}} &= -R \ln\left(\frac{RT}{V_m} \right) - \int_{\infty}^{V_m} \left(\frac{R}{v} - \left(\frac{\partial P}{\partial T} \right)_{V_m} \right) dv \\ s^{\mathrm{Dep}} &= R \ln\left(\frac{P(V_m - b)}{RT} \right) + \frac{1}{b} \frac{\partial a\alpha}{\partial T} \ln\left(\frac{V_m + b}{V_m} \right) \end{aligned} \tag{5.17}$$

s^{Dep} is the specific departure enthalpy in J K^{-1}mol^{-1}.

The ideal enthalpy and entropy can be calculated as if the fluid is treated as an ideal gas. The ideal gas properties have to consider the mixture properties as well. The enthalpy of mixing is non-existent (Nieto, 2015; Poling, 2007), so the enthalpy of an ideal gas is:

$$h^{\mathrm{IG}}(T) = \int_{T_0}^{T} c_p(\theta) d\theta \tag{5.18}$$

where h^{IG} is the specific enthalpy for an ideal gas in kJ kmol^{-1}, T_0 is a reference temperature in K, and $c_p(T)$ is the specific heat capacity of the fluid in kJ kmol^{-1}K^{-1} at temperature T. The heat capacity is obtained as a function of the temperature as:

$$\begin{gathered} c_{p,i}(T) = c_{p,i}^{\mathrm{A}} + c_{p,i}^{\mathrm{B}} T + c_{p,i}^{\mathrm{C}} \frac{T^2}{2} + c_{p,i}^{\mathrm{D}} \frac{T^3}{3} + c_{p,i}^{\mathrm{E}} \frac{T^4}{4} + c_{p,i}^{\mathrm{F}} \frac{T^5}{5} \\ \hat{c_p}(T) = \sum_i^C y_i c_{p,i}(T) \end{gathered} \tag{5.19}$$

where $c_{p,i}(T)$ is specific heat capacity in kJ kmol^{-1}K^{-1} of component i at temperature T, and $c_{p,i}^x$ are parameters characteristic to component i, and that can be found in the literature (Chase, 1998). In this case, due to the range of low temperatures, these parameters are difficult to find, so they are extracted from the Aspen database (AspenTech, 2001a), which gathers several physical properties databanks, and, other values have to be estimated with the Aspen physical properties methods (AspenTech, 2001b). The value of the thermodynamic parameters can be found in Appendix A.

Thus, the specific enthalpy of a fluid can be calculated as:

$$h = h^{\mathrm{Dep}} + h^{\mathrm{IG}} = PV - RT - \left(\frac{a\alpha - T \frac{\partial (a\alpha)}{\partial T}}{b} \right) \ln \left(\frac{V_m + b}{V_m} \right) + \int_{T_0}^{T} c_p(\theta) d\theta \tag{5.20}$$

Regarding the entropy, its ideal gas value does have a mixing term:

$$s^{\mathrm{mix}} = -R \left(\sum_i^C y_i \ln(y_i) \right) \tag{5.21}$$

where s^{mix} is the specific entropy of mixing in kJ kmol^{-1}K^{-1}. The specific entropy of an ideal gas can be written as:

$$s^{\mathrm{IG}}(T) = \int_{T_0}^{T} \frac{c_p(\theta)}{\theta} d\theta - \int_{P_1}^{P_2} \frac{R}{p} dp \tag{5.22}$$

where s^{IG} is the specific entropy of an ideal gas in J mol^{-1}K^{-1}, P_1 is the initial pressure in Pa, and P_2 is the final pressure in Pa. Therefore, the specific entropy of the fluid can be calculated as:

$$s = s^{\mathrm{Dep}} + s^{\mathrm{IG}} + s^{\mathrm{mix}} = R \ln\left(\frac{P(V_m - b)}{RT}\right) + \frac{1}{b}\frac{\partial a\alpha}{\partial T}\ln\left(\frac{V_m + b}{V_m}\right) + \int_{T_0}^{T} \frac{c_p(\theta)}{\theta} dT - \int_{P_1}^{P_2} \frac{R}{p} dp - R\left(\sum_{i}^{C} y_i \ln(y_i)\right) \tag{5.23}$$

5.3 Vapour and Liquid Equilibrium

If the stream presents just one phase, the model uses Eqs. 5.20 and 5.23. However, if the stream presents two phases, the model has to consider two additional terms, namely the vapour fraction, and the molar fractions in each phase. Both terms need the value of the vaporization equilibrium ratio for each component:

$$K_i = \frac{y_i}{x_i} \tag{5.24}$$

where K_i is the vaporization equilibrium ratio for component i, y_i is the molar fraction of component i in the vapour, and x_i is the molar fraction of components i in the liquid. To solve it, the model needs to find the fugacity of each phase. Fugacity measures the tendency of component i to escape from one phase to another. When there is an equilibrium fugacities reach an equality between their phases.

$$f_i^{\mathrm{V}} = f_i^{\mathrm{L}} \tag{5.25}$$

where f_i^{V} and f_i^{L} are the fugacities of component i in the vapour and in the liquid respectively with dimensions of pressure. Fugacities are calculated differently depending on the phase. For

the vapour phase:

$$f_i^V = y_i \phi_i^{\mathrm{V}} P \tag{5.26}$$

where ϕ_i^{V} is the fugacity coefficient of component i in the vapour phase. The fugacity coefficient is the ratio between the fugacity and the pressure in the system. The general equation for the fugacity coefficient is:

$$\ln\phi^{\mathrm{V}} = \int_0^P \left(\frac{V_m}{RT} - \frac{1}{p}\right) dp \tag{5.27}$$

and for the RKS EoS:

$$\begin{aligned} \ln(\phi_i^{\mathrm{V}}) = \frac{b_i}{\hat{b}}(Z-1) - \ln\left[Z\left(1-\frac{\hat{b}}{V_m}\right)\right] + \\ \frac{a\hat{\alpha}}{\hat{b}RT}\left[\frac{b_i}{\hat{b}} - \frac{2}{a\hat{\alpha}}\sum_j^C y_j(a\alpha)_{ij}\right]\ln\left(a+\frac{\hat{b}}{V_m}\right) \end{aligned} \tag{5.28}$$

The terms in Eq. 5.26 can now be solved. The fugacity term for the liquid phase is:

$$f_i^{\mathrm{L}} = x_i \gamma_i P_i^{\mathrm{sat}} \phi_i^{\mathrm{sat}} \exp\left[\frac{V_m(P - P_i^{\mathrm{sat}})}{RT}\right] \tag{5.29}$$

where γ_i is the activity coefficient (dimensionless) for component i, and measures the deviation from the ideal behaviour of a mixture, P_i^{sat} is the vapour pressure in Pa of component i, and ϕ_i^{sat} is the fugacity coefficient of i at the saturation point.

The excess Gibbs energy is used to derive γ:

$$\frac{g^E}{RT} = \sum_i^C x_i \ln(\gamma_i) \tag{5.30}$$

The Gibbs equation can be solved using the Wilson model:

$$\frac{g^E}{RT} = -\sum_i^C x_i \ln\left(\sum_j^C x_j \Lambda_{ij}\right) \tag{5.31}$$

where Λ_{ij} is the Wilson interaction parameter between i and j [1]; these parameters are extracted from Aspen, which gives the coefficients W_{ij}^{A}, W_{ij}^{B}, W_{ij}^{C}, W_{ij}^{D}, W_{ij}^{E} for the following equation:

$$\ln(\Lambda_{ij}) = W_{ij}^{\mathrm{A}} + \frac{W_{ij}^{\mathrm{B}}}{T} + W_{ij}^{\mathrm{C}} \ln(T) + W_{ij}^{\mathrm{D}} T + \frac{W_{ij}^{\mathrm{E}}}{T^2} \tag{5.32}$$

The equation can be truncated to the two first terms. The values for W_{ij}^{A} and W_{ij}^{B} can be found in Appendix A. Combining Eqs. 5.30 and 5.31, γ_i is calculated as:

$$\gamma_i^{\mathrm{L}} = -x_i \left(\sum_j^C x_j \Lambda_{ij}\right) + 1 - \sum_{k=1}^C \frac{x_k \Lambda_{ki}}{\sum_{j=1}^C x_j \Lambda_{kj}} \tag{5.33}$$

P_i^{sat} is calculated with parameters characteristic of each component:

$$\begin{gathered} \ln(P_i^{\mathrm{sat}}(T)) = f^{(0)}(T) + \omega f^{(1)}(T_r) \\ f^{(0)}(T) = 5.92714 - \frac{6.09648}{T_r} - 1.28862 \ln(T_r) + 0.169347 T_r^6 \\ f^{(1)}(T) = 15.2518 - \frac{15.6875}{T_r} - 13.4721 \ln(T_r) + 0.43577 T_r^6 \end{gathered} \tag{5.34}$$

Some terms in Eq. 5.29 are grouped together as:

$$\Pi_i = \exp\left[\frac{V_m(P - P_i^{\mathrm{sat}})}{RT}\right] \tag{5.35}$$

where Π_i is defined as the Poynting factor (dimensionless), and it is usually close to 1, unless the pressure is very high.

[1] Λ_{ij} is not equal to Λ_{ji}, and $\Lambda_{ii} = 0$.

Eqs. 5.25, 5.26, and 5.29 are rearranged as:

$$\begin{aligned} f^{\mathrm{V}} = f^{\mathrm{L}} \rightarrow y_i \phi_i^{\mathrm{V}} P = x_i \gamma_i P_i^{\mathrm{sat}} \phi_i^{\mathrm{sat}} \Pi_i \\ \frac{y_i}{x_i} = K_i = \frac{\gamma_i P_i^{\mathrm{sat}} \phi_i^{\mathrm{sat}} \Pi_i}{\phi_i^{\mathrm{V}} P} \end{aligned} \tag{5.36}$$

This equation calculates the molar fraction at each phase, the vapour fraction of the stream and the saturation points.

5.3.1 Rachford-Rice Algorithm

K_i is used for calculating relevant variables in a VLE through the Rachford-Rice algorithm. The Rachford-Rice (RR) algorithm calculates the vapour fractions, the composition of each phase, and the saturation points in a VLE using the K_i calculated with the RKS equations.

The RR algorithm is a series of steps that, given the temperature, pressure and composition of a stream:

1. Calculates the saturation points of the stream (bubble and dew points).
2. Defines, according to the given temperature, whether the stream consists of a liquid, a vapour, or a VLE
3. If there is a VLE, calculates the vapour fraction and the composition of each phase in the stream.

For deriving the algorithm, the mass balance of a flash drum is performed:

$$F z_i = V y_i + L x_i$$

$$F z_i = V(K_i x_i) + L x_i \rightarrow x_i = \frac{F z_i}{V K_i + L}$$

where F is the feed flow rate in mol s^{-1}, z_i is the molar fraction of component i in the feed, V is the vapour flow rate in mol s^{-1}, and L is the liquid flow rate in mol s^{-1}. Dividing both parts of the fraction by F, and noting that $F = V + L$

$$x_i = \frac{z_i}{\frac{VK_i}{F} + \frac{F-V}{F}}$$

$$x_i = \frac{z_i}{1 + \frac{V}{F}(K_i - 1)}$$

Considering that $\sum_i^C (y_i - x_i) = 0$, and that $\frac{V}{F} = \psi$, the former equation can be written as:

$$\sum_i^C \frac{z_i(K_i - 1)}{1 + \psi(K_i - 1)} = 0 \tag{5.37}$$

Eq. 5.37 is the RR flash equation, and it is solved by iterative methods. This algorithm is used when the temperature is between the two saturation points, otherwise, the value of ψ is less than 0 if the temperature its below the bubble point, or above 1, if the temperature is above the dew point. Thus, the model first calculates the saturation points.

5.3.2 Bubble Point and Dew Point Calculations

This subsection explains the algorithm for calculating the saturation points of a stream. The bubble point is, for a given pressure, the temperature at which the liquid starts vaporising. Thus, at the bubble point, the vapour fraction is zero: $\psi = 0$. From Eq. 5.37:

$$\sum_i^C z_i(K_i - 1) = 0$$

Even though at the bubble point there is no vapour, the algorithm assumes that there is a small amount of vapour so that it can calculate the vaporization equilibrium ratio at this temperature. Thus, the composition in the liquid at the bubble point can be assumed to be the same as the overall composition ($x_i = z_i$). The model assumes a bubble temperature and calculates K_i, and

consequently, it can calculate y_i ($= K_i\ x_i$). The sum of the molar fractions in the vapour is 1, otherwise, the assumed temperature is not the bubble point:

$$\sum_{i}^{C} y_i^{\text{Bub}}\ (T^{\text{Bub}}) = \begin{cases} =1 & \begin{array}{l}\text{The assumed temperature}\\ \text{is the bubble temperature}\end{array} \\ >1 & \begin{array}{l}\text{The assumed temperature}\\ \text{is higher than the bubble temperature}\end{array} \\ <1 & \begin{array}{l}\text{The assumed temperature}\\ \text{is lower than the bubble temperature}\end{array} \end{cases} \tag{5.38}$$

where T^{Bub} is the bubble temperature, and y_i^{Bub} is the molar fraction of the component i at the bubble point.

K_i depends on ϕ_i^{V} (Eq. 5.36), which is a function of the RKS coefficients $a\alpha$ and b (Eq. 5.28), which are also functions of y_i (Eq. 5.13). Thus, the analyst has to assume an initial value of y_i to calculate K_i.

Applying the iteration in Eq. 5.38 results in a new value for y_i and T_{Bub}. Because the calculated T_{Bub} has used the assumed value of y_i, the calculations requires an iteration using the new value of y_i. Therefore, the bubble point calculation consists of an iteration inside another iteration. The procedure is repeated until convergence of the calculation. Figure 5.2 shows the procedure for determining the bubble point.

The dew point is the temperature at which, for a given pressure, the vapour starts condensing. At that temperature $\psi = 1$, and the vapour composition is equal to the overall composition

($y_i = z_i$), so Eq. 5.37 becomes:

$$\sum_{i}^{C} \left(\frac{y_i}{K_i} \right) - 1 = 0$$

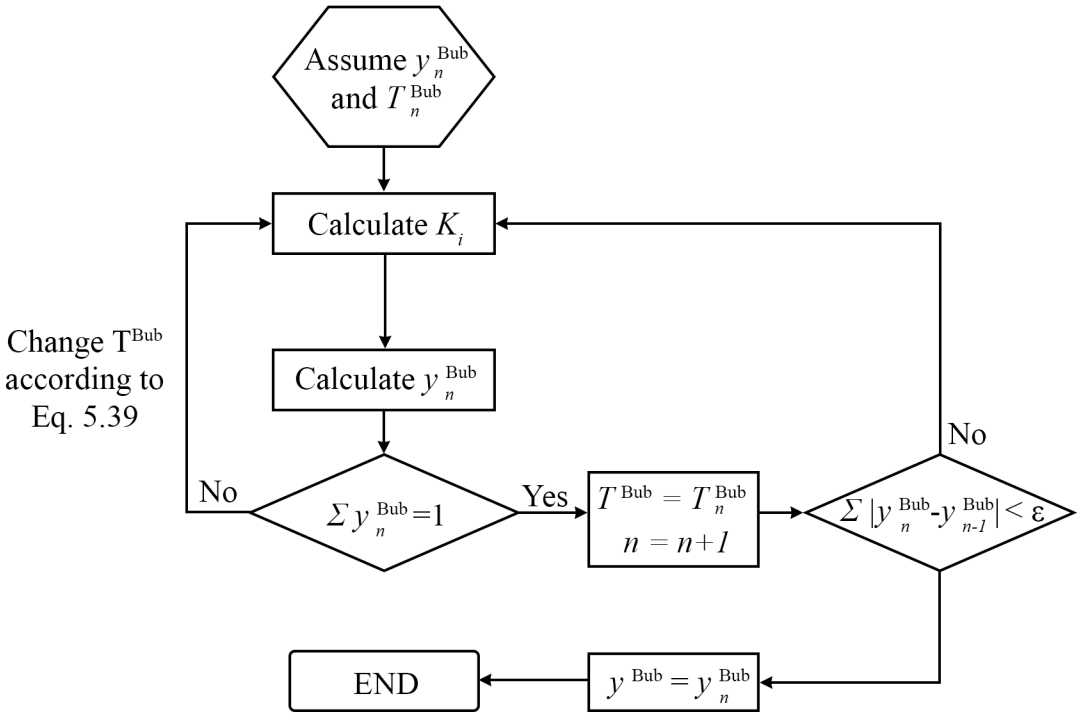


Figure 5.2: Flow diagram for determining the bubble point.

The procedure is the same as for the bubble point, but Eq. 5.38 becomes Eq. 5.39:

$$\sum_{i}^{C} x_i^{\text{Dew}}\,(T^{\text{Dew}}) = \begin{cases} = 1 & \text{The assumed temperature is the bubble temperature} \\ > 1 & \text{The assumed temperature is lower than the bubble temperature} \\ < 1 & \text{The assumed temperature is higher than the bubble temperature} \end{cases} \tag{5.39}$$

Using the RKS EoS and the vapour fraction, the model obtains the total enthalpy and entropy of a stream:

$$\begin{aligned} h &= h^{\text{V}}\psi + h^{\text{L}}(1-\psi) \\ s &= s^{\text{V}}\psi + s^{\text{L}}(1-\psi) \end{aligned} \tag{5.40}$$

where h^{V} and h^{L} are the specific enthalpies of the vapour and liquid phases respectively in kJ kmol^{-1}, and s^{V} and s^{L} are the specific entropies of the vapour and liquid phases respectively in kJ kmol^{-1} K^{-1}. To calculate the extensive forms of the enthalpy and the entropy, they have to be multiplied by the flow rate of the stream:

$$\begin{aligned} H &= F(h^{\text{V}}\psi + h^{\text{L}}(1-\psi)) \\ S &= F(s^{\text{V}}\psi + s^{\text{L}}(1-\psi)) \end{aligned} \tag{5.41}$$

Figure 5.3 shows a flow diagram for solving the RR algorithm

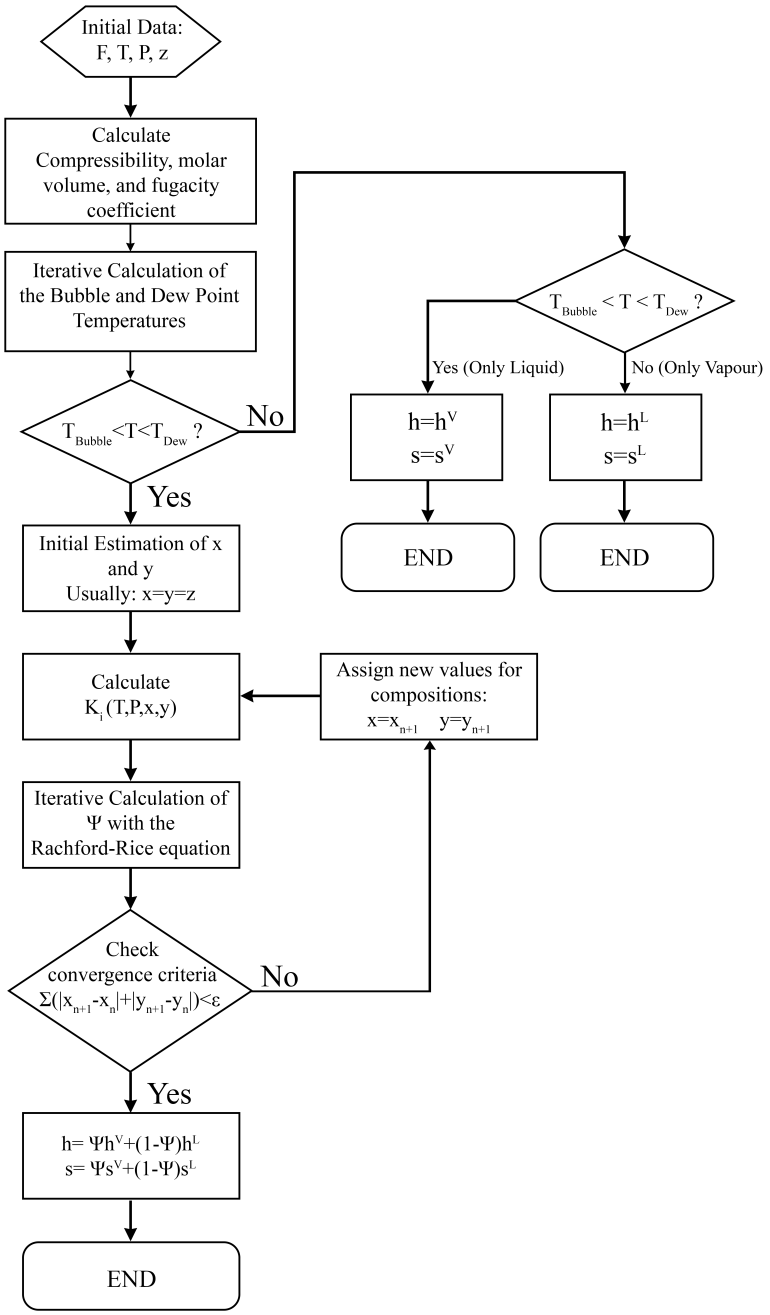


Figure 5.3: RR algorithm for calculating the specific enthalpy, specific entropy, vapour fraction, and vapour and liquid composition in a stream that might present a VLE.

5.4 Power Consumption of the Plant

The consumption of the plant is assumed to come solely from the electrical power consumption of the three motors attached to the compressors used in the refrigeration cycles.

$$W_{\text{Total}} = W_{\text{Prec}} + W_{\text{Liq}} + W_{\text{Sub}} = F_{\text{Prec}}\, w_{\text{Prec}} + F_{\text{Liq}}\, w_{\text{Liq}} + F_{\text{Sub}}\, w_{\text{Sub}}$$

5.4.1 Power Consumption of the Compressors

The consumptions of the compressors are calculated as the difference of enthalpies of the discharge and the suction streams. The model considers that the only efficiency that affects the discharge stream is the isentropic efficiency, which is explained in the next section. Thus, referring to Figure 5.1:

$$\begin{aligned} W_{\text{Total}} = {} & \psi_{\text{P4}}\, F_{\text{Prec}}\, (h_{\text{P5}} - h_{\text{P4}}) + \\ & \psi_{\text{L5}}\, F_{\text{Liq}}\, (h_{\text{L6}} - h_{\text{L5}})\ \psi_{\text{S6}}\, F_{\text{Sub}}\, (h_{\text{S7}} - h_{\text{S6}}) \end{aligned} \tag{5.42}$$

The analyst gives values to the temperature, pressure, and composition to calculate the specific enthalpy of each stream. However, the model needs to calculate temperature at the compressor discharge streams. The following subsection explains how the compressor model calculates this temperature.

5.4.2 Model of the Compressors

The compressor is assumed isentropic, so for a given discharge pressure, the model determines the enthalpy at the discharge pressure by calculating the isentropic enthalpy. The value of an isentropic property is the value of this property when it undergoes a process with constant

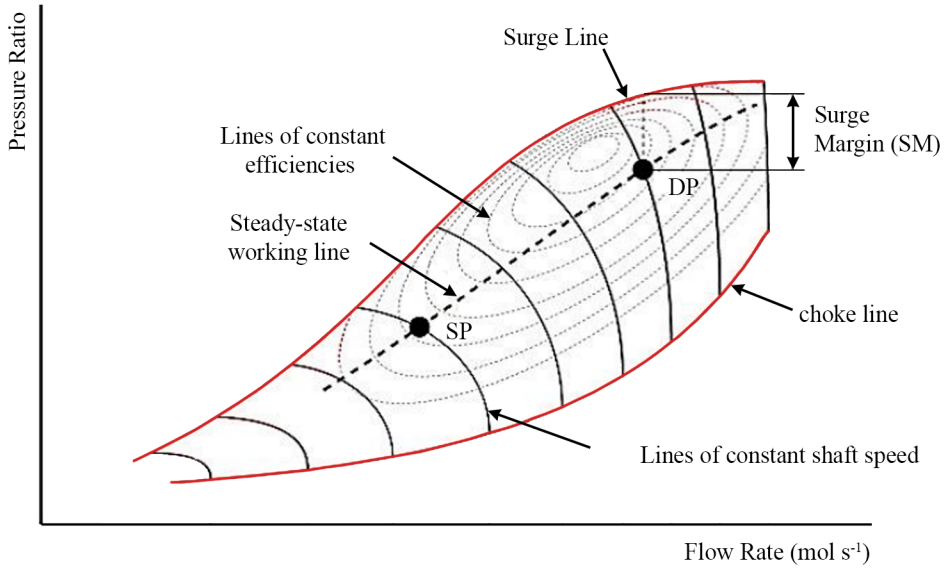


Figure 5.4: Example of a compressor map. The horizontal axis represents the flow rate, the vertical axis represents the pressure ratio, and the dotted lines show constant isentropic efficiencies. The solid black lines represent constant shaft speeds, the more to the left these lines are, the slower the compressor. The left red line represents the surge line, and the right hand side line is the choke line. This figure is extracted from Miller (2015)

entropy. For compressors, the enthalpy follows the equation:

$$\eta_{\text{isen}} = \frac{h_{\text{d}}^{\text{isen}} - h_{\text{s}}}{h_{\text{d}}^{\text{real}} - h_{\text{s}}} \tag{5.43}$$

where η_{isen} is the isentropic efficiency, which measures how close the process is to be ideal, h_{s} is the specific enthalpy of the suction stream in J mol^{-1}, $h_{\text{d}}^{\text{real}}$ is the enthalpy of the discharge stream in the actual process in J mol^{-1}, and $h_{\text{d}}^{\text{isen}}$ is the enthalpy of the discharge stream in an isentropic process in kJ kmol^{-1}.

A compressor map provides the value of the isentropic efficiency of a compressor by knowing the values of the flow rate, the pressure ratio ($P_{\text{d}}/P_{\text{s}}$), and the speed. Figure 5.4 gives an example of a compressor map to obtain the isentropic efficiency.

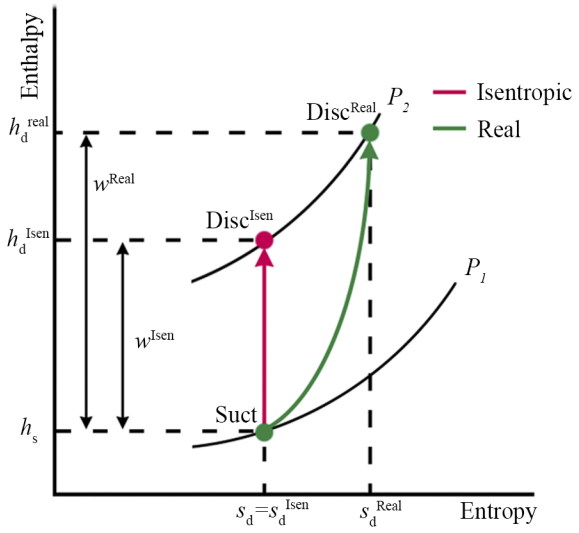


Figure 5.5: Entropy-enthalpy diagram for an isentropic and a real ceompression. The horizontal axis represents the entropy, and the vertical axis represents the enthalpy of the stream compressed. The figure shows the path followed by a real compression (green), and the path followed by an isentropic compression (pink).

Figure 5.5 depicts the differences between enthalpies in an isentropic process and the actual process. The temperature and the pressure at the suction stream are known, so the thermodynamic equations can calculate the entropy at this stream. Consequently, the entropy at the discharge stream in the isentropic process is also known because the suction and discharge streams have the same entropy. The temperature in the isentropic process is calculated by iteration, varying the isentropic temperature until the following equation is met:

$$s_{\mathrm{d}}^{\mathrm{isen}} - s_{\mathrm{s}} = 0$$

where $s_{\mathrm{d}}^{\mathrm{isen}}$ is the specific entropy at the discharge stream for the isentropic process in J mol^{-1} K^{-1} as a function of the isentropic temperature, and s_{s} is the specific entropy at the suction stream in J mol^{-1} K^{-1}.

From Eq. 5.43, $h_{\text{disc}}^{\text{real}}$ results in:

$$h_{\text{disc}}^{\text{real}} = \frac{h_{\text{disc}}^{\text{isen}} - h_{\text{suction}}}{\eta_{\text{isen}}} + h_{\text{suction}} \tag{5.44}$$

The temperature at the exit of the actual compression is obtained following the same procedure. In this case, however, instead of iterating with the entropies, the model iterates using the enthalpies until the following equation is met:

$$h_{\text{disc}}^{\text{real}}(T^{\text{isen}}) - h_{\text{disc}}^{\text{real}} = 0$$

From Eq. 5.42, the electrical energy consumption of a single compressor is:

$$w = h_{\text{disc}}^{\text{real}} - h_{\text{suction}} = \frac{h_{\text{disc}}^{\text{isen}} - h_{\text{suction}}}{\eta_{\text{isen}}} \tag{5.45}$$

Thus, the overall consumption of the plant is the sum of the consumptions of the three compressors. Figure 5.6 shows a flow diagram for calculating the consumption of the plant.

5.5 Joule-Thomson Cycle

This section examines the Joule-Thomson cycle undergone by the refrigerants in the MFC Linde process. Figure 5.7 shows the subcooling refrigeration cycle from Figure 5.1. The temperatures are fixed to avoid heat stress in the pipes, and there is no pressure drop (these assumption are explained in Appendix C.2).

The amount of heat absorbed by the refrigerants depends on its flow rate and the discharge pressure in its corresponding compressor. The flow rate of the refrigerants are established according to the temperature needed for the natural gas after performing an heat balance. Thus, this discussion considers the consequences of the discharge pressure of Comp3 on the absorbed heat. To obtain conclusions, in the first subsection, the compressor provides a nominal pressure that

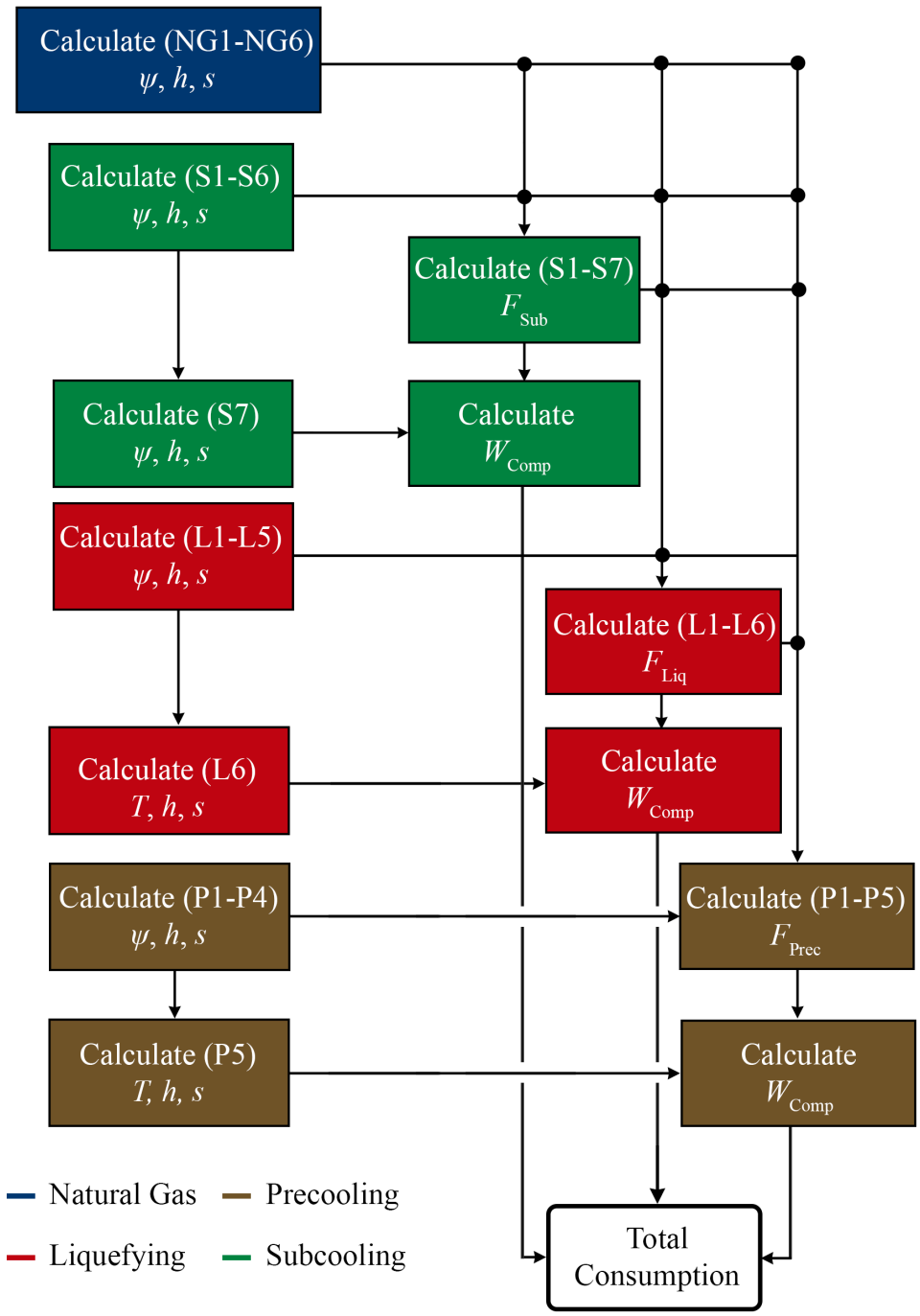


Figure 5.6: Algorithm for calculating the total electrical consumption of the plant. The names of the streams and the colours of the shapes are referred to Figure 5.1.

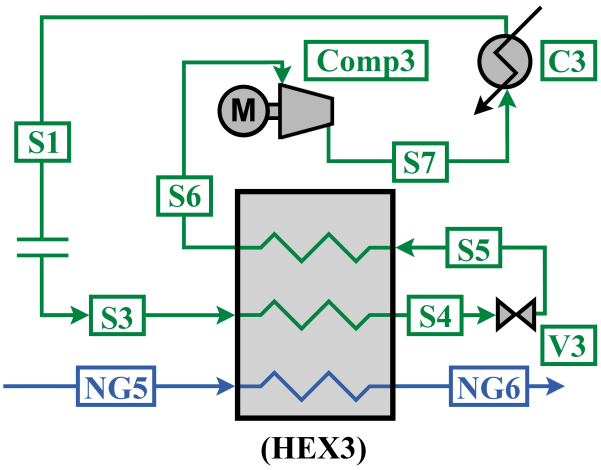


Figure 5.7: Subcooling cycle exploiting the Joule-Thomson effect. This example is extracted from the subcooling cycle in Figure 5.1.

causes S3 to be a subcooled liquid, in the second subsection, the compressor provides a lower pressure that causes S3 to present a VLE, and in the third subsection, the compressor provides a pressure that causes S3 to be close to its saturation point.

5.5.1 Joule-Thomson Cycle under Nominal Operation

Under nominal operation in an LNG process, stream S3 is a subcooled liquid. Figure 5.8 shows a graph relating the enthalpy and the pressure. Each point represents each stream in Figure 5.7. The blue curve delimits the vapour and the liquid equilibrium areas, with the liquid on the left of the curve. The black lines represent isotherms, curves in which the temperature is constant; the more on the left the isotherm, the lower the temperature. The top isotherm presents a small red section, which represents the division between the vapour and liquid phase. Starting from stream S1, the refrigerant decreases its temperature going through HEX1, HEX2, and HEX3, until it reaches stream S4. This temperature decrease happens with a constant pressure, so the lines are horizontal. Stream S4 undergoes an expansion in an isenthalpic valve, so the pressure decreases, and the enthalpy is kept constant. Thus, S5 has the same enthalpy as stream S4,

but a lower temperature. After that, the refrigerant enters again to the heat exchanger HEX3, but in this case it absorbs heat, thus increasing its enthalpy until reaching S6, which has the same temperature as S3 (S3 and S6 are in the same isotherm). Stream S6 is compressed until it reaches the pressure in stream S1. The refrigerant is cooled down in the sea cooler C3, until it reaches the sea temperature. The refrigerant exits the sea cooler and enters HEX1, so the cycle is closed.

The two enthalpies differences, $(h_{S6} - h_{S3})$ and $(h_{S7} - h_{S6})$ in the horizontal axis give, respectively, the specific heat that the refrigerant can absorb and the specific heat required by the

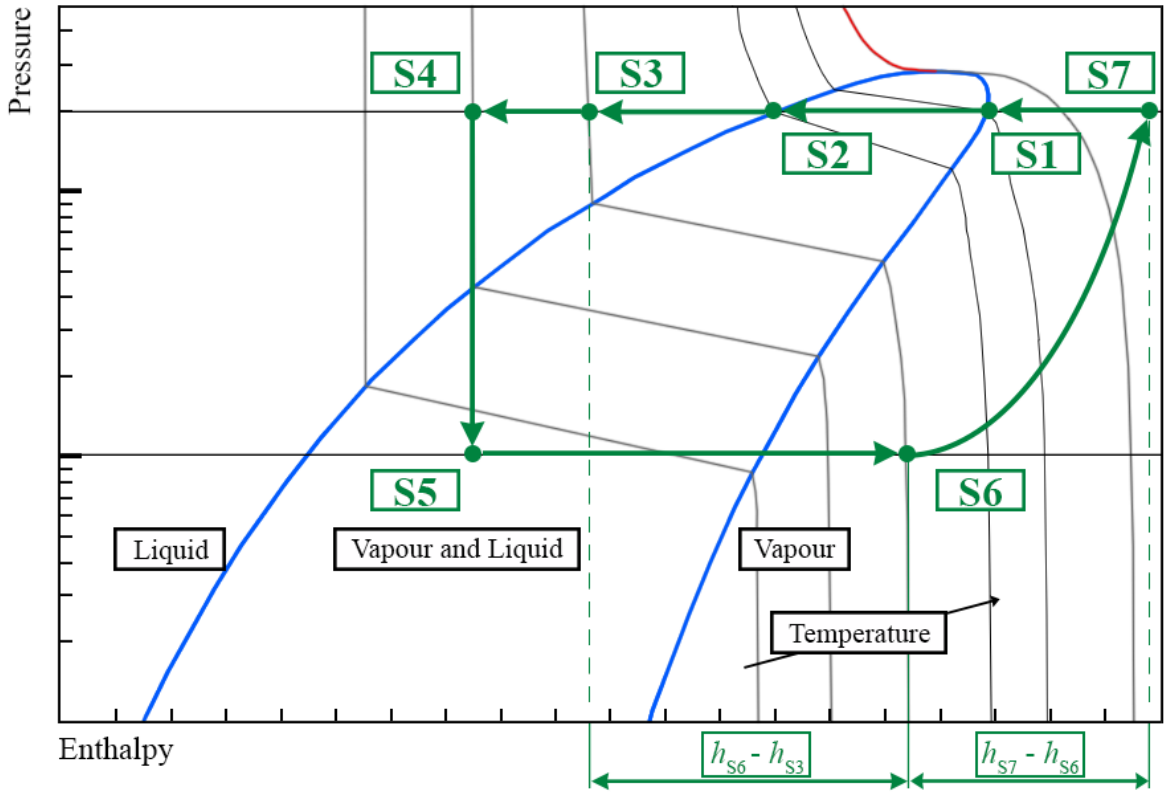


Figure 5.8: Pressure-Enthalpy diagram displaying the points of the subcooling refrigerant in Figure 5.7 undergoing a Joule-Thomson expansion. The horizontal axis shows the enthalpy, whereas the vertical axis represents the pressure (in a logarithmic scale). The blue line in the graph confines the vapour and liquid equilibrium area, and the black lines depicts the isotherms. The trajectory of the refrigerant is represented in green, and the green nodes are the streams in Figure 5.7.

compressor for reaching the needed pressure. Both differences are crucial for the following discussions.

5.5.2 Joule-Thomson Cycle in a Lower Pressure Operation

The analysis in this subsection proposes a lower discharge pressure that causes S3 to present a VLE. Figure 5.9 shows the same diagram as in Figure 5.8, but in this case, the yellow lines

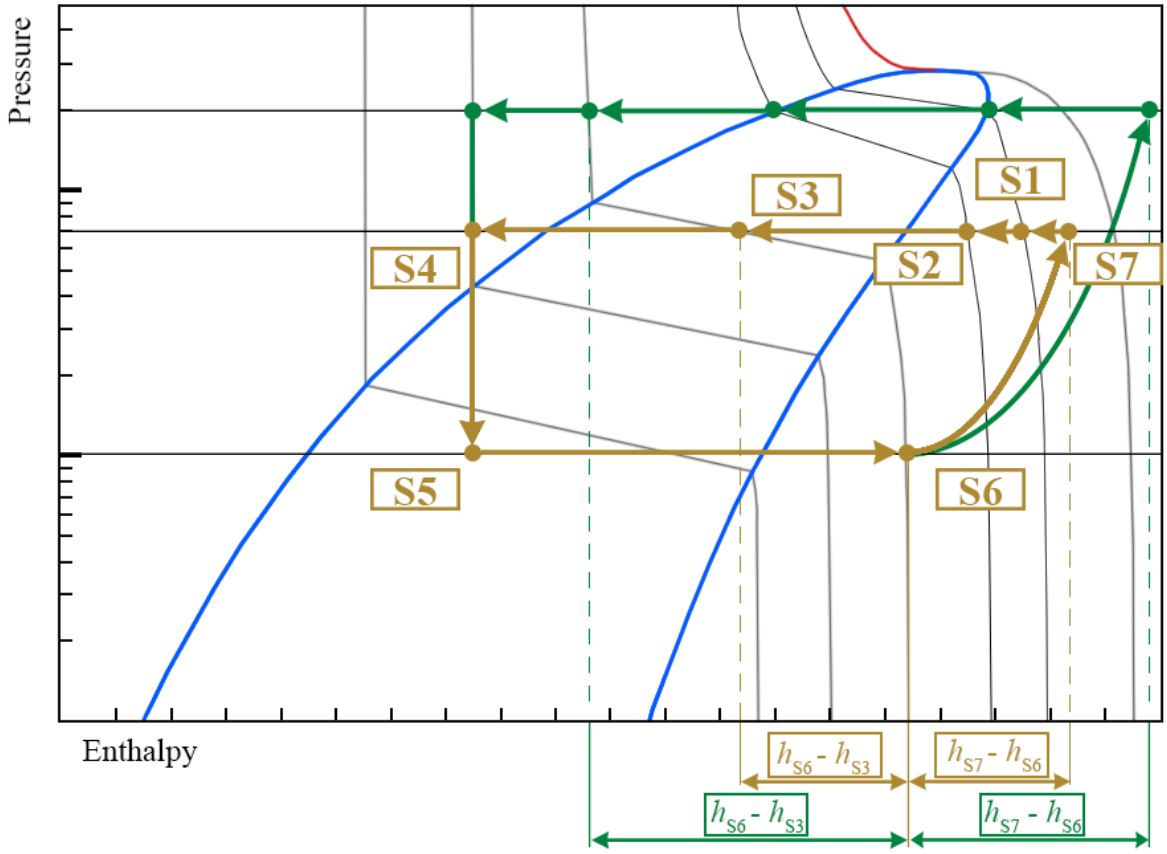


Figure 5.9: Pressure-Enthalpy diagram displaying the points of the subcooling refrigerant in Figure 5.7 undergoing a Joule-Thomson expansion. The green lines depict the same trajectory illustrated in Figure 5.8, and the yellow lines represents the trajectory of the subcooling refrigerant if the pressure in S3 corresponded to a pressure that causes it to be at a VLE.

represent the lower pressure operation. The height of the points S1-S4, and S7 in the graph is decreased, and S3 falls within the VLE region. Since they are in the same isotherm, in both operations (nominal and lower pressure) S3 has the same temperature.

In Figure 5.9, both $h_{S6} - h_{S3}$ and $h_{S7} - h_{S6}$ are smaller than their respective values in the nominal operation case. As mentioned, $h_{S7} - h_{S6}$ is the specific work that has to be done by the compressor for reaching the specified pressure, so this new smaller value should be beneficial for the overall consumption of the plant. However, from equation 5.6, the subcooling flow rate is inversely proportional to $h_{S6} - h_{S3}$, so the new smaller value of $h_{S6} - h_{S3}$ causes a larger refrigerant flow rate. Consequently, the extensive work done by the compressor has to increase. Thus, it is important to find a pressure in which the consumption and flow rate are minimised, or, from another perspective, a pressure in which $h_{S6} - h_{S3}$ is maximised, while $h_{S7} - h_{S6}$ is minimised.

5.5.3 Joule-Thomson Cycle in an Optimal Pressure Operation

Figure 5.10 shows the same cycle setting a different discharge pressure that causes S3 to be almost at its saturation point. The new value of $h_{S6} - h_{S3}$ is close to its respective value in the nominal operation, so, from Eq. 5.6, the subcooling flow rate is almost equal to the flow rate in the nominal operation. On the other hand, the new value for $h_{S7} - h_{S6}$ is lower than its respective value in the nominal operation. Thus, the consumption of the subcooling compressor is at its optimal point when S3 is at its saturation point. This can be generalized for the other cycles: the optimal consumption of each cycle is found at a discharge pressure which provokes the stream entering the heat exchanger to be at its bubble point.

5.6 Solution Approaches in the Study of the LNG Process

This section includes the assumptions made to solve the LNG process model. Additionally, it includes an analysis of the Degrees of Freedom (DoF) considering the made assumptions, so that the model determines the independent variables.

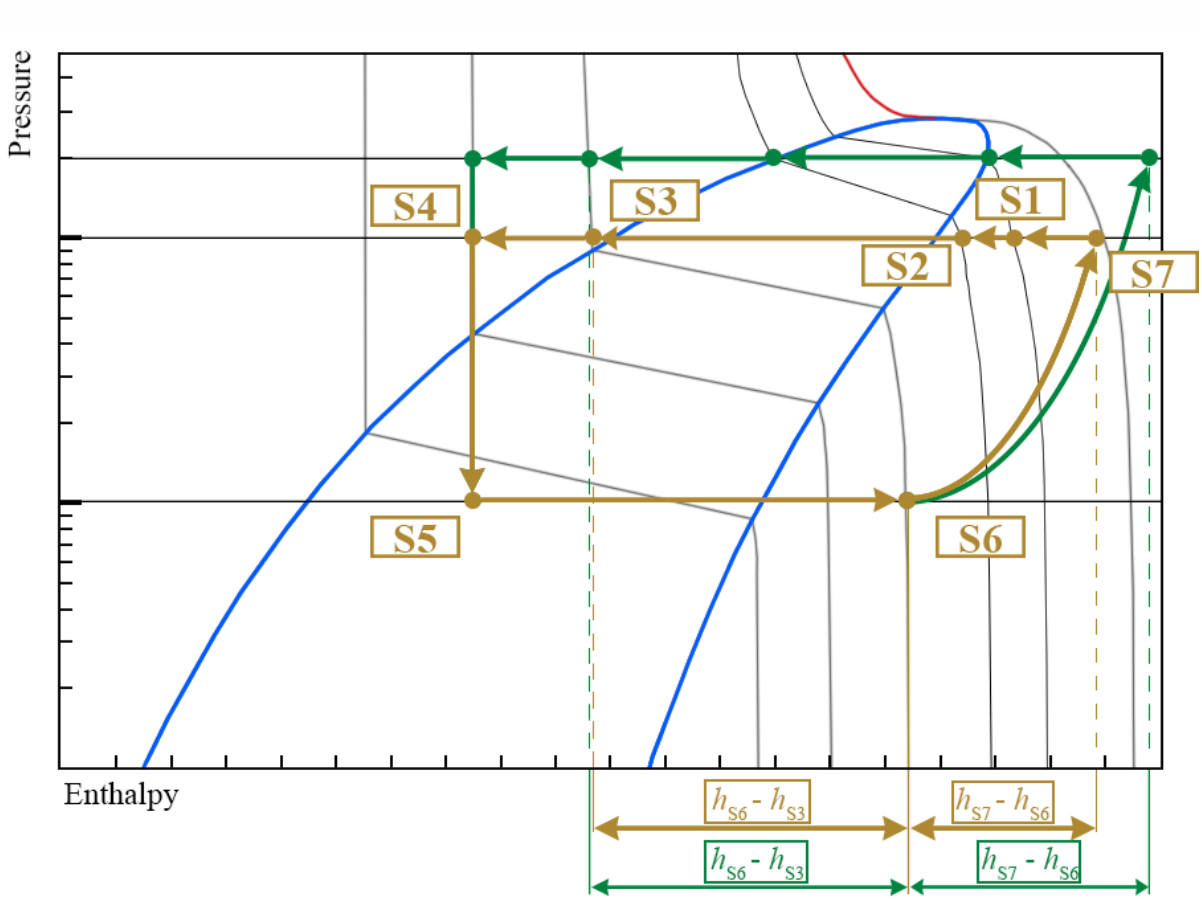


Figure 5.10: Pressure-Enthalpy diagram displaying the points of the subcooling refrigerant in Figure 5.7 undergoing a Joule-Thomson expansion. In this case, the yellow lines represents the trajectory of the subcooling refrigerant if the pressure in S3 corresponded to a pressure just above the saturation point pressure, so that it only presents a vapour phase.

5.6.1 Assumptions of the LNG model

Analysing the DoF is essential to identify what variables can be treated as independent. Before the analysis, this subsection shows the assumptions made in the model, so they are considered in the examination of the DoF.

1. Except for NG2 and NG6, all temperatures are fixed during the course of a single simulation. They are, however, changed for different simulations
2. The heat exchangers are assumed to be large enough for reaching the established temperatures. This means that the piping system within the heat exchangers is long enough, so that the necessary heat is completely transferred from the hot streams to the cold streams
3. There is no pressure drop due to the piping system
4. The pressures after the Joule-Thomson valves in the refrigerant cycles are fixed (streams P3, L4, and S5 in Figure 5.1)
5. The natural gas at the beginning of the liquefaction (NG1 in Figure 5.1) comes from the natural gas purification dryer system, so the natural gas pressure is assumed constant at 30 bar
6. The dynamic behaviour of the process is not considered, so the model calculates only the operating points when the process is at its steady state

Appendix C.2 gives reasoning of why these assumptions are sensible.

5.6.2 Degrees of Freedom and Input Values

The analysis of the DoF is included in Appendix C.1. The analysis shows that there are 28 DoF. The analyst provides the temperature of all streams except for streams NG2 and NG6, subtracting 14 DoF. Table 5.1 shows the values of the temperatures. The analyst has not fixed

the temperature in NG2 because that is the temperature in the flash drum (NG_ Flash in Figure 5.1). The vapour fraction in this flash drum changes the composition of the vapour natural gas, and therefore, varying the temperature at NG2 changes the composition of the LNG.

There are 14 DoF more. The analyst established the values of the discharge pressure of the valves (V1, V2, and V3), and the pressure of the natural gas streams. Table 5.2 specifies the pressures of each stream, which subtract four DoF, leaving the model with ten DoF.

The temperature and pressure in P4, L5, and S6 cause these streams to be at vapour state. If for a given pressure, the temperature varied, these streams might present a VLE, which would require the installation of flash drums and pumps after the heat exchangers. Appendix C.4 analyses this scenario and explains the behaviour of the pumps when the temperatures of P4, L5, and S6 vary.

Table 5.3 specifies the compositions (z) of each gas, which subtract four DoF, so the model has six DoF remaining. One degree of freedom is used for fixing the overall power consumption in the plant, which is defined by the available power. Therefore, the process has five variables remain to be fixed, as discussed in the next section.

Table 5.1: Input values for the temperatures in the LNG process

Natural Gas Stream	T(K)	Precooling Cycle Stream	T(K)	Liquefying Cycle Stream	T(K)	Subcooling Cycle Stream	T(K)
1	298.15	1	283.15	1	283.15	1	283.15
2	-	2	238.15	2	238.15	2	238.15
3	=NG2	3	-	3	173.15	3	173.15
4	=NG2	4	260.15	4	-	4	120.15
5	173.15	5	-	5	220.15	5	-
6	-	-	-	6	-	6	185.15
-	-	-	-	-	-	7	-

Table 5.2: Input values for the pressures in the LNG process

Natural Gas Stream	P(bar)	Precooling Cycle Stream	P(bar)	Liquefying Cycle Stream	P(bar)	Subcooling Cycle Stream	P(bar)
1	30	1	=P5	1	=L6	1	=S7
2	=NG1	2	=P1	2	=L1	2	=S1
3	=NG2	3	2	3	=L2	3	=S2
4	=NG2	4	=P3	4	2	4	=S3
5	=NG3	5	-	5	=L4	5	2
6	=NG5	-	-	6	-	6	=S5
-	-	-	-	-	-	7	-

Table 5.3: Compositions of the natural gas and the refrigerants

Component	Natural Gas	Precooling	Liquefying	Subcooling
Methane	0.8893	0	0.05	0.4
Ethane	0.0651	0.2	0.85	0.3
Propane	0.0392	0.8	0.1	0
Butane	0.0048	0	0	0
Pentane	0.0016	0	0	0
Ethylene	0	0	0	0.3

5.6.3 Fixed Variables

From Table 5.2, the analyst has not provided any of the discharge pressure of any cycle. One of the discharge pressures is determined by the two remaining cycles and the overall electrical power consumption, so the analyst can only fix two of them.

From the heat balances, the model determines the flow rate of the refrigerants using the thermodynamic properties and the production rate of natural gas. Thus, the five DoF are:

1. Discharge pressure of one of the refrigerant compressor
2. Discharge pressure of another refrigerant compressor
3. LNG production rate
4. NG2 temperature / LNG composition
5. NG6 temperature / LNG temperature at the exit of the process

Due to the nature of the Joule-Thomson cycle, the refrigerant cycles can work at an optimal point, so the pressure should be kept constant at that point. Hence, the first step towards studying flexible operation is determining the optimal pressures given by the compressors for given values of LNG production rate, exit temperature, and composition. These optimal pressures are inputs for the simulations where the LNG characteristics and production rate change.

Therefore, the results are divided into two chapters: (i) the first related to obtaining the optimal pressures in the refrigeration cycles for a given LNG production rate, exit temperature, and composition, and (ii) a second chapter related to obtaining envelope of feasible operating points for LNG flow rate, exit temperature and composition at a given set of compressor discharge pressures.

5.7 Summary of the Chapter

This chapter has introduced the mathematical model of the Liquefied Natural Gas (LNG) process. The process liquefies natural gas by cooling it down through three stages, namely precooling, liquefying, and subcooling stages. Each stage has a refrigerant that absorbs heat from the natural gas in a heat exchanger.

The model performs heat balances to each heat exchanger to calculate the flow rate of each refrigerant. The model needs to calculate the enthalpies of each stream to calculate the heat balances. Therefore, the model employs the Redlich-Kwong Soave (RKS) equations to calculate the thermodynamic properties of the streams. The model uses the Rachford Rice algorithm to calculate the vapour fraction and the composition of each stage in the streams presenting a Vapour and Liquid Equilibrium (VLE).

The model calculates the electrical power consumption of a compressor as the difference between the enthalpies at the suction and the discharge streams. The total consumption of the plant is the sum of the three compressors.

This chapter has presented the relevance of appropriately adjusting the discharge pressure of each compressor to exploit the Joule-Thomson cycle. Section 5.5 hypothesised that, in a refrigeration cycle, the optimal pressure causes the refrigerant to be right above its bubble point when entering the heat exchanger.

The model has five degrees of freedom, and the independent variables are:

- The discharge pressure of two compressors
- The LNG production rate
- The LNG temperature at the exit of the process
- The LNG temperature at the flash drum after the precooling stage (NG_ Flash), which is related to the LNG composition

For a given LNG production rate and LNG characteristics, the calculations of the model showed that there is a set of discharge pressures which minimises the electrical power consumption. Thus, the model divides the calculations into two groups:

- One for finding the optimal set of discharge pressures for fixed values of the LNG production and the LNG characteristics
- One for studying the effects of the LNG production and the LNG characteristics on the electrical power consumption using the optimal set of discharge pressures as input

Chapter 6

Optimization of the Pressures in the Refrigeration Systems

This section presents the results as graphical representations of the relationships between the discharge pressures and the overall electrical power consumption of the plant. As stated in Section 5, the pressure of the refrigerants affects the flow rate of the refrigerants, and the specific electrical consumption of the compressors, so the simulations are divided in two parts accordingly. The LNG characteristics are constant during these discussions, with the production rate fixed at 15 kmol s^{-1}, the temperature in the flash drum at 238.15 K, and the LNG temperature at the exit of the process at 107.15 K.

6.1 Effects of the Pressure on the Flow Rate of the Refrigerants

Section 5.5 mentioned that changing the discharge pressure has significant consequences on the overall electrical consumption if it causes a stream entering a heat exchanger to present a different phase. This section shows the relationship between the flow rate, the vapour fraction,

and the discharge pressures. This section divides the results into three groups of two rows, each group corresponding to a different heat exchanger. The upper row in each group represents the flow rate of the refrigerant corresponding to the analysed heat exchanger. The lower row depicts the vapour fractions of each stream entering or leaving the heat exchangers. Thus, the first group corresponds to the precooling heat exchanger; the upper row represents the precooling flow rate, and the lower row represents the vapour fraction of each stream in the precooling heat exchanger.

6.1.1 Effects of the Pressure on the Precooling Refrigerant

The upper row in Figure 6.1 shows the effects of varying the discharge pressure of each refrigerant on the precooling flow rate. The lower row shows the impact of changing the discharge pressure of each refrigerant on the vapour fraction of the streams involved in the first heat exchanger balance (P1, L1, L2, S1, and S2). The shadowed zones in each pair of graphs are the ranges of pressure in which the refrigerants present a Vapour and Liquid Equilibrium (VLE).

There is a strong relationship between the vapour fraction of each refrigerant and the precooling flow rate. Figure 6.1.a.2) shows that below 10 bars, stream P1 presents a VLE. In the same region, Figure 6.1.a.1) shows that the precooling flow rate is sensitive to any change of the precooling pressure. This is observed also when streams L1 or L2 have a VLE, and when S2 presents a VLE.

$$F_{\text{Prec}} = \frac{F_{\text{NG1}}(h_{\text{NG2}} - h_{\text{NG1}}) + F_{\text{Sub}}(h_{\text{S2}} - h_{\text{S1}}) + F_{\text{Liq}}(h_{\text{L2}} - h_{\text{L1}})}{h_{\text{P1}} - h_{\text{P4}}} \tag{5.4}$$

Eq. 5.4 is the heat balance in the first heat exchanger introduced in Section 5.1. F_{Prec}, F_{Liq}, and F_{Sub} are the flow rates of the precooling, liquefying, and subcooling refrigerants in kmol s^{-1}, F_{NG1} is the natural gas feed rate in kmol s^{-1}, and h_x is the specific enthalpy of stream x in kJ kmol^{-1} s^{-1}. From Eq. 5.4, the precooling flow rate is inversely proportional to the difference

between the enthalpies at the entrance and at the exit of the heat exchanger, $h_{P1} - h_{P4}$. Therefore, the flow rate decreases when h_{P1} decreases. [1]

Since the temperature of stream P1 is constant, raising the precooling pressure in the VLE region leads to a higher amount of liquid in the stream. Liquid has a lower enthalpy than vapour, so the enthalpy of the stream decreases when the vapour fraction decreases. Consequently, in the VLE region, the enthalpy in stream P1 decreases when the pressure increases. Thus, when

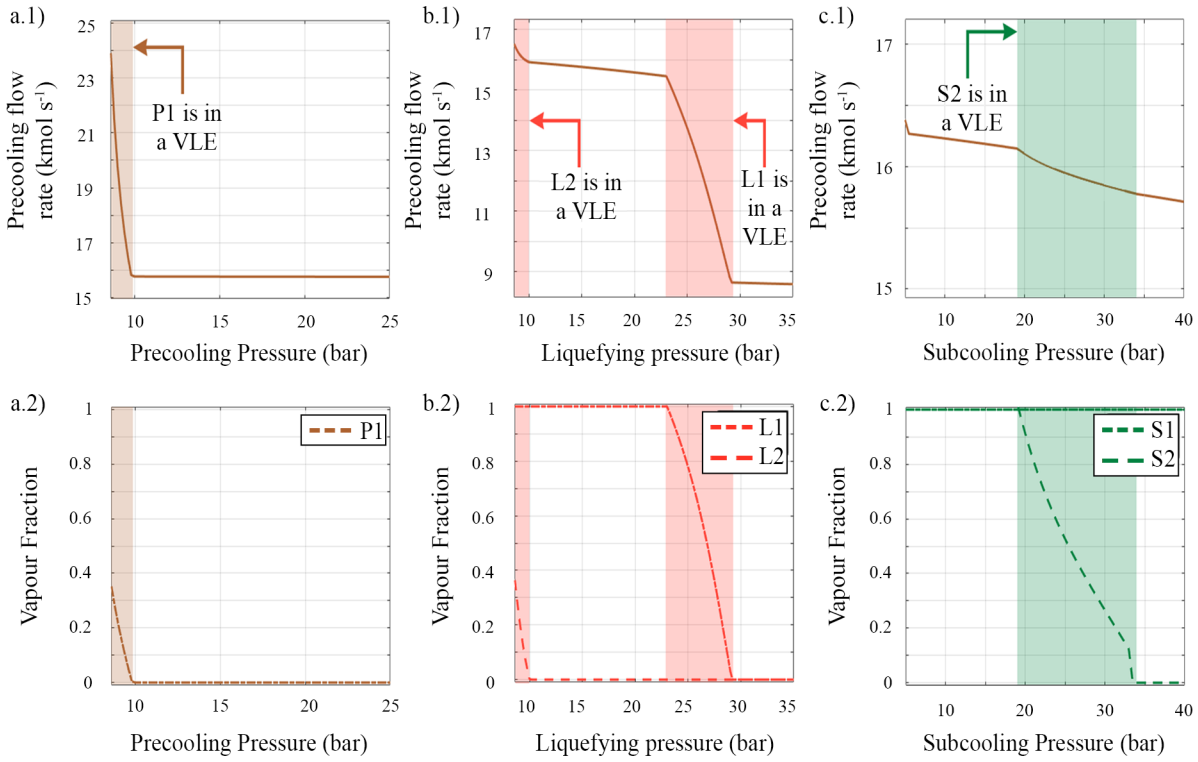


Figure 6.1: Effects of the discharge pressures of each refrigerant (bar) on (upper row) the precooling refrigerant flow rate (kmol s^{-1}), and on (lower row) their respective vapour fractions in the streams involving the first heat exchanger (HEX1 in Figure 5.1). Column a) represents the pressure of the precooling refrigerant (brown), b) represents the liquefying pressure (red), and c) represents the subcooling pressure (green).

[1] h_{P1} and h_{P4} are negative, and h_{P4} is higher than h_{P1}, so when h_{P1} decreases the magnitude of $h_{P1} - h_{P4}$ increases.

the precooling pressure increases from 8 to 10 bars, ψ_{P1} h_{P1} decreases, resulting in a lower precooling flow rate.

When there is only one phase, the effects of increasing the pressure on the enthalpy are not significant, so the flow rate barely changes. However, the power consumption in the compressor increases for reaching the desired pressure. The optimal pressure for the precooling cycle is a pressure that minimises the flow rate and maximises the specific power consumption. Thus, this point is found in the transition between having a VLE and having a liquid, which is where the precooling flow rate plateaus.

Figure 6.1.b) shows that the precooling flow rate significantly decreases when stream L1 or L2 present a VLE. This relationship follows the same reasoning as P1, h_{L1} decreases when L1 presents more liquid, so in the heat balance equation, $h_{L2} - h_{L1}$ decreases.

On the other hand, if h_{L2} decreased due to the presence of more liquid, $h_{L2} - h_{L1}$ would increase. Nevertheless, Figure 6.1.b.1) shows that the precooling flow rate decreases when L2 has more liquid in it. In this case, the pressure rise of L2 causes a decrease in its flow rate, so, even though the term $h_{L2} - h_{L1}$ is larger, the extensive difference of enthalpies $F_{Liq}(h_{L2} - h_{L1})$ is smaller.

6.1.2 Effects of the Pressure on the Liquefying Refrigerant

Figure 6.2 shows the effects of varying the liquefying and the subcooling pressures on the flow rate of the liquefying cycle. The graphs in Figure 6.2 refer to the streams entering or leaving the second heat exchanger (L2, L5, S2, and S3). The precooling refrigerant is not involved, so its effects on the liquefying flow rate are not included, leaving Figure 6.2 with four graphs.

$$F_{Liq} = \frac{\psi_{NG2} F_{NG1}(h_{NG5} - h_{NG3}) + F_{Sub}(h_{S3} - h_{S2})}{h_{L2} - h_{L5}} \tag{5.5}$$

Eq. 5.5 is the heat balance in the second heat exchanger introduced in Section 5.1. ψ_{NG2} is the vapour fraction in the flash drum (NG_ Flash). The same reasoning from the precooling heat exchanger is followed. Figures 6.2 a.1) and 6.2 a.2) show that, for the liquefying pressure, from

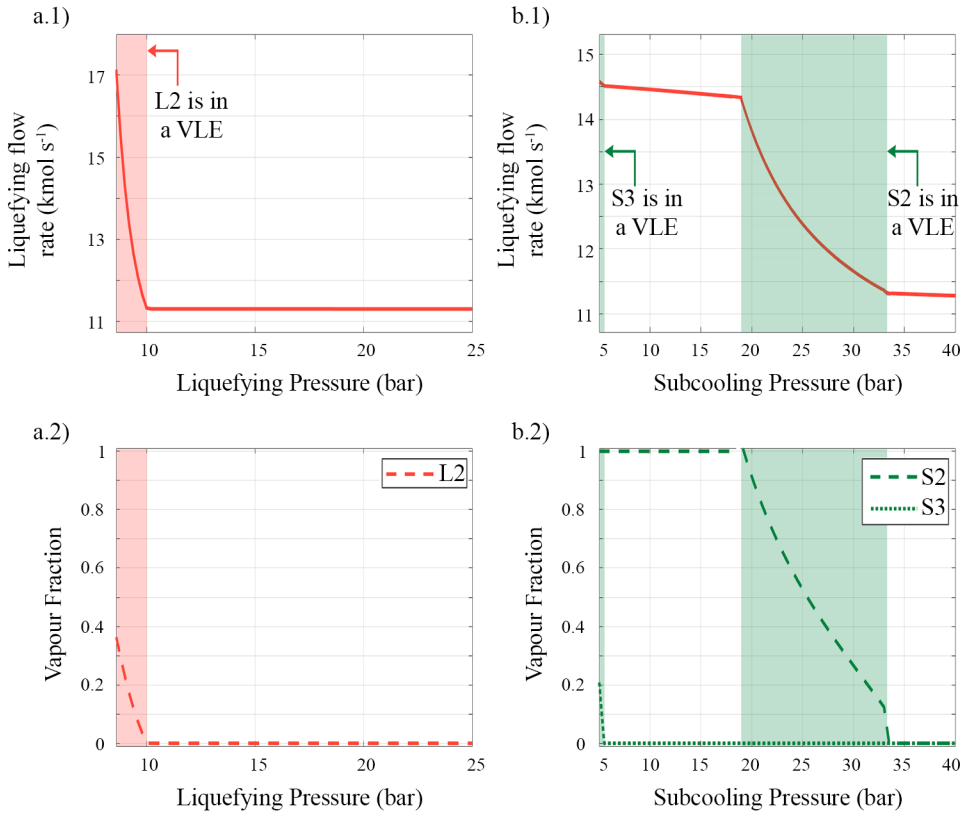


Figure 6.2: Effects of the discharge pressures (bar) of the liquefying and the subcooling refrigerants on (upper row) the liquefying refrigerant flow rate (kmol s^{-1}), and on (lower row) their respective vapour fractions in the streams involving the second heat exchanger (HEX2 in Figure 5.1).

7 to 10 bars, L2 is in a VLE, so an increase in the liquefying pressure provokes a drop in its enthalpy (h_{L2}), and the liquefying flow rate steeply decreases.

Between 10 and 22.5 bars, and from 29 bars onwards, L1 and L2 both present one phase, so increasing the pressure does not have a significant impact on their enthalpies. Therefore, increasing the pressure in these ranges has virtually no consequences on the liquefying flow rate. Nevertheless, the liquefying compressor consumes more electrical power. Hence, the optimal point is at either 10 bars, or at 29 bars, where the liquefying flow rate hits a plateau.

Figure 6.2 b.1) shows that, for the subcooling pressure, from 19 to 33.5 bars, S2 presents a VLE, which causes the liquefying flow rate to decrease when the subcooling pressure increases.

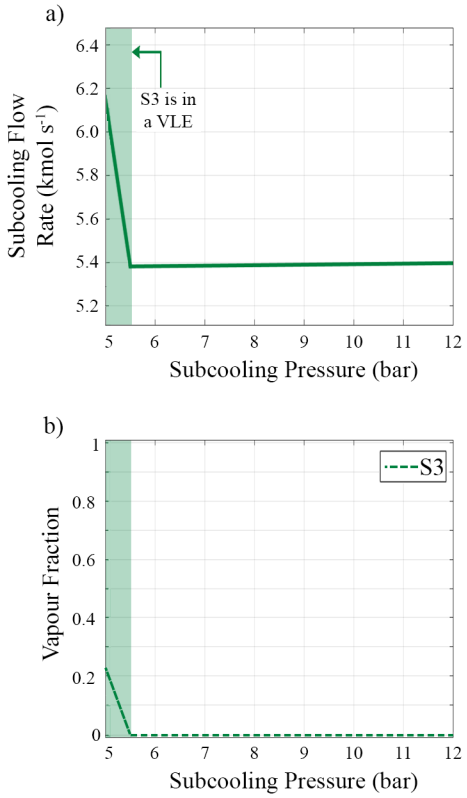


Figure 6.3: Effects of the discharge pressures (bar) of the subcooling refrigerants on (upper row) the subcooling refrigerant flow rate (kmol s^{-1}), and on (lower row) the subcooling vapour fractions in the streams involving the third heat exchanger (HEX3 in Figure 5.1).

6.1.3 Effects of the Pressure on the Subcooling Refrigerant

Figure 6.3 shows the effects of varying the subcooling pressure on the flow rate of the subcooling cycle, and the vapour fraction of S3. The analysis is performed to the third heat exchanger, in which the only refrigerant is the subcooling refrigerant.

$$F_{\text{Sub}} = \frac{\psi_{\text{NG2}} F_{\text{NG1}} (h_{\text{NG6}} - h_{\text{NG5}})}{h_{\text{S3}} - h_{\text{S6}}} \tag{5.6}$$

Eq. 5.6 is the heat balance in the third heat exchanger introduced in Section 5.1. Figure 6.3 indicates that S3 presents a VLE when the subcooling pressure is below 5.5 bars, and within

this region, the flow rate drops when the pressure increases. This is because, as Eq. 5.6 shows, the term $h_{S3} - h_{S6}$ increases when h_{S3} decreases.

6.2 Effects of the Pressure on the Electrical Power Consumption

The total power consumed in the process is the sum of the consumption of the three compressors. The consumption of each compressor is the product of its specific electrical consumption and the flow rate of the refrigerant it compresses. Both terms are functions of the pressure ratio of the compressors, so this section studies how they are related to the pressure ratio. Additionally, this section analyses the combination of the effects of the refrigerant pressures on the overall electrical consumption.

6.2.1 Electrical Consumption in a Compressor

Figure 6.4 shows the specific power consumption of each refrigerant compressor as a function of the discharge pressure. The specific power consumption increases as the discharge pressure increases. The darker regions in the graphs of Figure 6.4 represent the choke zone of the compressors (low pressures and high flow rates), so the cycle can not operate within these areas.

The overall consumption also depends on the flow rate of the refrigerants. Figure 6.5 shows the extensive power consumption of the compressors resulting from multiplying the specific consumption of each compressor by the respective flow rate. Each graph in Figure 6.5 shows the evolution of the electrical consumption of each individual compressor when the pressure of the refrigerant corresponding to the compressor is varied, and the rest of pressures remains constants. For instance, Figure 6.5 a) shows the consumption of Comp1 when its discharge pressure increases, and Comp2 and Comp3 have a discharge pressure of 15 bars and 35 bars respectively.

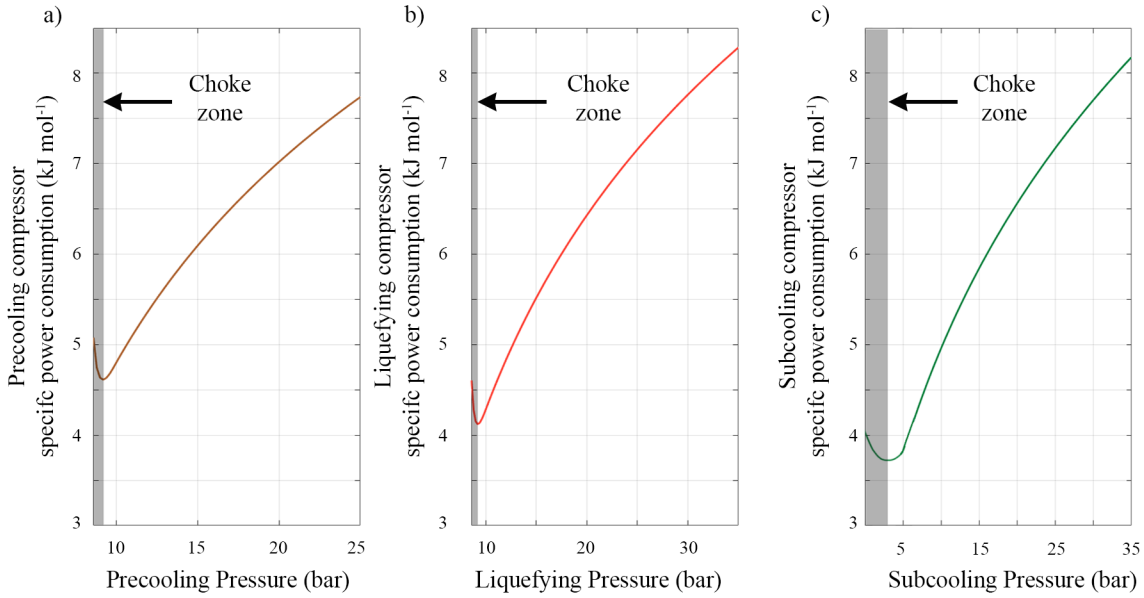


Figure 6.4: Relationship between the compressor specific electrical consumption (kJ mol $^{-1}$) and the discharge pressure (bar) for each refrigerant.

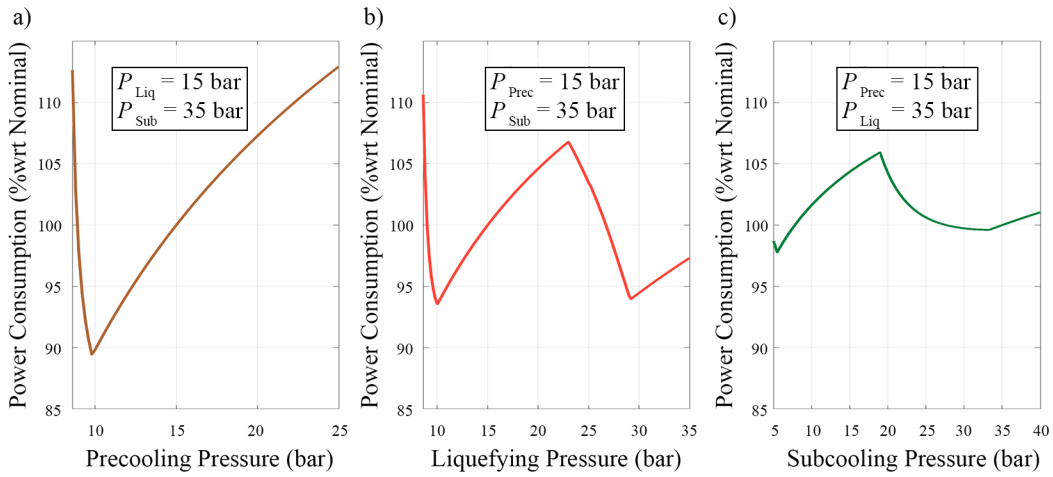


Figure 6.5: Relationship between the compressor electrical consumption (as a percentage with respect to the nominal power consumption) and the discharge pressure (bar) for each refrigerant. The graphs represent the consumption of the compressor taking into account that the discharge pressure has an effect on the flow rate of the refrigerant.

There is a relationship between the vapour fraction of each refrigerant and their consumption, and the minimum appears to be near the bubble point of the refrigerants. Thus, the minimum seems to be at 10 bars for the precooling refrigerant, 9.8 bars for the liquefying refrigerant, and 5.5 bars for the subcooling refrigerant. Nevertheless, the discharge pressure is not feasible for the subcooling compressor, because it would fall within the choke zone (Figure 6.4). Thus, it is necessary to observe the overall consumption of the plant when all pressures vary to obtain the optimal pressure for the subcooling cycle.

6.2.2 Overall Consumption of the LNG

The following graphs represent the overall electrical power consumption when two pressures are changed, and leaving the remaining pressure fixed. Figure 6.6 shows the consumption of the whole plant when the pressure of the liquefying and the subcooling cycles vary, and the

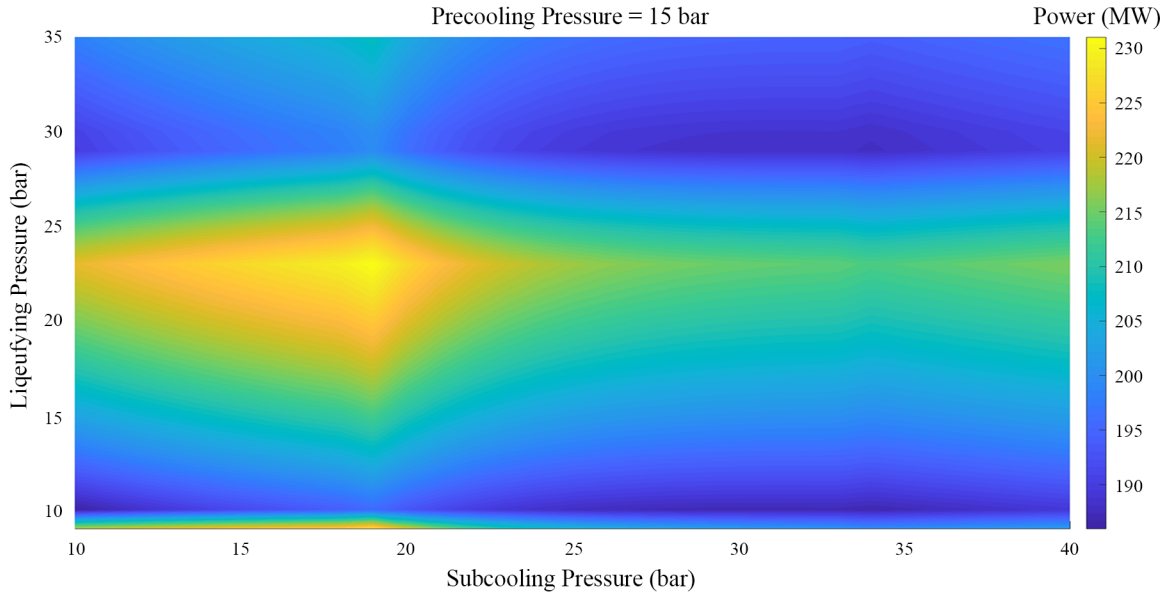


Figure 6.6: Consumption of the whole plant (MW) when the liquefying and the subcooling discharge pressures (bar) vary, and the precooling discharge pressure remains constant at 15 bar.

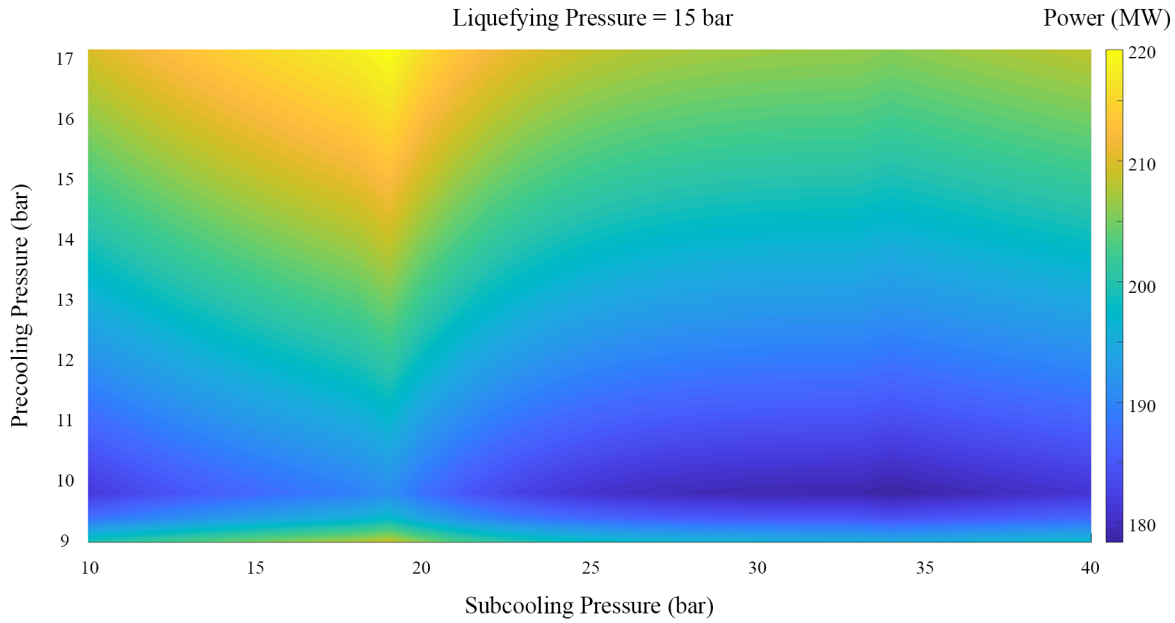


Figure 6.7: Consumption of the whole plant (MW) when the precooling and the subcooling discharge pressures (bar) vary, and the liquefying discharge pressure remains constant at 15 bar.

precooling pressure is constant at 15 bars. Figure 6.6 shows that the minimum consumption of the plant corresponds to a subcooling pressure of 33.5 bars.

Figure 6.7 shows the consumption of the whole plant when the discharge pressure of the precooling and the subcooling refrigerants vary. The liquefying discharge pressure is constant at 15 bars. In this case, it seems more clearly that the minimum for the consumption of the plant is at 33.5 bars for the subcooling discharge pressure, and 10 bars for the precooling cycle.

Figure 6.8 shows the consumption of the whole plant when the discharge pressure of the precooling and the liquefying refrigerant change. There is a minimum in the power consumption when the precooling pressure is at 10 bars, and the liquefying pressure is at 9.8 bars. As mentioned above, these pressures correspond to the saturation pressures of each refrigerant when the refrigerants enter their respective heat exchangers.

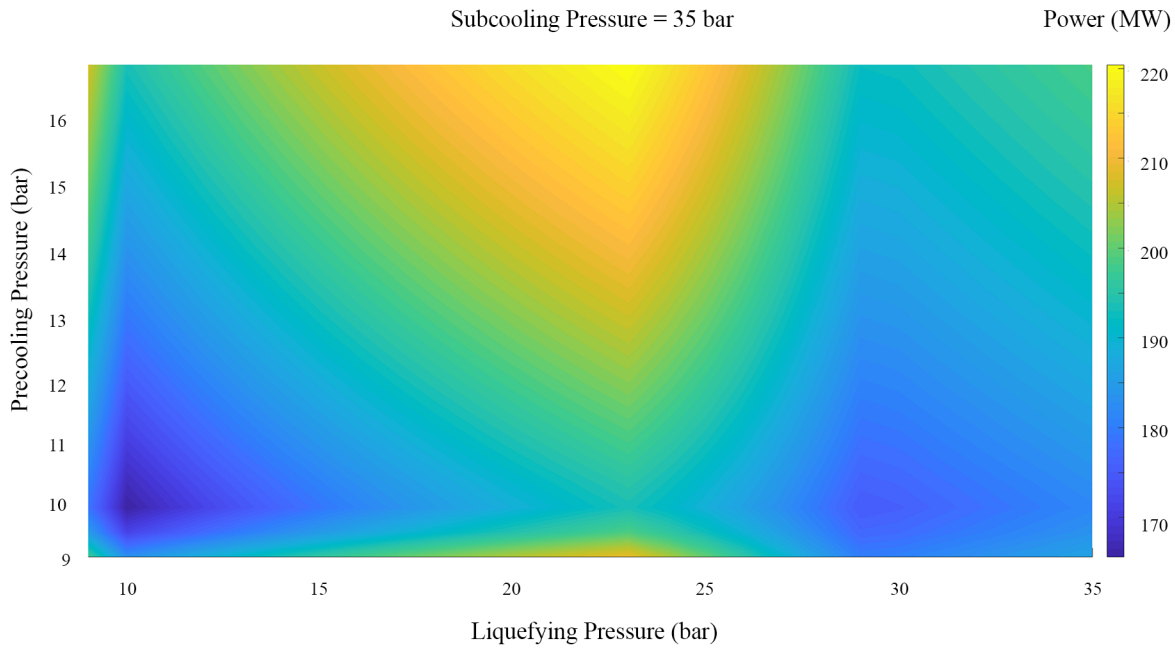


Figure 6.8: Consumption of the whole plant (MW) when the precooling and the liquefying discharge pressures (bar) vary, and the subcooling discharge pressure remains constant at 35 bar.

6.3 Discussion of the Effects of the Pressure

The obtained optimal points for the pressures are at 10 bars for the precooling cycle, 9.8 bars for the liquefying cycle, and 33.5 bars for the subcooling cycle. Nevertheless, comparing these results with those of a real industry (Stockmann et al., 2001), the used pressures are 15 bars, 15 bars, and 35 bars. The reason for setting the pressures higher than the results is to give some margin between the operation point and the saturation point. Figures 6.1, 6.2, and 6.3 show that, if the pressure of any refrigerant goes below its bubble point, then its flow rate steeply increases, resulting in a much higher consumption and a sudden rise of the flow rate that might trigger other variables to suddenly change.

The obtained pressures result in an optimal point for the process to operate, and changing them solely increases the consumption of the plant. Thus, during the following simulations, the pressures are established at the operational point suggested in the literature, with:

- Precooling pressure = 15 bar
- Liquefying pressure = 15 bar
- Subcooling pressure = 35 bar

6.4 Summary of the Chapter

This chapter has analysed the effects of varying the discharge pressures on the electrical power consumption of the compressors and the process.

The results showed that there is a strong relationship between the power consumption and the presence of a Vapour and Liquid Equilibrium (VLE). When a stream entering a heat exchanger presents a VLE, the enthalpy of the stream is more sensitive to changes in the pressure. The change of enthalpy affects the heat balance, causing the flow rate of the refrigerants to change.

When the refrigerant entering the heat exchanger is entirely liquid, the enthalpy of the stream will slightly change for a pressure increase. The compressor needs more energy to increase the pressure of the stream, which causes higher electrical consumption. However, the flow rate of the refrigerant does not virtually change when the pressure increases. Thus, the optimal pressure causes the refrigerant to be at the point where it is almost entirely liquid.

Industrial practice increases the optimal pressure to add a margin of operation and prevent a sudden rise in the flow rate of the refrigerants in case the pressure decreases. Therefore, the established set of pressures is 15 bars for the precooling refrigerant, 15 bars for the liquefying pressure, and 35 bars for the subcooling pressure.

Chapter 7

Results from the Study of Flexible Operation in the LNG Process

This chapter presents the impacts of varying the Liquefied Natural Gas (LNG) production rate and its characteristics on the consumption of the process. Chapter 5.6 specified that the LNG characteristics to be changed are its temperature at the exit of the process (NG6 in Figure 5.1), and its composition, which depends on the temperature of the flash drum after the precooling stage (NG_Flash in Figure 5.1). Each variable influences the electrical power consumption, either individually or in conjunction with the other variables. Hence, this chapter presents the influence of each variable separately, and then it exposes the combined effect.

7.1 Effects of the Production Rate

The LNG production rate determines the heat that the refrigerants need to absorb. The model assumes that the heat transfer area in the heat exchangers is large enough for the refrigerants to absorb the necessary heat. Thus, the flow rate of the refrigerants is proportional to the production flow rate, considering that the rest of the variables are kept consistent.

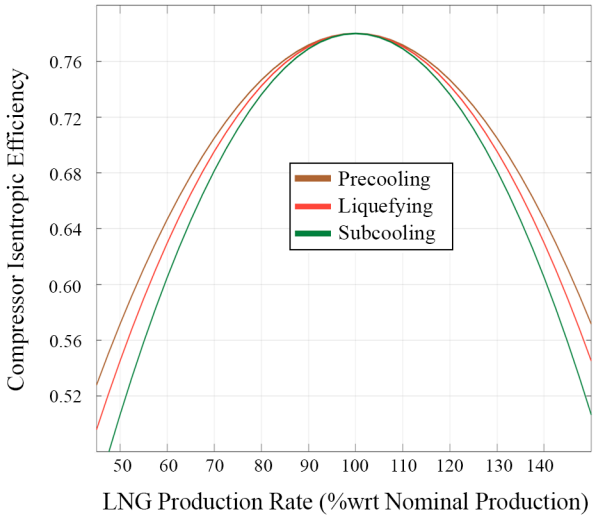


Figure 7.1: Relationship between the compressor efficiency and the natural gas production rate (as a percentage of its nominal value) for each compressor. The compressors are modelled so that the efficiency is at its maximum (η=0.77) for the nominal operation point.

The relationship between the overall power consumption and the production rate is not linear due to the isentropic efficiency of the compressors. The isentropic efficiency changes when the flow rate of the refrigerants changes. This efficiency is extracted from a lookup table according to the compressor maps in Miller (2015), setting the maximum efficiency of each compressor at 0.77. The model assumes that the compressors work at their maximum efficiency at the nominal LNG production rate. Figure 7.1 shows the relationships between the LNG production rate and the isentropic efficiency of each compressor. The efficiencies reach their maximum at 100% of the production rate, on the assumption that the compressors are optimal for the nominal as designed production rate. The minimum compressor efficiency achievable by the compressors before falling within the choke zone is 0.60. Figure 7.1 shows that when the LNG production rate decreases to around 59%, the efficiency of the subcooling compressor is 0.60. Thus, the maximum reduction of LNG production rate is 59%.

Figure 7.2 shows the relationship between the LNG production rate and the electrical consumption of the plant. Both axes are represented in percentages relative to their nominal operating point. For the power, this nominal operation is 200 MW, and the nominal production rate is at 7 MTPA (equivalent to 15 kmol s^{-1}). Thus, considering that a typical power trip decreases

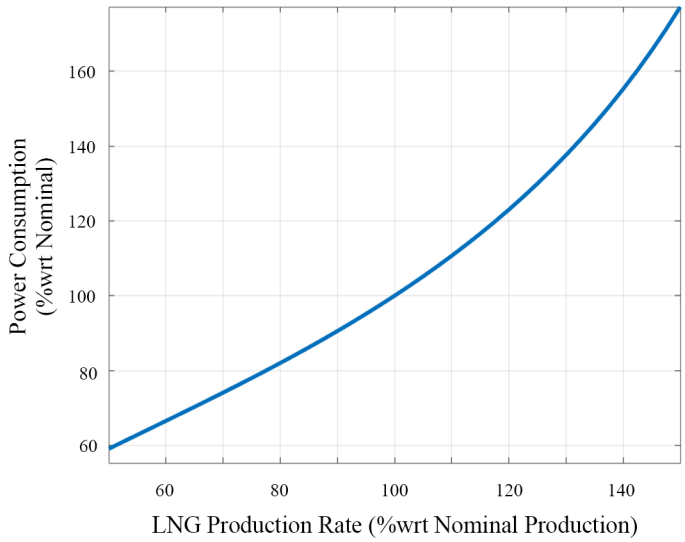


Figure 7.2: Relationship between the LNG production rate and the electrical power consumption, both terms as percentages of their nominal values.

the available power by 30 MW, the remaining power is 170MW, which makes up 85% of the nominal consumption of the plant.

In Figure 7.2, in the nominal operation point, the relationship is almost linear, so decreasing the power consumption to 90% causes the production rate to be at its 90%. However, the relationship loses linearity as the power decreases, and a slight reduction in the power consumption causes a sharper reduction in the production rate. For instance, reducing the power consumption to 60% causes the production rate to be reduced to 50%. The difference in relationships is due to the efficiencies of the compressors. Figure 7.1 illustrated that the lower the LNG production rate, the lower the efficiencies of the compressors, so they would need more electrical power per unit of production.

Figure 7.1 showed that the production rate can decrease up to 59%, and according to Figure 7.2, the LNG production rate reduction corresponds to 65%. Thus, the LNG production can reduce its electrical power consumption up to 65% by decreasing the LNG production to 59%.

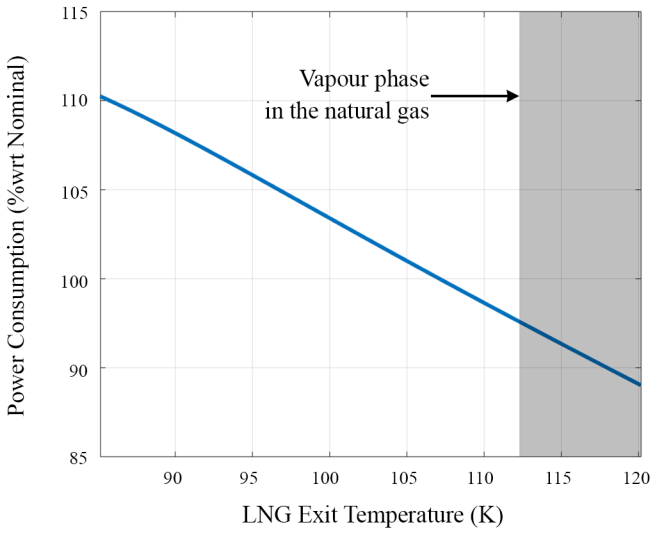


Figure 7.3: Relationship between the temperature of the natural gas at the end of the process (K) and the overall consumption of the plant (as a percentage of the nominal consumption) for a constant production rate and composition. The shaded area on the right represents the area in which the natural gas presents a vapour phase.

The production rate does not need to be reduced as much if other variables are adjusted. The two remaining variables are the LNG temperature at the exit of the process, and the temperature at the flash drum after the precooling stage.

7.2 Effects of the LNG Exit Temperature

The temperature at the exit of the process is established at a lower temperature to provide a comfortable operating buffer. Thus, the LNG temperature at the exit for the nominal operation is -167°C. Figure 7.3 shows, for a constant production rate and composition, how the consumption of the plant varies when the LNG temperature at the exit of the process is adjusted.

The horizontal axis, in this case, represents the LNG temperature at NG6 in K, and the vertical axis shows the power consumption as a percentage of the nominal operation power. Additionally, the black area in the graph represents the range of temperatures at which the natural gas

presents a vapour phase, so the operating point must always be on the left-hand side of that area. Hence, by changing only the LNG exit temperature, the maximum power reduction achievable is 2% of the nominal power.

7.2.1 Discussion of the Effects of the LNG Exit Temperature

When the LNG exit temperature increases, the flow rate of the subcooling cycle decreases, leading to two consequences:

- The consumption of the subcooling compressor decreases
- The subcooling refrigerant carries less heat than when the LNG is at its nominal value, so the precooling and the liquefying cycles do not need to absorb that much heat from the subcooling cycle. This involves two more consequences:
  - The power consumption of the liquefying compressor decreases
  - The reduced liquefying flow rate causes the flow rate of the precooling cycle decreases. Thus, the power consumption of the precooling compressor decreases

Thus, overall, the three compressors will have their consumption reduced by increasing the LNG exit temperature. Figure 7.4 shows the variation of the flow rate of the refrigerants when the LNG exit temperature changes.

When the LNG exit temperature increases, the flow rate of the refrigerants decreases at a slower rate than it does when the LNG production rate decreases. This indicates that this method is not as effective or direct as decreasing the production rate, but it is a manner of obtaining an extra power reduction without decreasing the production rate as much.

Thus, the higher the exit temperature, the lower the power consumption of the plant. As the power reduction gets lower, the LNG exit temperature becomes closer to the saturation point, so it is important to consider this trade-off: the process is reducing the power consumption

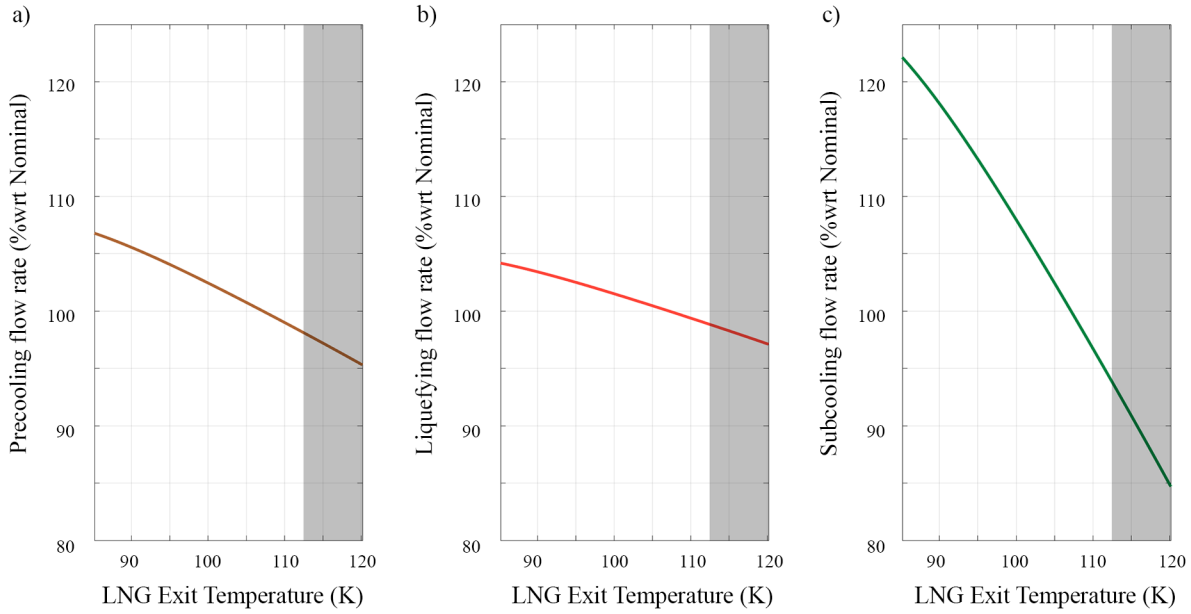


Figure 7.4: Effects of varying the LNG exit temperature (K) on the flow rate of the refrigerants (% wrt their nominal values). The shaded areas represent the temperatures at which the natural gas presents a vapour phase.

but with the added risk of obtaining a natural gas that is not completely liquid. In practice, the natural gas at the end of the process might present a vapour state, but that vapour can be recycled to cool it down further to become liquid.

7.3 Effects of the LNG Flash Drum Temperature

The natural gas flash drum separates the heavy compounds of the natural gas that condensed in the precooling cycle. After the precooling stage, in the nominal operation, around the 8% of the natural gas has condensed, and the resultant vapour has a higher concentration of lighter components than the natural gas before the precooling stage. As a measure of purity, the results refer to the methane mole fraction.

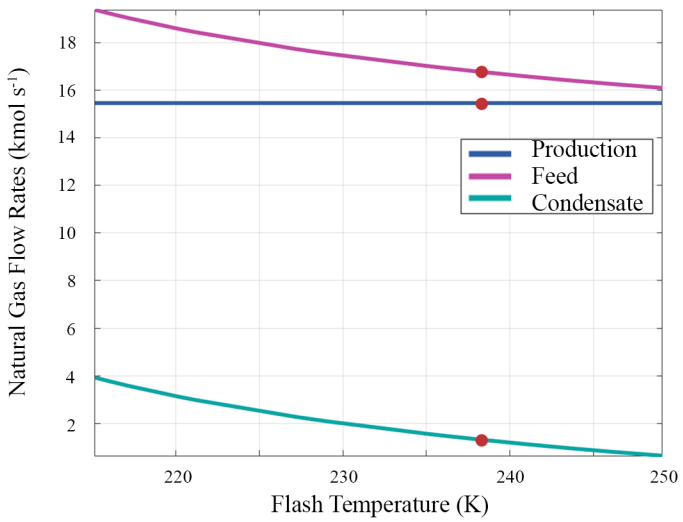


Figure 7.5: Relationships between the natural gas flow rates (kmol s^{-}1) entering and exiting the flash drum and the temperature in the flash (K). The red dots represent the nominal operating temperature (238.15 K)

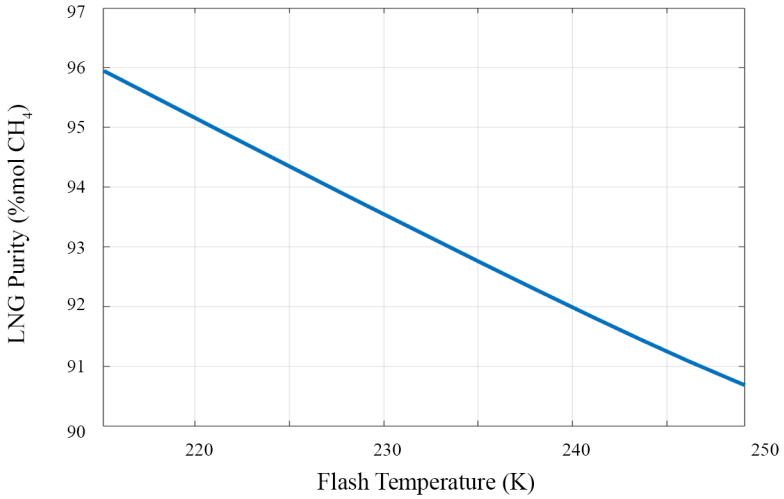


Figure 7.6: Relationship between the purity of the natural gas at the end of the process (measured as its CH_4 content in % mol) and the temperature of the flash drum (K)

The temperature in the drum is the same as the temperature of the stream entering in it (NG2), and the streams coming out from it (NG3, and NG4). The lower the temperature, the more natural gas condenses, and vice versa. The calculations keep the production rate constant as the flash drum temperature changes to isolate this variable from the LNG production rate. Thus, the production rate is maintained constant by varying the natural gas feed according to the amount of natural gas that condenses in the flash drum. Figure 7.5 shows the variation of the flow rates of the natural gas feeding, the vapour rate, and the condensate rate when the temperature in the flash varies.

The horizontal axis shows the temperature at NG2, NG3, and NG4 in K, and the vertical axis represents the flow rates of the feed, vapour, and condensate in kmol s^{-1}. The red points represent the nominal operating point found at 238.15 K. The sum of flow rates of the vapour and liquid is always equal to the flow rate of feeding, and the vapour exiting the flash drum is constant.

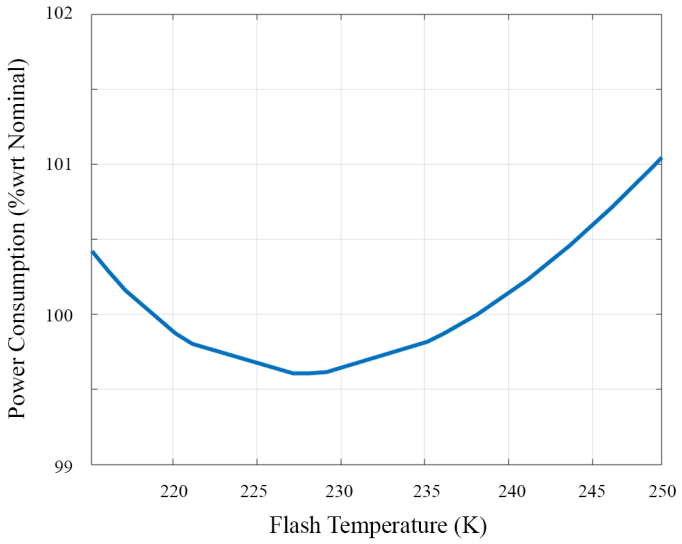


Figure 7.7: Relationship between the overall consumption of the plant (as a percentage of its nominal value) and the temperature of the flash drum (K).

The presence of lighter components increases as the flash temperature decreases. Figure 7.6 shows this relationship. In the figure, the horizontal axis represents the flash temperature in K, and the vertical axis is the purity of the vapour measured as the CH_4 content in % mol. Figure 7.7 shows the consumption of the plant when the temperature in the flash changes. The horizontal axis is the temperature of the flash separator, and the vertical axis is the process consumption percentage with respect to the nominal power.

Figure 7.7 shows that the consumption of the plant slightly varies from the nominal point when the temperature in the flash drum varies. The minimum power consumption corresponds to a temperature of 227 K, with a reduction of less than 0.5%.

7.3.1 Discussion of the Effects of the LNG Flash Separator Temperature

From Figure 7.5, at lower temperatures, there is more feed to be treated. This feeding increase causes the precooling refrigerant flow rate to be higher. Figure 7.8.a) shows the precooling

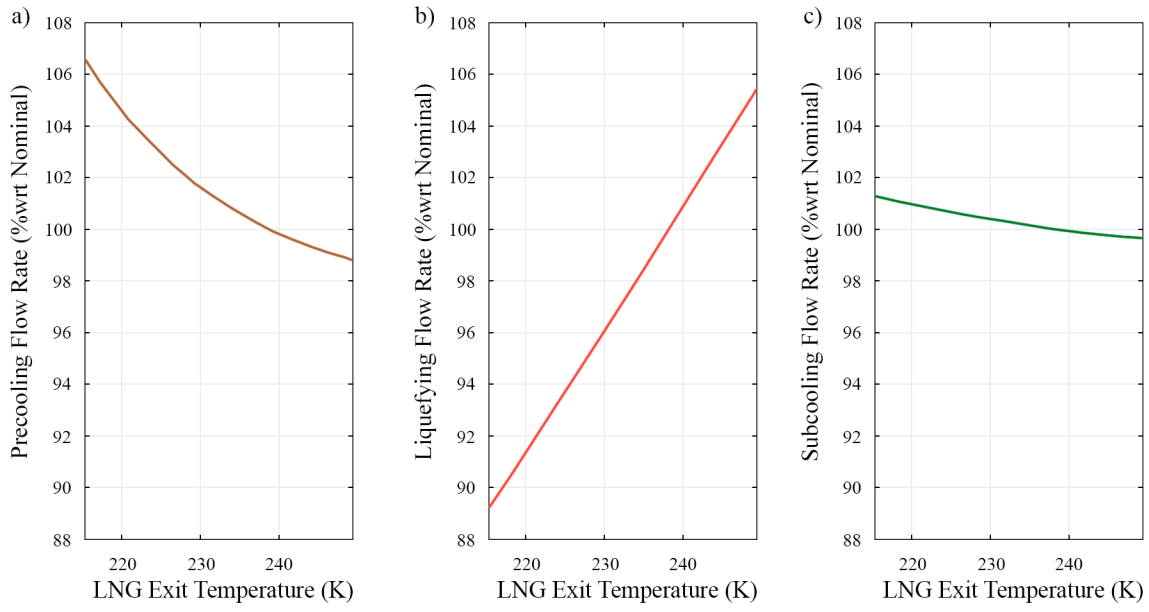


Figure 7.8: Effects of varying the temperature in the flash drum (K) on the flow rate of the refrigerants (% wrt their nominal values).

refrigerant flow rate when the temperature of the flash changes. The power consumption of the precooling compressor is increased due to the increase of flow rate.

Figure 7.5 illustrated that the flow rate of vapour after the flash does not depend on the temperature of the flash. Figure 7.8 shows that the liquefying refrigerant flow rate depends on the flash temperature, even though it absorbs heat from the same amount of natural gas flow rate. This is due to the change of specific enthalpy of the natural gas stream due to the presence of other hydrocarbons.

Two main variables cause the specific enthalpy to vary, the temperature, and purity. Figure 7.6 shows that the concentration of lighter components increases with a lower flash temperature. A lighter component, such as methane, has a lower heat capacity than a heavier component. Thus, a lower temperature in the flash drum implies a lighter mixture, that, in turn, means a lower heat capacity.

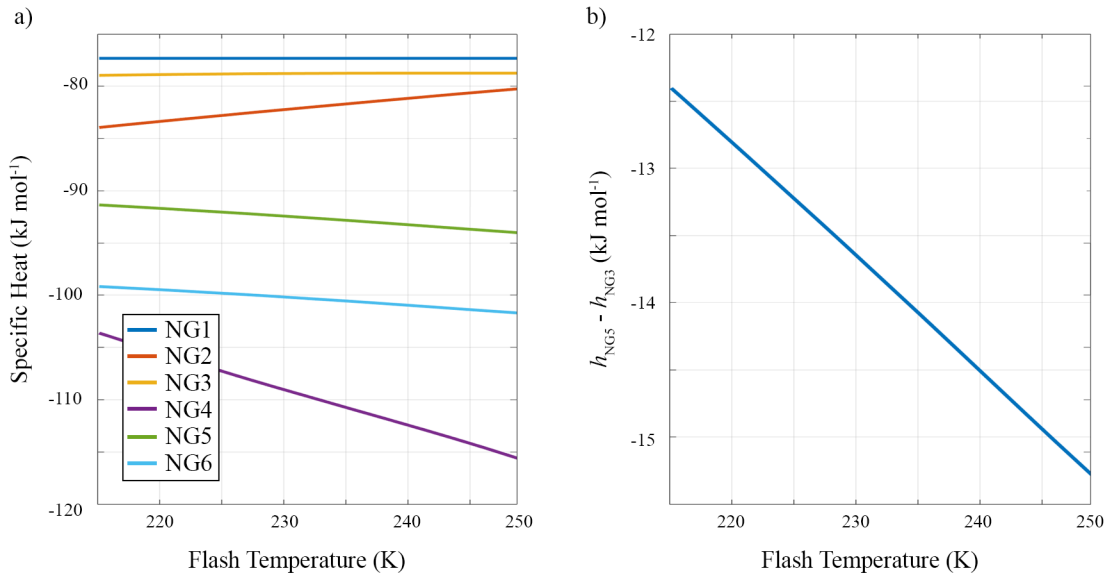


Figure 7.9: a) Relationships between the enthalpies of each stream of the natural gas (kJ mol^{-1}) and the temperature of the flash separator (K), and b) relationship of the difference of enthalpies between NG5 and NG3 (kJ mol^{-1}) and the temperature of the flash separator (K)

Figure 7.9.a) shows the relationship between the flash temperature and the specific enthalpies of the natural gas streams. The graph gives the values of the specific enthalpies as their absolute values, without taking any reference. Thus, the lower in the graph, the higher the difference with respect to the reference.

The difference $h_{\mathrm{NG5}} - h_{\mathrm{NG3}}$ is the specific heat that the liquefying refrigerant has to absorb. The specific enthalpy at stream NG5 increases as the flash temperature increases, whereas the specific enthalpy at stream NG3 is almost constant. The specific enthalpy h_{NG3} is virtually constant because the decrease in heat capacity offsets the increase in specific enthalpy caused by the increase of temperature. Figure 7.9.b) shows the difference between the specific enthalpies in streams NG5 and NG3 ($h_{\mathrm{NG5}} - h_{\mathrm{NG3}}$). The higher the temperature in the flash separator, the more heat to be absorbed by the liquefying refrigerant, and therefore, the higher the liquefying refrigerant flow rate.

Thus, from Figure 7.7, the power consumption does not notably vary because the flow rate of the refrigerants acts inversely to each other when the temperature in the flash drum change. For instance, when the temperature in the flash drum increases, the flow rate of the precooling and subcooling cycles decrease, but the flow rate of liquefying refrigerant increases.

7.4 Effects of the Combined Variables

One of the objectives in an industrial plant is to obtain the maximum possible amount of product. Thus, this research studies how to reduce the power consumption of the LNG plant while minimising the production rate reduction. Adjusting the LNG temperature at the exit or the temperature in the flash separator alleviates the reduction of production rate.

The individual effects of varying the LNG temperature at the end of the process or the temperature in the flash separator are not significant. Nevertheless, combining their effects can increase their individual impact for obtaining more production rate. This section shows the results of adjusting more than one variable.

7.4.1 Flow rate and LNG Exit Temperature

Figure 7.10 shows the consequences of changing the production rate and the LNG exit temperature on the consumption of the plant. The horizontal axis illustrates the LNG production rate as a percentage of the nominal production rate, the vertical axis is the electrical power consumption as a percentage of the nominal power consumption, and each curve represents an isotherm for the LNG exit temperature. The shaded area is the area in which the natural gas is in the vapour phase at 1 bar, so the operating point cannot be within that area.

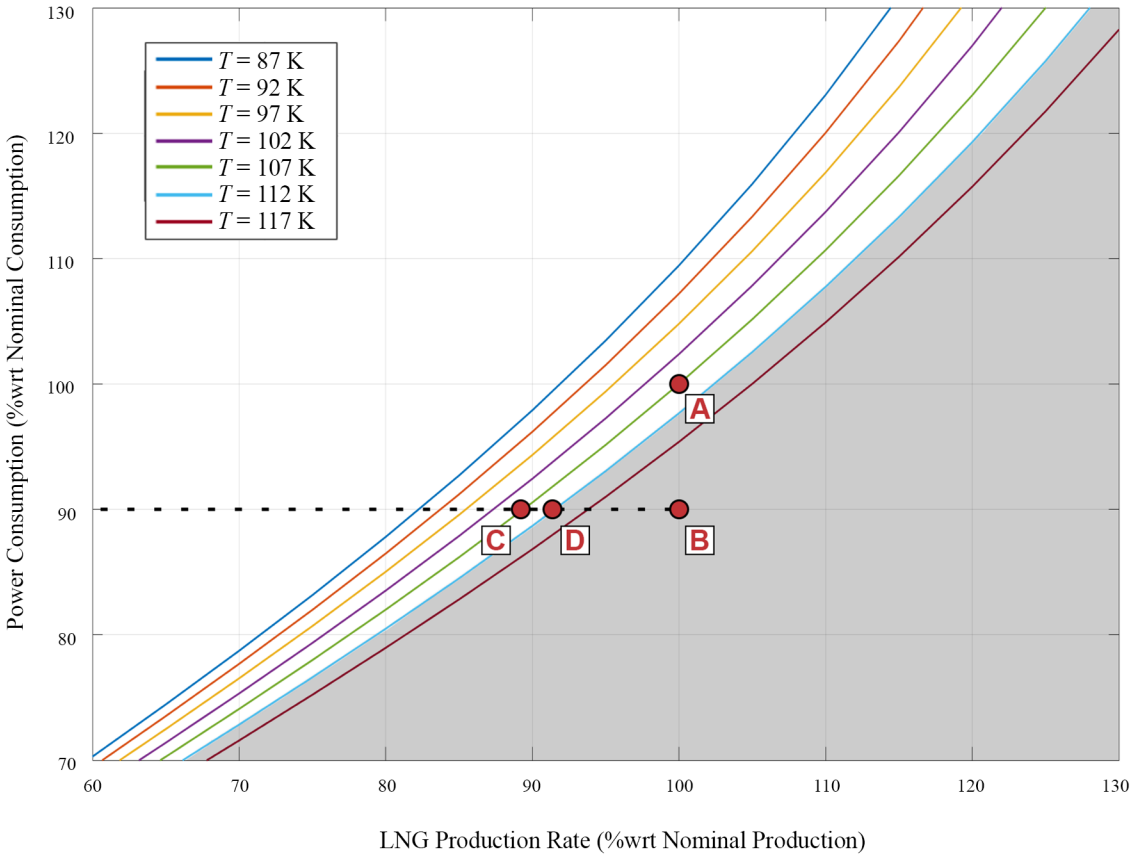


Figure 7.10: Overall consumption of the whole LNG plant (as a percentage of its nominal value) when the natural gas production rate (as a percentage of its nominal value) varies. Each curve represents the natural gas temperature at the end of the process. The shaded area represents the temperatures at which the natural gas presents a liquid phase. Each red dot indicates a different operating point.

Changing an additional variable apart from the production flow rate can result in the same power reduction without reducing the production flow rate as much. For example, in Figure 7.10, the nominal point is at point A. If the power is reduced to 90%, there are three alternatives:

- **Changing the temperature**: The LNG exit temperature can be increased to reach point B. However, this point falls within the shaded area mentioned before. This means that it is infeasible to obtain that power reduction by solely changing the LNG exit temperature
- **Changing the production flow rate**: The production flow rate can be reduced to reach point C. This point implies a reduction in the production flow rate to 89%
- **Changing both temperature and production flow rate**: If both variables are changed, without the temperature reaching the saturation point, the operating point can be at point D. In this point, the reduction flow rate is reduced to 92%

Thus, increasing the exit temperature less than 5 K can increase the production rate by 3%. In this case, it implies going from 13.35 kmol $s^{-1}$to 13.8 kmol s^{-1}, which makes a difference of 622 tonnes of LNG per day.

7.4.2 Flow rate, LNG Exit Temperature, and Flash Temperature

Section 7.3.1 showed that changing the temperature of the flash temperature is not very effective. Nevertheless, during that section, the production flow rate remained constant by changing the feed flow rate. Figure 7.11.a) shows the consequences of varying the temperature in the flash drum while keeping the feed rate constant. Figure 7.11.b) shows the vapour fraction in the flash drum when the temperature in it changes. The red dots represent the nominal operation at 238.15 K. In contrast to Figure 7.5, in which the production rate is fixed, this graph let the production rate to vary, while keeping the feed rate fixed.

From Figure 7.11, due to the lower vapour fraction, the LNG production rate decreases when the flash temperature is reduced. Thus, if the natural gas feed rate is constant, the LNG production

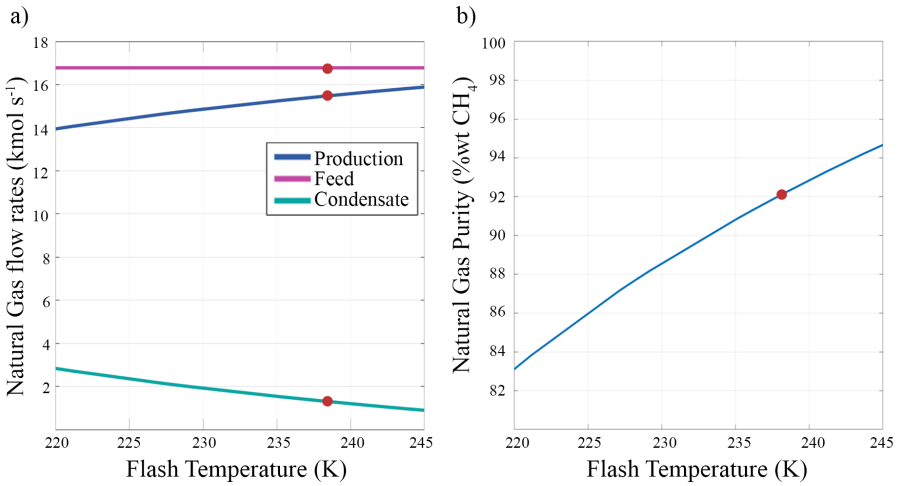


Figure 7.11: Effects of varying the flash drum temperature (K) on the a) natural gas flow rates (kmol s^{-1}) of the streams exiting the flash drum when the feed rate is kept constant, and on the b) composition of the LNG (% wt CH_4). The red dots represent the nominal operating temperature.

rate varies with the flash temperature according to the following equation:

$$F_{\text{LNG}} = F_{\text{Feed}}\ \psi$$

where F_{Feed} is the feed rate in kmol s^{-1}, F_{LNG} is the production rate in kmol s^{-1}, and ψ is the vapour fraction in the flash drum.

The graphs in the following analysis show the electrical power consumption of the plant when two variables are changed, and the remaining one is kept at its nominal value.

Flash Temperature and LNG Production Rate

Figure 7.12 illustrates the change in the power consumed when the production rate and the flash temperature are varied, and maintaining the LNG exit temperature constant.

The LNG production rate has a greater impact on the power consumption than the temperature of the flash drum. When the temperature in the flash drum changes, the natural gas feed rate

has to change accordingly for reaching the same LNG production rate. Therefore, changing the temperature in the flash drum also changes the LNG production rate.

Flash Temperature and Exit Temperature

Figure 7.13 illustrates the change in the power consumed when the LNG exit temperature and the flash temperature are varied, maintaining the LNG production rate constant.

The only variable that can make a significant difference is the exit temperature. Varying the exit temperature can cause variations of up to 10% on the the nominal power consumption.

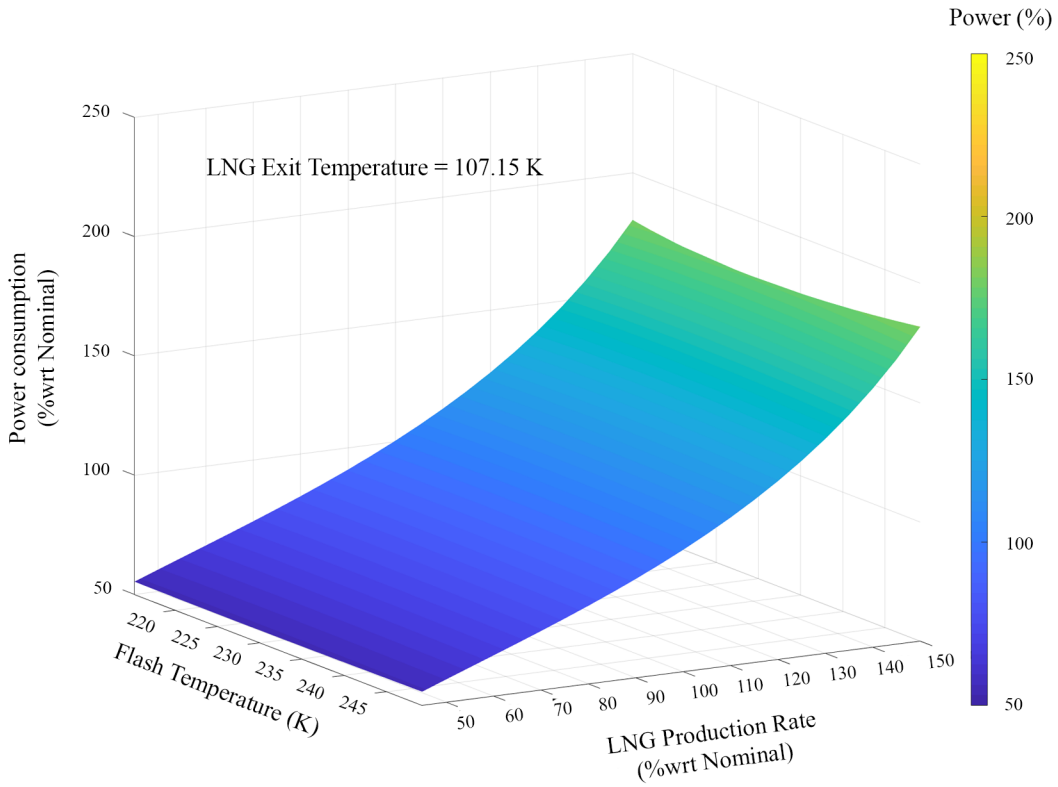


Figure 7.12: Effects of varying the LNG production rate (as a percentage of its nominal value) and the temperature at the flash separator (K) on the overall electrical power consumption of the plant (MW), when the natural gas temperature at the end of process is constant at 107.15 K.

LNG Production Rate and Exit Temperature

Figure 7.14 illustrates the change in the power consumed when the LNG exit temperature and the LNG production rate are varied while maintaining the flash temperature constant.

The effect of varying the LNG exit temperature on the power consumption is higher when the LNG production rate is higher. This is observed in the slope of the curve when the LNG production is at 110%, which, compared to the slope when the LNG production is at 50%, is much more pronounced. This is because both factors cause a high flow rate of refrigerants, reaching points where the isentropic efficiency has acutely decreased (Section 7.1). This causes

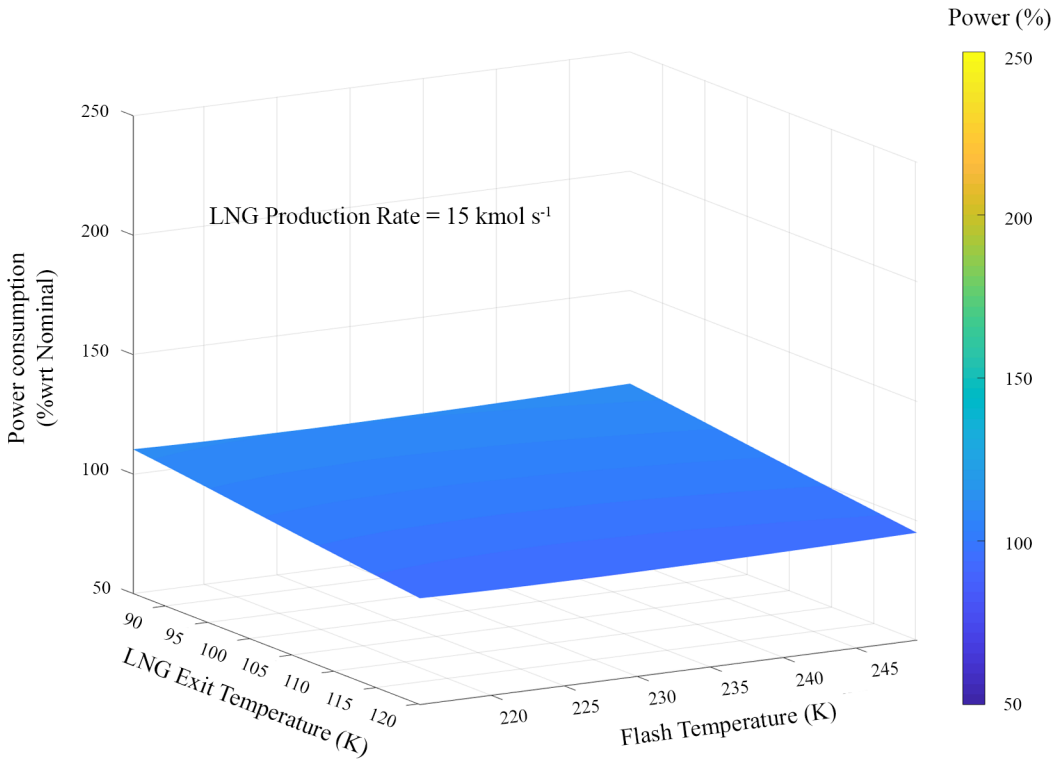


Figure 7.13: Effects of varying the natural gas temperature at the end of process (K) and the temperature at the flash separator (K) on the overall electrical power consumption of the plant (MW), when the LNG production rate is constant at 15 kmol s^{-1}.

the power consumed by the compressors to be much more pronounced for achieving the same discharge pressure.

This section has presented the influence of changing two variables on the electrical power consumption, while keeping the third one constant. Appendix C.5 shows a methodology for plotting the three variables, creating an envelope of operation.

7.5 Discussion of the Results

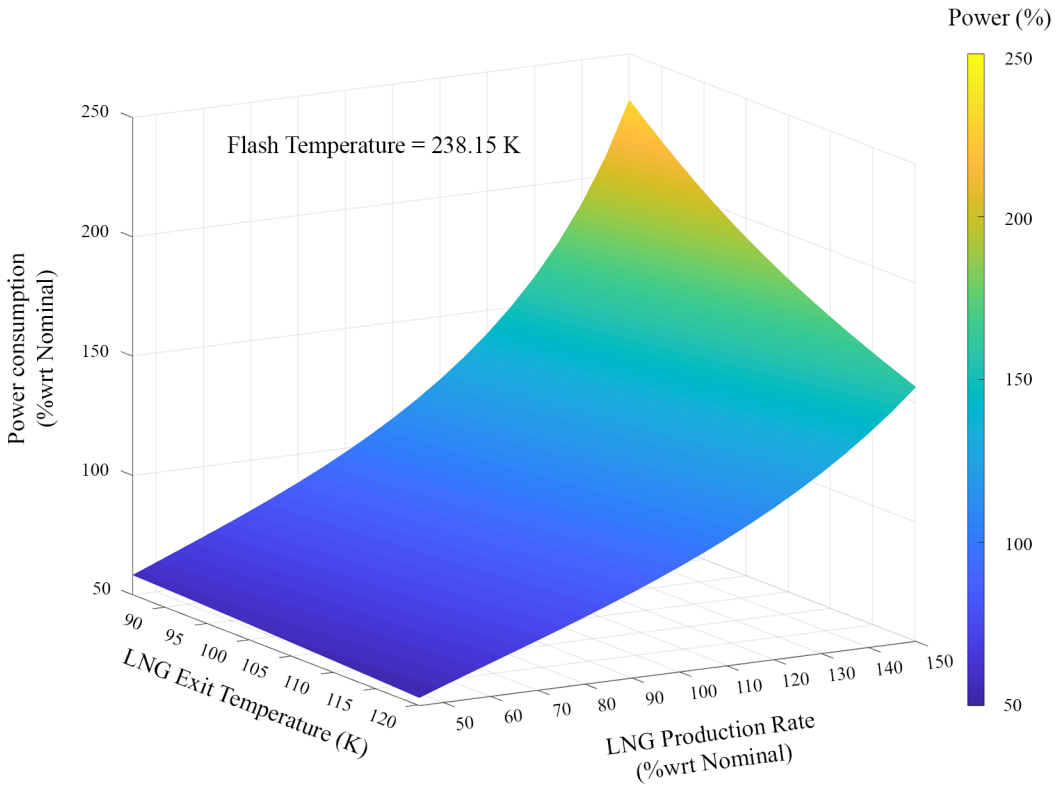


Figure 7.14: Effects of varying the natural gas temperature at the end of process (K) and the LNG production rate (as a percentage of its nominal value) on the overall electrical power consumption of the plant (MW), when the temperature at the flash separator is constant at 238.15 K.

Table 7.1: Maximum production rate that can be achieved if one or more process variables are changed for a given power reduction. The exit temperature and the drum temperature that maximise the production rate are, respectively, 112.15 K and 227.15 K

Power (%)	Production Rate	LNG Exit Temperature and Production Rate	Flash Drum Temperature and Production Rate	Exit Temperature, Flash Drum Temperature, and Production Rate
100%	100	102	100.5	104
95%	95	98	96.5	99
90%	88	92	89	94
85%	83	86	84	87.5
80%	77	79	77.5	81
75%	70	72	70.5	73

The results in Table 7.1 show that changing the LNG production rate has the highest impact on the power consumption. Other variables, such as temperature or pressure also influence the total electrical power consumption, but the consequences of varying these properties are not as great. Varying the LNG exit temperature or composition can reduce the decrease of LNG production rate.

Table 7.1 shows the maximum achievable production rate when varying only the production rate, when varying the production rate and the exit temperature, when varying the production rate and the flash temperature, and when all three variables are varied.

Changing two variables increases the maximum achievable production rate compared to only varying the production rate. The achievable production rates in the third column (changing exit temperature and production rate) are higher than the achievable production rates in the fourth column (changing flash drum temperature and production rate). Thus, if the temperature at the exit of the process and the production rate vary, the achievable production rate does not decrease as much as it would decrease if only one variable changed.

The obtained production rate is not just the sum of each effect because the influence of each variable complements each other. For example, for an 85% power reduction, varying the exit

temperature implies 3% more achievable production rate compared to solely changing the production rate. Adjusting the flash drum temperature means 1% more achievable production rate compared to solely changing the production rate.

If all three variables are changed, the achievable production rate increases by 4.5% of its nominal value. The reason for this increase is because of the combined effects of the exit temperature and the composition of the LNG. Adjusting the temperature in the flash drum affects the heat capacity of the LNG. Moreover, increasing the LNG temperature at the exit of the process makes the amount of heat to be absorbed lower. Therefore, the combination of both factors makes the heat that the refrigerants need to absorb to be smaller, so the electrical consumption of the compressors decreases as well.

The results obtained in this chapter provides an envelope of feasible operation that the PPM can use. In an electrical contingency, the PPM can use the envelope to reduce the electrical consumption, and establish values to the LNG production rate, the LNG exit temperature, and the temperature in the flash drum. The established values of the process variables have to be consistent with the available electrical power.

7.6 Summary of the Chapter

This chapter has analysed the effects of varying the Liquefied Natural Gas (LNG) production rate, the LNG exit temperature, and the LNG composition on the electrical power consumption. During the analysis, the discharge pressure of the compressors is constant at the operating point found in Chapter 6.

The results have shown that the relationship between the LNG production rate and electrical power consumption is not linear due to the isentropic efficiency of the compressors. The results have shown that the electrical power consumption can be reduced to 65%. A power reduction below this point causes the subcooling compressor to fall within the choke region. A power reduction of 65% corresponds to a reduction in the LNG production rate of 59%.

The results have shown that the electrical power consumption decreases when the LNG exit temperature increases. However, varying the LNG exit temperature does not significantly affect the electrical power consumption. Thus, changing the LNG exit temperature could be more useful for alleviating the reduction in LNG production rate.

The analysis of the LNG composition showed that an LNG stream richer in lighter compounds requires less electrical power consumption. Lighter components have lower heat capacities, and therefore, decreasing their temperature requires less heat absorbed.

Combining the effects of the LNG exit temperature and the LNG composition is not the addition of each effect. Each individual effect contributes to the other process variables. If combined, for a given electrical power consumption, the effects of both variables can increase the achievable LNG production rate to 104%.

Chapter 8

Summary of the Analysis of the LNG Process

This part has shown a deep insight into the physical mechanisms in the Liquefied Natural Gas (LNG) process. The analysis includes the mathematical model of the process and the procedure for solving it. The model contains the thermodynamic equations of the system, and the description of the main effects in the process needed to understand the modelling, and the results of the simulations carried out with the mathematical model.

An essential aspect of the description of the thermodynamics is the Joule-Thomson effect. This effect is crucial for understanding the operating point of the compressors in the process, and it also reflects the importance of having an accurate Vapour and Liquid Equilibrium (VLE) model.

The model uses the Redlich-Kwong Soave (RKS) equations of state, and they are formulated for a mixture of real fluids. Modelling accurately the RKS has been crucial for obtaining accurate results, especially when there is a VLE present in the stream that is modelled.

The model has five degrees of freedom, which are used for varying the discharge pressure of two compressors, the LNG temperature at the exit of the process (NG6), the temperature in the flash drum (NG2), and the LNG production rate.

Results showed that the operating point reaches a minimum power consumption when the pressures in the streams entering their corresponding heat exchangers are just above their bubble point (stream P1 for the precooling refrigerant, L2 for the liquefying refrigerant, and S3 for the subcooling refrigerant). These pressures are 10 bars for the precooling refrigerant, 9.8 bars for the liquefying refrigerant, and 5.5 bars for the subcooling refrigerant. However, the limits of the compressors establish that the subcooling refrigerant, for the necessary flow rate, cannot be below 8 bars. Thus, the next optimal point is at the bubble point of the subcooling stream entering the second heat exchanger (S2), which corresponds to 33.5 bars.

The industrial practice is to operate the compressors with a margin. Thus, a disturbance in the discharge pressure would not change the phase of the refrigerants abruptly. Therefore, the model set the discharge pressures at 15 bars for the precooling refrigerant, 15 bars for the liquefying refrigerant, and 35 bars for the subcooling refrigerant.

With the pressure fixed, the three remaining variables are changed to observe their influence on the electrical consumption of the plant. The results have shown that power consumption mainly depends on the production rate. The relationship is not linear, however, because the efficiency of the compressors reduces when operated away from their normal operating point.

Two other variables also affect power consumption, namely the LNG temperature at the exit of the process, and the composition of the LNG, which is varied adjusting the temperature in the flash drum. These variables change the specific enthalpy of the natural gas streams, so they can be adjusted to a certain limit to increase the achievable LNG production rate.

The results ultimately are used for creating an envelope of feasible operation. In an electrical contingency event, the process power management system uses this envelope to reduce the power consumption of the compressors and to provide new set points to the process variables according to the power reduction.

Flexible operation is intended to be used as a tool for establishing the new operating point by giving a family of set points that are going to make the process suitable for the upcoming power consumption. The results have demonstrated the potential of flexible operation in an LNG plant,

giving not only a wide range of possible power consumptions in which the LNG process could work but also a wide range of possible families of curves that would achieve the desired power consumption.

Part III

Flexible Operation in the Aluminium Smelter

Chapter 9

Modelling of the Aluminium Smelting Process

The model determines how electrical energy is transformed into other forms of energy in the aluminium smelting process. The process involves chemical energy used to develop the reactions, thermal energy to keep high temperatures and the aluminium molten, and electrical energy for the reduction reaction. Additionally, the electrical current heats the electrolyte bath as a result of the Joule heating effect.

Due to the high temperatures in the bath, if the electrical power consumed is reduced, the residual heat keeps the temperature at acceptable levels during a certain period of time. This duration depends on the magnitude of the power reduction, the surroundings of the bath, and the bath properties, such as the heat capacity, conductivity, or temperature.

Figure 9.1 shows the electrolyte cell where the aluminium reduction takes place. The electrical input is at the anode bridge, which transports the current to the anode rods, and then to the anode blocks. The blocks are submerged in the cryolite bath, whose operating temperature is around 1250 K, and the dissolved alumina undergoes an electrochemical reaction, whereby aluminium is produced, collected in the cathode, and transported outside of the cell by the collector bars.

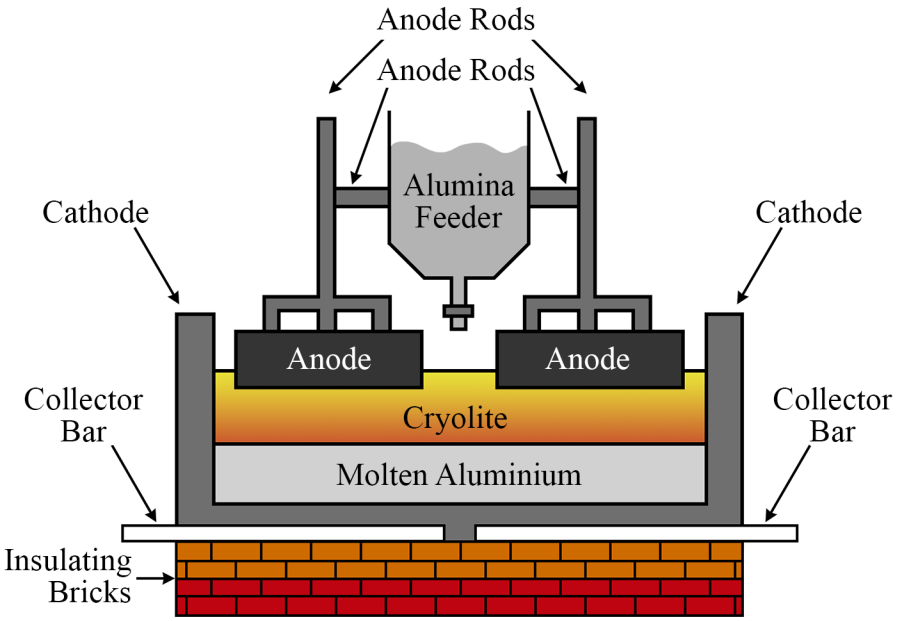


Figure 9.1: Scheme of an electrolytic cell. A regular aluminium smelting plant has several cells in parallel, with a total consumption of hundreds or thousands of megawatts (The Norðurál plant has an electrical consumption of 1.4 GW (Norðurál, 2019)). Electric current enters from the anode rods to the cathode. The cryolite bath dissolves the alumina, which is added using the feeder at the top. The produced aluminium is extracted at the bottom of the bath, and it flows through the collector bars, so that it can be stocked.

9.1 Modelling Principles

This section introduces the process basics for each part of the whole model. The model is divided into three sub-models, namely the mass balance model, the electrical model, and the heat balance model.

9.1.1 Principles of the Mass Balance Model

This subsection introduces the basic principles in the mass balance, involving the composition of the bath, and the reactions that affect the composition. The concentration of each component defines the properties of the electrolyte, such as the heat capacity, or the electrical conductiv-

ity. These properties are used as inputs to the heat balance model, and to the electrical model respectively.

Theoretical Production Rate of Aluminium

The main reaction for aluminium production is:

$$2\,Al_2O_3 + 3\,C \longrightarrow 4\,Al + 3\,CO_2 \tag{9.1}$$

Reaction 9.1 is a reduction reaction, so it needs an electrical potential. This is provided by an electrical current flowing through the bath containing the dissolved alumina, which will cause electrons to move from the cathode to the anode. The redox form of 9.1 is:

$$4\,Al \longrightarrow 4\,Al^{3+} + 12\,e^-$$

$$3\,O_2 + 12\,e^- \longrightarrow 6\,O^{2-}$$

Thus, for every mole of aluminium formed, there are three electrons moving from the cathode to the anode. Hence, the aluminium production rate can be calculated using the Faraday's law of electrolysis. This law relates the production rate to the average current passed through the electrolyte:

$$n = \frac{C}{F n_{e^-}} \tag{9.2}$$

where n is the number of moles generated in the electrolysis, C is the electric charge in coulombs (C), F is the Faraday constant equal to 96485.33 C mol $^{-1}$, and n_{e^-} is the number of electron flowing from the cathode to the anode. The electric charge is a measure of the current over time, $\Delta C(t) = \int_0^t I(\tau) d\tau$, where t is the elapsed time of electrolysis:

$$n = \frac{I\,t}{96485.33 \times 3} \rightarrow n = 3.455 \times 10^{-6} I \quad \text{mol s}^{-1} \tag{9.3}$$

The molar mass of aluminium is 26.98 g mol $^{-1}$, so Eq. 9.3 in mass terms is:

$$m = 9.321 \times 10^{-8}\, I \quad \mathrm{kg_{Al} s^{-1}} \tag{9.4}$$

Electrolyte Components

While the melting point of aluminium is 933.47 K, the cryolite (Na_3AlF_6) used for dissolving alumina has a melting point of 1284.15 K. Thus, the operating temperature must be above 1284.15 K, but keeping high temperatures is very energy demanding. Therefore, additives are included to decrease the cryolite melting point. The basic additives are aluminium fluoride (AlF_3), and calcium fluoride (CaF_2). Lithium Fluoride (LiF), and magnesium fluoride (MgF_2) are also added for reducing even more the melting point, and for increasing the electrical conductivity of the bath. With these additives, the melting point can be lowered to 1153.15 K.

Bath Ratio

A mole of cryolite is composed of three moles of sodium fluoride (NaF), and one mole of AlF_3:

$$Na_3AlF_6 \longrightarrow 3\,NaF + AlF_3$$

The ratio between the amount of NaF with respect to the AlF_3 present in the bath is called bath ratio (R_b).

$$R_b(\text{mol }\%) = \frac{3\ \text{NaF}}{1\ \text{AlF}_3} = 3$$

$$R_b(\text{wt }\%) = \frac{3 \times 41.988}{83.9767} = 1.5$$

The excess AlF_3 has to be differentiated from the cryolite AlF_3. The cryolite AlF_3 is the minimum AlF_3 to form cryolite. In industrial practice, the bath ratio varies between 1.00 and 1.25. To adjust this ratio, sodium carbonate (Na_2CO_3) or more AlF_3 is added to the bath. The max-

imum R_b mol% is 3, which is the corresponding to the ratio of the cryolite with no excess AlF_3.

9.1.2 Principles of the Electrical Model

The voltage drop depends on the characteristics of the bath, and the necessary electrical current depends on the established production rate and the temperature of the bath.

Current Efficiency

Eq. 9.4 defined the theoretical aluminium production rate per ampere in kilograms. In reality, however, the production rate is smaller due to the reaction between the aluminium and the carbon dioxide that appears during the reduction reaction:

$$2\,Al + 3\,CO_2 \longrightarrow Al_2O_3 + 3\,CO \tag{9.5}$$

The ratio between the actual production rate and the theoretical production rate is known as current efficiency (η), and it is represented as a percentage. Thus, the actual production rate is:

$$m = 9.321 \times 10^{-8}\, I\, \eta \quad \mathrm{kg_{Al} s^{-1}} \tag{9.6}$$

The current efficiency depends on the electrolyte properties, such as the viscosity, density, and the solubility of aluminium in the electrolyte. The calculation of this efficiency will be further explained in Section 9.1.4.

Anode Effect

Increasing the conductivity of the bath also improves the efficiency of the plant, since a lower voltage drop is achieved. In industrial practice, the usual voltage drop of the whole cell is

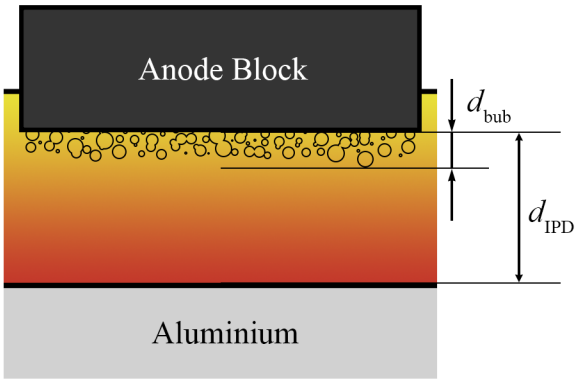


Figure 9.2: Schematic representation of the IPD and the bubble layer thickness to calculate the voltage drop in the electrolyte bath

between 4 and 4.5 V. This voltage drop is affected by the composition of the bath, as mentioned above, but it can also be affected by the anode effect.

In regular operation, a layer of CO_2 bubbles is present in the anode surface due to the reduction reaction taking place in the bath. The *anode effect* consists of the thickening of the layer of bubbles, offering a higher electrical resistance, which causes the voltage to rise from around 4 V to 80 V. The anode effect appears when the alumina concentration in the bath falls below a critical value that depends on the operating conditions, varying from 0.5 to 2 % wt.

Voltage Drop in the Electrolyte

The distance between the anode and the aluminium pad is named Interpolar Distance (IPD). This distance can be varied by lowering or raising the anode within some limits.

Figure 9.2 shows the layers within the electrolyte bath. To calculate the voltage drop, the model considers the bubble layer thickness d_{bub}, so the IPD free from bubbles is $d_{IPD} - d_{bub}$. The current does not flow inside the bubbles, so the effective area in which current is flowing through the anode can be defined as $A_{eff} = A_{an} - A_{bub}$, where A_{eff} is the effective area, A_{an}, is the area of the anode, and A_{bub} is the cross-sectional area of the bubbles attached to the anode.

Considering that κ is the electrical conductivity of the electrolyte, the voltage drop is:

$$\begin{aligned} V = R\,I = \kappa\,\frac{L}{A}\,I \\ V = I\,\kappa\,\left(\frac{d_{\mathrm{IPD}} - d_{\mathrm{bub}}}{A_{\mathrm{an}}} + \frac{d_{\mathrm{Bub}}}{A_{\mathrm{bub}}}\right) \end{aligned} \tag{9.7}$$

where d_{IPD} is the magnitude of IPD in cm. Eq. 9.7 shows that there are two factors that increase the voltage drop: a larger IPD, and a thicker bubble layer. For a fixed electrical current a higher voltage drop means more electrical power is consumed, and at the same time, means more heat generated in the cell due to the Joule heating effect.

9.1.3 Principles of the Heat Balance Model

The temperature of the bath depends on the heat generated or absorbed by the mechanisms involved during the electrolysis.

Enthalpy and Gibbs Energy

The electricity provided to the cell is used for increasing the internal energy of the products with respect to the reactants (ΔU in W), and for providing heat to the cell (Q_{cell} in W):

$$W_{\mathrm{cell}} = \Delta U + Q_{\mathrm{cell}} \tag{9.8}$$

Where W_{cell} is the electrical power provided to the electrolyte cell in W. ΔU is used for increasing the work and the heat of the system. Applying Eq. 9.8 to the reduction reaction (Eq. 9.1) work can be divided into two terms, the electrical power deployed to carry out the reaction, and the work for expanding the gases produced by the reaction. In a reversible reaction, the heat is equal to $T\Delta S$, where T is the temperature in K and S is the entropy in J mol^{-1} K^{-1}. Therefore:

$$\Delta U = W_{\mathrm{Reaction}} - p\Delta V + T\Delta S \tag{9.9}$$

where W_{Reaction} is the power needed by the alumina reduction in W, and $p\Delta V$ is the work for expanding the gases that appear from the reaction. Considering that enthalpy is the sum of the internal energy and the work for expanding the system:

$$\begin{aligned} \Delta H &= \Delta U + p\Delta V \\ \Delta H &= (W_{\text{Reaction}} - p\Delta V + T\Delta S) + p\Delta V \\ \Delta H &= W_{\text{Reaction}} + T\Delta S \end{aligned} \tag{9.10}$$

Thus, the necessary power for carrying out the alumina reduction is:

$$W_{\text{Reaction}} = \Delta H - T\Delta S \tag{9.11}$$

where W_{Reaction} is the power needed by the alumina reduction in W. The term $(\Delta H - T\Delta S)$ is known as *Gibbs Energy* (ΔG), and is the minimum energy needed for the reaction to happen. The Gibbs energy for a chemical reaction is the sum of the Gibbs energies of formation of the products minus the Gibbs energies of formation of the reactants. Thus, for Reaction 9.1, the Gibbs energy is:

$$\Delta G = 1.5\ G_f(\text{CO}_2) - G_f(\text{Al}_2\text{O}_3)$$

where G_f is the Gibbs energy of formation in kJ mol^{-1}, which is zero for pure substances. The values for this term can be found in the literature (Chase, 1998).

9.1.4 Electrolyte Properties

The properties of the electrolyte have consequences on the mass and energy balances, and on the electrical model. This section outlines each property in the bath.

Current Efficiency

The current efficiency is the ratio between the actual aluminium production rate and the theoretical aluminium production rate. This efficiency is a function of the solubility and mass transfer of the metal in the bath. Therefore, the ratio between the mass transfer rate and the production rate gives the current efficiency:

$$\eta = 100 \left(1 - \frac{r_{\text{mass}}}{r_{\text{prod}}} \right) \tag{9.12}$$

where η is the current efficiency, r_{mass} is the rate of mass transfer of aluminium, and r_{prod} is the aluminium production rate. As seen in Eq. 9.3, and noticing that the rate is the production divided by the time, this rate can be written as:

$$r_{\text{prod}} = \frac{I}{3\,F} \quad \text{mol s}^{-1}$$

therefore, Eq. 9.12 results in:

$$\eta = 1 - \frac{3\,F\,r_{\text{mass}}}{I}$$

According to (Mamantov and Marassi, 1987), the rate of mass transfer of aluminium in a cryolite bath can be expressed as:

$$r_{\text{mass}} = k_m\,A\,c_{\text{Al}}^{\text{max}}\,(1-f) \quad \text{mol s}^{-1}$$

where k_m is the mass transfer coefficient of the metal in m s^{-1}, A is the area of the aluminium pad, which is assumed to be the same as the cathode area in m^2 (Figure 9.1), $c_{\text{Al}}^{\text{max}}$ is the maximum solubility of the aluminium in the cryolite as a weigth percentage, and f is an empirical factor that involves the concentration of aluminium and its maximum solubility. According to Haupin (1995), this factor is assumed to be 0.113.

The mass transfer k_m is calculated considering the Sherwood (Sh), the Reynolds (Re) and the Schmidt (Sc) numbers. From Incropera et al. (2011), these number are related as:

$$\mathrm{Sh} = 0.023\mathrm{Re}^{5/6}\mathrm{Sc}^{1/3} \tag{9.13}$$

Individually, each term can be written as:

$$\mathrm{Sh} = k_m \frac{d_{\mathrm{IPD}}}{D}$$

$$\mathrm{Re} = \frac{\rho\ v_s\ D}{\mu}$$

$$\mathrm{Sc} = \frac{\mu}{\rho\ D}$$

where D is the diffusivity of aluminium in the cryolite in $\mathrm{m}^2\ \mathrm{s}^{-1}$, ρ is the electrolyte density in $\mathrm{kg\ m}^{-3}$, v_s is the interfacial speed between the cryolite and the aluminium pad in $\mathrm{m\ s}^{-1}$, and μ is the dynamic viscosity of the electrolyte in $\mathrm{kg}^{-1}\ \mathrm{m\ s}^{-1}$. These values can be substituted in Eq. 9.12:

$$\eta = 100 - 2.2 \times 10^5 \frac{A\ D^{2/3} \rho^{3/2} v_s^{5/6}}{I\ \mu^{1/2}\ d_{\mathrm{IPD}}} c_{\mathrm{Al}}^{\max}(1-f) \quad (\%)$$

The current efficiency ranges between 90 and 96 % (Sterten and Solli, 1996). According to Grjotheim and Welch (1988), the diffusivity can be assumed to be 3 x 10^{-8} $\mathrm{m}^2\ \mathrm{s}^{-1}$, and the interfacial speed 0.15 $\mathrm{m\ s}^{-1}$. The density, viscosity, and solubility are properties that depend on the electrolyte composition.

Density

Most of the electrolyte properties are calculated by means of empirical relationships. The equation from the density is extracted from Korenko et al. (2015):

$$\rho = 0.1 \left[\frac{c_{\text{Cryo}}}{3.305 - 9.38 \times 10^{-4}\, T_b} + \frac{c^{\text{Exc}}_{\text{AlF}_3}}{1.987 - 3.19 \times 10^{-4}\, T_b + 0.094 c^{\text{Exc}}_{\text{AlF}_3}} \right.$$
$$+ \frac{c_{\text{CaF}_2}}{3.177 - 3.91 \times 10^{-4}\, T_b + 0.0005 c^2_{\text{CaF}_2}} + \frac{c_{\text{Al}_2\text{O}_3}}{1.449 + 0.0128 c_{\text{Al}_2\text{O}_3}}$$
$$\left. + \frac{c_{\text{MgF}_2}}{3.392 - 5.24 \times 10^{-4}\, T_b + 0.01407 c_{\text{MgF}_2}} + \frac{c_{\text{LiF}}}{2.358 - 4.9 \times 10^{-4}\, T_b} \right] \quad \text{kg m}^{-3}$$

where T_b is the bath temperature in K.

Viscosity

The empirical equation of the viscosity of the electrolyte cell is extracted from (Grjotheim and Welch, 1988):

$$\mu = 11.557 - 9.158 \times 10^{-3}\, T_{bc} - 1.587 \times 10^{-3}\, c^{\text{Exc}}_{\text{AlF}_3}$$
$$+ \left[-2.094 \times 10^{-3} + 1.853 \times 10^{-5} (T_{bc} - 1000) \right] \left(c^{\text{Exc}}_{\text{AlF}_3} \right)^2$$
$$-2.168 \times 10^{-3}\, c_{\text{Al}_2\text{O}_3} + \left[5.925 \times 10^{-3} - 1.938 \times 10^{-5} (T_{bc} - 1000) \right] c^2_{\text{Al}_2\text{O}_3} \quad \text{m}^2\text{s}^{-1}$$

T_{bc} is the bath temperature in Celsius degrees.

Aluminium Solubility

The empirical relationship for the aluminium solubility is given by Skybakmoen et al. (1997):

$$\log(c^{\text{max}}_{\text{Al}}) = 1.8251 - \frac{0.2959}{R_b} - \frac{3429}{T_b} - \frac{0.0339\, c_{\text{Al}_2\text{O}_3}}{c^{\text{max}}_{\text{Al}_2\text{O}_3}} -$$

$$0.0249\, c_{\text{LiF}} - 0.0241\, c_{\text{MgF}_2} - 0.031\, c_{\text{CaF}_2}$$

where $c^{\max}_{Al_2O_3}$ is the alumina solubility as a weight percentage, which can be calculated with another empirical equations:

$$\begin{aligned} c^{\max}_{Al_2O_3} = \big[&11.9 - 0.062\, c^{\text{Exc}}_{AlF_3} - 0.0031 (c^{\text{Exc}}_{AlF_3})^2 \\ &-0.20\, c_{CaF_2} - 0.5\, c_{LiF} - 0.3\, c_{MgF_2} + \frac{42\, c^{\text{Exc}}_{AlF_3}\, c_{LiF}}{200 + \text{LiF}\, c_{LiF}} \Big] \left(\frac{T_{bc}}{1000} \right)^A \\ A = 0.048\, &(100 - c^{\text{Exc}}_{AlF_3}) + \frac{2.2\, c^{1.5}_{LiF}}{10 + c_{LiF} + 0.001\, (c^{\text{Exc}}_{AlF_3})^3} \quad \% \text{ wt} \end{aligned} \tag{9.14}$$

Electrical Conductivity

The electrical conductivity in S cm^{-1} can be expressed with the following empirical Eq. (Hiveš et al., 1996):

$$\begin{aligned} \ln(\kappa) = 1.977 &- 0.02\, c_{Al_2O_3} - 0.0131\, c^{\text{Exc}}_{AlF_3} - 0.006\, c_{CaF_2} - 0.0106\, c_{MgF_2} \\ &-0.0019\, c_{KF} - 0.0121\, c_{LiF} - \frac{1204.3}{T_b} \end{aligned} \tag{9.15}$$

where c_{KF} is the mass fraction of potassium fluoride in the bath, which, in this case, is zero.

Heat capacity

The heat capacity is expressed as a combination of effects of each component in the bath (Tingaev, 2013; Wijayaratne et al., 2018). Thus, the heat capacity can be reduced as:

$$\begin{aligned} c_p = &(12.02 + 0.95 \times 10^{-3} T_b)\, c_{MgF_2} + (-21.94 + 28.9 \times 10^{-3} T_b)\, c_{Al_2O_3} + \\ &(7.686 + 6.35 \times 10^{-3} T_b)\, c_{NaF} + (10.82 + 1.2 \times 10^{-3} T_b)\, c_{AlF_3} \\ &(7.129 + 4.4 \times 10^{-3} T_b)\, c_{CaF_2} + 24.74\, c_{LiF} \quad \text{J g}^{-1}\text{K}^{-1} \end{aligned} \tag{9.16}$$

where c_p is the heat capacity of the electrolyte in J $g^{-1}K^{-1}$.

9.2 Mass Balances

The mass balance has to consider the feed material, the material exiting the cell, and the net production of material due to the chemical and electrochemical reactions. This section discusses each element in the mass balance.

$$\frac{dm}{dt} = \frac{dm_{\text{Input}}}{dt} + \frac{dm_{\text{Output}}}{dt} + \frac{dm_{\text{Reaction}}}{dt}$$

where dm/dt is the rate of mass change in the cell, dm_{Input}/dt and dm_{Output}/dt the mass flow rate going to and going out from the cell, and dm_{Reaction}/dt is the net production rate of each component caused by the reactions.

9.2.1 Reactions in the Bath

The processes that affect the mass balance are gathered into three groups: (i) aluminium production reaction, (ii) hydrogen fluoride reaction, and (iii) vaporization.

Aluminium Production Reaction

The main reaction in the cell is the reduction of alumina as already introduced in Eq. 9.1 as:

$$2\,Al_2O_3 + 3\,C \longrightarrow 4\,Al + 3\,CO_2$$

The current efficiency is caused by the recombination of aluminium and CO_2, defined by Reaction 9.5:

$$2\,Al + 3\,CO_2 \longrightarrow Al_2O_3 + 3\,CO$$

Considering that a fraction (1-η) of aluminium undergoes the recombination Reaction 9.5, the two reactions can be combined:

$$\begin{array}{r} 4\,(1-\eta)\mathrm{Al} + 6\,(1-\eta)\mathrm{CO_2} \longrightarrow 2\,(1-\eta)\mathrm{Al_2O_3} + 6\,(1-\eta)\mathrm{CO} \\ 2\,\mathrm{Al_2O_3} + 3\,\mathrm{C} \longrightarrow 4\,\mathrm{Al} + 3\,\mathrm{CO_2} \qquad + \\ \hline 2\,\eta\,\mathrm{Al_2O_3} + 3\,\mathrm{C} \longrightarrow 4\,\eta\,\mathrm{Al} + 3\,(2\,\eta\ -\ 1\,)\mathrm{CO_2} + 6\,(1-\eta)\mathrm{CO} \end{array} \tag{9.17}$$

For every 4 η mol of produced aluminium, 2 η mol of alumina are consumed, 3 mol of carbon are consumed, 3(2η-1) mol of CO_2 are generated, and 6(1-η) mol of CO are generated.

$$\frac{dm_{\mathrm{Al_2O_3}}}{dt} = -\frac{dm_{\mathrm{Al}}}{dt}\frac{MM_{\mathrm{Al_2O_3}}}{MM_{\mathrm{Al}}}\frac{2\eta}{4\eta}$$

where $dm_{\mathrm{Al_2O_3}}/dt$ is the consumption rate of alumina, dm_{Al}/dt is the production rate of aluminium, MM_x is the molecular weight of component x, with $MM_{\mathrm{Al_2O_3}} = 101.96$ g mol^{-1} and $MM_{\mathrm{Al}} = 26.98$ g mol^{-1}.

$$\frac{dm_{\mathrm{Al_2O_3}}}{dt} = -1.761 \times 10^{-8}\, I\, \eta \quad \mathrm{kg\ s^{-1}}$$

For the remaining components present in the reaction, the same procedure is followed:

$$\frac{dm_{\mathrm{C}}}{dt} = -3.111 \times 10^{-8}\, I \quad \mathrm{kg\ s^{-1}}$$

$$\frac{dm_{\mathrm{CO}}}{dt} = 1.452 \times 10^{-7}\, I\, (1-\eta) \quad \mathrm{kg\ s^{-1}}$$

$$\frac{dm_{\mathrm{CO_2}}}{dt} = 1.140 \times 10^{-7}\, I\, (2\eta - 1) \quad \mathrm{kg\ s^{-1}}$$

Hydrogen Fluoride Reaction

Hydrogen fluoride (HF) is produced in the cell due to two reactions, and it leaves the cell as a gas. The two reactions are:

$$2\,Na_3AlF_6 + 3\,H_2 \longrightarrow 2\,Al + 6\,NaF + 6\,HF \tag{9.18}$$

$$2\,AlF_3 + 3\,H_2O \longrightarrow Al_2O_3 + 6\,HF \tag{9.19}$$

The reacting water enters the cell as moisture in the alumina feed, whereas the hydrogen is present in the cell because it is trapped in the anodes. Haupin (1995) provided an empirical equation for calculating the rate of HF production as a function of the aluminium production rate in the main reaction (Reaction 9.1).

$$\begin{aligned}\frac{dm_{\mathrm{HF}}}{dt} = 1.454\times10^{7}\,\exp\left[0.78127R_b^2 - 3.1733R_b - \frac{8444}{T_b}\right]\left(\frac{462-191R_b}{P_b\,\eta}\right)\\ \left(\frac{c_{\mathrm{H_2O}}}{37.44}+\frac{c_{\mathrm{H}}}{21.5}\right)^{0.5}\left(\frac{c_{\mathrm{Al_2O_3}}}{c^{max}_{\mathrm{Al_2O_3}}}\right)^{-0.462}\ \mathrm{kg\ ton_{Al}^{-1}}\end{aligned} \tag{9.20}$$

where P_b is the barometric pressure in bar, and $c_{\mathrm{H_2O}}$ and c_{H} are, respectively, the concentration of water in the feed and the concentration of hydrogen captured in the anodes in % wt. In this project, the values used for the two concentrations are the ones suggested by (Haupin, 1995), which are 2.8% for the water, and 0.093% for the hydrogen. The production or consumption rates of the components present in the reactions can be approximated as:

$$\frac{dm_{\mathrm{Al}}}{dt} = \frac{dm_{\mathrm{HF}}}{dt}\frac{MM_{\mathrm{Al}}}{MM_{\mathrm{HF}}}\frac{2}{12} = 0.2247\,\frac{dm_{\mathrm{HF}}}{dt}\quad \mathrm{kg\ ton_{Al}^{-1}}$$

$$\frac{dm_{\mathrm{Al_2O_3}}}{dt} = \frac{dm_{\mathrm{HF}}}{dt}\frac{MM_{\mathrm{Al_2O_3}}}{MM_{\mathrm{HF}}}\frac{1}{12} = 0.4246\,\frac{dm_{\mathrm{HF}}}{dt}\quad \mathrm{kg\ ton_{Al}^{-1}}$$

$$\frac{dm_{\mathrm{AlF_3}}}{dt} = -\frac{dm_{\mathrm{HF}}}{dt}\frac{MM_{\mathrm{AlF_3}}}{MM_{\mathrm{HF}}}\frac{2}{12} = -0.6994\,\frac{dm_{\mathrm{HF}}}{dt}\quad \mathrm{kg\ ton_{Al}^{-1}}$$

$$\frac{dm_{\mathrm{NaF}}}{dt} = \frac{dm_{\mathrm{HF}}}{dt}\frac{MM_{\mathrm{NaF}}}{MM_{\mathrm{HF}}}\frac{6}{12} = 1.049\,\frac{dm_{\mathrm{HF}}}{dt}\quad \mathrm{kg\ ton_{Al}^{-1}}$$

Eq. 9.20 shows that the fluoride production is mainly a function of R_b and the alumina concentration. An increase of any of these two variables causes a decrease of the production rate of HF.

Vaporization

The presence of sodium fluoride and aluminium fluoride produces a very volatile component, sodium tetrafluoroaluminate, which is present in two forms: as a monomer ($NaAlF_4$) and a dimer ($Na_2Al_2F_8$). Both of them are produced from the reaction between sodium fluoride and aluminium fluoride:

$$NaF + AlF_3 \longrightarrow NaAlF_4 \tag{9.21}$$

Once the sodium tetrafluoroaluminate is formed, it leaves the bath as a gas. The rate of gas losses depends on the saturation vapour pressure and the number of moles. According to Haupin (1995), this rate is:

$$\frac{dm_{NaAlF_4}}{dt} = \frac{2040}{\eta}\frac{P_m + 2P_d}{P_b} \quad \text{kg ton}_{\text{Al}}^{-1} \tag{9.22}$$

where dm_{NaAlF_4}/dt is the flow rate of sodium tetrafluoroaluminate in kg $\text{ton}_{\text{Al}}^{-1}$, and P_b, P_m, and P_d are respectively, the barometric pressure, the monomer partial pressure, and the dimer partial pressure in bar.

Considering that the total pressure is the sum of the pressures of the monomer and the dimer. (Grjotheim and Welch, 1988) and (Haupin, 1995) provide the equations for the monomer partial pressure and the total pressure respectively, and therefore, the dimer partial pressure can be

deduced as the difference. The total pressure is:

$$\log(P_T) = B - \frac{A}{T_b}$$

$$A = 7101.6 + 3069.7\ R_b - 635.77\ R_b^2 + \frac{764.5\ c_{Al_2O_3}}{1 + 1.0817\ c_{Al_2O_3}} + 13.2\ c_{CaF_2}$$

$$B = 7.0174 + 0.6844\ R_b - 0.08464\ R_b^3 + \frac{1.1385\ c_{Al_2O_3}}{1 + 3.2029\ c_{Al_2O_3}} + 0.0068\ c_{CaF_2}$$

The monomer partial pressure can be expressed as:

$$P_m = \frac{\sqrt{1 + 4K\ P_T} - 1}{2K}$$

$$K = \exp\left(\frac{-21414}{T_b} + 15.6\right)$$

where K is the dimerization constant. Thus, the dimer pressure is:

$$P_d = B - \frac{A}{T_b} - \frac{\sqrt{1 + 4K\ P_T} - 1}{2K}$$

From Eq. 9.22, the consumption rate of NaF and AlF_3 results in:

$$\frac{dm_{NaF}}{dt} = -\frac{dm_{NaAlF_4}}{dt}\frac{MM_{NaF}}{MM_{NaAlF_4}} = -0.5525\ \frac{dm_{NaAlF_4}}{dt} \quad \text{kg ton}_{Al}^{-1}$$

$$\frac{dm_{AlF3}}{dt} = -\frac{dm_{NaAlF_4}}{dt}\frac{MM_{AlF_3}}{MM_{NaAlF_4}} = -1.105\ \frac{dm_{NaAlF_4}}{dt} \quad \text{kg ton}_{Al}^{-1}$$

9.2.2 Material Feed

The main feed is the alumina that gets dissolved in the cryolite, and undergoes the reduction reaction. There are two more feeds, AlF_3, and Na_2CO_3, which are fed to the cell for two purposes: (i) maintaining the bath ratio (R_b) at a desired level, and (ii) maintaining the total mass (and therefore all components mass fractions) constant.

The alumina fed to the cell is not pure, and it has 1.5 % wt of AlF_3, 0.2 % wt of Na_2O, and 2.75 % wt of water. This composition is extracted from the alumina used in the Norðurál plant in Iceland (Norðurál, 2019). Alumina enters as a solid, and, in order for it to react and produce aluminium, it has to be dissolved. The dissolution rate has been studied by Biedler (2003), who stated that this rate can be modelled as two mechanisms, one slower than the other. Both mechanisms are governed by a first order differential equation, 75% of the alumina dissolves at a higher speed with a dissolution constant of 0.099 s^{-1}, and the 25% remaining has a dissolution constant of 0.005 s^{-1}. Thus, the dissolution rate is:

$$\text{Quicker dissolution} \quad \frac{dC_{Al_2O_3}}{dt} = -0.099 C_{Al_2O_3}$$

$$\text{Slower dissolution} \quad \frac{dC_{Al_2O_3}}{dt} = -0.005 C_{Al_2O_3}$$

$$\text{Alumina dissolved} \quad \frac{dm_{Al_2O_3}}{dt} = 0.75\ (0.099 C_{Al_2O_3}) + 0.25\ (0.005 C_{Al_2O_3})$$

where $C_{Al_2O_3}$ is the concentration of undissolved alumina in kg s^{-1}. In practice, the alumina is added in batches. However, in the model, it is continuously added, so the dissolved alumina concentration is constant throughout the whole operation.

The additions of fluoride are considered to be continuous as well, and they are assumed to dissolve instantly. As Grjotheim and Welch (1988) suggested, the reason for adding Na_2CO_3 rather than just NaF is because the Na_2CO_3 reacts with the AlF_3, so the bath ratio can be manipulated more easily. The reaction is:

$$3\,Na_2CO_3 + 2\,AlF_3 \longrightarrow 6\,NaF + Al_2O_3 + 3\,CO_2 \tag{9.23}$$

A 0.3% of the Na_2CO_3 fed to the bath is Na_2O, which reacts with the AlF_3 as well:

$$3\,Na_2O + 2\,AlF_3 \longrightarrow 6\,NaF + Al_2O_3 \tag{9.24}$$

9.3 Electrical Model

The electrical model calculates the difference in voltage between the anode rods and the cathode. Electricity enters the cell through the anode rods, providing a direct current to the bath frame and the bath itself. The electrolyte bath has an ohmic resistance, which, along with the current flowing through the bath, causes a voltage drop. Figure 9.3.a) shows the current flowing through the cell and the ohmic resistances, and Figure 9.3.b) shows the corresponding circuit diagram.

Thus, the total voltage drop in the cell is divided into three parts: (i) ohmic voltage, (ii) decomposition voltage, which is the voltage drop caused by electrolysis reactions, and (iii) overvoltages.

The voltage drop and the electric current provide an electrical power that converts to heat. Heat is used in the cell to (i) help developing the endothermic reactions, to (ii) heat up the material fed to the cell, and to (iii) provide enough power to offset the heat lost to the surroundings. The

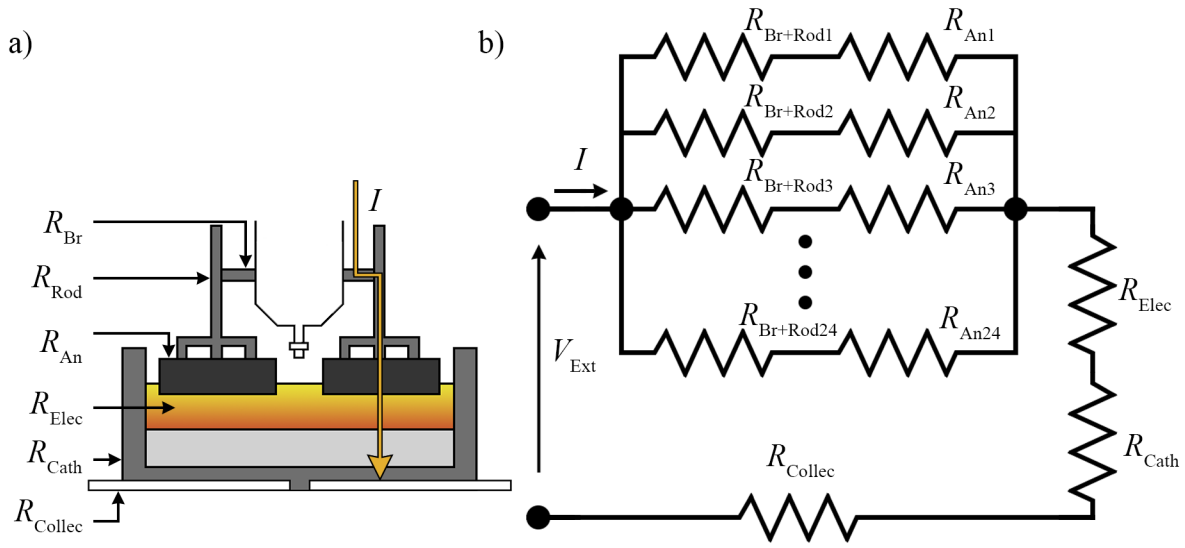


Figure 9.3: a) Schematic representation of the electrolyte cell, and b) its corresponding electrical circuit diagram.

electrical power consumption of the cell is constant, and the model establishes the values of the variables to meet the power requirements.

9.3.1 Ohmic Voltage

This is the voltage drop caused by the ohmic resistance of various sections in the cell. This voltage drop is divided into two groups: the outer part, which is the (i) external voltage drop, and the inner part, named as (ii) electrolyte voltage drop.

External Voltage Drop

This voltage drop is caused by the frame of the electrolyte cell, which consists on the anode block, the anode bridge, the anode rods, the cathode, and the collector bars.

Empirical data for the resistances is taken from the work by Molenaar et al. (2016). According to this work, there are 24 anodes, and they can be considered to be connected in a parallel arrangement. In each anode, the anode block has a resistance of 2.2×10^{-5} Ω, and the sum of the anode rod and the anode bridge has a resistance of 7.8×10^{-6} Ω. The cathode resistance is assumed to be 1.55×10^{-6} Ω, and the collector bars has a resistance of 1×10^{-6} Ω.

Figure 9.3.b) shows a simplification of the electric diagram corresponding to the voltage drop due to the external ohmic drops. The electrolyte voltage drop is included between the anode and the cathode.

Since the ohmic resistance are not changing with temperature, Ohm's law can be used for calculating the ohmic voltage drop. The total external resistance can be calculated considering the arrangement of the elements in Figure 9.3.b).

$$\begin{gathered} R_{\text{Ext}} = \left(\frac{R_{\text{An}} + R_{\text{Br+Rod}}}{24}\right) + R_{\text{Cat}} + R_{\text{Collector}} \\ R_{\text{Ext}} = 1.49\times10^{-6} + 1.55\times10^{-6} + 1\times10^{-6} = 4.04\times10^{-6} \quad \Omega \end{gathered} \tag{9.25}$$

where R_{An}, $R_{\text{Br+Rod}}$, R_{Cat}, and $R_{\text{Collector}}$ are, respectively, the ohmic resistance of the anode block, the anode and bridge, the cathode, and the collector bars, all in Ω. Thus, the external ohmic drop is:

$$V_{\text{Ext}} = 4.04 \times 10^{-6}\, I \quad \text{V} \tag{9.26}$$

Electrolyte Voltage Drop

The electrolyte voltage drop is the difference of potential from the anode to the cathode. This voltage drop is affected by the electrical conductivity, which has already been introduced as:

$$\begin{aligned} \ln(\kappa) = 1.977 - 0.02\, c_{\text{Al}_2\text{O}_3} - 0.0131\, c^{\text{Exc}}_{\text{AlF}_3} - 0.006\, c_{\text{CaF}_2} - 0.0106\, c_{\text{MgF}_2} \\ -0.0019\, c_{\text{KF}} - 0.0121\, c_{\text{LiF}} - \frac{1204.3}{T_b} \end{aligned} \tag{9.15}$$

The equation shoes that the temperature of the bath, and the concentration of alumina can potentially affect the conductivity of the bath. Figure 9.4 shows the relationships between the electrolyte conductivity and the alumina concentration, and the bath temperature:

From Figure 9.4, conductivity decreases when the alumina concentration increases. Hence, for a fixed distance between anode and cathode, if the alumina concentration increases, the ohmic resistance decreases. Additionally, when the bath temperature increases, the conductivity increases as well, so increasing the temperature decreases the ohmic resistance.

Considering that the current is uniform throughout the bath, the electrolyte resistance is expressed as:

$$R_{\text{Eb}} = \kappa \left(\frac{d_{\text{IPD}} - d_{\text{Bub}}}{A_{\text{An}}} + \frac{d_{\text{Bub}}}{A_{\text{eff}}} \right) \tag{9.27}$$

where R_{Eb} is the ohmic resistance of the electrolyte bath, and A_{eff} is the surface area in which the current is flowing through the bubbles. In the model, A_{eff} is considered large enough to

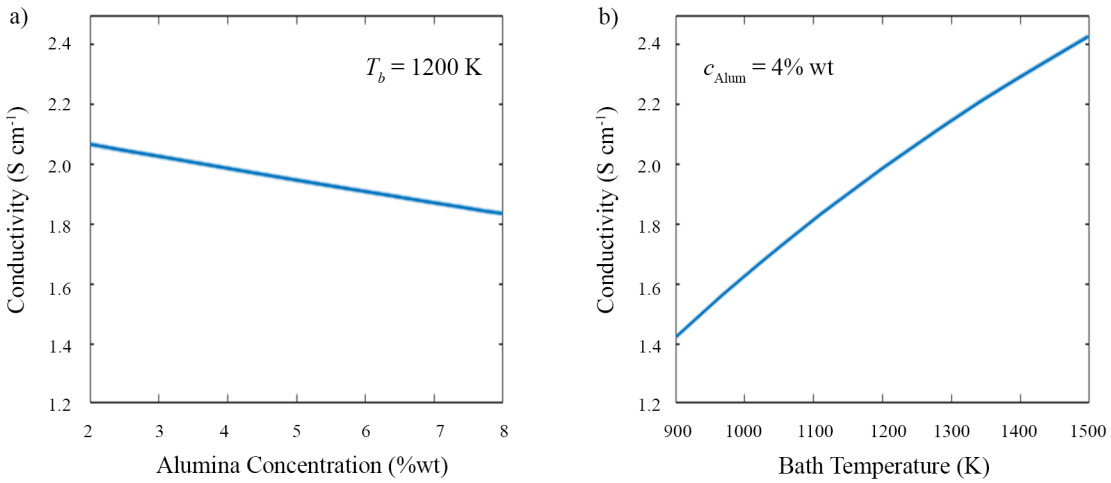


Figure 9.4: Conductivity of the electrolyte bath as a function of the a) alumina concentration in %wt and b) bath temperature in K. In both graphs, the vertical axis is the electrical conductivity in S cm $^{-1}$

neglect the second term of Eq. 9.27. The term d_{bub} is the bubble layer thickness in cm, which depends on the current flowing through the cell. According to Drengstig et al. (2003), the bubble layer thickness can be expressed as:

$$d_{\text{Bub}} = \frac{0.5517 + j_{\text{An}}}{1 + 2.167 j_{\text{An}}} \quad \text{cm} \tag{9.28}$$

where j_{An} is the anode current density in A m^{-2} expressed as the current divided by the anode effective area

Figure 9.5 shows the bubble layer thickness variation when the current is varied. The bubble thickness does not significantly change when the electrical current varies. Thus, the changes of the bubble layer thickness caused by a variation of the electrical current are not enough to make a difference in the total resistance.

From Eqs. 9.27 and 9.28, the ohmic resistance of the bath is a function of the IPD, the bubble layer, and the conductivity. The bubble layer is a function of the electrical current, so ultimately, the ohmic resistance depends on the temperature, the alumina concentration, the IPD, and the

current. Figure 9.6 shows the relationships between the voltage drop in the electrolyte and these variables.

As Figure 9.6 shows, the voltage drop increases when either the alumina concentration, the electrical current, or the IPD increases, and it decreases when the temperature increases.

The bubble layer also presents an ohmic resistance. In the work by Drengstig et al. (2003), the voltage drop in the bubble layer is expressed as:

$$V_{\text{Bub}} = \frac{d_{\text{Bub}}\ j_{\text{An}}}{\kappa}\frac{\phi}{1-\phi}$$

$$\phi = 0.5090 + 0.1823\, j_{\text{An}} - 0.1723\, j_{\text{An}}^2 + 0.05504\, j_{\text{An}}^3 +$$

$$\frac{0.4322 - 0.3781 R_b}{1 - 1.1637 R_b} + \frac{0.431 - 0.1437(c_{Al_2O_3} - c_{Al_2O_3}^{\text{AE}})}{1 + 7.353(c_{Al_2O_3} - c_{Al_2O_3}^{\text{AE}})}$$

The voltage drop in the bubble layer is a function of the electrical current, the alumina concentration, the bath ratio, and the temperature. Figure 9.7 shows the voltage drop in the bubble layer as a function of these four variables.

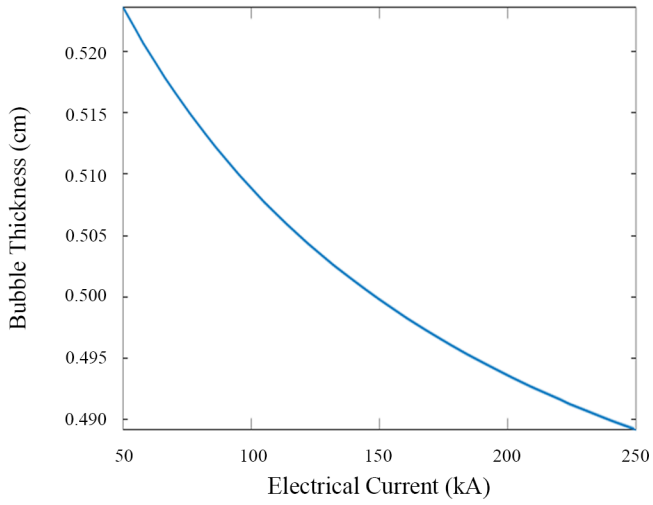


Figure 9.5: Bubble layer thickness (cm) as a function of the electrical current (kA).

Figure 9.7 shows that the voltage drop increases when the electrical current or the bath ratio increase, and it decreases when the temperature or the alumina concentration increase. There is an asymptote in Figure 9.7.a) when the alumina concentration gets close to the anode effect concentration, and makes the voltage drop tend to infinity[1].

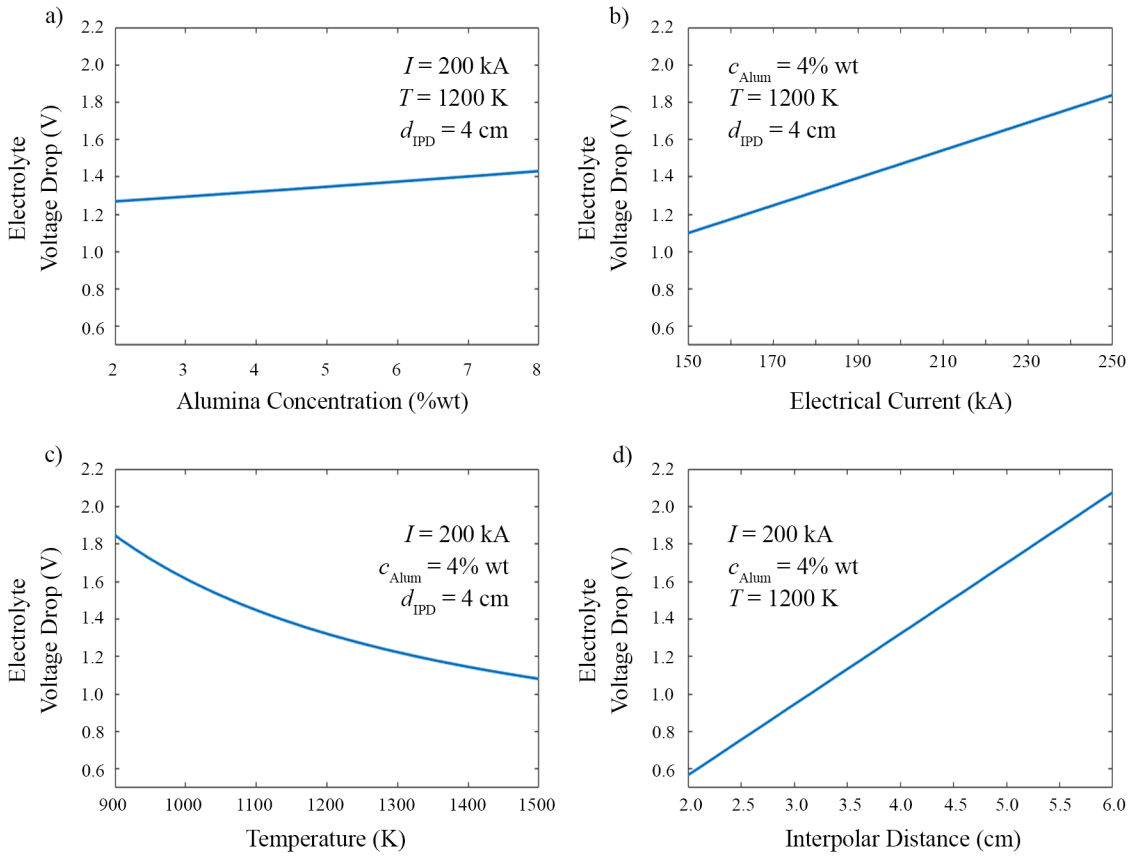


Figure 9.6: Voltage drop in the electrolyte in V as a function of a) the alumina concentration in %wt, b) the bath temperature in K, c) the electrical current in kA, and d) the IPD in cm.

[1]In practice, the voltage will not become infinite. Rather, it will meet a constraint, and the current will reduce

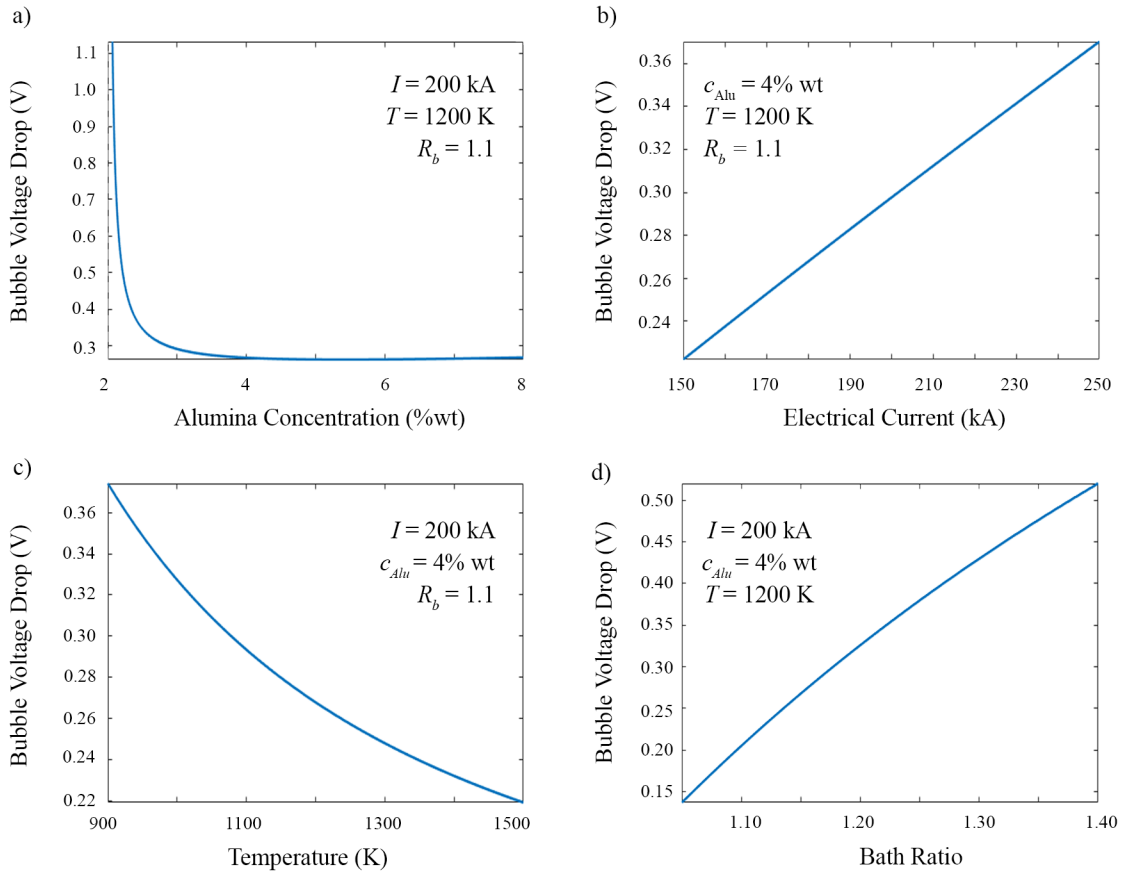


Figure 9.7: Voltage drop in the bubble layer in V as a function of a) the alumina concentration in %wt, b) the bath temperature in K, c) the electrical current in kA, and d) the bath ratio.

9.3.2 Decomposition Voltage

The decomposition voltage is the voltage drop used for decomposing the alumina. Section 9.1 introduced the thermodynamics of the aluminium redox reaction, as well as the Gibbs energy:

$$\Delta G = 1.5\ G_f(CO_2) - G_f(Al_2O_3)$$

Table 9.1: Gibbs Free Energy of Formation in kJ mol^{-1} for the relevant compounds in the aluminium reduction

Temperature	1000	1100	1200	1300	1400
Alumina	-1361.437	-1328.286	-1295.228	-1262.264	-1229.393
CO_2	-395.886	-396.001	-396.098	-396.177	-396.240

At standard conditions, the voltage drop necessary to provide the Gibbs energy is named as standard electrode potential, expressed as E^0, and its units are Volts (V).

$$\Delta G = n_e E^0 F \quad \text{kJ mol}^{-1}$$

where n_e is the number of electron interchanged during the redox reaction. For the main reaction, n_e is six electrons[2]. Thus, the standard electrode potential can be expressed as:

$$E^0 = \frac{\Delta G}{n_e F} = \frac{1.5\ \Delta G_f(CO_2) - \Delta G_f(Al_2O_3)}{6 \times 96485}$$

The thermodynamic data for the Gibbs energy of formation of each component can be found in Chase (1998). The tables provided give values for the Gibbs energy at various temperatures. For the aluminium reduction, the relevant compounds are the alumina and the carbon dioxide (the Gibbs energy of formation for the elements is zero, so aluminium and carbon do not affect the Gibbs energy of the reaction). Since the temperature might change during the process, the Gibbs free energy of formation is calculated as a function of the temperature by linear interpolation of the values given in Table 9.1.

Thus, an expression for the Gibbs free energy as a function of the temperature is:

$$\Delta G_f(\text{Alumina}) = -1690.6 + 0.3295 T_b \qquad \text{kJ mol}^{-1}$$

$$\Delta G_f(CO_2) = -394.902 - 9.77 \times 10^{-4} T_b \qquad \text{kJ mol}^{-1}$$

[2]It is important not to confuse this term with n_{e^-} which is the number of electrons flowing from cathode to anode, defining only half-reaction

Therefore, the standard potential is:

$$E^0 = 1000\ \frac{1.5\ (-394.902 - 9.77 \times 10^{-4}) - (-1690.6 + 0.3295\ T_b)}{6 \times 96485} = \\ 1.897 - 5.717 \times 10^{-4}\ T_b \quad \text{V} \tag{9.29}$$

The factor of 1000 in Eq. 9.29 converts kV to V. The standard electrode potential is the potential when the conditions in the bath are the standard conditions. Also, the standard potential takes place when the reaction has reached equilibrium. The Nernst equation is used to obtain the actual potential, or the decomposition voltage:

$$E_0 = E^0 - \ln(Q_r)\frac{RT}{n_e F} \tag{9.30}$$

where Q_r is the reaction quotient, and it is a measurement of the progress of a reaction. It is a function of the activities of the reaction. For a generic reaction $m\text{A} + n\text{B} \rightarrow p\text{C} + q\text{D}$ it is expressed as:

$$Q_r = \frac{a_{\text{C}}^p\ a_{\text{D}}^q}{a_{\text{A}}^m\ a_{\text{B}}^n}$$

Thus, for the aluminium reduction, the reaction quotient is:

$$Q_r = \frac{a_{\text{Al}}^4\ a_{\text{CO}_2}^3}{a_{\text{Al}_2\text{O}_3}^2\ a_{\text{C}}^3}$$

where a_i is the activity of compound i. The aluminium, carbon and carbon dioxide are close enough to their standard conditions, so their activities are equal to one. On the other hand, the activity of the alumina has to be deduced with empirical measurements. According to Martínez-Velasco and González-Molina (2014), the activity of the alumina is expressed as a function of the alumina concentration ($c_{\text{Al}_2\text{O}_3}$) as follows:

$$a_{\text{Al}_2\text{O}_3} = -0.03791\frac{c_{\text{Al}_2\text{O}_3}}{c_{\text{Al}_2\text{O}_3}^{\max}} + 2.364\left(\frac{c_{\text{Al}_2\text{O}_3}}{c_{\text{Al}_2\text{O}_3}^{\max}}\right)^2 - 2.194\left(\frac{c_{\text{Al}_2\text{O}_3}}{c_{\text{Al}_2\text{O}_3}^{\max}}\right)^3 + 2.8686\left(\frac{c_{\text{Al}_2\text{O}_3}}{c_{\text{Al}_2\text{O}_3}^{\max}}\right)^4$$

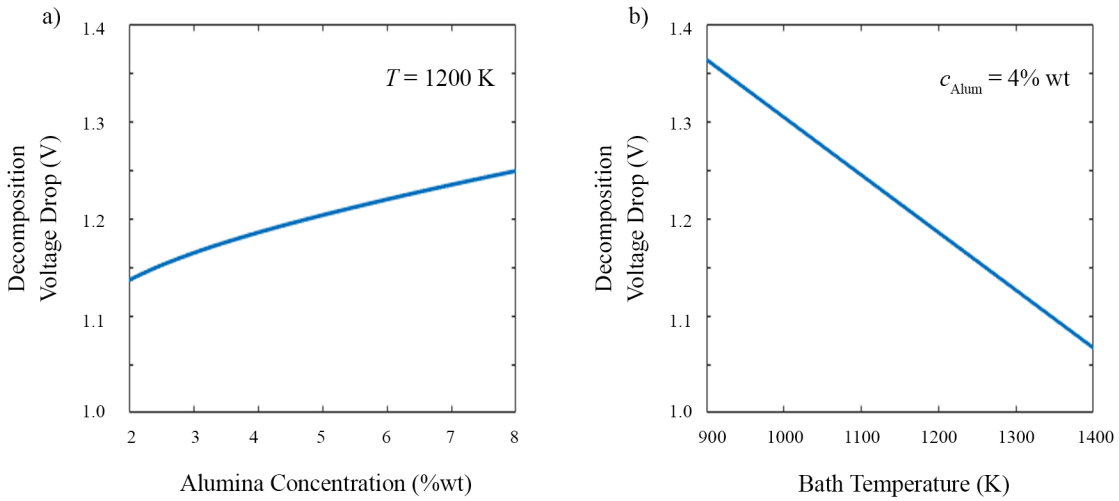


Figure 9.8: Decomposition voltage (V) as a function of the a) alumina concentration (%wt) and b) bath temperature (K). In both graphs, the vertical axes are the decomposition voltage drop.

where $c^{max}_{Al_2O_3}$ is the alumina solubility explained by Eq. 9.14. The decomposition voltage is mainly a function of the alumina concentration and the bath temperature. Figure 9.8 shows the graphical representation of Eq. 9.30 when the temperature or the alumina concentration varies.

As Figure 9.8 shows, the voltage drop increases as the alumina concentration becomes larger. If the electrical power consumption of the cell is to be constant, a higher alumina concentration implies a lower electrical current, and consequently, the aluminium production rate is reduced. A higher bath temperature leads to a lower decomposition voltage drop, and, if the electrical consumption is constant, the electrical current increases, increasing then the aluminium production.

9.3.3 Overvoltage

Overvoltage occurs when there is a gradient of concentration in the bath. This takes place specially in the interfaces between the electrolyte and the electrodes. Another type of overvoltage is the reaction overvoltage, which occurs when a reaction needs to take place so a specific electron transfer happens. Thus, overvoltage can be divided into three types: (i) anode con-

centration overvoltage, (ii) cathode concentration overvoltage, and (iii) reaction concentration overvoltage.

Anode Concentration Overvoltage

In the interface between the anodes and the electrolyte bath, the concentration has a gradient that causes the voltage drop to increase. The anode overvoltage is expressed using a variation of the Nernst equation:

$$OV_{\mathrm{AC}} = \frac{RT}{n_e F} \ln\left(\frac{j_{\mathrm{crit}}}{j_{\mathrm{crit}} - j_{\mathrm{An}}}\right) \quad \mathrm{V} \tag{9.31}$$

where OV_{AC} is the anode concentration overvoltage in V, and j_{cr} is the critical current density, which is the current density at which the reaction in the anode is governed by the anode effect explained in Section 9.1. According to Pietrzyk (2008) the critical current density is:

$$j_{\mathrm{crit}} = \frac{(1.443 - 1.985R_b + 1.131R_b^2)\, c_{\mathrm{Al_2O_3}} + (0.4122 - 0.2037R_b)\, c^2_{\mathrm{Al_2O_3}}}{(1.443 - 1.985R_b + 1.131R_b^2)\, c^{\mathrm{AE}}_{\mathrm{Al_2O_3}} + (0.4122 - 0.2037R_b)(c^{AE}_{\mathrm{Al_2O_3}})^2}\, j_{\mathrm{An}} \quad \mathrm{A\ m^2}$$

where $c^{\mathrm{AE}}_{\mathrm{Al_2O_3}}$ is the critical alumina concentration at which the anode effect starts as a weight percentage. The critical alumina concentration is assumed to be 2% wt. Eq. 9.31 suggests that the anode concentration overvoltage depends on the temperature, the bath ratio, and the alumina concentration. Figure 9.9 shows the relationships between the anode concentration overvoltage and the alumina concentration in the bath, and the bath ratio. The relationship with the temperature is directly proportional with a gradient of $R/(n_e F)$ V K^{-1}.

Figure 9.9 shows that a higher alumina concentration leads to a lower voltage drop, and that a higher bath ratio leads to a higher voltage drop. Nevertheless, the voltage drops are not very significant compared to the voltage drop caused by the decomposition voltage.

Additionally, Figure 9.9.a) shows that the voltage drop tends to infinity when the alumina concentration gets closer the anode effect concentration.

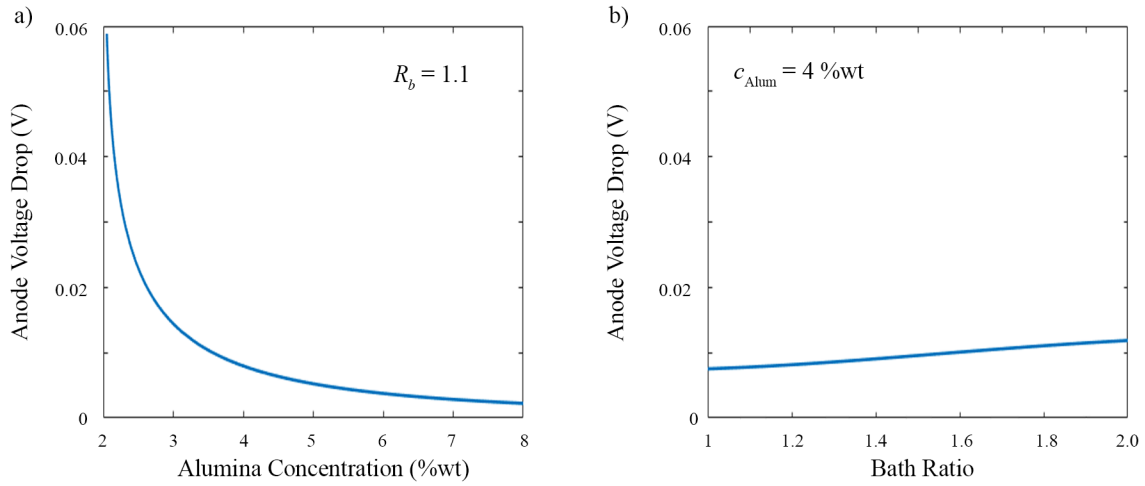


Figure 9.9: Voltage drop caused by the anode concentration overvoltage (V) as a function of the a) alumina concentration (%wt) and b) bath ratio. In both graphs, the vertical axes are the decomposition voltage drop.

Cathode concentration overvoltage

The interface between the cathode and the electrolyte has a gradient of concentration that causes an overvoltage. According to Pietrzyk (2008), it can be expressed as:

$$OV_{\text{CC}} = \frac{RT}{n_e F} \frac{1.375 - 0.125 R_b}{1.5} \ln\left(\frac{j_{\text{Cat}}}{0.283}\right) \tag{9.32}$$

where OV_{CC} is the cathode concentration overvoltage in V, and j_{Cat} is the current density of the cathode in A m^{-2}. Eq. 9.32 suggests that the cathode concentration overvoltage is affected by the temperature of the bath, and the bath ratio. Figure 9.10 only shows the relationship between the voltage drop and the bath ratio. The relationship with the temperature is proportional with a gradient of $R/(n_e F)$ V K^{-1}

Figure 9.10 shows that the bath ratio has little effect on the voltage drop, and that changing the bath ratio can barely achieve a voltage variation of 2 mV.

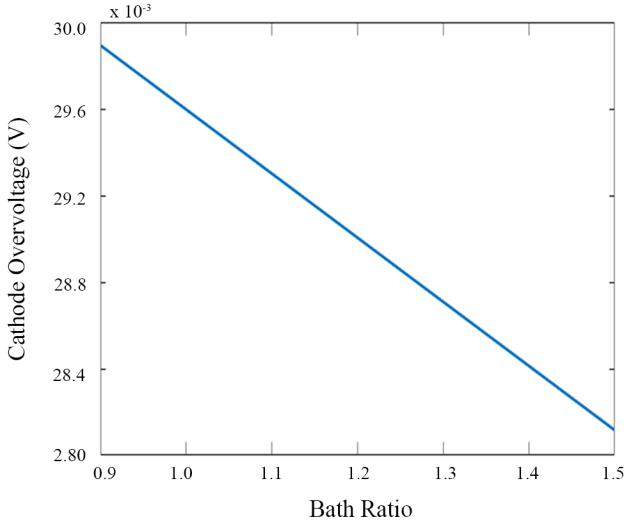


Figure 9.10: Voltage drop caused by the cathode concentration overvoltage in V as a function of the bath ratio. The horizontal axis represents the bath ratio, and the vertical axis is the voltage drop in V.

Reaction concentration overvoltage

The reactions necessary for the mass transfer lead to an overvoltage needed for the reaction to first take place. According to Haupin (2016), in the aluminium bath, the reaction that needs to happen is the dissociation of the oxygen. The oxygen that appears during the reaction causes bubbles to appear in the interface between the anode and the electrolyte. Haupin (2016) gave an empirical equation for determining the overvoltage caused by both the reaction and the bubbles:

$$\begin{aligned} OV_R &= 1.978\,\frac{RT}{n_e F}\ln\left(\frac{j_\mathrm{A}}{j_\mathrm{R}}\right) \quad \mathrm{V} \\ j_\mathrm{R} &= \exp\left[0.56\ln\left(c_{\mathrm{Al2O_3}}+\frac{c_\mathrm{LiF}}{4}\right)+0.276\,(R_b-1.5)-5.849\right] \quad \mathrm{A\ m^{-2}} \end{aligned} \tag{9.33}$$

Eq. 9.33 suggests that the reaction overvoltage depends mainly on the temperature, the alumina concentration, and the bath ratio. Figure 9.11 represents the voltage drop due to the reaction concentration overvoltage when the alumina concentration and the bath ratio change. The relationship with the temperature is proportional with a gradient of $1.978\,R/(n_e F)$ V K^{-1}

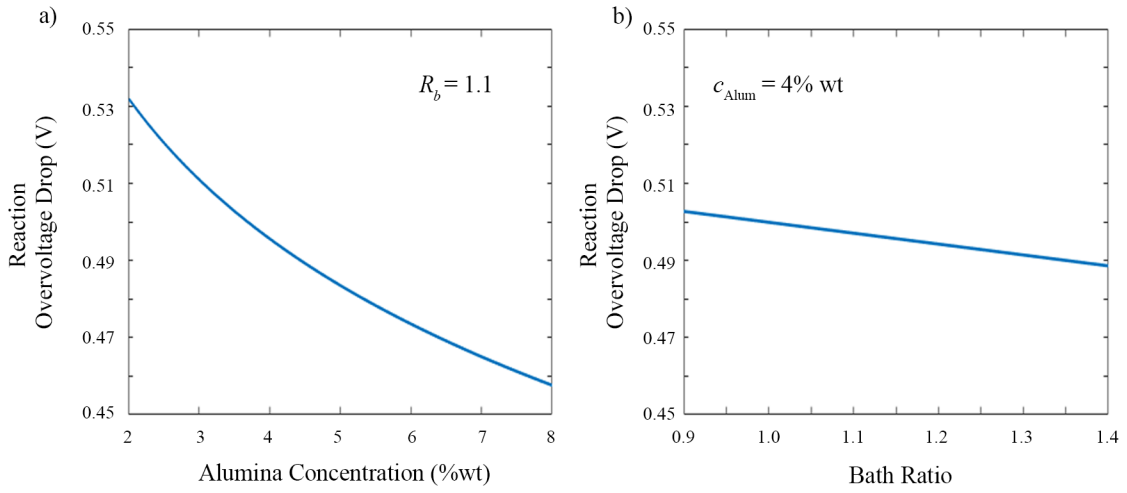


Figure 9.11: Voltage drop caused by the reaction concentration overvoltage in V as a function of the a) alumina concentration (%wt) and b) bath ratio. In both graphs, the vertical axes are the decomposition voltage drop.

Figure 9.11 shows that increasing either the alumina concentration or the bath ratio results in a decrease of the voltage drop. The voltage drop caused by this overvoltage is much higher than the two electrode concentration overvoltages.

9.3.4 Overall Electrical Model

As an overall view of the voltage drop in the electrolyte, there are five main variables that affect the voltage drop:

- Temperature of the bath
- Alumina concentration
- Electrical current
- Bath Ratio
- IPD

Figure 9.12 shows how the total voltage drop in the cell is affected by these five variables. In order to reduce the amount of graphs, each graph includes three curves, each one corresponding to a different value of electrical current.

Figure 9.12 shows that the total voltage drop increases when the bath ratio, the IPD, or the current increase, and it decreases when the temperature of the bath increases. This suggests that operating at higher temperatures would be desirable. However, the bath temperature has to be controlled to be between two limits. The upper limit is set at 1350K, so the cryolite ledges remain solid, and the lower limit is set at 1150K, so the cryolite bath does not solidify. Thus, the operating point is usually halfway between both limits, at 1250K. Figure 9.12.a) shows that there is a minimum in the voltage drop when the alumina concentration is at 3.39% wt, independently of the current. It would be recommended then to operate at that alumina concentration, nevertheless, alumina is being consumed continuously, and below that minimum, the concentration is getting closer to the anode effect concentration, which steeply raises the voltage drop. Therefore, the operating point for alumina is usually 4% wt.

9.4 Heat Balances

The heat balances consider all the energy going to or coming from the cell, as well as the energies generated or absorbed in the cell to maintain the aluminium reduction operative:

$$P_{\text{in}} = (P_{\text{out}} + P_{\text{loss}}) - (P_{\text{gen}} - P_{\text{abs}}) \quad \text{W} \tag{9.34}$$

In Eq. 9.34, H_{in} is the power entering the cell (both as an electrical input, or as a material feed) in W, H_{out} is the heat carried by the compounds leaving the cell in W, H_{loss} is the heat lost to the surroundings in W, H_{gen} is the heat generated by the exothermic reactions in W, and H_{abs} is the heat absorbed by the endothermic reactions in W.

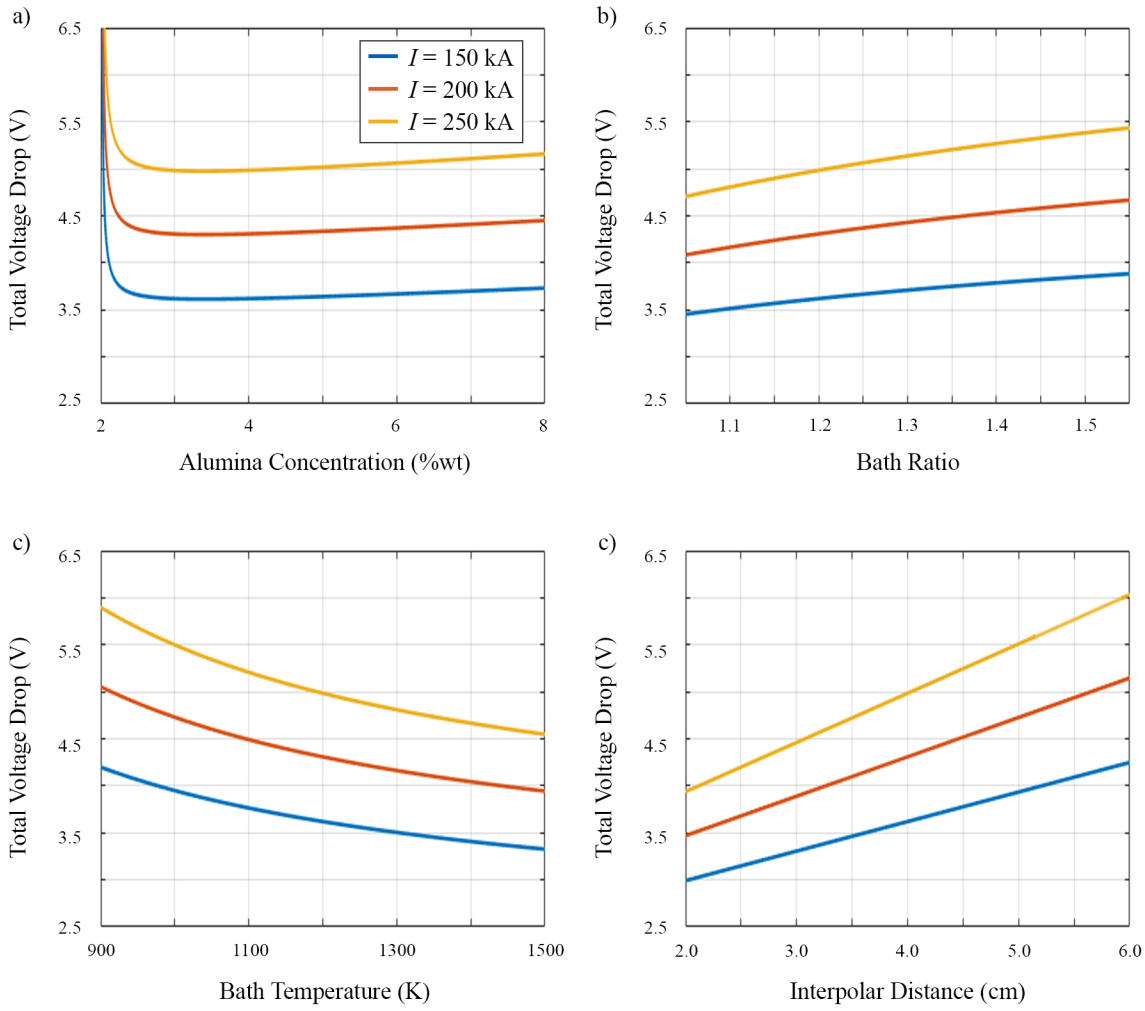


Figure 9.12: Total voltage drop in electrolyte cell in V as a function of a) the alumina concentration in %wt, b) the bath temperature in K, c) the bath ratio, and d) the IPD in cm. Each curve represents a different current flowing through the cell

Material leaves the cell at the same temperature as the bath, so the enthalpy related to the thermal energy of the bath does not vary. Thus, the energy of the compounds leaving the cell only corresponds to the reactions and the feeds, that are already considered in H_{gen} and H_{abs}, and H_{in}.

The temperature of the cell varies depending on the heat balance, according to:

- If $H_{\text{in}} > H_{\text{loss}} - (H_{\text{gen}} - H_{\text{abs}})$, the temperature of the cell increases
- If $H_{\text{in}} < H_{\text{loss}} - (H_{\text{gen}} - H_{\text{abs}})$, the temperature of the cell decreases
- If $H_{\text{in}} = H_{\text{loss}} - (H_{\text{gen}} - H_{\text{abs}})$, the temperature of the cell remains steady

The rate of temperature change depends on the heat capacity and the mass of the bath:

$$\frac{dT}{dt} = \frac{H_{\text{in}} - H_{\text{loss}} - (H_{\text{gen}} - H_{\text{abs}}))}{m\, c_p} \quad \text{K s}^{-1}$$

where m is the mass of the bath in kg, and c_p is the heat capacity of the bath in J kg $^{-1}$ K^{-1}. The heat capacity depends on the properties of the bath (Eq. 9.16).

9.4.1 Heat Entering the Cell

When electrical current flows through a resistance, this current generates heat, this process is known as Joule heating. The Joule heat can be expressed as:

$$H_{\text{Joule}} = V\, I \quad \text{W} \tag{9.35}$$

where H_{Joule} is the heat generated due to the Joule heating effect in the cell in W. The external parts of the cell do not interact with the electrolyte cell, so the Joule heat is only caused by the voltage drop within the electrolyte bath. This means that the voltage drop caused by the external ohmic resistance of the cell does not contribute to the Joule heating.

Thus, in Eq. 9.35, the voltage is the sum of each voltage drop within the bath.

$$V = E_0 + OV_{\text{AC}} + OV_{\text{CC}} + OV_{\text{R}} + V_{\text{Elec}} + V_{\text{Bub}}$$

where E_0 is the decomposition voltage, OV_{AC}, OV_{CC}, OV_{R} are the anode, cathode, and reaction overvoltages, V_{Elec} is the voltage drop in the electrolyte, and V_{Bub} is the voltage drop due to the

bubble layer in the anode surface; all these voltages are in V, and were already introduced in the electrical model of the cell.

9.4.2 Heat Absorbed by the Compounds Entering

Compounds entering the cell are at a lower temperature than the electrolyte bath. These compounds have to absorb energy from the bath in order to reach thermal equilibrium with the bath. The equation for calculating the differences of enthalpies is the Shomate equation:

$$\Delta H = H^A_{\text{Sho}}\, t_r + H^B_{\text{Sho}}\, \frac{t_r^2}{2} + H^C_{\text{Sho}}\, \frac{t_r^3}{3} + H^D_{\text{Sho}}\, \frac{t_r^4}{4} - \frac{H^E_{\text{Sho}}}{t_r} + H^F_{\text{Sho}} - H^H_{\text{Sho}}$$

$$t_r = \frac{T_b}{1000}$$

where $H^A_{\text{Sho}}, H^B_{\text{Sho}}, H^C_{\text{Sho}}, H^D_{\text{Sho}}, H^E_{\text{Sho}}, H^F_{\text{Sho}}, H^G_{\text{Sho}}$, and H^H_{Sho} are the Shomate coefficients, and can be found in the NIST-JANAF database (Chase, 1998). The material entering the cell is assumed to reach the bath temperature very rapidly.

9.4.3 Heat Lost to the Surroundings

Heat flows from the cell to the surroundings because of the difference between temperatures. The cell is represented as a cuboid, whose faces are insulated to retain as much heat as possible. Figure 9.13 shows a scheme of how the aluminium cell is insulated.

The heat lost to the surroundings is a function of the bath temperature, the temperature of the surroundings, and the thermal resistance of the cell:

$$Q_{\text{Loss}} = \frac{T_b - T_{\text{Ext}}}{R'_{\text{Tot}}}$$

In the equation, Q_{Loss} is the total amount of heat lost to the surroundings in W, T_{Ext} is the temperature of the surroundings in K, and R'_{Tot} is the thermal resistance of the cell in K W^{-1}.

The cuboid is divided according to each face to calculate the thermal resistance. Thus, it is divided into four sub-models: (i) the upper face, (ii) the lower face, (iii) two side faces, and (iv) the front and back faces. Each face adds its own thermal resistance, which, altogether results in the total thermal resistance. The total thermal resistance is:

$$\frac{1}{R'_{\text{Tot}}} = \frac{1}{R'_{\text{Up}}} + \frac{1}{R'_{\text{Low}}} + \frac{1}{R'_{\text{Side}}} + \frac{1}{R'_{\text{Side}}} + \frac{1}{R'_{\text{Front}}} + \frac{1}{R'_{\text{Back}}} \tag{9.36}$$

where R'_{Up}, R'_{Low}, R'_{Side}, R'_{Front}, and R'_{Back} are, respectively, the upper face, lower face, side face, front face, and back face thermal resistances of the cell in K W^{-1}. The model for calculating the thermal resistances considers only two forms of heat transfer, convection and conduction. Convection is given in the interface between two bodies of different densities, in this case, the fluids can be either the electrolyte, the molten aluminium, or the air.

Upper face

On top of the electrolyte cell, there is a thin layer of frozen electrolyte and alumina powder that acts as an insulation. This layer is called crust. Thus, the upper face of the cell is insulated by the crust and the anode blocks. Figure 9.14 shows a scheme of this arrangement. Thus, the

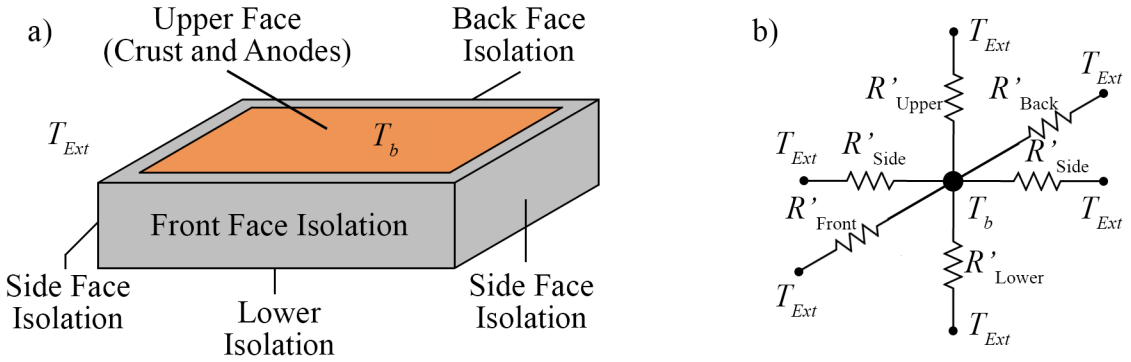


Figure 9.13: a) Representation of the insulation of the aluminium cell, and (b) its equivalent thermal circuit for heat transfer through the layers.

contribution of the upper face to the overall thermal resistance can be simplified considering that the anodes and the crust are arranged in parallel:

$$\frac{1}{R'_{\text{Up}}} = \frac{N}{R'_{\text{An}}} + \frac{1}{R'_{\text{Cr}}}$$
$$R'_{\text{An}} = \frac{1}{A_{\text{An}}}\left(\frac{1}{h_{\text{Air-An}}} + \frac{L_{\text{An}}}{k_{\text{An}}} + \frac{1}{h_{\text{Elec-An}}}\right) \tag{9.37}$$
$$R'_{\text{Cr}} = \frac{1}{A_{\text{Cr}}}\left(\frac{1}{h_{\text{Air-Cr}}} + \frac{L_{\text{Cr}}}{k_{\text{Cr}}} + \frac{1}{h_{\text{Elec-Cr}}}\right)$$

where N is the number of anodes (24 in this model) R'_{An} and R'_{Cr} are, respectively, the anode thermal resistance in K W^{-1}, A_{An} and A_{Cr} are the surface areas of the anode and crust in contact with the electrolyte bath in m^2, L_{An} and L_{Cr} are the height of the anode and the crust in m, $h_{\text{Air-An}}$ and $h_{\text{Air-Cr}}$ are the convection heat transfer coefficients between the air surrounding the cell and the anode and the crust in W m^{-2} K^{-1}, $h_{\text{Elec-An}}$and $h_{\text{Elec-Cr}}$ are the convection heat transfer coefficients between the electrolyte bath and the anode and the crust in W m^{-2} K^{-1}, and k_{An} and k_{Cr} are the thermal conductivity of the anode and the crust in W m^{-1} K^{-1}.

The data for the convection coefficients and the thermal conductivities are taken from Gheribi et al. (2017), Incropera et al. (2011) and Severo and Gusberti (2016). The measurements of the cell are taken from Kuschel and Welch (2016) and Peterson and Wang (2016). From Eq. 9.37, R'_{Up} is 0.0099 K W^{-1}.

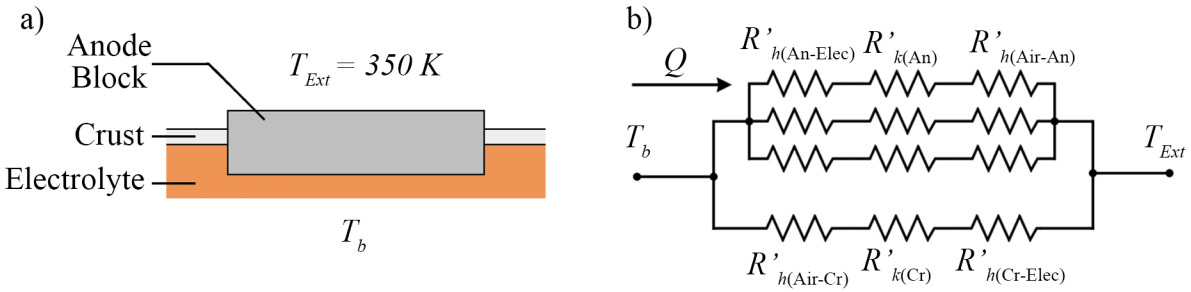


Figure 9.14: a) Schematic representation of the upper face of the insulation of the electrolytic cell, and b) its corresponding thermal resistance circuit.

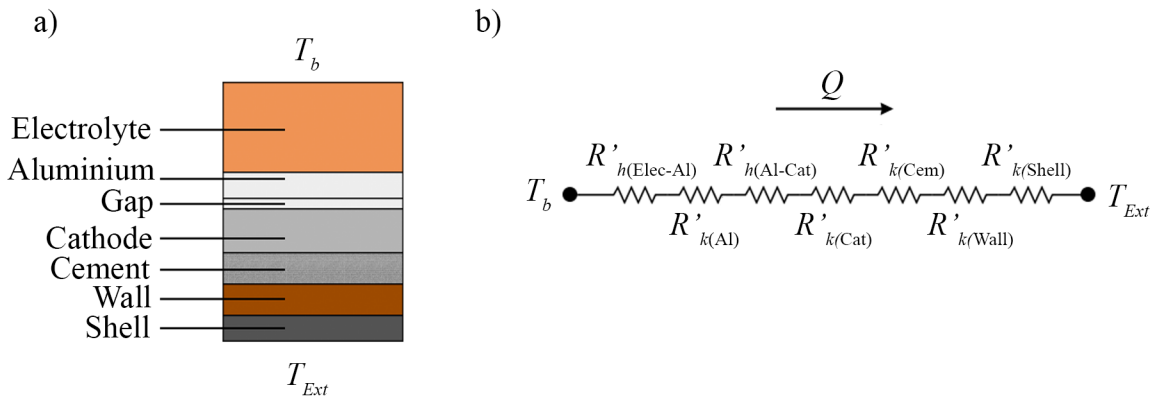


Figure 9.15: a) Schematic representation of the lower face of the insulation of the electrolytic cell, and b) its corresponding thermal resistance circuit.

Lower face

Figure 9.15 shows a schematic representation of the layers that form the lower face of the electrolytic cell.

The resistivity of the lower face is determined with the heat transfer coefficients of each layer. Thus, the contribution of the lower face to the overall thermal resistance is:

$$R'_{\text{Low}} = \frac{1}{A_{\text{Low}}}\left(\frac{1}{h_{\text{Elec-Al}}} + \frac{L_{\text{Al}}}{k_{\text{Al}}} + \frac{1}{h_{\text{Al-Cat}}} + \frac{L_{\text{Cat}}}{k_{\text{Cat}}} + \frac{L_{\text{Cem}}}{k_{\text{Cem}}} + \frac{L_{\text{Wall}}}{k_{\text{Wall}}} + \frac{L_{\text{Shell}}}{k_{\text{Shell}}}\right)$$

where A_{Low} is the area of the lower face of the bath, in m^2, $h_{\text{Elec-Al}}$ and $h_{\text{Al-Cat}}$ are the convection heat transfer coefficients between the bath and the molten aluminium, and between the molten aluminium and the cathode in $\text{W m}^{-2}\ \text{K}^{-1}$. L_i is the thickness of the layer i in m, and k_i is the thermal conductivity of the layer i in $\text{W m}^{-1}\ \text{K}^{-1}$. The floor has a thermal resistance of 1.27 K W^{-1}.

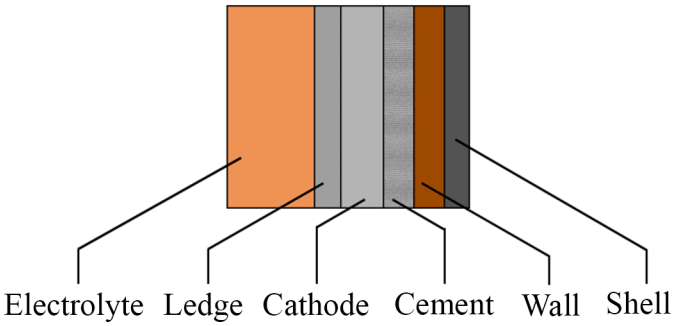


Figure 9.16: Schematic representation of one of the side faces of the insulation of the electrolytic cell.

Side faces

Figure 9.16 shows the layers of insulation of the sides of the cell.

The ledge layer in Figure 9.16 is the frozen layer of electrolyte that prevents the cathode from corroding. Thus, the contribution of the side faces to the overall thermal resistance is:

$$R'_{\text{Side}} = \frac{1}{A_{\text{Side}}}\left(\frac{1}{h_{\text{Bath-Ledge}}} + \frac{L_{\text{Ledge}}}{k_{\text{Ledge}}} + \frac{L_{\text{Cat}}}{k_{\text{Cat}}} + \frac{L_{\text{Cem}}}{k_{\text{Cem}}} + \frac{L_{\text{Wall}}}{k_{\text{Wall}}} + \frac{L_{\text{Shell}}}{k_{\text{Shell}}} + \frac{1}{h_{\text{Shell-Air}}}\right)$$

where A_{Side} is the area of one of the lateral faces of the bath, in m^2, $h_{\text{Elec-Ledge}}$ and $h_{\text{Shell-Air}}$ are the convection heat transfer coefficients between the bath and the frozen electrolyte, and between the outer layer and the surrounding air in $\text{W m}^{-2}\ \text{K}^{-1}$. L_{Ledge} is the thickness of the frozen electrolyte in m, and k_{Ledge} is the thermal conductivity of the frozen electrolyte in $\text{W m}^{-1}\ \text{K}^{-1}$. Each lateral face of the cell has a thermal resistance of $5.177\ \text{K W}^{-1}$.

Front and back faces

The front and back faces of the cell have the same structure as the lateral sides shown in Figure 9.16. The contact area, however, changes, so the thermal resistance can be calculated using Eq. 9.4.3 and substituting A_{Side} for the area of the front or back face of the cell. Thus, the thermal resistance of the front or the back face of the cell is 1.78 K W^{-1}.

Total thermal resistance

Therefore, the overall thermal resistance in Eq. 9.36 is 3.308 $\times$ 10^{-3} K W^{-1}. Higher thermal resistance is reflected in a higher thermal resistance value. Thus, the numerical values in this section show that most of the heat is lost through the upper face.

9.4.4 Heat Absorbed and Released by the Reactions

Chemical reactions also contribute to the heat balance of the cell. These reactions can either absorb or release heat. The enthalpy of reaction is calculated as the difference between enthalpies of formation of the products and the enthalpies of formation of the reactants. If the enthalpy of reaction is negative, the reaction is exothermic and the reaction releases energy to the bath, and if it is positive, it is endothermic, and the reaction absorbs energy from the bath. For a generic reaction $m\text{A} + n\text{B} \rightarrow p\text{C} + q\text{D}$, the enthalpy of reaction is:

$$\Delta H_{\text{Reaction}} = (p\Delta H_{f,\text{C}} + q\Delta H_{f,\text{D}}) - (m\Delta H_{f,\text{A}} + n\Delta H_{f,\text{B}})$$

where H_{Reaction} is the enthalpy of reaction in kJ mol^{-1}, and $\Delta H_{f,i}$ is the enthalpy of formation of component i in kJ mol^{-1}. The enthalpies of formation of the compounds in the process can be found in the NIST-JANAF database (Chase, 1998).

Section 9.2.1 introduced the alumina reduction reaction considering the current efficiency as:

$$2\,\eta\ \mathrm{Al_2O_3} + 3\,\mathrm{C} \longrightarrow 4\,\eta\ \mathrm{Al} + 3\,(2\,\eta\ -\ 1\,)\mathrm{CO_2} + 6\,(1\,-\eta)\mathrm{CO}$$

Considering that, for a pure substance, the enthalpy of formation is zero, the enthalpy of reaction is:

$$\Delta H_{\text{Reaction}} = \frac{3}{4}\left(2-\frac{1}{\eta}\right)\Delta H_{f,\mathrm{CO_2}} + \frac{3}{2}\left(\frac{1}{\eta}-1\right)\Delta H_{f,\mathrm{CO}} - \frac{1}{2}\,\Delta H_{f,\mathrm{Al_2O_3}}$$

Table 9.2 shows the enthalpy of formation for the three compounds related to the enthalpy of reaction equation.

Thus, the enthalpies of formation for the compounds presented in Table 9.2 can be written as a function of the bath temperature as:

$$\Delta H_{f,\mathrm{Al_2O_3}} = -1.705\times10^{3} + 1.120\times10^{-2}\,T \quad \text{kJ mol}^{-1}$$

$$\Delta H_{f,\mathrm{CO_2}} = -3.925\times10^{2} - 2.097\times10^{-3}\,T \quad \text{kJ mol}^{-1}$$

$$\Delta H_{f,\mathrm{CO}} = -1.056\times10^{2} - 6.400\times10^{-3}\,T \quad \text{kJ mol}^{-1}$$

Assuming a current efficiency of 95%, the heat of reaction, as a function of the temperature can be written as:

$$\Delta H_{\text{Reaction}} = 565.282 - 0.0076\,T \quad \text{kJ mol}^{-1} \tag{9.38}$$

Eq. 9.38 shows that to produce a mole of aluminium, the reaction needs around 560 kJ . Using the same approach, the enthalpy of reaction of the remaining reactions can be calculated. The

Table 9.2: Enthalpy of Formation in kJ mol^{-1} for the relevant compounds in the aluminium reduction

Temperature	1000	1100	1200	1300	1400
Alumina	-1693.394	-1692.437	-1691.366	-1690.190	-1688.918
CO_2	-394.623	-394.838	-395.050	-395.257	-395.462
CO	-111.983	-112.586	-113.217	-113.870	-114.541

reactions involved in the cell were included in the mass balance model included the reactions involved in the cell (Reactions 9.18, 9.19, 9.21, 9.23, and 9.24). The enthalpies of reaction presented in the next equations are in kJ mol^{-1}

$$3\,Na_3AlF_6 + \frac{3}{2}\,H_2 \longrightarrow Al + 3\,NaF + 3\,HF \qquad \Delta H_{\text{Reaction}} = 793.26 - 0.1258\,T$$

$$2\,AlF_3 + 3\,H_2O \longrightarrow Al_2O_3 + 6\,HF \qquad \Delta H_{\text{Reaction}} = 324.03 - 0.0759\,T$$

$$NaF + AlF_3 \longrightarrow NaAlF_4 \qquad \Delta H_{\text{Reaction}} = 895.21 - 0.9347\,T$$

$$3\,Na_2CO_3 + 2\,AlF_3 \longrightarrow 6\,NaF + Al_2O_3 + 3\,CO_2 \qquad \Delta H_{\text{Reaction}} = 24.784 - 0.1498\,T$$

$$3\,Na_2O + 2\,AlF_3 \longrightarrow 6\,NaF + Al_2O_3 \qquad \Delta H_{\text{Reaction}} = 844.58 + 0.1860\,T$$

The cell uses energy for dissolving the undissolved alumina. The undissolved form of alumina is the gamma phase, and the dissolved alumina is the alpha phase. Thus, the enthalpy of dissolution is:

$$\Delta H_{\text{Diss}} = \Delta H_{f,\alpha} - \Delta H_{f,\gamma} \quad \text{kJ mol}^{-1}$$

where ΔH_{Diss} is the enthalpy of dissolution in kJ mol^{-1}, and $\Delta H_{f,\alpha}$ and $\Delta H_{f,\gamma}$ are the enthalpy of formation of the alpha and gamma phase respectively in kJ mol^{-1}. Both values can be found in Chase (1998). As a function of the temperature, the enthalpy of dissolution can be written as:

$$\Delta H_{\text{Diss}} = -17 - 0.006\,T \quad \text{kJ mol}^{-1}$$

Combining all the enthalpies of reactions and the enthalpy of dissolution with the mass balance model, it is possible to obtain the overall energy requirements for the process to carry out the alumina reduction and the necessary reactions to maintain balance in the cell.

9.5 Solution Approaches in the Study of the Aluminium Smelter

This section includes the assumptions made to solve the aluminium smelter model. It also describes the calculations and simulations that were performed to analyse the influence that the process variables have on the electrical power consumed by the cell.

9.5.1 Assumptions of the Aluminium Smelter

The main assumption in the model is that the system is lumped, meaning that the temperature and the concentration in the electrolyte bath are homogeneous. The only gradient that is considered in the model is the concentration gradient in the interface between the anode and the bath, and between the bath and the cathode. However, for all the remaining calculations, the concentrations and temperatures are constant through space, and the thickness of frozen bath is assumed to be constant.

Another assumption involves the transfer of heat from the bath to the surroundings. The cell is assumed to be a rectangular block, in which each face has a series of layers. There are two factors that have not been considered

- The heat balance does not include the losses due to radiation
- The model does not consider the joints between the faces or in the corners

According to Rye et al. (2013), the losses to the surroundings due to radiation are much lower than the losses due to convection, so the contribution of the radiation to the heat losses can be neglected in this case. Namboothiri et al. (2009) stated that the losses to the surroundings through the joints and through the corners are negligible compared to the losses through the faces.

As the aluminium reduction progresses, the anode carbon block is consumed, and therefore the height of the carbon block decreases. This would lead to a decreased surface contact area between the anode and the electrolyte bath. In practice, the block is lowered, so both the surface contact area and the distance between anode and cathode remain constant. In practice, the anode block is changed around every 28 days (Jessen, 2008). Since the period of operation simulated in this project is no more than 24 hours, the block replacement is neglected.

9.5.2 Degrees of Freedom and Fixed Variables

Contrary to the LNG study, the degrees of freedom in the aluminium smelter can be easily deduced after modelling the process. There are nine degrees of freedom. One degree of freedom corresponds to the temperature of the surroundings, whose value is 350K. The analyst gives values to the concentration of LiF, MgF_2, and CaF_2, whose values are respectively 1% wt, 1% wt, and 6% wt.

Therefore, the analyst needs to fix five independent variables to solve the model. These five variables are the temperature of the bath, the electrical power consumption, the alumina concentration, the mass of bath, and the bath ratio.

The model calculates the dependent variables, namely the distance between the anode and the cathode (IPD), the electrical current, the alumina feed rate, the AlF_3 feed rate, and the Na_2CO_3 feed rate.

9.5.3 Solution Approaches

The model is calculated to observe the relationships between the process variables and the electrical consumption of the cell in steady state operation. The simulation of the model provides the transient behaviour of the cell. The results of the calculations and the simulations give a range of operability that forms the envelope of feasible operation that the Process Power Management can use for adjusting the power consumption in the aluminium smelter.

Steady State Operation of the Aluminium Smelter

The model calculates the IPD, the electrical current and the feed rates for given values of the bath temperature, electrical power consumption, alumina concentration, bath ratio, and bath mass. Every calculation changes the value of each independent variable (except the bath mass) at a time, and the observed variable is the production rate, which is a function of the electrical current.

The calculations are carried out in Matlab. The model establishes the limits of the IPD as 2 cm for the lower limit and 6 cm for the upper limit. If the fixed variables cause the IPD to exceed any limit, the calculations adjust the temperature for meeting the established limits. For instance, if the given values of the temperature and power consumption caused the IPD to be higher than 6 cm, the calculations provide the temperature that corresponds to an IPD of 6cm, and that is closest to the fixed temperature. During these conditions, the other fixed independent variables do not change their values. Chapter 10 shows and discusses the results of the calculations.

Transient Behaviour of the Aluminium Smelter

The model simulates a sudden power reduction to observe the transient behaviour of the process. The transient behaviour of the temperature and the heat balances are introduced in Section 11.1. The nominal power consumption is set at 850kW, and after two hours of operation, it is reduced to a certain percentage of its nominal value during a certain period of time. The range of power reduction goes from 50% to 100% of its nominal value, and the range of the period of time in which the power is reduced goes from one to six hours. The established values for the temperature, the alumina concentration and the bath ratio are constant during the simulation, and the observed variables are the production rate, and the temperature of the bath.

The reason for changing the amount of time of the power reduction is to observe how the stored energy in the bath decays when the power consumption is reduced. If the stored energy

decreases, so does the temperature, and it is important to determine for how long the temperature can be kept within the limits.

The simulations are carried out in Simulink. The simulations use the calculations from Matlab to establish the initial operating point. Chapter 11 shows and discusses the results of the simulations.

9.6 Control Systems in the Aluminium Smelter

This section explains, for the dynamic simulations, the mechanism used in the model for controlling the electrolytic cell. For comparison, this section describes the control system in industrial practice.

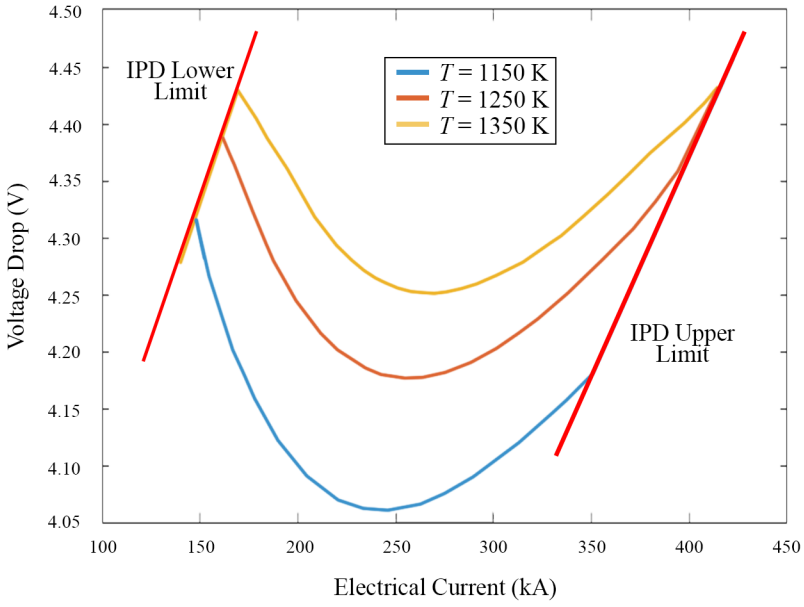


Figure 9.17: Optimal operating window in an aluminium electrolytic cell as a function of the voltage drop and the electrical current. The operating window is delimited by the temperature limits (1150K in blue and 1350K in yellow) and the minimum and maximum IPD (red).

9.6.1 Control Systems in Industrial Practice

In industrial practice, the operator adjusts the process variables to minimise the power consumption per unit of produced aluminium. Figure 9.17 shows the optimal operating window in an aluminium electrolytic cell as a function of the electrical current and the cell voltage drop.

The operating window in Figure 9.17 depends on the properties of the bath, such as the resistivity, the bath temperature, the alumina concentration, and the bath ratio. The heat and mass balances establish the temperature and IPD limits. According to the patents by Blatch et al. (1996); Michard (2018), the process determines the electrical current according to the established production rate. The electrical current affects the properties of the bath, so the operators

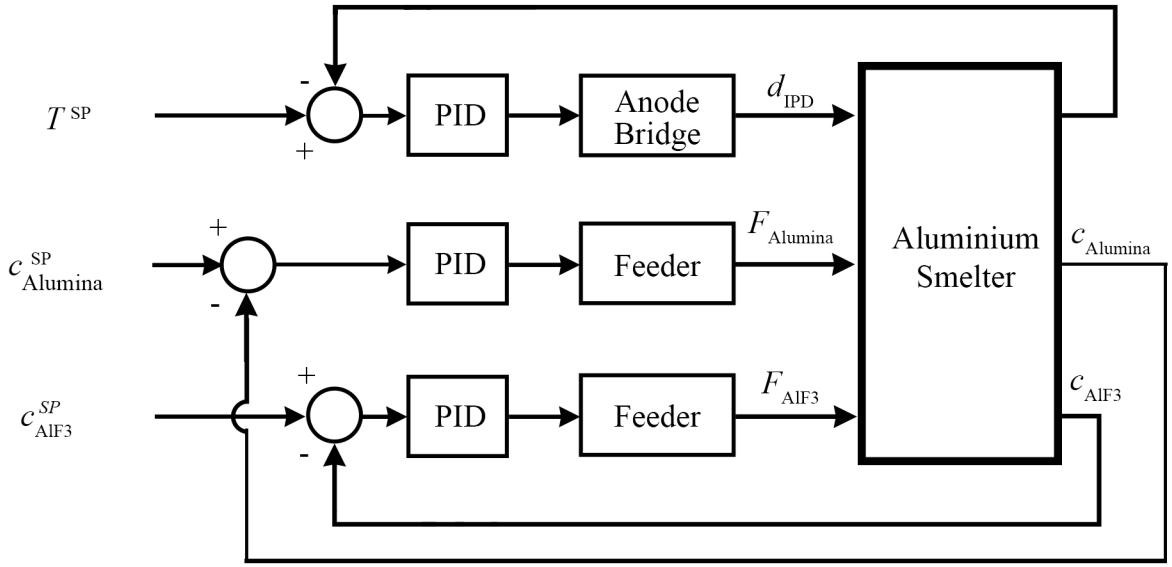


Figure 9.18: Control loops of an aluminium smelter in the industry. The temperature of the bath is adjusted by varying the IPD, the concentration of the AlF_3 and consequently the bath ratio are controlled by adjusting the AlF_3 feed rate, and the alumina concentration is controlled by adjusting the alumina feed rate.

adjusts these properties to optimise the electrical costs of producing aluminium for a given electrical current.

Industrial electrolytic cells usually have three manipulated variables, the alumina and AlF_3 feeds, and the IPD (Blatch et al., 1996; Michard, 2018). In some industries, the feed rate of Na_2CO_3 is manipulated for controlling the total mass of the bath (Jessen, 2008; Kolås and Støre, 2009; McFadden et al., 2006).

The controlled variables are the temperature of the bath, the concentration of alumina, and the concentration of AlF_3. Figure 9.18 shows the control loops used in industry.

The temperature is controlled by adjusting the IPD, which modifies the electrical resistance of the bath, and consequently, the Joule heat generated. The bath ratio changes when the AlF_3 concentration changes, which is adjusted by varying the AlF_3 feed rate. The smelter draws as much electrical power as it needs for operating the plant.

9.6.2 Control Systems in the Model

The model in this thesis controls the power consumption of the cell by adjusting the electrical current. Additionally, the model controls the bath mass by adjusting the Na_2CO_3 feed rate. The AlF_3 feed rate is adjusted to control the bath ratio instead of controlling the AlF_3 concentration.

The model is simulated in Simulink, and the controllers are PIDs that have been tuned according to the PID tuning algorithm developed by Mathworks (Matlab, 2010). The PID controller for the IPD establishes the upper and lower limit so that the maximum IPD is 6cm and the minimum IPD is 2cm.

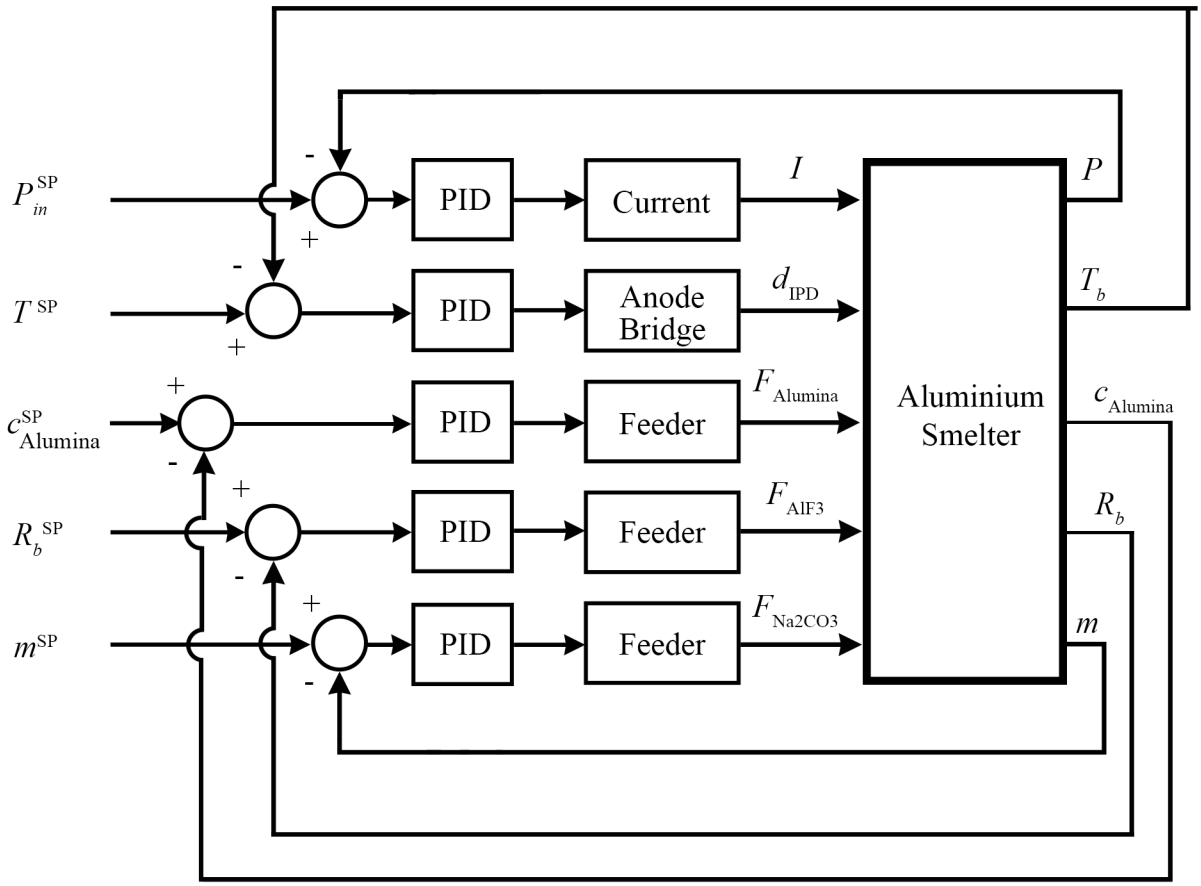


Figure 9.19: Control loops of the aluminium smelter model. The temperature of the bath is controlled by adjusting the IPD, the AlF_3 concentration and the bath ratio (R_b) are controlled by adjusting the AlF_3 feed rate, the alumina concentration is controlled by adjusting the alumina feed rate, the mass of the bath is controlled by adjusting the The Na_2CO_3 feed rate, and the electrical power consumption is controlled by adjusting the electrical current.

9.7 Summary of the Chapter

This chapter has described the mathematical model of the aluminium smelting process, and the solution approaches. Additionally, this chapter has found the independent variables and has described the control system in a real aluminium smelter to introduce the control system in the

model of this thesis. This chapter has described the three sub-models that form the aluminium smelter model.

The three sub-models are the mass balance model, the electrical model, and the heat balance model. This chapter mentions that the three sub-models have to be calculated simultaneously because of the links amongst sub-models.

The mass balance model considers the reactions in the bath, the material fed to the cell, and the products exiting the cell. This model also calculates the heats of reaction and the heats absorbed by the feeds. The electrical model takes into account the voltages that contribute to the overall voltage of the cell. The voltage drop in the electrolyte cell and the electrical current generate heat due to the Joule heating effect. Additionally, the voltage drop in the external parts of the cell and the electrical current absorb electrical power which does not heat the bath. The heat balance model receives inputs from the mass balance model and the electrical model to calculate the bath temperature. This model also calculates the heat lost to the surroundings.

The model of the aluminium smelter has five degrees of freedom. The fixed variables are the bath temperature, the electrical power consumption, the mass of the bath, the bath ratio ($R_b = \mathrm{NaF}/\mathrm{AlF_3}$), and the alumina concentration.

The model is calculated giving a different value to each independent variable every calculation. The results of the calculations are presented in Chapter 10. The model simulates 24 hours of operation, and reduces the electrical power consumption suddenly to observe the transient behaviour of the process. The results of the simulations are presented in Chapter 11.

This chapter has also explained the control system in industrial practice. Industries control the temperature of the bath by adjusting the distance between the anode and the cathode. The alumina concentration is controlled by adjusting the alumina feed rate, and the AlF_3 concentration is controlled by adjusting the AlF_3 feed rate. In addition to the controlled variables in industry, the power is also controlled by adjusting the electrical current, and the bath mass is controlled by adjusting the Na_2CO_3 feed rate. This thesis uses the PID controllers that Simulink offers, and tuned the controllers using the PID Tuner App.

Chapter 10

Steady State Operation of the Aluminium Smelter

This chapter studies the steady state operation in an aluminium smelting process. The analysis studies the range of operability of the process at steady state, and then shows the results of the calculations for various values of the independent variables. The nominal operation point corresponds to an alumina concentration of 3% wt, a bath temperature of 1250K, a bath ratio of 1.15, and the bath mass of 10000 kg.

10.1 Calculations of the Steady State Operation

This section shows the results of the calculations made for operational points when the process variables are varied. The calculations varies the electrical power consumption, the alumina concentration, the bath ratio, and the temperature of the bath.

10.1.1 Effects of Varying the Alumina Concentration

Figure 10.1 shows the dependence of the aluminium production rate on electrical power consumption. The horizontal axis shows the concentration of alumina in the bath as a weight percentage, and the vertical axis is the aluminium production rate in kg s^{-1}. Each curve represents a different level of electrical power consumption.

From Figure 10.1, the effect of the alumina concentration on the aluminium production rate is not as notable as the effect of the electrical power consumption. However, increasing the alumina concentration or the power consumption leads to a higher aluminium production rate.

For a fixed alumina concentration in the bath, the electrical current and the voltage increase when the power consumption increases. Thus, according to the Faraday's law of electrolysis (Eq. 9.2), the aluminium production rate increases when the power consumption rises.

For a fixed power consumption, when the alumina concentration in the bath increases, the overall voltage of the bath increases (Section 9.3) as seen in Figure 10.2.a) [1]. Figure 10.2.b) shows

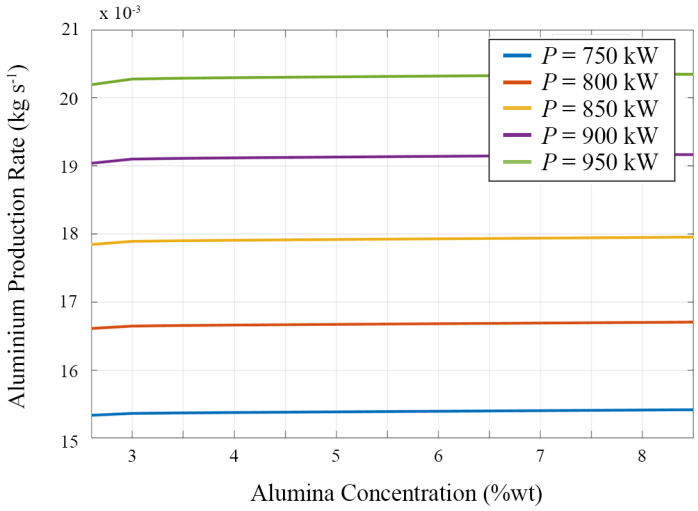


Figure 10.1: Effects on the aluminium production rate (kg s^{-1}) of varying the alumina concentration (% wt), for various levels of power consumption (kW).

[1] Figure 10.2 should not be confused with Figure 9.12, where the electrical power consumption is not fixed. In this case, the consumption is fixed, and therefore, the voltage is compensating the electrical current increase

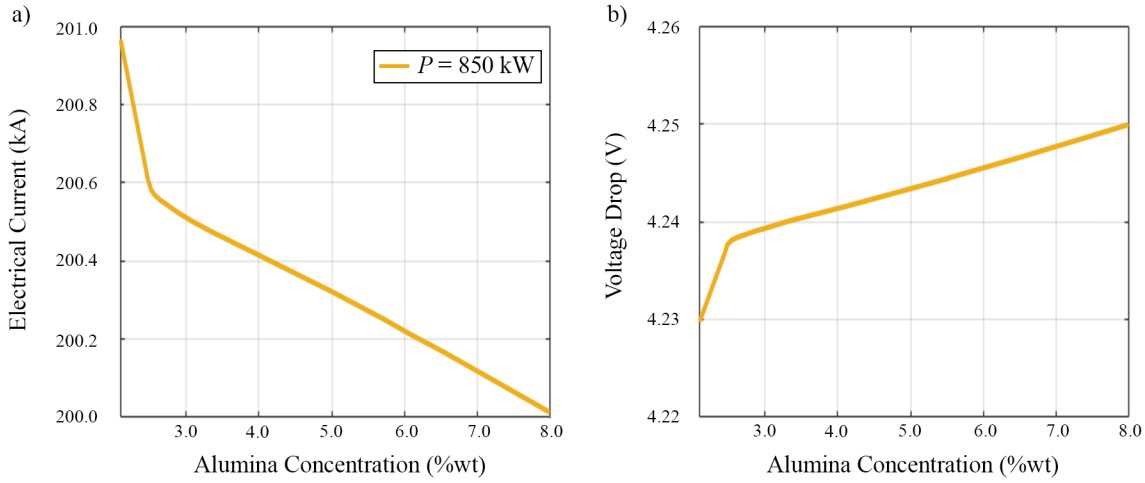


Figure 10.2: Effects on the a) voltage drop in the cell (V) and b) the electrical current (kA) of varying the alumina concentration (% wt), for a power consumption of 850kW

that the electric current decreases when the alumina concentration increases, so it compensates the increase of voltage drop.

According to the Faraday's law, an increase of electrical current would result in an increase of aluminium production rate, but this does not correspond to the increase of aluminium production rate seen in Figure 10.1. This is explained considering the current efficiency, which considers the amount of current that is actually being used for producing aluminium:

$$\frac{dm_{Al}}{dt} = 9.321 \times 10^{-8}\, I\, \eta \quad \mathrm{kg_{Al} s^{-1}} \tag{9.2}$$

Thus, the aluminium production rate not only depends on the current, but also on the current efficiency. Figure 10.3 shows that the current efficiency increases as the alumina concentration is raised. This increment overcompensates the electric current decrease, and therefore, the aluminium production increases when the alumina concentration increases.

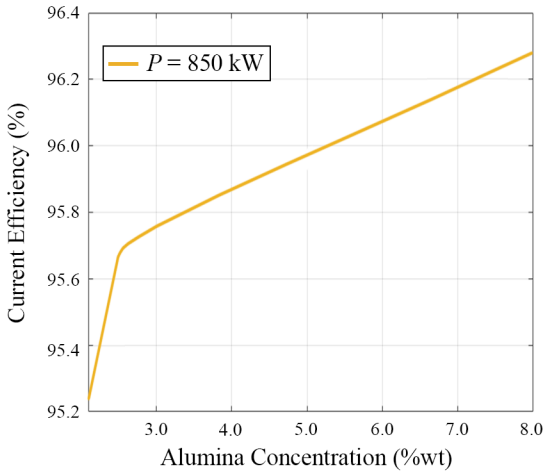


Figure 10.3: Effects on the current efficiency (%) of varying the alumina concentration (% wt), for a power consumption of 850kW

Figures 10.2 and 10.3 shows a shows a rapid reduction of current efficiency when the alumina concentration is below 2.8% wt. This is because the concentration is getting close to the anode effect concentration, which is assumed to be 2 % wt [2].

10.1.2 Effects of Varying the Bath Ratio

Figure 10.4 shows the dependence of aluminium production rate on the bath ratio, for an electrical power consumption of 850 kW [3].The units of the vertical axis in Figure 10.4 are in kg day^{-1} because if they were given in kg s^{-1}, the evolution would be imperceptible.

The aluminium production rate does not change significantly with bath ratio. There is a bath ratio in which the production is at its maximum for a given power consumption. The reason for this is the behaviour of the current, that, in turn is imposed by the behaviour of the voltage drops. Figure 10.5 shows the consequences of varying the bath ratio on the current and on the

[2]Figure 10.2 should not be confused with Figure 9.12, where the electrical power consumption is not fixed. In this case, the consumption is fixed, and therefore, the voltage is compensating the electrical current increase

[3]In this case, the plot only shows one level of power consumption, because otherwise it would be difficult to appreciate the curvature of the relationship.

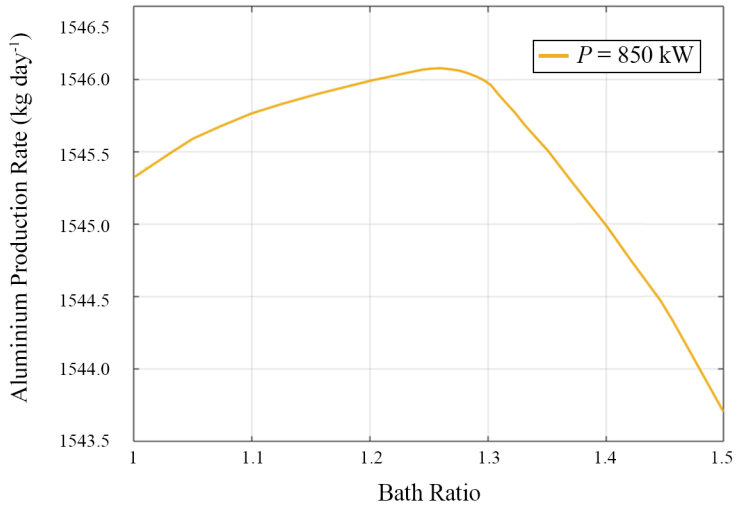


Figure 10.4: Effects on aluminium production rate (kg day^{-1}) of varying the bath ratio, for a power consumption of 850kW.

voltage drop. There is a minimum in the electrical current (and consequently a minimum in the voltage drop) when the bath ratio is at 1.15.

Figure 10.6 shows the behaviour of the voltage observed in Figure 10.5. Figure 10.6 shows the contribution of each factor to the total voltage drop. The bubble voltage drop and the electrolyte voltage drop behave in opposite directions, but the decrease of electrolyte voltage drop is larger than the increase of bubble voltage drop. However, before the bath ratio reaches 1.15, the bubble voltage drop increases more rapidly compared to the rate of decrease of the electrolyte voltage drop. Therefore, when the bath ratio is below 1.15, the voltage drop increases when the bath ratio increases, and when the bath ratio is above 1.15, the voltage drop decreases when the bath ratio increases.

From Figures 10.4 and 10.5.a), when the electrical current increases, the production rate decreases. This is due to the behaviour of the current efficiency. Figure 10.7 shows the current efficiency when the bath ratio changes. From Figures 10.7 and 10.5 the rate of decrease of the current efficiency is larger than the rate of increase of the electrical current, and therefore, from Eq. 9.2, the aluminium production tends to drop due to the current efficiency.

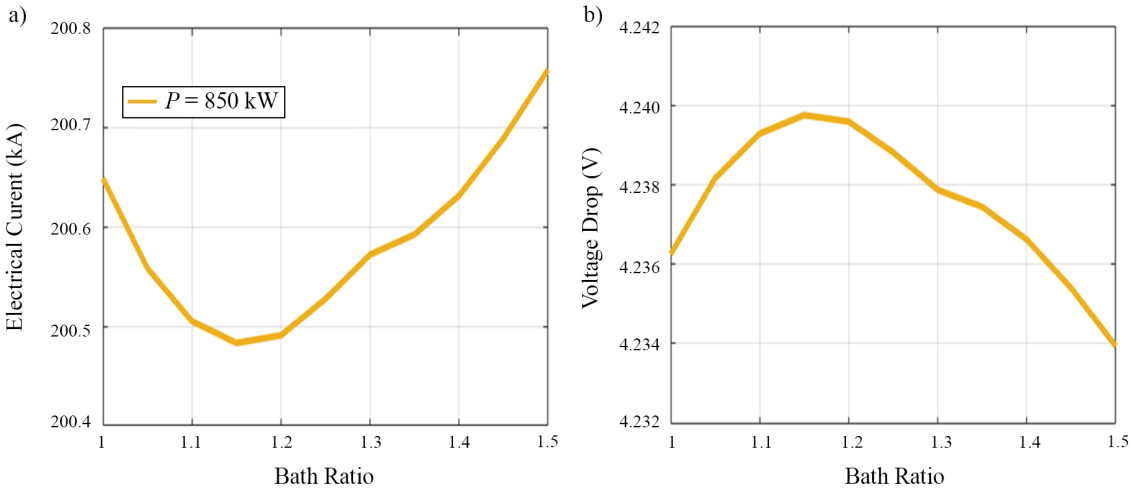


Figure 10.5: Effects on a) the electrical current (kA) and b) the voltage drop of varying the bath ratio, for a power consumption of 850 kW.

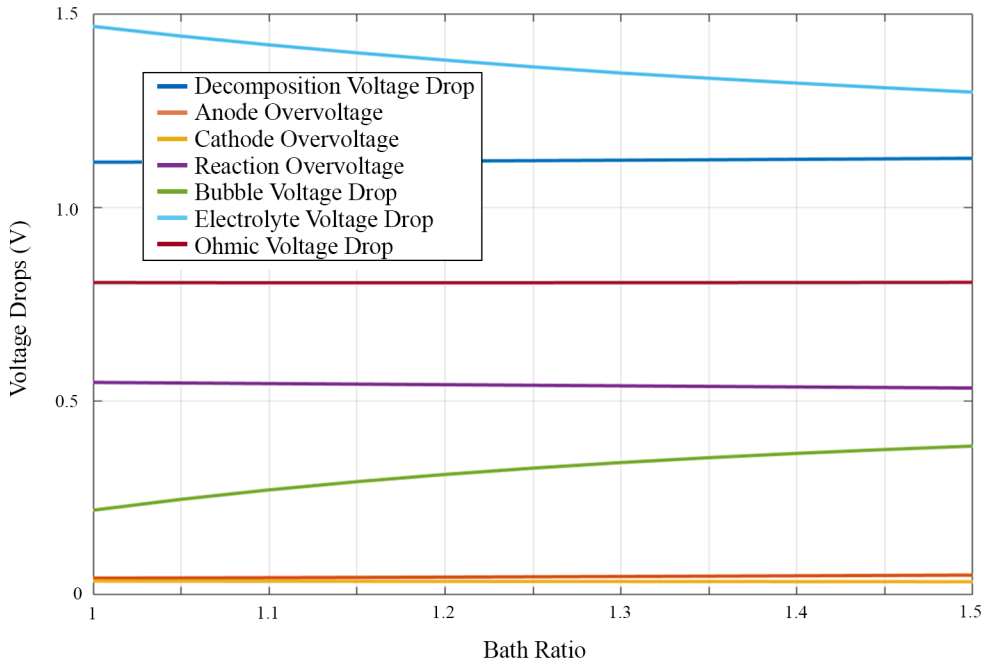


Figure 10.6: Effects on the contributions to the total voltage (V) of varying the bath ratio, for a power consumption of 850 kW.

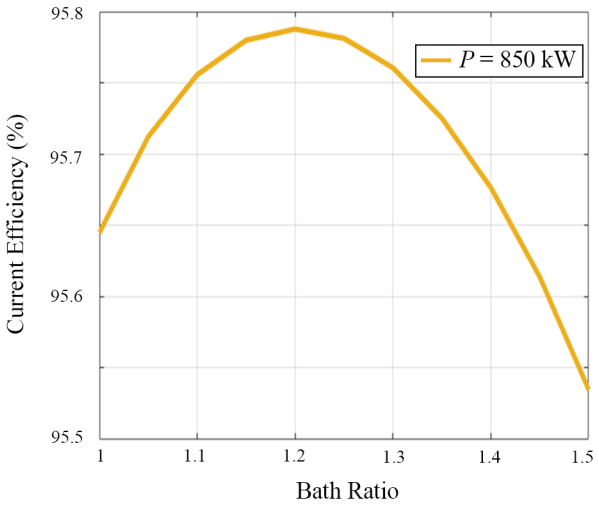


Figure 10.7: Effects on the current efficiency (%) of varying the bath ratio, for a power consumption of 850 kW.

10.1.3 Effects of Varying the Bath Temperature

Figure 10.8 shows how the aluminium production rate changes when the bath temperature varies. The aluminium production rate decreases more rapidly than when the alumina concentration or the bath ratio change, meaning that varying the temperature is a more effective mechanism for changing the production of aluminium.

Increasing the temperature of the bath increases the IPD (Figure 10.11). When the IPD increases, the electrolyte voltage increases, and, for fixed electrical power consumption, the electrical current decreases for offsetting the voltage increase. Figure 10.9 shows the effects on the contributions to the total voltage when the bath temperature varies. The electrolyte voltage drop increases when the temperature increases because the IPD increases.

Figure 10.10 shows the effects on the electrical current and the voltage drop when the bath temperature varies. The electrical current decreases when the temperature increases, which ultimately causes the aluminium production rate to decrease (Figure 10.8).

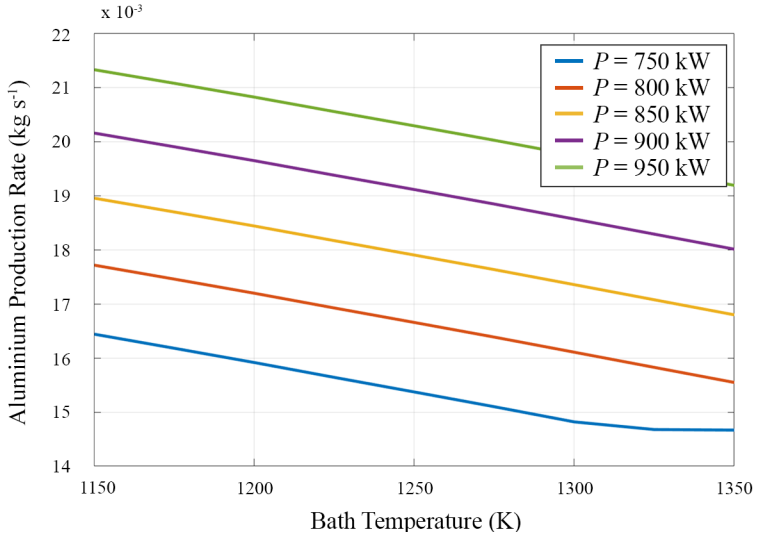


Figure 10.8: Effects on the aluminium production rate (kg s^{-1}) of varying the bath temperature (K), for various levels of power consumption (kW).

10.2 Envelope of Feasible Operation in an Aluminium Smelter

As mentioned in Section 9.5.3, the model sets an upper limit for the IPD at 6 cm. For fixed values of the independent variables, if the model calculates an IPD higher than 6 cm, the model returns the closest temperature that corresponds to an IPD of 6 cm.

The temperature of the bath changes when the IPD varies: when that distance is significant, the voltage drop caused by the electrolyte ohmic resistance is high. Therefore, for a fixed power consumption and temperature, the IPD is adjusted to change the heat caused by electrolyte ohmic resistance accordingly. For instance, if the established temperature is high, the IPD increases, so the available power is used to increase the electrolyte voltage drop, and the temperature is raised. Figure 10.11 shows the IPD when the temperature and the power changes, supporting the argument proposed above.

Figure 10.11 shows that, when the electrical power is 750 kW and the temperature is 1310 K the IPD reaches its limit. Thus, for a power consumption of 750 kW, the steady state operation becomes infeasible if the temperature is higher than 1310 K. In this case, when the bath temper-

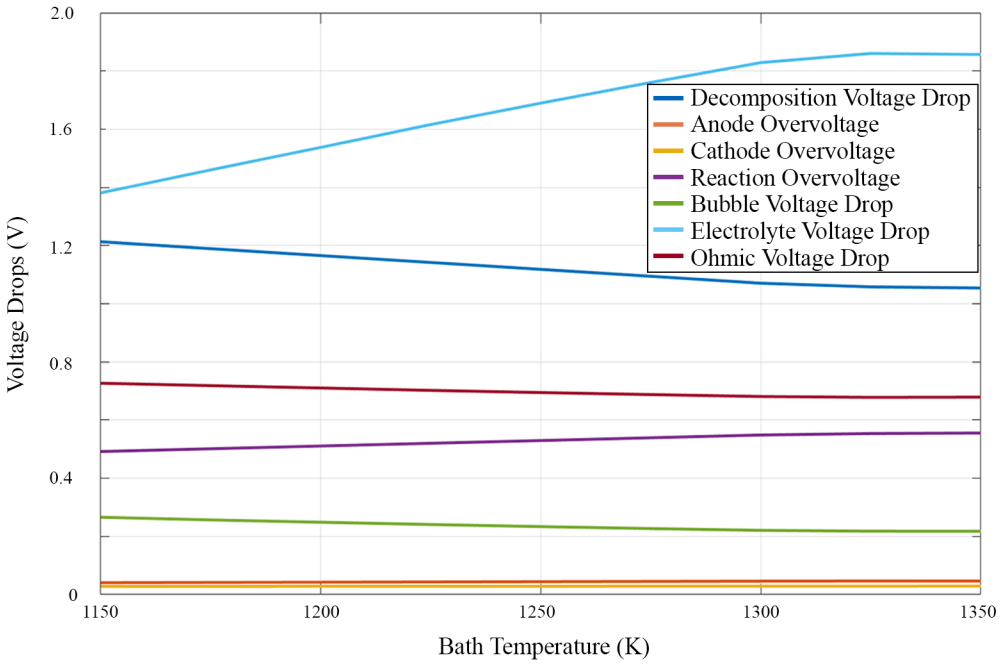


Figure 10.9: Effects on the contributions to the total voltage (V) of varying the bath temperature (K), for a power consumption of 750 kW. The shaded area indicates the region in which the operation is not feasible at steady state according to Section 10.2

ature is fixed at 1350 K, the calculations detects that the IPD exceeds 6cm, so the model fixes the IPD at 6 cm and returns the bath temperature that is the closest to 1350 K, which is 1310 K.

This analysis is extended to a wider range of power consumption and bath temperatures to obtain the envelope of feasible operation. The analysis has been performed by establishing the bath temperature at its two limits, 1150 K for the lower limit, and 1350 K for the upper limit, and varying the power consumption of the plant. Figure 10.12 shows that the envelope of feasible operation is between 625 kW and 1800 kW (73.52% and 211.74%).

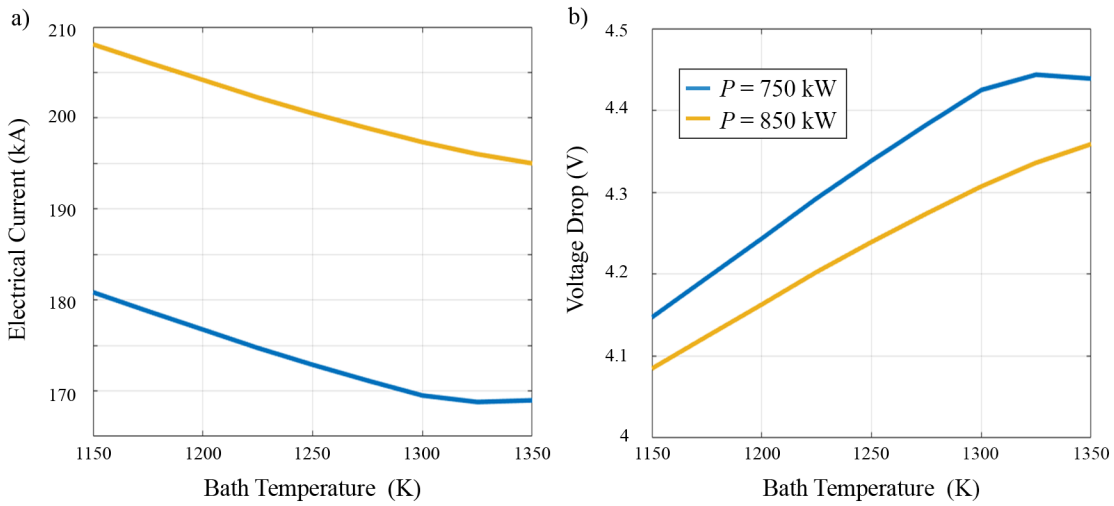


Figure 10.10: Effects on the a) electrical current (kA), and b) voltage drop (V) of varying the bath temperature (K), for the electrical power consumption at values of 750 kW and 850 kW. The shaded area indicates the region in which the operation is not feasible at steady state according to Section 10.2

From Figure 10.12, the cell can operate steadily if the bath temperature meets the following equations:

$$\begin{aligned} 625\text{kW} < P < 780\text{kW} &\rightarrow 1150\text{K} < T_b < (1.28P + 350)\text{K} \\ 800\text{kW} < P < 1400\text{kW} &\rightarrow 1150\text{K} < T_b < 1350\text{K} \\ 1450\text{kW} < P < 1800\text{kW} &\rightarrow (0.571P + 321.43)\text{K} < T_b < 1350\text{K} \end{aligned} \tag{10.1}$$

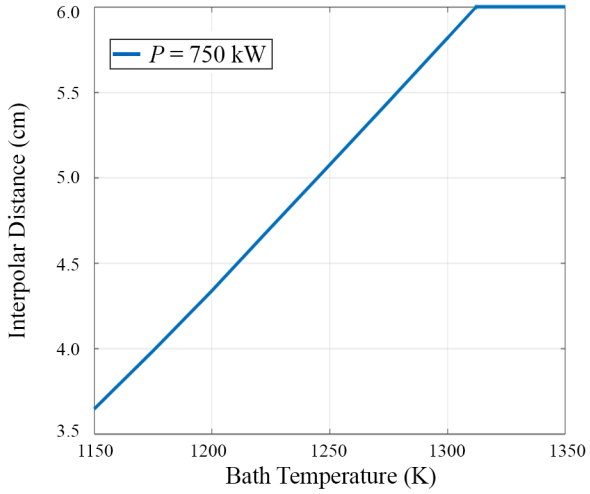


Figure 10.11: Effects on the the distance between electrodes (cm) of varying the bath temperature (K), for a power consumption of 750kW.

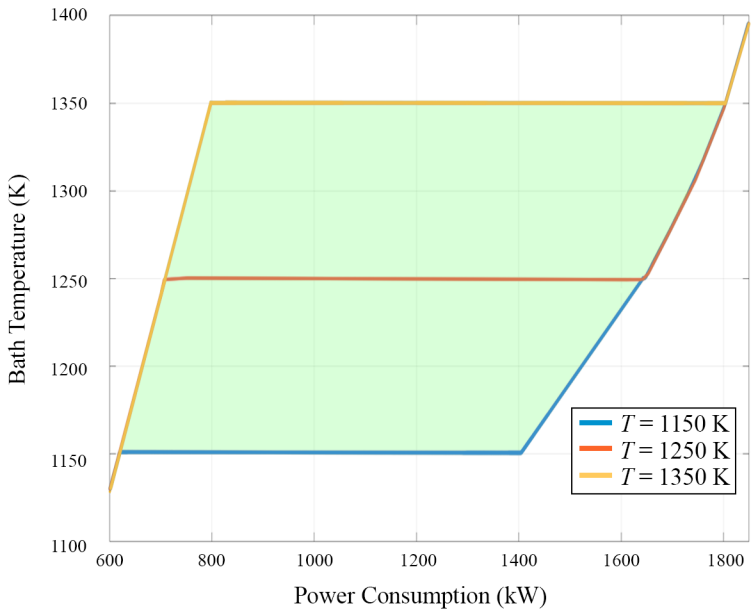


Figure 10.12: Relationship between the bath temperature (K) and the power consumption (kW). The plot shows that there are feasible solutions to the model giving a bath temperature of between 1150 K (blue) and 1350 K (yellow) when the power consumption is between 625 kW and 1800 kW

Figure 10.13 shows the electrical current and the aluminium production rate for the range of power consumption operability in the range of feasible bath temperatures. From the graph 10.13, the production rate corresponding to the minimum electrical power consumption is 12.7 g s^{-1}, and the production rate corresponding to the maximum electrical consumption is 34.96 g s^{-1}.

The model has calculated that the power consumption limits are between 625 kW and 1800 kW. These power consumption limits can be exceeded during a certain amount of time if the power is restored before the bath temperature reaches one of its limits. This will be demonstrated in the next chapter.

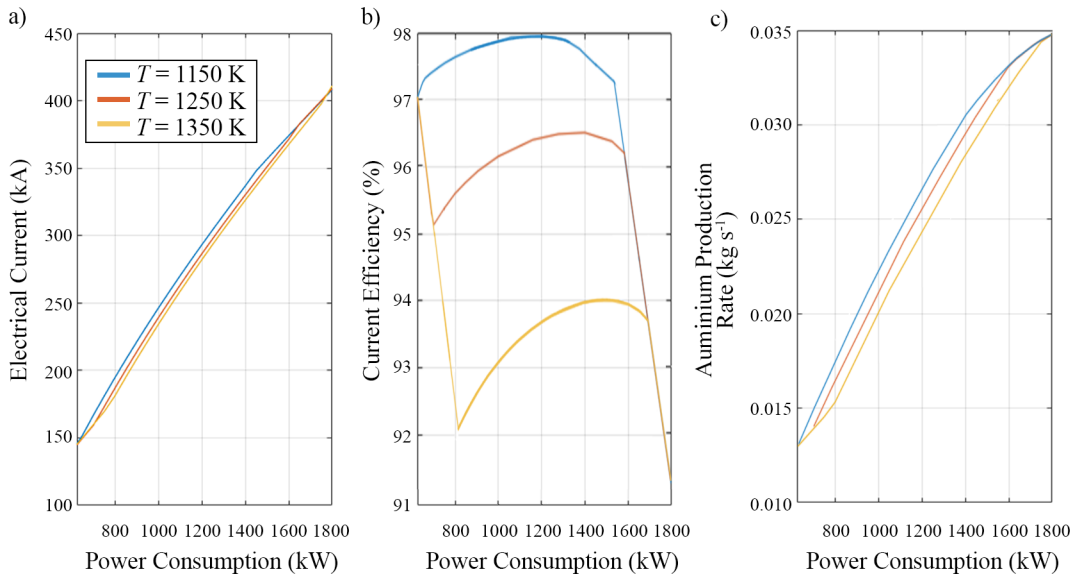


Figure 10.13: Effects on the a) electrical current (kA), b) electrical current (%), and c) aluminium production rate (kg s^{-1}) of varying electrical power consumption for the bath temperature at values of 1150 K (blue), 1250 K (orange), and 1350 K (yellow).

10.3 Summary of the Chapter

This chapter has shown the calculations of the model for steady state operation. The results showed the effect on the aluminium production rate of varying the bath temperature, the bath ratio, the alumina concentration, and the electrical power consumption. The power consumption has significant effects on the aluminium production rate. This suggests that, when the power consumption needs to be reduced, inevitably, the aluminium production rate has to be reduced accordingly.

The alumina concentration and the bath ratio has little influence on the aluminium production rate, but they can be adjusted to increase the current efficiency, and consequently, the production rate. The aluminium production rate is higher when the alumina concentration increases. However, the alumina concentration has to be between 2% and 8%. For the other independent variables fixed, when the bath ratio is 1.25, the aluminium production rate presents a maximum.

The results showed that the aluminium production rate increases when the bath temperature decreases. However, the bath temperature must be between 1150 K and 1350 K. The calculations have demonstrated that the temperature does not exceed if the power consumption is between 625 kW and 1800 kW. These results provide an envelope of feasible operation for steady state operation. The range of aluminium production rate in this envelope is between 12.7 g s^{-1} and 34.96 g s^{-1}

Chapter 11

Transient Behaviour of the Aluminium Smelter

This chapter studies the dynamic behaviour of the aluminium smelting process. The model simulates 24 hours of operation. After two hours of operation, the fixed electrical power consumption suddenly reduces to observe the transient behaviour of the process.

This chapter introduces the transient behaviour of an aluminium smelting process by giving an example of its robustness, and then presents the results of the simulations.

11.1 Dynamic Behaviour

The electrolyte bath in the aluminium smelter is bulky, so that it can hold all the necessary electrolyte to dissolve the alumina. The electrolyte bath can store large amounts of energy, so the process responds very well against changes in the energy input. Thus, in case the cell is not receiving any electricity, the temperature does not suddenly drop. The rate of temperature change depends on the mass, the heat capacity of the bath, and the sum of heats entering and

leaving the cell:

$$\frac{dT}{dt} = \frac{P_{in} - P_{loss} - (P_{gen} - P_{abs}))}{m\, c_p} \quad \mathrm{K\ s^{-1}}$$

This analysis gives values to the equation for providing an idea of the bath robustness. The analysis considers that the average heat capacity of the bath is 1510 J $\mathrm{kg^{-1}}$ $\mathrm{K^{-1}}$. The temperature decrease can be calculated as a function of the mass when the power is completely lost. If power is completely lost, there is no current, so the reactions stop.The flows of feed and product also stop, and the only heat flowing in the cell is the heat lost to the surrounding:

$$\frac{dT}{dt} = \frac{0 - P_{\mathrm{loss}} - 0}{m\, c_p} \quad \mathrm{K\ s^{-1}}$$

$$\frac{dT}{dt} = -\frac{\frac{T-350}{0.003308}}{m\ 1510} \quad \mathrm{K\ s^{-1}}$$

Integrating the equation gives:

$$\begin{aligned} \frac{dT}{T-350} &= -\frac{dt}{4.995m} \\ T(t) &= 900 \exp\left[-\frac{t}{4.995m}\right] + 350 \end{aligned} \tag{11.1}$$

Figure 11.1 plots the obtained equation for different bath masses to see how the mass affects the dynamic transient of the temperature.

Figure 11.1 and the Eq. 11.1 suggest that the bath temperature tends to be equal to the temperature at the surroundings, which is 350 K. The dotted line at 1150 K represents the temperature at which the cryolite starts freezing, so the bath temperature has to be always above that dotted line. Figure 11.1 shows that the temperature decreases faster when the cryolite mass is lower.

Figure 11.1 shows that there is a linear relationship between the temperature decrease rate and the mass. Thus, if the mass increased, the temperature decreases more slowly. In practice, the reactions affect the heat balance, and the heat capacity is a function of the temperature.

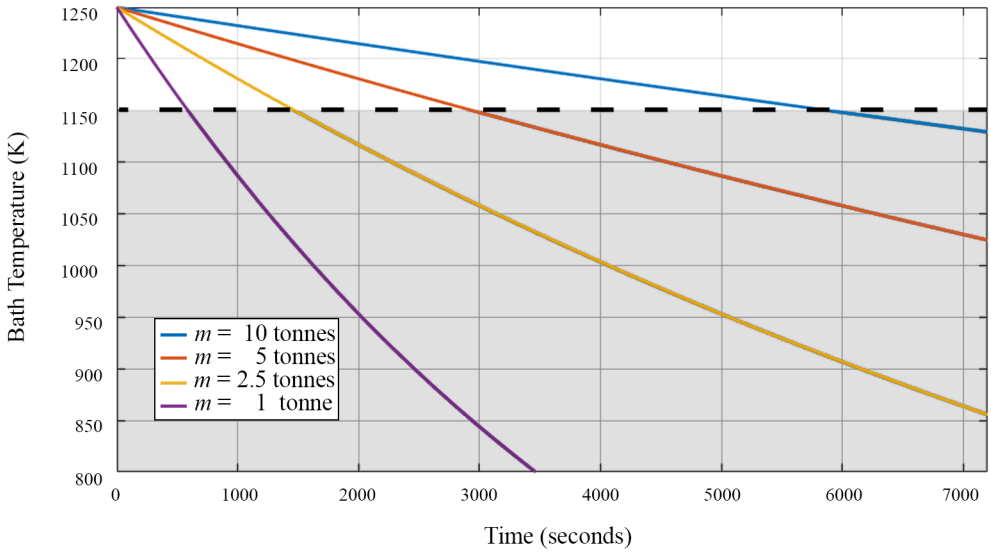


Figure 11.1: Progression of the temperature of the electrolytic bath when the power supply is cut for various bath masses.

Nevertheless, Figure 11.1 gives an idea of how robust the system is against changes in the power input.

The analysis in this section was made with the power completely turned off. If the power supply were reduced rather than stopped, the Joule heat would still be present, and the temperature will last longer within the valid limits. The ability of the bath to store energy is a useful feature for increasing the flexibility of the plant.

11.2 Simulations of a Power Reduction in the Aluminium Smelter

This section presents the results of the simulations in which the electrical power consumption is reduced during the operation, reproducing the behaviour of the cell when a power reduction takes place. The model simulates 24 hours of operation, and the power reduction happens after

two hours. The duration and magnitude of the power reduction is varied in every simulation, and the results show how the temperature and aluminium production rate vary with time.

The results are classified according the duration of the power reduction, starting with a one-hour power reduction, and then simulating four-hour and six-hour power reductions. The power reductions range between 50% and 90% with steps of 10% of the nominal value. Thereby, the simulations determine the duration and magnitude of the power reduction in which the temperature remains at admissible values. The temperature must be between 1150 K and 1350 K.

11.2.1 Power Reduced for One Hour

Figure 11.2 shows the progress of the temperature and the aluminium production rate for a one-hour power reduction. When the power input is lower, the temperature decreases faster, and the aluminium production rate is lower.

Evolution During the Power Reduction

This subsection discusses the behaviour of the temperature and the aluminium production rate during the power reduction.

The electrical power input provides power for the reactions and also for keeping the temperature of the cell constant. Figure 11.2 shows that for a one-hour curtailment, the temperature is kept between the acceptable levels (1150 K and 1350 K).

When the power input decreases, the electrical current decreases and consequently, the aluminium production rate decreases. When the electrical power is reduced to 70%, the aluminium production reaches a plateau, and the same happens when the power input is lowered to 60 and 50%. This suggests that, at those points, the current does not further decrease because the voltage drop has reached a plateau as well. Figure 11.3 shows the evolution of the current and the

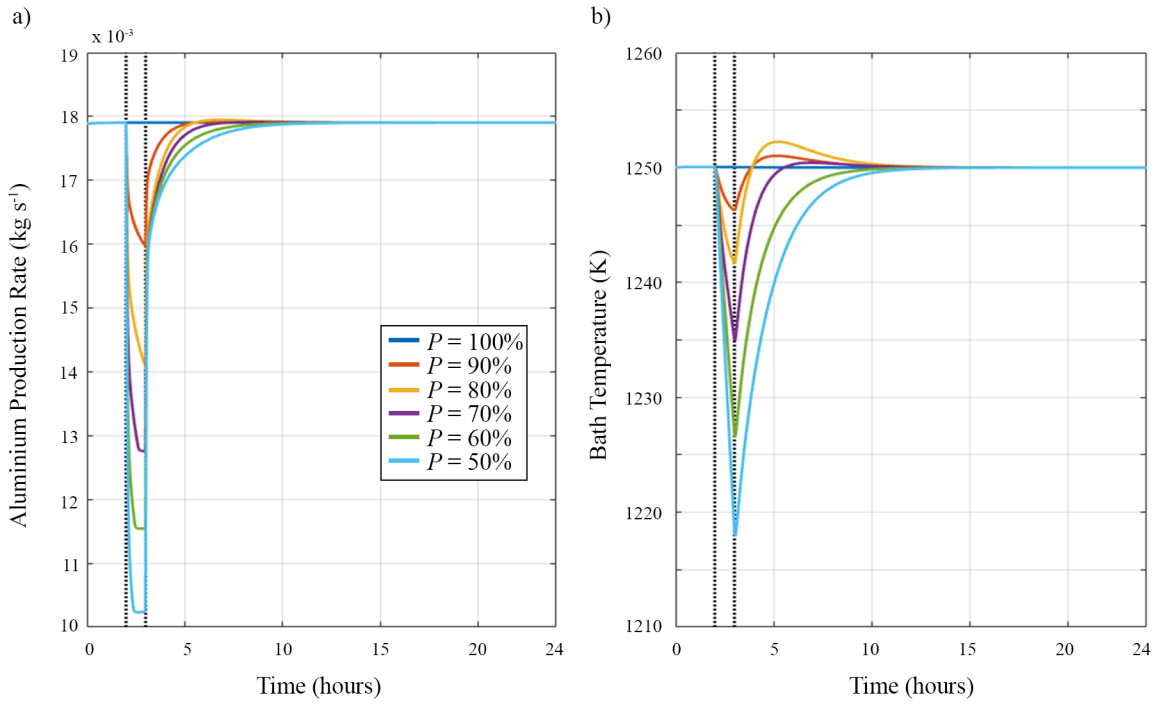


Figure 11.2: Evolution of a) the and aluminium production rate (kg s^{-1}) and b) the bath temperature (K) in 24 hours operation for various levels of power consumption. The power reduction takes place after two hours of operation, and it lasts one hour.

voltage drop for the one-hour reduction at 50% of nominal value. As predicted, both variables reach a plateau when the aluminium production rate does.

The reason for the plateau is because the IPD cannot get any larger. As mentioned, the temperature is controlled by adjusting the IPD, whose limit is at 6 cm. If the temperature falls below its set point (1250 K), the IPD starts to increase, so the electrolyte voltage drop increases. When the IPD reaches its upper limit, the electrolyte voltage drop plateaus, so the electrical current can be adjusted (almost) freely for adapting the power consumption to the power input. Figure 11.3.a) shows the evolution of the distance between electrodes. This evolution also explains the different curvatures in the temperature seen in Figure 11.2. When the IPD reaches 6 cm, it can no longer control the temperature, which drops at a constant rate. On the other hand, if the IPD does not hit the upper limit (for the 90% consumption for instance), the temperature can be controlled, and after the power recovery, it returns to its set point quickly.

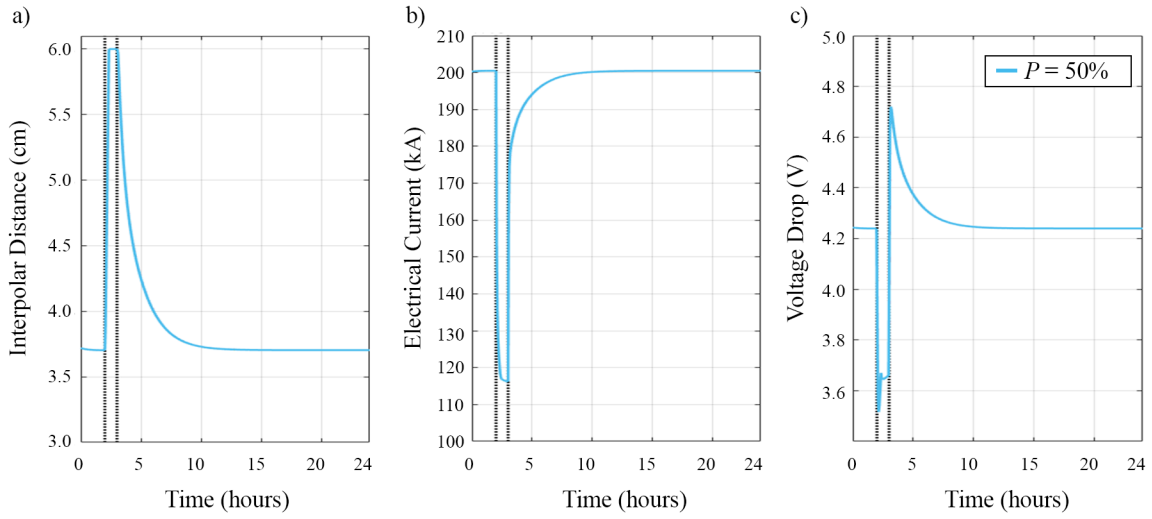


Figure 11.3: Evolution of the a) IPD (cm), b) the electrical current (kA), and c) the voltage drop in the cell (V) for a one-hour power reduction. The power is reduced to 50%.

Evolution After the Power Restoration

When the power is restored, the aluminium production rate returns to its nominal value because the electrical current also returns to the nominal operating value. When the IPD starts decreasing because the temperature is becoming more stable, the electrolyte voltage drop decreases as well, and the current can return to its nominal value.

From Figure 11.3, after the power restoration, the IPD is still at its upper limit because the temperature is still below its set point (1250 K). However, the power input electrical power is at its nominal value, so the electrical current increases. Nevertheless, because the IPD is at its upper limit, the electrolytic voltage drop is high, so the current can not return to its nominal value. Figure 11.4 shows the evolution of the voltages that form the overall voltage for a power reduction of 50%.

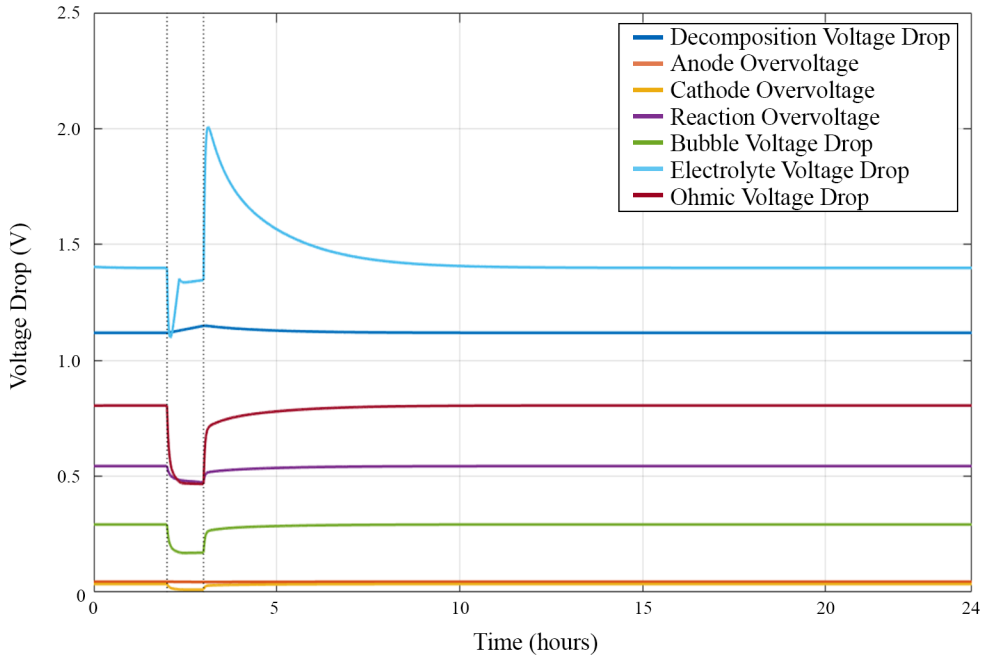


Figure 11.4: Evolution of the contributions to the total voltage for a one-hour power reduction. The power is reduced to 50%.

11.2.2 Power Reduced for Four Hours

Figure 11.5 shows the transient behaviour of the aluminium production rate and the temperature when the power consumption is reduced during four hours. The behaviour can be explained as it was explained for the one-hour reductions.

Evolution During the Power Reduction

When the power is reduced to 50%, the temperature falls below 1150 K after five hours and a half of operation, so it is nor feasible to maintain a four-hours reduction at 50%.

During the power reduction, the voltage drop increases, causing the current to reduce. Figure 11.6 shows that the current decreases, but Figure 11.5 shows that the aluminium production rate

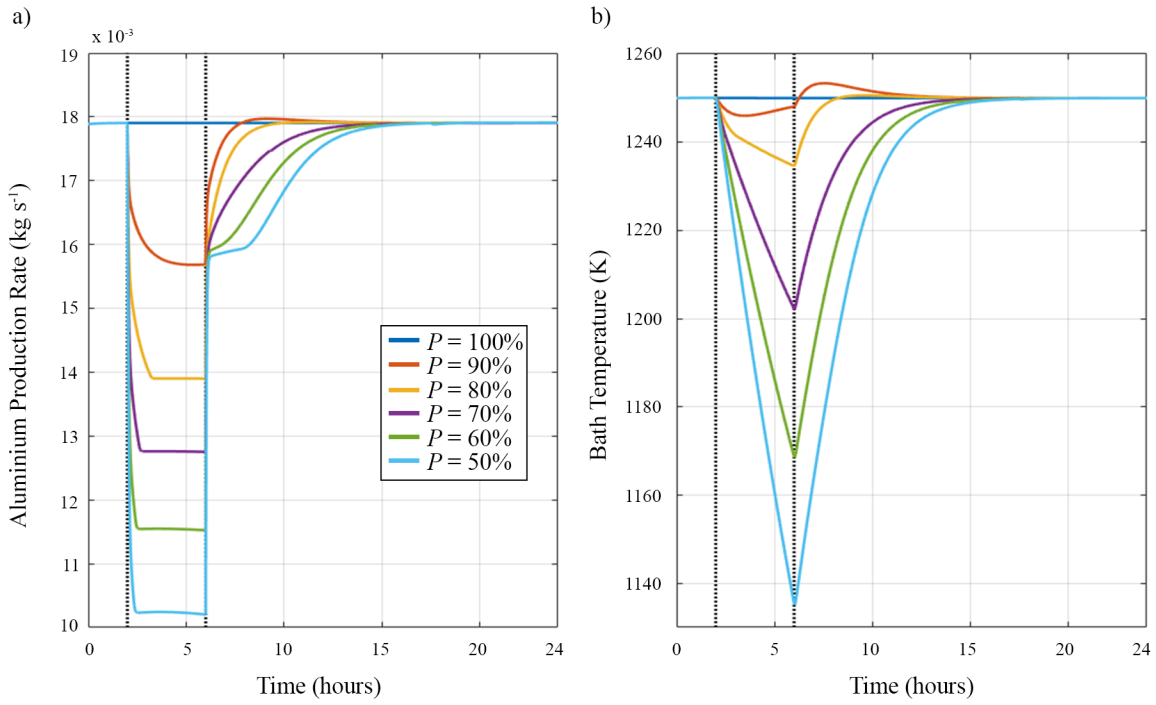


Figure 11.5: Evolution of a) the and aluminium production rate (kg s^{-1}) and b) the bath temperature (K) in 24 hours operation for various levels of power consumption. The power reduction takes place after two hours of operation, and it lasts four hours.

seems flat. However, according to Faraday's law, the aluminium production rate decreases with an electrical current decrease.

The reason for the aluminium production to remain flat is because the current efficiency increases when the electrical current decreases. The increase in current efficiency offsets the electrical current reduction. Figure 11.7 shows the evolution of the current efficiency when the power is reduced to 50% for four hours.

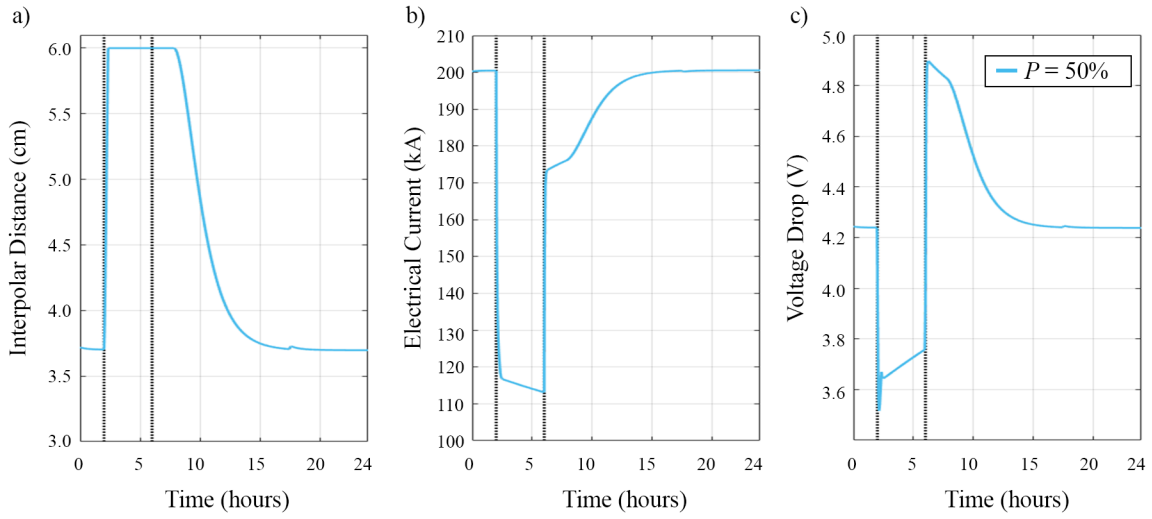


Figure 11.6: Evolution of the a) IPD (cm), b) the electrical current (kA), and c) the voltage drop in the cell (V) for a four-hour power reduction. The power is reduced to 50%.

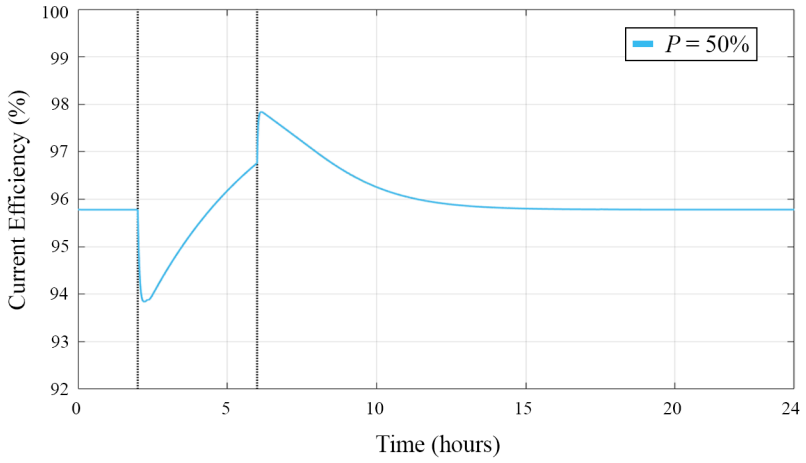


Figure 11.7: Evolution of the current efficiency (%) for a four-hour power reduction. The power consumption is reduced to 50%.

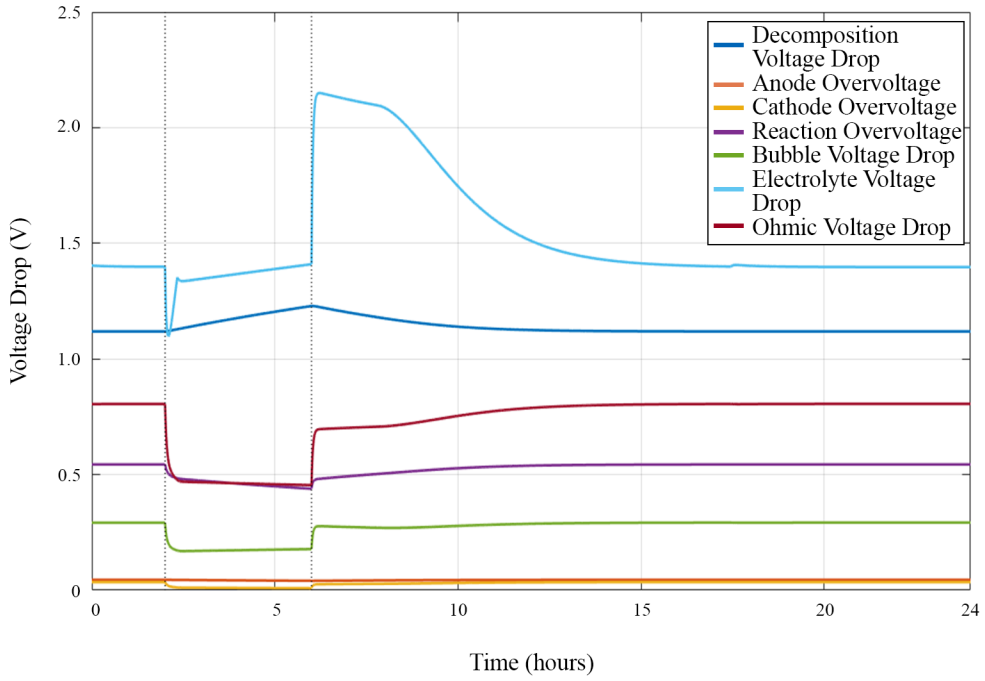


Figure 11.8: Evolution of the contributions to the total voltage for a four-hour power reduction. The power is reduced to 50%.

During the reduction, the voltage increases because the temperature of the bath increases. Figure 11.8 shows the evolution of the voltages when the power is reduced to 50% for four hours. The figure shows that during the reduction, the decomposition and the electrolyte voltages increase. The decomposition voltage increases because the temperature is lower, and the difference of potentials in the reduction reaction increases (Section 9.3.2, Eq. 9.30). Right after the power reduction, the electrolyte voltage drop abruptly decreases, because the electrical current decreases, but the increase of IPD offsets the decrease of electrolyte drop. After that, it starts increasing because the temperature decreases, which causes the conductivity of the bath to decrease.

Evolution After the Power Restoration

The voltage drop decreases because the temperature of the bath starts increasing, and consequently, the current increases. As the current increases, the current efficiency decreases, so the overall result is a flat aluminium production rate.

Figure 11.5 shows that the lower the power consumption, the more time the temperature needs to return to its nominal value due to all the lost energy. Thus, when the power input is lower, the energy losses are higher, and the bath needs to absorb energy during a more extended period.

11.2.3 Power Reduced for Six Hours

Figure 11.9 shows the transient behaviour of the aluminium production rate and the temperature when the power is reduced during six hours. For both reductions of 60 and 50%, the lack of energy in the cell makes infeasible reaching a steady state by the end of the day. For the 50% reduction, the temperature overshoot is so high that it crosses the upper limit.

The temperature when the power is reduced to 50% crosses the 1150 K at around five hours and a half of operation. When the power is reduced to 60%, the temperature reaches the 1150 K limit at approximately seven hours and a half of operation.

When the power is reduced to 90%, it seems that the temperature would reach the steady state even before the power recovery, but the aluminium production rate would be lower. This suggests that the cell can operate at a lower level of power consumption indefinitely, with the trade-off of having a lower production rate.

Figure 11.10 shows that the IPD when the power is cut by half remains most of the operation time in its upper limit, but the voltage significantly changes. This suggests that a great component of the total voltage is not only determined by the electrolyte voltage drop, but also it is determined by the bath temperature.

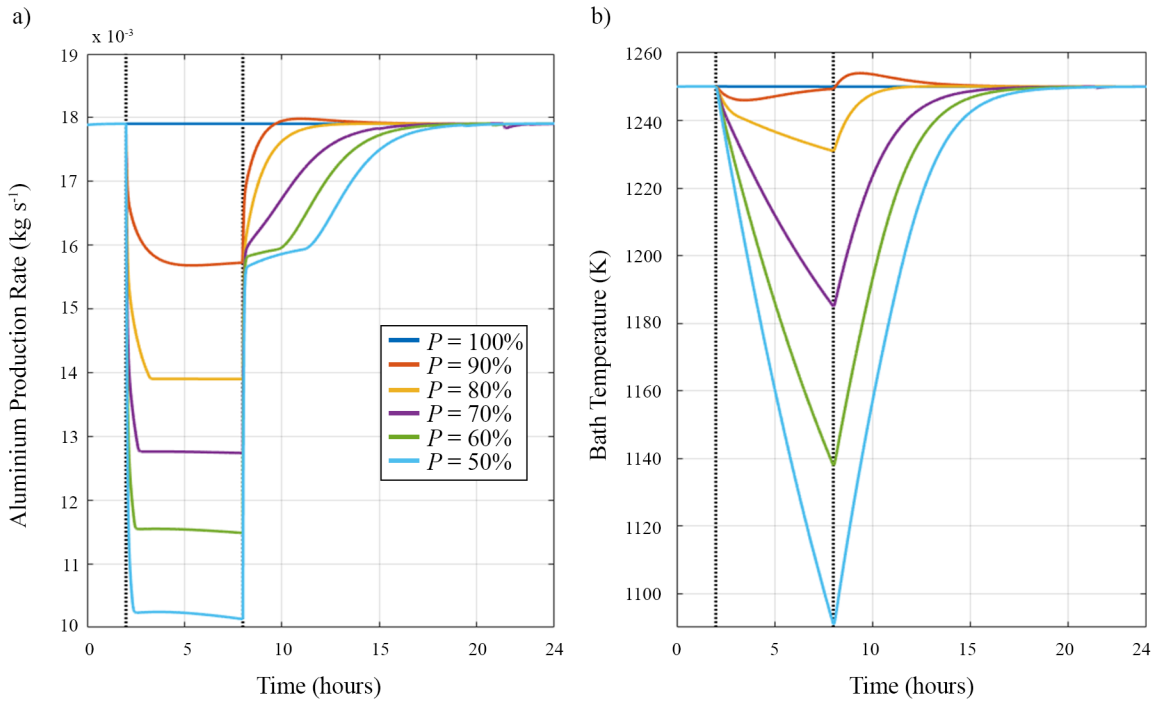


Figure 11.9: Evolution of a) the and aluminium production rate (kg s^{-1}) and b) the bath temperature (K) in 24 hours operation for various levels of power consumption. The power reduction takes place after two hours of operation, and it lasts six hours.

11.3 Relationship Between Duration and Magnitude of a Power Reduction

Observing the rates of temperature decrease in Figures 11.2 to 11.9, the temperature decreases at the same rate for a given power reduction. This feature can be used for determining the maximum duration for each power reduction. Eq. 11.1 showed that the change of bath temperature can be considered as an exponential function.

$$\frac{dT}{dt} = \frac{H_{\text{in}} - H_{\text{loss}} - (H_{\text{gen}} - H_{\text{abs}}))}{m\, c_p}$$

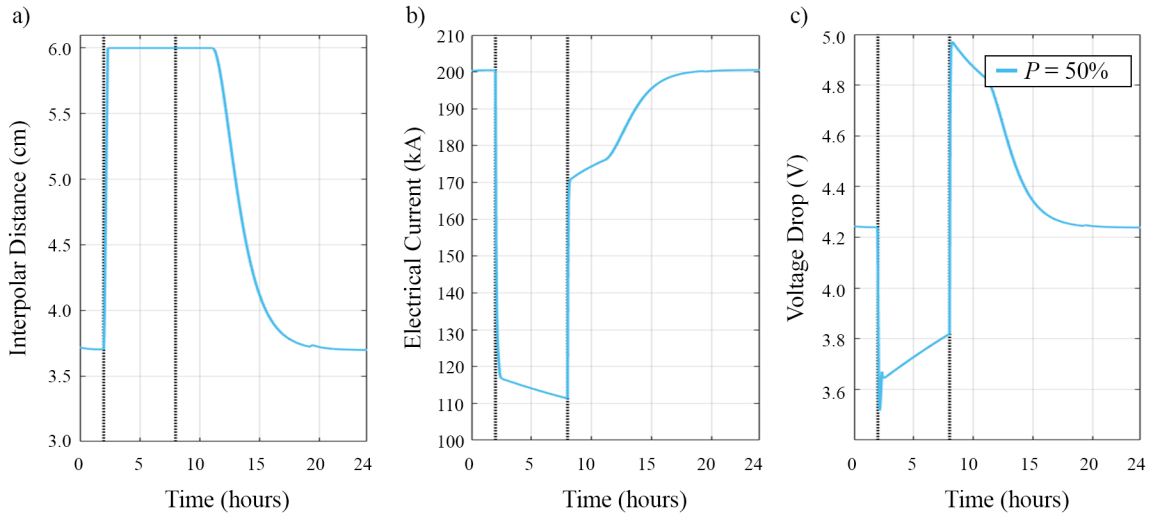


Figure 11.10: Evolution of the a) IPD (cm), b) the electrical current (kA), and c) the voltage drop in the cell (V) for a six-hour power reduction. The power is reduced to 50%.

If the heat capacity is considered constant with a value of 1510 J kg $^{-1}$ K $^{-1}$ and the mass is 10000 kg:

$$\frac{dT}{dt} = \frac{P_{\text{in}} - H_{\text{loss}} - (H_{\text{gen}} - H_{\text{abs}})}{10000 \times 1510}$$

where P_{in} is the electrical power consumption in W. The heat consumed by the reactions comes mainly from the reduction reaction. Thus, for simplicity reasons, the heat absorbed only considers the alumina reaction, which was calculated to be around 560 kJ per mole of aluminium produced (20.756 kJ per gram of aluminium).

Figure 10.13.c) can be used to deduce the equation that relates the power consumption with the aluminium production rate by regression. With a coefficient of determination of 97.98%, the relationship between power consumption and aluminium production can be written as:

$$\frac{dm_{Al_2O_3}}{dt} = 1.9064 \times 10^{-8} P_{\text{in}} + 0.0017 \quad \text{kg s}^{-1}$$

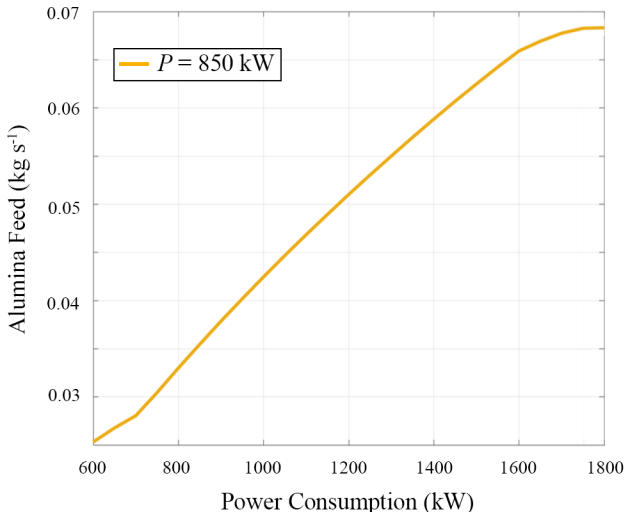


Figure 11.11: Relationship between the alumina feed (kg s^{-1}) and the power consumption (kW) in steady state.

Thus, the heat absorbed by the reactions is:

$$H_{\text{abs}}^{\text{Reac}} = 20756 \times 1000 \left(1.9064 \times 10^{-8} P_{\text{in}} + 0.0017\right) \quad \text{W}$$

Heat is also used to raise the temperature of the feed to the temperature of the bath. The main feed going to the bath is the alumina. Figure 11.11 shows the variation of the alumina feed when the power consumption changes. The equation relating the alumina feed and the power consumption can be found by regression, and the calculations gave the following result:

$$\frac{dF_{\text{Al}_2\text{O}_3}}{dt} = 3.7409 \times 10^{-8} P_{\text{in}} + 0.0045 \quad \text{kg s}^{-1}$$

From the Shomate equations, the heat necessary for raising the alumina temperature from the feed temperature (373 K) to 1250 K is 1015 kJ kg^{-1}. Thus, the heat necessary for raising the temperature of the feed is:

$$H_{\text{abs}}^{\text{Feed}} = 1.015 \times 10^{6} \left(3.7409 \times 10^{-8} P_{\text{in}} + 0.0045\right) \quad \text{W}$$

Additionally, there are power losses due to the ohmic drop due to the external parts of the cell. The voltage drop due to the external ohmic resistance is V_{Ext} = 4.04 $\times$ 10^{-6} I. From Figure 10.13.a) the relationship between the current and the power consumption can be deduced by regression, and the equation obtained is:

$$I = 0.2259\, P_{\text{in}} + 9.872 \times 10^{3}$$

Therefore, the power losses are:

$$H_{\text{Loss}}^{\text{Ext}} = 4.04 \times 10^{-6}\, (0.2259\, P_{\text{in}} + 9.872 \times 10^{3})^{2}\text{W}$$

Thus, Eq. 11.1 results in:

$$\frac{dT}{dt} = \frac{P_{\text{in}} - \frac{T_b - T_{\text{Out}}}{R'_{\text{Tot}}} - H_{\text{abs}}^{\text{Reac}} - H_{\text{abs}}^{\text{Feed}} - H_{\text{Loss}}^{\text{Ext}}}{m\, c_p}$$

$$\frac{dT}{dt} = \frac{P_{\text{in}} - \frac{T_b - 350}{0.003308} - 20756 \times 1000\, (1.9064 \times 10^{-8} P_{\text{in}} + 0.0017) -}{10000 \times 1510}$$

$$\frac{1015(3.7409 \times 10^{-8} P_{in} + 0.0045) - 4.04 \times 10^{-6}\, (0.2259\, P_{\text{in}} + 9.872 \times 10^{3})^{2}}{10000 \times 1510}$$

where T_{Out} is the outside temperature in K, and R'_{Tot} is the total thermal resistance in K W^{-1}. Substituting values:

$$49950.8\, \frac{dT}{dt} = 1.814 \times 10^{-3}\, P_{\text{in}} - 133.135 - 6.820 \times 10^{-10}\, P_{\text{in}}^{2} - T_b + 350 \tag{11.2}$$

when time is zero, the temperature is at its set point, 1250 K. Integrating the equation above:

$$\begin{aligned} T(t) &= (900 + f(P_{\text{in}}))\, \exp\left(-\frac{t}{49950.8}\right) + (350 - f(P_{\text{in}})) \\ f(P_{\text{in}}) &= 6.82 \times 10^{-10}\, P_{\text{in}}^{2} - 1.814 \times 10^{-3} P_{\text{in}} + 133.135 \end{aligned} \tag{11.3}$$

The equation above gives an approximation of the bath temperature as a function of the electrical power consumption and its duration. For instance, if the power is reduced to 60%,

$f(P_{in}) = -614.62$, so the equation above results in:

$$T(t) = 285.38 \exp\left(-\frac{t}{49950.8}\right) + 964.62$$

This equation tells that, when time is infinite, the temperature of the bath would decrease to 1054.78 K, which is not feasible. Also, it tells that the bath temperature reaches 1150 K after:

$$t = -49950.8 \ln\left(\frac{1150 - 964.62}{285.38}\right) = 21549.46 \quad \text{s}$$

This means that a power reduction of 60% can last for five hours and 59 minutes before the temperature reaches the lower limit, which is very close to the results in Figure 11.9.

This demonstrates that determining the duration of the power reduction can be achieved by approximations using the obtained envelope of feasible operation.

11.3.1 Maximum Power Reduction without Power Recovery

Eq. 11.3 can determine the maximum magnitude of power reduction that does not cause the bath temperature to exceed the lower limit. If at $t = \infty$ the temperature is at its lower limit, the process can continue without restoring the power. Eq. 11.3 has been calculated with parameters for an initial temperature of 1250K, so if the initial temperature were different, Eq. 11.3 would be different, and the results would consequently differ.

At $t = \infty$, and $T = 1150$K, Eq. 11.3 is:

$$1150 = (350 - f(P_{\text{in}}))$$

$$0 = 6.82 \times 10^{-10} P_{\text{in}}^2 - 1.814 \times 10^{-3} P_{\text{in}} + 133.135$$

The feasible solution of the quadratic equation is $P_{\text{in}} = 697.11$kW, which corresponds to 82% reduction. Thus, if the cell operates at a temperature of 1250 K, the power consumption can be reduced indefinitely to 82% without causing the bath temperature to exceed the lower limit.

If the electrical power consumption is reduced to a value above 82%, the temperature eventually returns to 1250 K. If the power is reduced to a value below 82%, the temperature will eventually exceed the lower limit.

11.4 Summary of the Chapter

This chapter has analysed the transient behaviour of the aluminium smelting process when power consumption suddenly decreases. The chapter has discussed the robustness of an electrolyte cell describing an example in which the power is completely curtailed. In the example, the temperature of the bath decreases more slowly when the mass of the bath increases. In the simulations, the power consumption is reduced rather than stopped so that the power reduction can last longer.

To asses the duration of the reductions, the model simulated the process for 24 hours of operation. After two hours of operation, the simulation suddenly reduces the power consumption to observe the transient behaviour of the plant. The simulations change the magnitude and the duration of the reductions. During the simulations, the temperature has to be within the upper limit, 1350 K, and the lower limit 1150 K. The results have shown that the temperature decreases more rapidly when the magnitude of the power reduction is higher. Therefore, the duration of the power reduction is shorter when the size of the power reduction increases.

The simulations have shown that the power consumption can be reduced to values in which the process would not be steady. However, the power has to be restored before the temperature exceeds its lower limit at 1150 K. The results of the simulations have been used for finding a relationship between the magnitude and duration of a reduction, and the temperature of the bath. This relationship has found that, for an initial temperature of 1250 K, the maximum power reduction that does not require a power recovery is 82%.

Chapter 12

Discussion of the Results

The results were classified into two groups, in the first group the model calculates the steady state operating points, and in the second group, the model simulates the transient behaviour of the aluminium process. In both cases, the main effect of reducing the power consumption is the reduction of aluminium production rate.

- A power decrease causes the current to decrease
- For a fixed current efficiency, the aluminium production rate is proportional to the current
- A change in current efficiency can offset the change in electric current
- The bath ratio does not have a great impact on the aluminium production rate
- The bath ratio can be adjusted for changing the voltage drops
- The alumina concentration does not have a great impact on the production rate, but it can improve the current efficiency of the cell
- A higher alumina concentration causes higher overvoltages, and therefore, it is recommendable to keep it low enough for not increasing those voltage drops, but not too low, so that the anode effect is avoided

12.1 Discussion of the Steady State Results

The model calculates the electrical current, the IPD, and the feed rates for various values of the bath temperature, the electrical power consumption, the bath ratio, and the alumina concentration. When the electrical power consumption is reduced, the limiting variable is the bath temperature, so the results have shown the envelope of feasible operation of the cell as a function of the electrical power consumption and the bath temperature.

The Process Power Management (PPM) system can use the envelope of feasible operation to know how to operate the cell in steady state operation. According to the envelope, the process can operate at steady state when the power consumption is between 625 kW and 1800 kW. Within that range, the temperature can be adjusted from 1150 K and 1350 K, as long as the temperature meets Eqs. 10.1. The envelope shows that, for a fixed power consumption, the aluminium production rate increases for lower temperatures. The trade-off is that the temperature gets closer to the cryolite solidification point. In an electrical contingency, the PPM system can also use the envelope of feasible operation to establish the values of the process variables that correspond to the available power.

Eqs. 10.1 shows that between 800 kW and 1400 kW, the temperature in steady state operation can be between 1150 K and 1350 K. Observing Figure 10.13.b), for a given temperature, the power consumption for producing a kilogram of aluminium does not vary significantly. For instance, in Figure 10.13.b), at 1250 K, for a power consumption of 850 kW, the production rate is 17.9 $g_{Alum}\ s^{-1}$, for a power consumption of 1000 kW, the aluminium production rate is 21.1 $g_{Alum}\ s^{-1}$, and for a power consumption of 1400 kW, the aluminium production rate is 29.5 $g_{Alum}\ s^{-1}$. The three points correspond, respectively, to an electrical consumption of 13.19 kWh kg^{-1}_{Alum}, and 13.16 kWh kg^{-1}_{Alum}, and 13.18 kWh kg^{-1}_{Alum}. These results agree with the results from Deign (2017).

Thus, if the electrical power consumption is between 800 kW and 1400 kW, the aluminium production rate will be proportional to the electrical power consumption. The PPM system can

use the envelope of feasible operation in Figure 10.13.b) to know the aluminium production rate by adjusting the temperature and the power consumption.

If the electrical power consumption is between 625 kW and 800 kW, or between 1400 kW and 1800 kW, the effect on the aluminium production rate depends on the established bath temperature. In the lower range of power consumption, a lower temperature has more effects on the power consumption per aluminium produced. On the other hand, in the upper range of power consumptions, a higher temperature has more effects on the power consumption per aluminium produced.

The other independent variables can affect the envelope of feasible operation. The alumina concentration and the bath ratio affect the aluminium production rate. The production rate increases for higher concentrations of alumina. Nevertheless, the alumina concentration must be below 8% wt to avoid undissolved alumina in the bath. The aluminium production rate has a maximum when the bath ratio ($R_b = \mathrm{NaF}/\mathrm{AlF_3}$) is at 1.25.

Thus, for obtaining the maximum aluminium production rate for a given electrical power consumption, the process has to set the temperature as low as the lower limit allows, the concentration as high as the upper limit allows, and the bath ratio at 1.25.

12.2 Discussion of the Dynamic Behaviour Results

The results from the calculation provide an envelope of feasible operation for steady state operation. During an electrical contingency, the PPM system accommodates the process to the corresponding power available. Due to the stored energy in the aluminium smelter, the PPM can reduce the power consumption outside the envelope of feasible operation during a specific period.

The magnitude and duration of a power reduction are related to the bath temperature using the results. The relationship is developed for an initial temperature of 1250 K and tells the

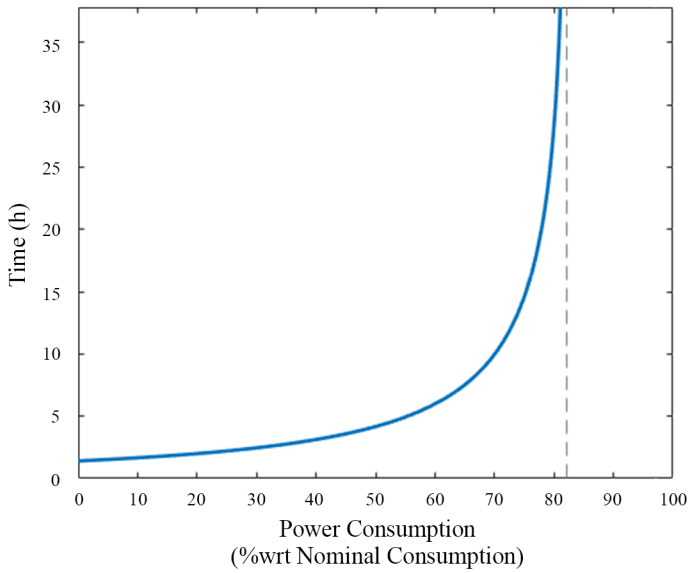


Figure 12.1: Maximum feasible duration of a power reduction as a function of the magnitude of the power reduction.

temperature of the bath for a given power reduction after a specific time. Figure 12.1 shows a graphical representation of Eq. 11.3 when the bath temperature is set at its lower limit.

Figure 12.1 provides the maximum duration of a power reduction according to the magnitude of this reduction. The asymptote at P=82% represents the maximum power reduction that does not cause the temperature to exceed its lower limit. Figure 12.1 shows that the electrolyte bath can operate flexibly, especially if the power reduction remains above 60%. In these conditions, the power reduction can last for more than 5 hours. During the power reduction, the aluminium smelter keeps producing aluminium, and the aluminium production rate can be deduced observing Figures 11.2 to 11.9,

Figure 12.1 and Eq. 11.3 provide an envelope of feasible operation that adds information to the envelope derived for steady state operation by including the time as a variable. The PPM system can use the envelope to know the duration of the power reduction. Figure 12.1 is derived from an initial temperature of 1250 K and a final temperature of 1150 K. Thus, PPM can use Eq. 11.3 to update the envelope at any moment. The envelope of feasible operation was determined using

the results from this simulation, but the PPM system can use the same procedure for obtaining an envelope specific to each process.

A further interesting finding in the transient graphs is that the bath temperature can return to its former initial value without an electrical power consumption boost, meaning that the power consumption does not increase above its nominal point to compensate the power reduction. The Joule heat generated provides chemical energy to the endothermic reactions, to heat the fed materials, and to offset the heat lost to the surroundings. If the available heat is lower than the combination of these three heats, the temperature of the bath decreases, and vice-versa. After the electrical power restoration, the system uses less heat for the aluminium reaction and more power to overcompensate the heat lost to the surroundings, so the temperature of the system increases without the need for an extra electrical power boost.

12.3 Summary of the Chapter

The Process Power Management (PPM) system can use the envelopes of feasible operation found during the calculations and the simulations for adjusting the power consumption of the plant. The envelope for steady state operation shows the power consumption in which the temperature does not exceed any limit. The values of these power consumptions can be exceeded during a certain period as long as the temperature remains within limits.

During an electrical contingency, the PPM system can exploit the energy stored in the aluminium smelter to adjust the power consumption and using the envelope of feasible operation. The PPM system knows the maximum duration of these power reductions.

This chapter has also discussed that the aluminium smelter can return to its nominal operating point without an electrical consumption boost. While the process variables return to their nominal values, the aluminium production rate is lower than the nominal rate. This is because the electrical power is used for heating the cell instead of producing more aluminium.

Chapter 13

Summary of the Aluminium Smelter

This part has studied flexible operation in an aluminium smelting process. Aluminium production is an electricity-intensive operation, in which electrical power is used to carry out an electrolysis reaction and to heat the electrolyte bath in which the reaction takes place. For this case study, the study of flexible operation assessed the operability of the electrolyte cell during an electrical contingency, so it determines how the process would work when the available power is reduced.

The aluminium smelter model has several variables affecting the power consumption in the process, and therefore it is important to find every relationship to set the available power consumption without any variable going out of limits. The most important limits are the temperature and the alumina concentration:

- If the temperature is too low, the cryolite bath will freeze
- If the temperature is too high, the cathodes of the cell will be damaged
- If the alumina concentration is too low, the cell undergoes the anode effect in which the voltage drop significantly rise
- If the alumina concentration is too high, the alumina will not dissolve in the bath

The model is divided into three sub-models, the mass balance model, the electrical model and the heat balance model. The model has five degrees of freedom, and the five fixed variables are the temperature of the bath, the bath ratio, the electrical power consumption, the alumina concentration, and the bath mass.

The model is calculated for obtaining the steady state operating points. The simulations of the model provides the transient behaviour of the process. The control loops adjust:

- The current for controlling the power consumption
- The Interpolar Distance (IPD) for controlling the temperature
- The alumina feed for controlling the alumina concentration
- The AlF_3 feed for controlling the AlF_3 concentration, and consequently, the bath ratio (R_b=NaF/AlF_3)
- The Na_2CO_3 feed for controlling the total mass

In the aluminium smelter, energy can be accumulated to eventually be released as different forms of energy. Power comes from the electrical input, and it is transformed into heat by the Joule heating effect. This heat is used for:

- Providing chemical power to the endothermic reactions
- Heating up the material entering the cell
- Compensating the heat flowing to the surroundings

If the electrical power consumption is not enough to compensate the heat lost to the surroundings, the bath uses the accumulated energy as heat. The temperature of the system decreases, but the process can still be operative.

The calculations determined an envelope of feasible operation. The process can operate at steady state if the electrical power consumption is between 625 kW and 1800 kW. If the electrical power consumption is below that range, the steady bath temperature exceeds its lower limit of 1150 K. If the electrical power consumption is above that range, the steady bath temperature exceeds its upper limit of 1350 K. The Process Power Management (PPM) system can use the envelope of feasible operation to know how to operate the smelter at steady state. In an electrical contingency, the PPM system can use the envelope to establish the values of the process variables that correspond to the available power after the power reduction.

The model also calculated the effects on the aluminium production rate of varying the temperature of the bath, the bath ratio, and the alumina concentration:

- The bath temperature is set lower in order to increase the aluminium production rate, but must not exceed its lower limit of 1150 K
- The alumina concentration is set higher in order to increase the aluminium production rate, but must not exceed its upper limit of 8% wt
- The bath ratio is set 1.25 to maximise the aluminium production rate

The simulations have explored the envelope of operation when the power consumption decreases suddenly. The steady state envelope obtained with the calculations set the power consumption limits at 625 kW and 1800 kW. These power consumption can exceed these limits during a certain period, as long as the bath temperature does not exceed any limit. After the power reduction, it is possible to return to the former operating point without increasing the power consumption to a level higher than its former value.

The results of the simulations obtained a relationship between the duration and magnitude of a power reduction, and the bath temperature. The PPM can use this relationship to know for how long the power reduction can take place, depending on the magnitude of the power reduction and the temperature in the bath. The results showed that, for an initial temperature of 1250 K, the maximum achievable power reduction that can last indefinitely is 82%. The results showed that

the aluminium smelter is robust, if the power is reduced above 60%, the bath of the temperature will not exceed the lower limit for at least five hours.

Aluminium smelter is a good candidate for implementing flexible operation because of its ability to store energy, whereby it can stand an electrical power reduction for a prolonged period of time. The PPM system can use this feature to facilitate the regulation of power consumption in the process. To that end, the PPM can use the envelope of feasible operation derived in the analysis if the dynamic behaviour if the aluminium smelting process. This dynamic analysis is a novel contribution towards the study of flexible operation of electricity-intensive processes.

Part IV

Discussions and Conclusion

Chapter 14

Discussion of Flexible Operation

This chapter discusses the similarities and differences between the results obtained in the liquefaction of natural gas and the alumina reduction process, so that a series of hypothesis for implementing, assessing, and applying flexible operation to other processes can be proposed.

This chapter starts enumerating the commonalities of the Liquefied Natural Gas (LNG) and aluminium smelting process. The shared characteristics of the processes are focused on the results and on the procedure for converting the electrical energy into a form of energy that is useful for the process. The dynamic analysis of the aluminium smelter adds a new variable to its model, which is the time. The comparison provides conclusions that are useful for a future implementation of flexible operation in industrial practice. This chapter finishes suggesting future work in the field of flexible operation and potential processes for the study of flexible operation.

14.1 Comparison of the Results between LNG and Aluminium Smelter

This section compares the range of electrical power reduction for both processes, as well as the range of production rate that they can achieve. For both cases, it seems inevitable to lower the production of the process for reducing the electrical power consumption. This decrease can be alleviated if other process variables are adjusted.

For a given power reduction, in the LNG case, the reduction of LNG production rate can be lessened if the LNG composition and its temperature at the end of the process are adjusted. In the aluminium smelting process, the reduction of aluminium production rate can be lessened if the temperature of the bath, the alumina concentration, and the bath ratio are adjusted.

It is important to establish the limits of these adjustments in the steady state and during the transient state. The models obtained the envelope of operation of each process that relates the power consumption and the process variables. These envelopes, along with the limits, provide the envelope of feasible operation that the Process Power Management (PPM) can use to adjust the electrical power consumption of the plant.

14.1.1 Duration of the Power Reduction

The LNG model did not consider the transient state. The power is cut instantly, but the process takes time to adapt to the new consumption. In spite of that, the transient state in the LNG process is not an issue because the refrigerants will respond to the change of production rate accordingly (Fazlollahi et al., 2015; He and Ju, 2016). Hence, this analysis does not take into account the duration of the power reduction in the LNG process.

On the other hand, for the aluminium smelter, the duration of the power reduction presents an important question, since, the longer the duration of power reduction, the more the bath

temperature decreases. Results have shown that the duration of the power reduction depends on its magnitude.

The bath temperature during an electrical power reduction in the aluminium process can be approximated using Eq. 11.3:

$$\begin{aligned} T(t) &= (900 + f(P_{\text{in}})) \exp\left(-\frac{t}{49950.8}\right) + (350 - f(P_{\text{in}})) \\ f(P_{\text{in}}) &= 6.82 \text{ x } 10^{-10} P_{\text{in}}^2 - 1.814 \times 10^{-3} P_{\text{in}} + 133.135 \end{aligned} \tag{11.3}$$

where t is the power reduction time elapsed in seconds, $T(t)$ is the temperature at time t in K, P_{in} is the electrical power input in W, H_{loss} are the heat losses to the surroundings in W. Thus, the duration of the power reduction depends on the initial and limit temperature, and the magnitude of the power input.

Eq. 11.3 can be used to calculate the time it takes for the bath temperature to reach the lower limit by substituting T=1150K:

$$t = 49950.8 \ln\left(\frac{900 + f(P_{\text{in}})}{800 + f(P_{\text{in}})}\right)$$

14.1.2 Magnitude of the Power Reduction

The maximum achievable power reduction for the LNG is a 50% of its nominal consumption. If the power consumption is further reduced, the compressors might undergo surge problems, and the process has to be stopped. On the other hand, the maximum power increase of the plant is a 60% of its nominal consumption (consuming then a 160% in total), and the problem is given by a possible choke problem in the compressors.

As mentioned, the magnitude of the power reduction in the aluminium smelter depends on the duration of it. Thus, this paragraph only considers the steady state of the aluminium smelter. The power consumption at which the smelter can operate indefinitely depends on the process variables, and as the results showed the temperature is the limiting variable. As the graphs

showed, the higher the power reduction, the lower the production rate. The graphs showed that, in steady state, the power consumption ranges from 625 kW to 1800 kW (73.52% and 211.74%)., which correspond to 11.35 g s $^{-1}$ and 30.52 g s^{-1} (63.41.52% and 170.5%).

The relationship between the temperature and the power consumption in a steady state operation can be approximated considering that, in Eq. 11.2, $\frac{dT}{dt}$ is zero.

$$49950.8\,\frac{dT}{dt} = 1.814\times10^{-3}\,P_{in} - 133.135 - 6.820\times10^{-10}\,P^2 - T_b + 350$$

$$T_b = -6.820\times10^{-10}\,P^2 + 1.814\times10^{-3}\,P_{in} + 216.865$$

The equation above can approximately determine the temperature of the bath as a function of the power consumption.

14.1.3 Minimising the Reduction of Production Rate

Both processes can reduce their power consumption by reducing the production rate [1]. For a given power reduction, the decrease in production rate can be alleviated if other variables in the process are adjusted. These process variables can either affect the process or the product. This section gives a comparison between both processes regarding how the process variables or the product characteristics can be changed in order to maximize the production rate for a fixed electrical power consumption.

Changing the Process Variables in the LNG Process

For the LNG process, the values of the operating points are established so that the electrical power consumption is adapted to the available power while at the same time, the process is at a feasible operating point. For the LNG, the process variables that can be changed in the

[1] For the LNG case, however, a power reduction of the 2% of its nominal power can be achieved by solely adjusting the composition and the temperature of the LNG; for further reductions, the production rate has to be changed

process are the discharge pressure of the refrigerants, and the flash temperature at the exit of the precooling stage.

Regarding the pressures, the model found a set of discharge pressures that minimizes the power consumption for a given production rate. An adjustment to the temperature of the flash causes the composition of the natural gas stream to change. The composition of the liquefied gas is specified by customers, so, the range of operability for the flash temperature is not wide. Moreover, for a given production rate, the temperature of the flash does not significantly change the electrical power consumption of the process.

A possibility not discussed so far in the thesis is to allow the temperatures of the refrigerants at the exit of their respective heat exchangers to vary. This would lead to variation of the vapour fraction. Appendix D.4 will provide an initial analysis of this idea, which will require the use of pumps in the Joule-Thomson refrigeration cycles in addition to the compressors, increasing the flexibility of the process.

Changing the Process Variables in the Aluminium Smelter

For the aluminium smelter, the aluminium production rate is directly proportional to the electrical current flowing through the cell. For a given electrical power consumption, the current depends on the process variables, so, ultimately, adjusting a process variable has consequences on the amount of aluminium produced. For instance, for a given power consumption, a higher bath temperature requires a longer distance between the cathode and the anodes, so the voltage drop in the bath increases, and consequently the heat provided to the cell increases. When the voltage between the electrodes in the cell increases. for a given power consumption, the current has to decrease, and therefore, increasing the temperature of the process decreases the aluminium production rate.

The main limits in the aluminium smelter are set by the temperature of the bath and the alumina concentration. A low temperature freezes the cryolite, and a high temperature damages the cathode. A low alumina concentration causes a thick bubble layer under the anodes, and a high

concentration can not be dissolved by the cryolite. Nevertheless, the stored energy in the cell makes it possible to have a good dynamic response against possible changes of the incoming energy, and therefore, both variables do not abruptly fluctuate when an alteration occurs. This can be exploited for reducing the power consumption of the cell during a period of time, until any of the variables approaches a risky value (as shown in Section 11).

When an electrical contingency takes place, aluminium production is not the priority, and the process must be adapted to keep the production running at a lower power input. The points presented above suggest that varying the bath temperature is a good choice for achieving the power reduction while maximizing the aluminium production, as long as it does not cross any limit. Additionally to the temperature, the alumina consumption and the bath ratio can be adjusted for reducing the power consumption and maintaining the aluminium production rate as high as possible.

There is significant stored energy due to the energy content of the cryolite bath, so the bath temperature does not significantly vary when there is a change in the available power. Thus, the ability of the process to store energy is a key element when assessing the flexibility of the plant.

Product Characteristics in the LNG Process

The product characteristics of the LNG are the LNG temperature and composition at the end of the process. For a given power consumption, the production rate increases the higher this temperature. However, the LNG can not be above its saturation temperature, otherwise it would present a vapour phase. On the other hand, a very low temperature decreases the production rate, so it is desirable for the exit temperature to be as close to its saturation point as possible.

The composition of the LNG depends on the flash temperature after the precooling stage. For a given power consumption, including hydrocarbons other than methane in the natural gas stream leads to a higher overall production rate. However, it is not desirable to have LNG that has too high a percentage of other hydrocarbons because the product would not meet the product specification.

Both characteristics can be adjusted simultaneously to increase the production rate further than it would do if they are adjusted separately. If the LNG presents more methane, its heat capacity will decrease, making it easier to release energy with a temperature change. Thus, if the temperature also varies, the refrigerants would require less flow rate to absorb heat from the natural gas stream.

Furthermore, the LNG process has a by-product, which is the natural gas liquid, as a result of the condensation in the flash drum after the precooling stage. If the LNG stream is richer in methane, that implies a lower temperature in the flash, and a higher natural gas liquid rate.

Product Characteristics in the Aluminium Smelter

The product characteristics do not significantly affect the electrical consumption of the plant. The only characteristic that can be changed is the temperature of the aluminium, and it is established by the temperature of the electrolyte bath and has no consequences on the product itself (unless it drops to its melting point).

However, there are other factors such as additives or emissions, whose rates can be calculated according to the process state. The feeds are manipulated to control the concentrations of the bath, as well as the total mass of it. The concentration of fluorides (ALF_3 and NaF) regulate the bath ratio, so if the desired bath ratio is adjusted, the feeds will vary.

The emission rates, such as fluorides or CO_2, depend on the electrical current and the concentration of different compounds present in the bath. If the process adjusts the emissions, other variables, such as the conductivity will change, and consequently, the voltage between electrodes changes. For a fixed power consumption, if the voltage changes, the electrical current varies as well, which results in the aluminium production rate changing. Ultimately, varying the emission rate changes the aluminium production rate. Thus, there might be some needs in the process that can become a first concern, overriding the product characteristics.

Comparison of the Production Rate Maximisations

In both processes, for a given power consumption, the main priority is maintaining the production rate as high as possible. There are other factors that can play a crucial role in the development of the process, either from a process or a economic standpoint. Therefore, flexible operation has to consider every aspect of the process.

The composition of the LNG at the end of the process is not a critical factor for the process itself, so the limits set by this characteristic are established by what the customer needs. Tight limits, such as the temperature of the LNG at the end of the process, indicates that some characteristics have to be very well controlled. If the control is accurate, the product characteristics can be adjusted in order to help the process to meet the electrical power demands, and at the same time, maintaining the production losses to a minimum.

The presence of a by-product, like the natural gas liquid in the LNG process, increases the flexibility of the process. Not all the by-products can be sold, for example, the fumes from the aluminium smelter are unwanted emissions rather than a by-product.

14.1.4 Comparison of the Energy Transformations between LNG and Aluminium Smelter

The consumed electrical power during a period is a form of energy. Energy has several forms, such as electrical, mechanical, thermal, or chemical. Flexible operation has considered all the equipment in the processes, modelling them and the interactions amongst them, so that the electrical energy consumed by the electrical equipment could be translated to other types of energies.

For instance, the LNG process can be seen as a heat pump, in which electricity is used to move the heat from the natural gas to the sea. Thus, the electrical power is transformed into heat. In the aluminium smelter, electrical energy is transformed into chemical energy for reducing the

alumina, and into thermal energy for maintaining the temperature of the bath between 1150K and 1350K.

This section reviews how energy is transformed to change different process variables, from the electrical energy withdrawn to the final product. The analysis compares the transformations in both processes to draw a series of conclusions.

Energy Transformations in the LNG Process

The LNG process consumes energy to power the electrical motors attached to the compressors. Compressors transform this electrical energy into mechanical energy, which is transferred to the refrigerants to either vary its flow rate or its pressure. In both cases, the internal energy of the refrigerant is changed:

- **Flow rate:** The extensive property of the internal energy makes it proportional to the flow rate.
- **Pressure:** Internal energy can be divided into heat energy (Q), and work (W) which is a function of the pressure.

If a source of heat is introduced to the refrigerant, the temperature of the refrigerant varies. Thus, if the heat comes from the natural gas, the refrigerant increases its temperature. The absorbed heat by the refrigerant is ultimately released to the sea as thermal energy. It is worth mentioning that, during the Joule-Thomson expansion occurring in the valve, the internal energy of the refrigerant varies as it expands, and consequently, changing the pressure-volume work of the refrigerant.

Thus, the crucial form of energy for liquefying the natural gas is the thermal energy absorbed by the refrigerant, and that is determined by the desired temperature of the natural gas and the temperature of the natural gas entering the process. The LNG process has a series of equipment,

and it is necessary to find the relationships between one equipment and the following one. These relationships are the energy flows in the LNG process.

Figure 14.1 shows a graphical representation the energy flows in the LNG process, including the incoming electrical power and how it is distributed in the process. Each arrow in Figure 14.1 represents energy flow rates.

The arrows entering the dotted box represent the power inputs, with the yellow arrows representing the electrical power input, and the blue arrow representing the energy flows of the natural gas streams. Each colour represents a different refrigerant or the natural gas streams, agreeing to the colours in Figure 5.1. The energy exchanged between the liquefying refrigerant and the natural gas is the largest, because the natural gas is liquefied in that stage and it releases its latent heat. The arrows exiting the dotted box represent the power outputs, with the black arrows representing the mechanical power losses due to the isentropic efficiency of the compressors, the blue lines representing the energy flows of the natural gas liquid and LNG flows, and the navy arrows representing the heat released to the sea by the refrigerants.

The values in Figure 5.1 shows the values corresponding to the production of 1 kmol s^{-1}. The values of the energy flows are expressed considering the LNG stream as the baseline.

Figure 14.1 shows that the exchange of power is continuous, and that there is no energy storage. This suggests that any change in any arrow will propagate to the other arrows, and due to the interactions between refrigerants, a slight change might have great consequences. Section 14.1 discussed that changing the characteristics of the LNG product have impacts on the power consumption. Therefore, changing the LNG production rate or the LNG exit temperature, affects the blue arrows in Figure 14.1. Changing the thickness of the blue arrows will affect the rest of the diagram, varying then the electrical consumption of the process.

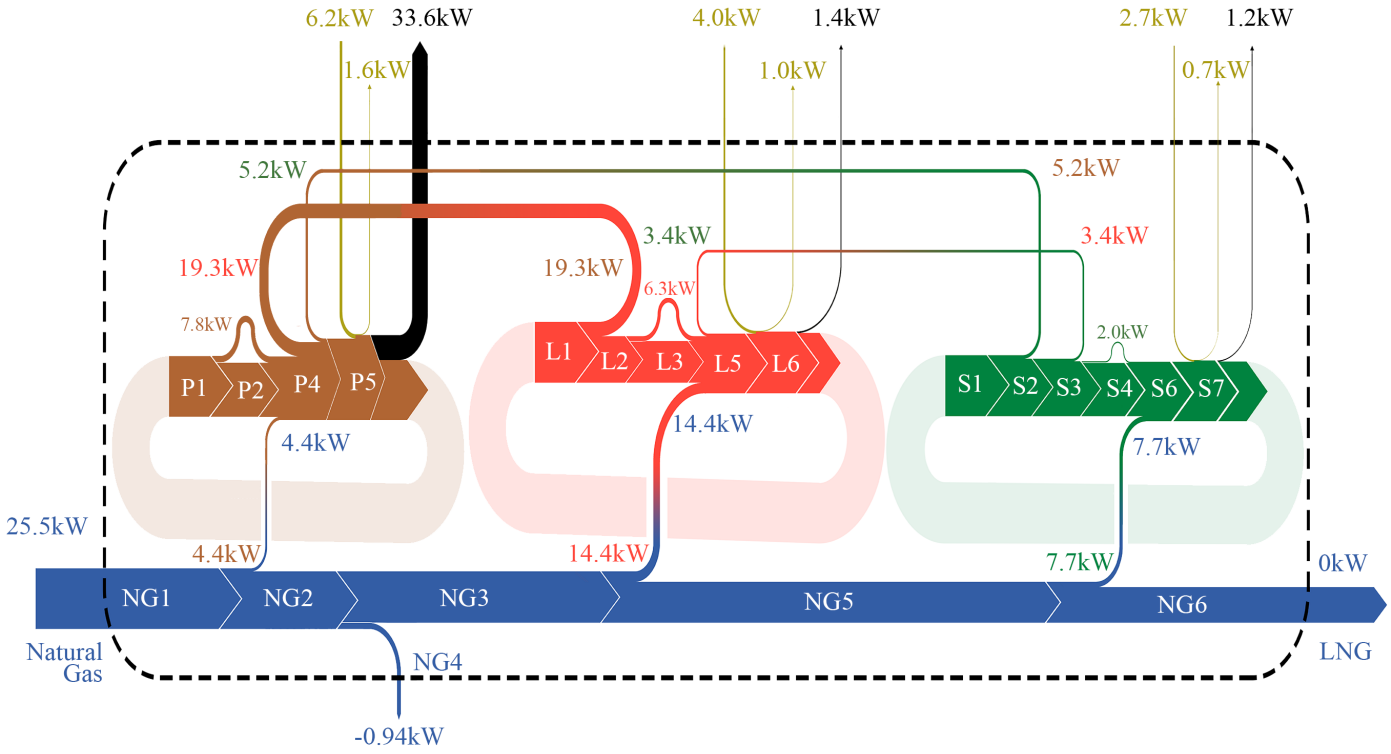


Figure 14.1: Sankey Diagram for the LNG process. The values are expressed based on the production of 1 kmol s^{-1} of LNG. Each circle represents a refrigerant cycle. The colour palette corresponds to the colours used in Figure 5.1. Additionally, the picture represents electrical power (yellow), and heat exchanged in the sea coolers (black).

Energy Transformation in the Aluminium Smelter

In the aluminium cell, electricity is provided to the bath via the anodes. Electrical energy is used for supplying the chemical energy to carry out the reactions in the bath, the thermal energy to maintain the temperature of the bath at the desired value, and the thermal energy to heat the material entering the cell.

The cell gets the thermal energy by transforming the electrical energy via the Joule heating of the bath. The Joule heating is the production of heat with the flow of electric current through an electrical resistance. The generated heat is equal to the product between the current and the voltage drop in the bath.

The external parts of the cell, such as the anode bridge or the rods, consume electrical power. However, these parts are not in contact with the bath, so the Joule heat produced in these parts does not contribute to the thermal energy in the bath.

The magnitude of the voltage in the bath is a function of the properties of the bath, as explained in Section 9.3.

The thermal energy in the bath is then used for three objectives:

- To heat the material fed to the bath
- To provide the energy needed by the endothermic reactions
- To maintain high temperatures in the bath

This implies that the amount of energy transformed into chemical energy or to rise the temperature of the bath can be changed if the variables in the bath are adjusted.

The main reaction in the cell is the reduction of alumina, which needs thermal energy for providing the difference of chemical energy between the products and the reactants, and electrical energy for providing the difference of potential between the products and the reactants.

The difference of potentials between the product and the reactants, is named decomposition voltage (Section 9.3). The amount of chemical energy is the product of the decomposition voltage and the current flowing through the system during a certain period of time. The difference of potential does not cause an absorption of energy, but it contributes to the total voltage drop that converts the electrical energy into thermal energy via the Joule heating effect.

The difference of chemical energy between the products and the reactants is known as enthalpy of reaction. If the enthalpy of reaction is positive, the products have a higher energy than the reactants, which, in this case, is absorbed from the thermal energy in the system; this means that the reaction is endothermic. On the other hand, if the enthalpy of reaction is negative, the reaction releases chemical energy, which is transformed into thermal energy. Enthalpy of reaction depends on the temperature of the system. For instance, in the aluminium bath, most of the reactions are endothermic, and the higher the bath temperature, the less enthalpy of reaction they would require.

Thermal energy has to be constantly provided to the cell, so it compensates the thermal energy losses to the surroundings. Therefore, if the electrical power consumption stops, the bath temperature decreases because thermal energy is flowing to the surroundings.

Figure 14.2 shows the energy transformations in the aluminium smelting process. The picture represents a Sankey diagram for the aluminium smelter in a nominal operation when the electrical power is 850 kW. In the diagram, the yellow line entering the dotted box represents the electrical power consumption of the cell. This arrow is then divided into two: (i) one arrow representing the electrical power caused by the external ohmic losses (red), which does not contribute to increase the thermal energy of the bath, and (ii) the other arrow representing the resulting thermal energy generated by the voltage drop within the bath. The chemical energy flow due to the exothermic energy (blue) increases the thermal energy in the bath.

Figure 14.2: Sankey Diagram for the aluminium smelter. The diagram represents how electrical energy is transformed in the process in a nominal operation at 850 kW, a bath temperature of 1250K, an alumina concentration of 4%wt, and a bath ratio of 1.15.

The resulting thermal energy is divided into three: (i) one arrow represents the heat needed for raising the temperature of the material that is fed to the bath (green), (ii) other arrow represents the heat absorbed by the endothermic reactions (blue), and (iii) other arrow represents the heat lost to the surroundings (orange). The blue arrow is divided into two, one represents solely the heat absorbed by the alumina reaction, and the other arrow represents all the remaining endothermic reactions.

Figure 14.2 shows the energy flows in the cell in a steady state. However, time is an important factor in this process, so the dynamic behaviour of the aluminium cell during a power reduction has to be observed.

One of the findings in the study was that there is no need to increase the electrical power consumption above its nominal value after the power restoration to restore the bath to its former value. Instead, the aluminium production rate was reduced during a period of time, increasing the voltage drop by increasing the distance between anode and cathode, and consequently, the heat provided to the bath increased.

Figure 14.3 shows the power corresponding to each arrow in Figure 14.2 during 24 hours of operation, in which the electrical power consumption is reduced to 80% during four hours. Figure 14.3.a) represents the power absorbed from the cell, which will cause a decrease in the temperature. Figure 14.3.b) represents the power provided to the cell, which will cause an increase in the temperature. Figure 14.3.c) overlaps both figures to see at what moments one is higher than the other. Figure 11.5 showed the temperature profile and the aluminium production rate for a four-hour power reduction (Section 11.2).

Figure 14.3 does not show the power losses due to the ohmic resistance of the external parts of the cell. This power does not affect the energy stored in the bath and is not relevant to the temperature.

Figure 14.4 shows the energy flows when the generated heats are different from the lost heats. Figure 14.4.a) shows the energy flows when the generated heats are higher than the lost heats, and the heat needed for bringing the system to equilibrium is taken from the stored energy of

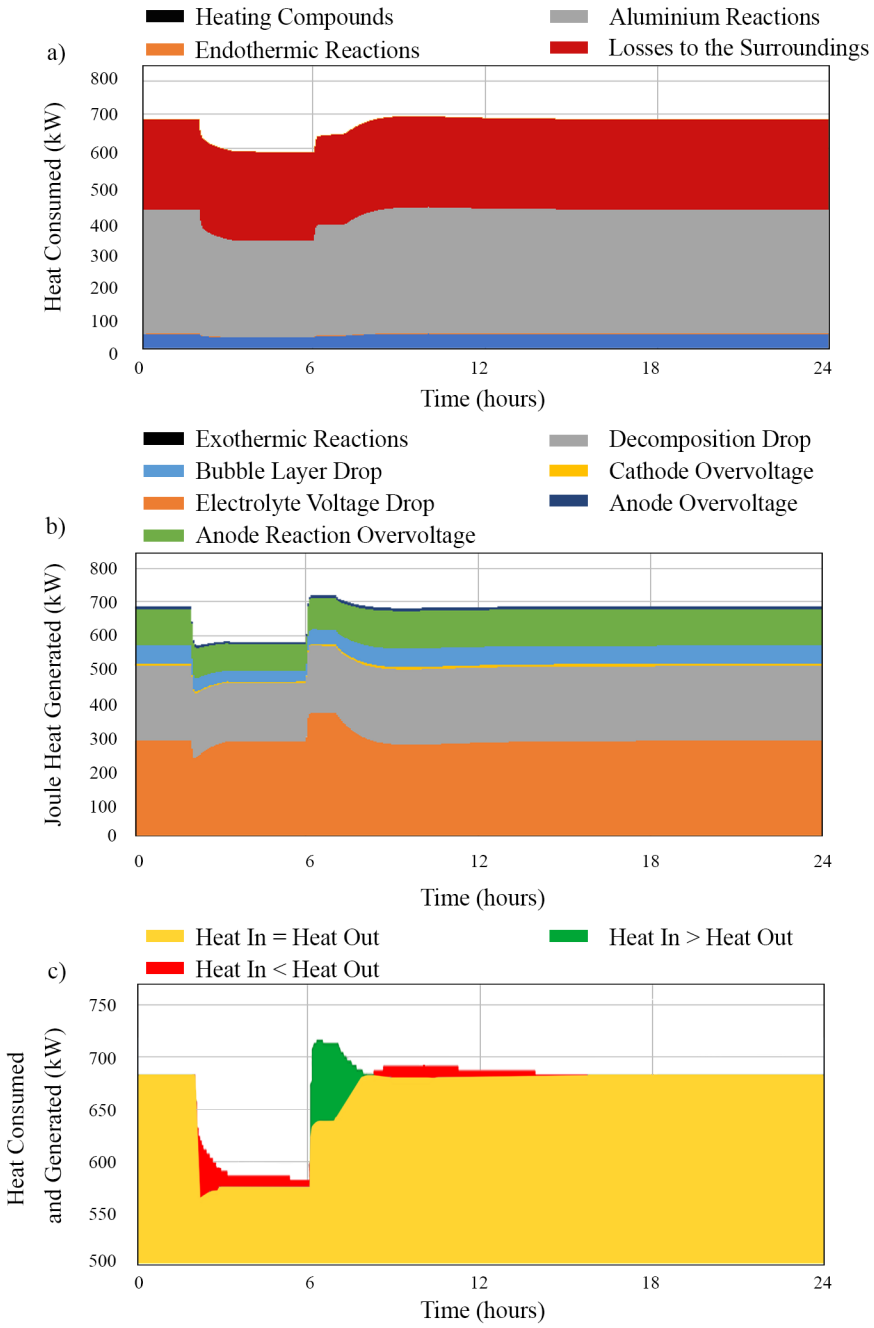


Figure 14.3: Time trends of the a) heat consumed in the cell (kW) b) Joule heat generated in the cell (kW), and in c) the generated heats overlaps the lost heats. If the generated heat are higher than the lost heat (green), the thermal energy in the bath increases, and if the generated heats are lower than the lost heat (red), the thermal energy in the bath decreases.

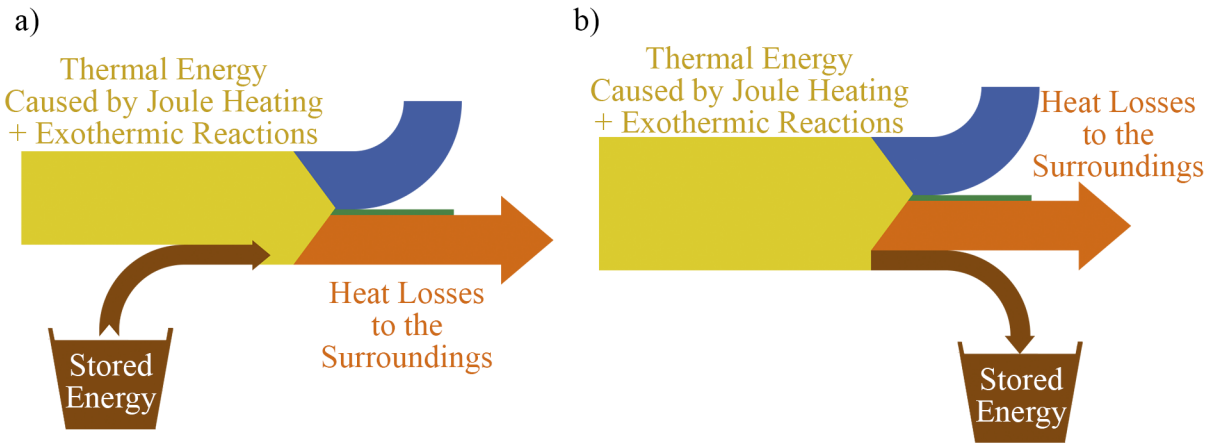


Figure 14.4: Sankey Diagram for the aluminium smelter when the a) heat generated is lower than the heat consumed, and b) when the heat generated is higher than the heat consumed. In a), the lack of heat is consumed by the thermal energy from the bath, and in b), the heat surplus is addressed to increase the thermal energy of the bath.

the cell as thermal energy. Figure 14.4.b) shows the energy flows when the generated heats are lower than the lost heats, and the excess heat is stored in the cell as thermal energy. If both heats are equal, the cell maintains the same energy.

From Figure 14.3, during the power reduction, the generated heats are lower than the lost heats, and the difference of heats is withdrawn from the stored energy in the bath. The stored energy is in the form of thermal energy, so the difference of heats causes the temperature to decrease. After the power is recovered, the generated heats are higher than the lost heats, and the difference of heats is is stored in the bath. Thus, after the power recovery, the temperature rises. The temperature will rise until the difference of heats becomes zero. At this point, the temperature reaches the temperature set point.

When the temperature is lower than the temperature set point, the temperature control loop increases the distance between electrodes, so the voltage drop in the electrolyte increases. Consequently, the generated Joule heat increases, and more heat is addresses to increase the temperature of the cell. However, the power controller reduces the electrical current, so the electrical

power consumption ($V \times I$) matches the electrical power available. The aluminium production rate is proportional to the electrical current, thus, the whole control loop addresses more electrical power to heat the cell, and less to produce aluminium[2].

When power is restored, the temperature controller still sends the signal to the IPD actuator to increase the distance between electrodes and increase the temperature of the cell, causing the voltage drop in the cell to be higher than the nominal. The electrical power available is at its nominal value, and since the voltage is larger, the electric current is lower than its former value. As a consequence, the production rate is lower until the temperature controller sends the signal to decrease the IPD. Thus, after the power restoration, the control loops uses more electrical power to heat the cell, and less to produce aluminium until the temperature returns to its set point.

This evolution leads the temperature to return to its former state without increasing the power consumption to a value above its nominal value.

14.2 Possible Implementation in Industrial Sites

This section analyses the differences between both processes in terms of energy transformations, so that, a series of conclusions can be extracted and used for being implemented in the industry.

14.2.1 Conclusions from Comparing the LNG and the Aluminium Smelter

In terms of the analysis of energy transformation, aluminium smelter differs from the LNG process in several ways: the exploitation of its (i) dynamic behaviour, presenting (ii) chemical

[2]The electrical current affects the ohmic losses due to the external parts, so a higher current means more electrical consumption, more power losses, and a higher aluminium production rate. The power consumption is the product between the overall voltage drop and the electrical current, but the Joule heat is the product between the voltage drop between the electrical current. The aluminium production, on the other hand, does not depend on the voltage drop, it depends on the current

reactions, having different (iii) propagation effect, the (iv) flexibility of the production, and the (v) equipment used in the process.

Dynamic Behaviour

The LNG process is a continuous process in which natural gas is constantly flowing, and therefore, it does not store energy. On the other hand, the aluminium smelter stores energy because it involves a large mass held at high temperature.

This allows the cell to absorb or provide energy, making it easier to respond against changes in the power input. Therefore, having the possibility of storing energy in the system improves its flexibility for possible power reductions.

Chemical Reactions

Producing aluminium requires several chemical reactions. Generally, chemical reactions exchange chemical energy for going to one state to another; this chemical energy in turn, is provided by the thermal energy in the system. In the aluminium smelter, most of the reactions are endothermic, reducing the temperature of the cell, and thus, the electrical energy input to the cell the plant has to increase. But, if the chemical reactions were exothermic, the electrical input could be decreased if the temperature is intended to increase to a certain level. This suggests that the chemical energy can be used for regulating the temperature of the system, and not relying as much on electricity, which increases the flexibility of the plant.

Propagating Effect

The LNG process has high connectivity and multiple recycles. Due to all these connections a small change in some variables in the LNG process can have large impacts on others. Thus, when the available power changes, virtually all the set points in the plant have to change to be

prepared for the incoming modifications. Flexible operation has to take into account all these interactions between equipment and process variables.

Product Flexibility

Aluminium produced in the smelter has no room of possibilities in terms of characteristics, so the product characteristics in this process have no effect on the power consumption of the plant. The LNG, on the other hand, either or both of the temperature and composition of the LNG can change, which causes a difference on the power consumption of the process.

Therefore, energy transformations can also take place by changing the product of the process, but it is crucial that these changes do not affect the established needs of the product, or that they do not make the product exceed any limit.

Process Equipment

The LNG process uses uses rotating machines that transform electrical energy into mechanical energy. The compressors transform the mechanical energy into internal energy of the refrigerants, which has the potential to become thermal energy or pressure volume work. The process also has valves, that transforms the internal energy into the pressure volume work.

The aluminium smelter converts the electrical energy into thermal energy. Additionally, the smelter transforms the electrical energy into chemical energy used for providing the difference of electric potential to the aluminium reduction reaction.

14.2.2 Questions for Implementing Flexible Operation in Industrial Practice

During the research, the author was given the following scenario by the industrial adviser: *"Imagine you are a consultant trying to sell Flexible Operation to an industry. if you have to give an answer by the end of the day, what are the question you would ask for assessing its implementation?"*

After all the simulations, adjusting all the variables, and observing ultimately what is relevant for both the process side and the electrical side, the author came with the following questions:

"Assuming that we know what the process is producing:

1. What is the main electrical consumer?
2. Within the process, what is the electrical consumer connected to?
3. What properties of the product can be adjusted? and to what extent?
4. What is the objective of the plant for reducing its power consumption?"

Clearly, these questions have to be extended to know the details of each equipment, but, as a main structure, it gives the necessary steps to implement flexible operation.

Question number 1 gives a rough idea of how electrical energy is going to be transformed. Electrical energy is not instantly converted, and depending on the electric equipment that consumed electricity, the process will be able to know how fast the response can be. It also gives the first range of operability by setting the boundaries of the equipment.

Question number 2 gives the answer for the propagating effect mentioned in the conclusions above, and also, it gives the operating limits of the equipment and for the energy transformations and the process variables involved in that equipment.

Both questions 1 and 2 should reveal if the process has the ability of storing energy, which is very useful when implementing flexible operation. Also, the combinations of both questions gives an idea of the presence of a chemical reaction, and the exchanged heat or mass amongst the equipment, which will affect the flexibility in the process.

Question 3 set the limit by establishing a threshold the process does not want to exceed in terms of production. It also answers how the product can be changed, so its characteristics could be exploited for changing the electrical consumption of the plant.

Question 4 refers to the uses of flexible operation introduced in Chapter 2. The motivations help the PPM system to have preprogrammed preferences according to economical reasons, process robustness, ancillary services, or sustainability reasons. For a given power reduction, there are several sets of operational points and depending on the motivations for implementing flexible operation, the decision of choosing one set over another depends on the preferences of the plant managers.

These questions should be enough for addressing an initial assessment of the flexible operation implementation, and giving an answer by the end of the day, which is the situation given to the author. However, it should be noted that, for a more detailed assessment, the questions should be more detailed as well. For instance, a P& ID of the process, a detailed map of the site power system that provides electricity to the process, and the specifications of the equipment could give much more information for an accurate assessment. With that, it is possible then to model the process and start the calculations and simulations as it has been done in this work.

14.3 Further Work

Flexible operation is a concept still in development, and it is a new field that has to be widely explored. This work is intended to set the first steps towards its study, and to bridge a gap between the process operation and the electrical system by establishing an envelope of feasible operation that the PPM can use to coordinate both parties. However, this envelope still needs

to be more exhaustively detailed. The model presented in this work has focused on the process rather than on the electrical system,.

The case studies in this work were developed from mathematical models in the literature and some concepts and ideas from real industries during the research of the author.

14.3.1 Further Work in the Study of Flexible Operation

Flexible operation is intended to be utilised by process power management (PPM) systems. As mentioned in Section 2, if there is an electrical contingency, the current PPM uses circuit breakers to interrupt the power supply to some machinery, so that the overall consumption of the site is reduced. When an electrical contingency takes place, the response of the circuit breakers is virtually immediate, so the electrical equipment does not suffer any damage. If flexible operation is implemented, when an electrical contingency occurs, the set points of the process variables and the new electrical consumption have to change immediately.

The main difference is that circuit breakers are used for stopping electrical flow to non-critical equipment, whereas flexible operation lowers the electrical consumption of both critical and non-critical equipment. As seen in the LNG process, the electrical consumption is simultaneously changed in all rotary machinery. What is missing in this model is the dynamic response of the power grid when more than one circuit suddenly reduces the consumption.

Thus, one of the following steps for improving the flexible operation concept is a more detailed model of the electrical system in the site, for both steady state and dynamic transients. Additionally, the conclusions drawn during this section were extracted from analysing two different processes. Thus, the study of flexible operation could be benefited if more case studies were researched, so more thorough conclusions could be drawn. This is further discussed below. Section 14.3.2 describes some improvements that could be made to the studies in this thesis. Then, section 14.3.3 discusses potential processes that can be researched for improving the study of flexible operation.

14.3.2 Further Work in the LNG and Aluminium Smelter Models

The LNG process and the aluminium smelter were modelled considering a series of assumptions for simplifying the model, and due to the lack of equations corresponding to empirical situations or specific equipment. Both models could be enhanced by having access to the specifications or to the empirical data that would allow to model some behaviours in the plant. The next list enumerates what can be improved for each process.

Further Work in the LNG Model

The assumptions made in this model and the feasibility of implementing them were explained in Section 5.1. The reason for this was the lack of data from real heat exchangers, which makes it complicated to model a multistream heat exchanger. To date, the available literature regarding this type of heat exchanger only gives an approximate behaviour, providing the necessary data from the real heat exchanger (Ghosh et al., 2010; Kamath et al., 2009; Watson and Barton, 2016) , so the most accurate manner for modelling this is by obtaining empirical data from a real plant. With that, the dynamic behaviour of the streams exchanging heat can be determined, and therefore, the evolution of the temperatures when the power reduction takes place would be more accurate.

The data for the compressors maps were taken from a generic compressor from Honeywell (Stephenson, 2011). Using the real compressor maps should give an improved accuracy to the model. The dynamic behaviour of the compressor is also an issue for the model. When the compressor starts slowing down due to the reduced consumption of the motor, the flow rate of the refrigerants will start to decrease as well. Another issue that has not been addressed during this work is the dynamic response between the motor and the compressor when the motor receives less electrical power. During his research, the author asked about these issues to workers at ABB, and as a conclusion, he was told that the dynamic response of the motors would be satisfactory.

Thus, the LNG model has to implement empirical data and equipment specifications, so that it will be able to simulate the dynamic response from the motor, the compressor and the heat exchangers.

Further Work in the Aluminium Smelter Model

Temperature and alumina concentration are two of the most important variables in the aluminium smelter. It is very important to control them, so the equipment is not damaged and the process is not jeopardized. One of the assumptions made for the aluminium smelter is that the system is lumped, meaning that the temperature and the concentration are homogeneous within the cell. Another assumptions related to the temperature is that the heat balance does not consider the losses due to radiation or from the corners of the cell. Thus, to increase accuracy in the model, it can include a distributed system in which the temperature and alumina concentration are also a function of the space, and additionally, add a model for including the heat transfer by radiation and the heat transfer through the vertices of the cell. While including the radiation and the vertices are not making a significant difference (Rye et al., 2013), the distributed system will determine the thickness of the cryolite ledge, which has a direct impact on the heat losses to the surroundings.

The consumption of the carbon in the anodes has to be taken into account. The rate at which the anodes are consumed depends on the rate of reduction reaction, which in turn depends on the magnitude of the electric current. The height of the anode affects the ohmic resistance of the cell, and therefore, the voltage drop. Although the simulation runs for 24 hours, the carbon anodes have to be changed at least every month (Jessen, 2008), so it is another factor to bear in mind if the model is intended to simulate a longer operation. To alleviate this issue, a real aluminium smelter could provide the data for the usual consumption rate of the anodes, as well as the thickness of the blocks, so that the voltage drop and the time between replacements can be obtained.

14.3.3 Potential Processes to be Researched

The conclusions that could be drawn by comparing the LNG process and the aluminium smelter gave a good understanding of how to proceed if flexible operation is intended to be implemented. Nevertheless, some aspects are not observed in both processes. For example, the type of operation or process of both plants do not give the full spectrum of possibilities in which flexible operation can be implemented.

The LNG process is a continuous process, and the aluminium smelter is a semi-batch process. Thus, a batch process could give another perspective of how time can be used for increasing the flexibility in the plant. In a batch process, the stored energy is not flowing, and therefore its transformation would differ from the two studied processes.

The equipment used during the process another consideration for having more processes to observe. In the LNG process, rotating equipment, heat exchangers, and expansion valves have been examined, whereas in the aluminium smelter, a mixture of an arc furnace and a chemical reactor has been studied. Something in common in both processes is that the electrical energy is transformed into thermal energy at some point of the process, but the mechanism for that transformation is completely different.

Cement Production

Cement production is an electricity-intensive process with potential for flexible operation. One of the steps in the process is the rock crushing, in which the surface area is increased by using crushers and grinders. The crushed limestone goes to a kiln, in which the following decomposition takes place:

$$CaCO_3 \longrightarrow CaO + CO_2 \tag{14.1}$$

A higher surface area has more energy than the bulk material, so the electrical energy is used to provide that energy. Consequently, the size of the raw material affects the energy consumption

of the grinder, so observing the behaviour of the electrical consumption as a function of the material fed gives additional input for more conclusions. An aspect to consider in the cement grinder is that it works in batches, so the rocks are fed to the grinder, then they are ground, and once ground, they leave the grinder. To some extent, it makes the process independent of the time factor, so if studied more conclusions can be deduced.

The production of cement can undergo two processes, the wet and the dry process. Compared to the dry process, the wet process consumes less electrical power, but the kiln needs more fuel. The product quality in the wet process is higher, but the process time also increases. The difference of operations come from the beginning of the process, where the process adds water to the raw material, but the equipment does not need to change.

If the questions from section 14.2.2 were answered for this plant, the answers to the three first questions would be:

Q. What is the main electrical consumer?

A. The main consumers are the crushers and the grinders.

Q. Within the process, what is the electrical consumer connected to?

A. After crushing the limestone, it goes to a kiln where the crushed limestone is decomposed.

Q. What properties of the product can be adjusted?

A. Quality of the product or time production.

The answer to question 3 refers to the way of operating the plant. If the grinders can work under the wet process, they will consume less energy. However, that might affect to the overall quality of the product, as well as the time for producing it. The answer of the fourth question depends on the plant and what are their objectives at that specific moment.

Chloralkali Process

Other potential process is the chloralkali process, in which chlorine and caustic soda are produced. One of the reasons for including this process is that it is a high energy consumption, and therefore it can be an active member for regulating the power balance in the grid. Apart from that, when the caustic soda is purified, this purification process has a chemical reactor, in which (unlike most of the reactions in the aluminium smelter) exothermic reactions take place (Schlafer et al., 2000). As mentioned above, for exothermic reactions, temperature is crucial, so it would be interesting to observe how to control the temperature when the consumption in the plant varies. Additionally, the process has also an electrolysis cell, so it can be compared to the electrolysis reactions carried out in the aluminium smelter. Figure 14.5 shows a simplification of the chloralkali process. In the process, a salt solution is electrolysed in an electrolytic cell to obtain sodium hydroxide, hydrogen, and chlorine, which is the primary product of the process. The cell is the most consuming equipment of the plant, and it is between a heat exchanger that raises the temperature of the salt solution, and a membrane that concentrates the product from the electrolysis. The redox reaction takes place in the cell, so the power consumed in it affects the heat balance in the process.

If the questions from Section 14.2.2 were answered for this plant, the answers to the three first questions would be:

Q. What is the main electrical consumer?

A. The main consumer is the electrolytic cell.

Q. Within the process, what is the electrical consumer connected to?

A. It is connected to a heat exchanger that increases the temperature of the salt solution, and a membrane that concentrates the sodium hydroxide.

Q. What properties of the product can be adjusted?

A. Quality of the product and production rate of each compound.

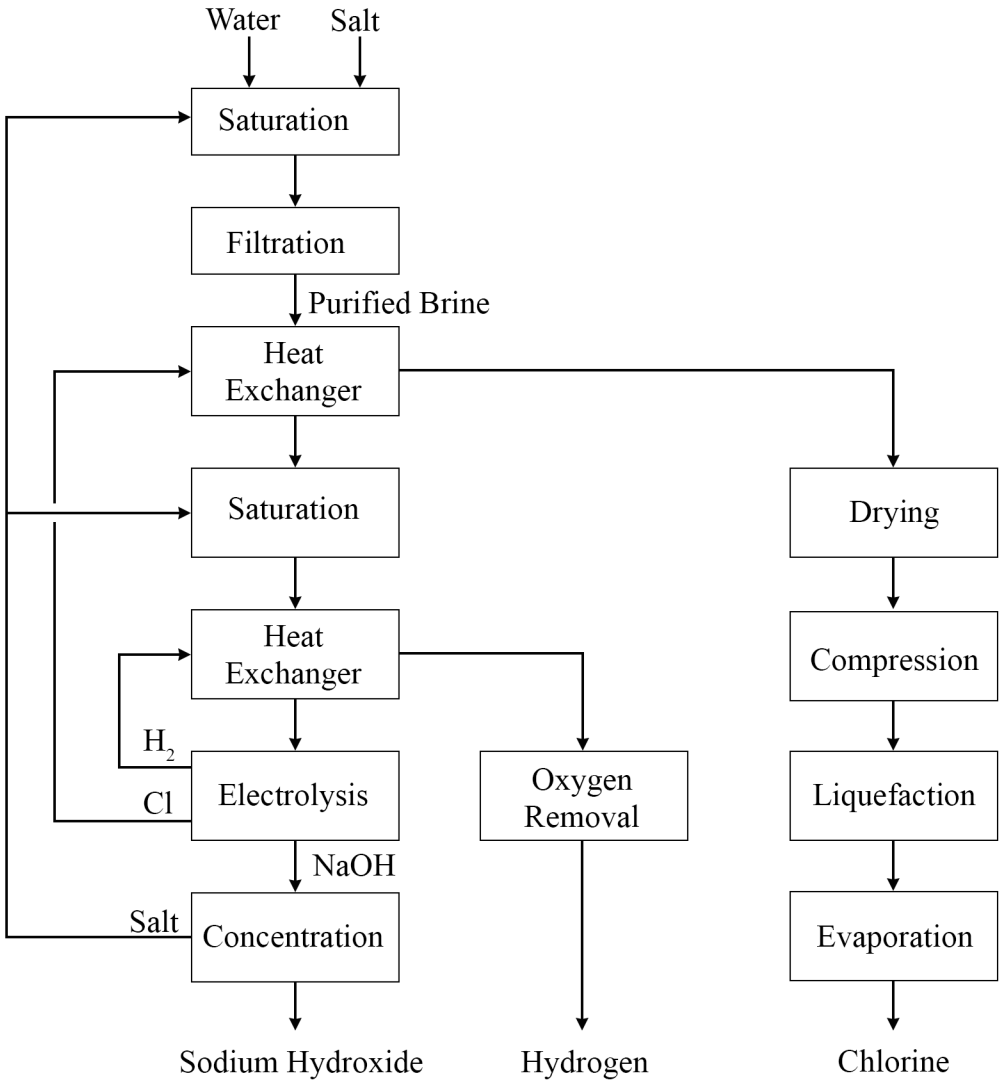


Figure 14.5: Simplified diagram of the chloralkali process.

The answer to question 3 is due to the reaction yield of the electrolysis, which depends on the current and the temperature in the electrolysis cell. Thus, not only the production rate, but also the quality of the NaOH, the hydrogen and the chloride streams depend on the power addressed to the cell.

These examples are a suggestion for future work in the study of flexible operation in electricity-intensive processes. The author encourages other researchers to explore flexible operation in

different processes using the guidelines provided during this chapter, adopting a critical thinking for expanding the concept of flexible operation.

Chapter 15

Conclusions

Flexible operation allows industrial processes to accommodate the process variables when a disturbance occurs. In electricity-intensive processes, a possible disturbance is a reduction in the available power. This thesis has studied flexible operation in electricity-intensive processes when there is a reduction in the available power.

Electricity-intensive processes are often in a microgrid, which is a group of loads and power generators that can connect or disconnect from the public power grid. Process Power Management (PPM) systems ensure that the generated and consumed power in the microgrid are balanced. In an electrical contingency, the available power suddenly reduces, and the PPM system disconnects electrical loads in the process until the electrical power consumption is lower than the available power. This operation is called load shedding.

PPM starts by shedding non-essential equipment, but if the electrical power consumption is not low enough, PPM might disconnect essential equipment, and the process then needs to shut down. In that context, if the process has low granularity, i.e. a small number of large loads, it is more likely that the PPM will have to shed an essential load. If the process stops, the economic impacts are significant due to the loss of production and the costs of restarting the plant. Thus, this thesis proposes an approach whereby the PPM controls the consumption of the

plant by reducing the consumption of the equipment rather than disconnecting it. This approach is named flexible operation.

If the plant operates flexibly, the process can continue producing during an electrical contingency, but at a lower production rate. During an electrical contingency, the process has to immediately operate with lower electrical power consumption. The process variables have to move towards an operating point consistent with the available power. Thus, PPM reduces the electrical power available the process, and at the same time, it sends set points to the process control system to move towards an operating point consistent with the available power.

The solution approach is observing the electrical power consumption when various process variables were adjusted so that a relationship between these variables and the electrical power consumption is determined. It is possible to know the behaviour of the process when the electrical power consumption is reduced using the relationships. These relationships are useful for:

- Obtaining an envelope of feasible operation giving a family of possible set points that corresponds to the available electrical power. A single value of electrical power consumption can be achieved by adjusting different values for different variables. Thus, maintaining some values within a specified range will depend on the necessities and preferences.
- Determining preprogrammed actions to carry out, so, in case there is an electrical contingency, the process can respond as fast as possible. The power reduces very rapidly (within 200ms). Therefore it is crucial to send new set points to the process control system within 200ms. Thus, the plant can immediately start to move towards a new operating point that is consistent with the available power.
- Estimating a range of power consumption that provides the PPM system with the limitations of their power reduction.

The hypothesis at the beginning of this document suggested that during an electrical contingency, it is possible to operate an electricity-intensive process flexibly to exploit the remaining available power. This thesis has exposed arguments that proved the veracity of this hypothesis

by studying flexible operation for electricity-intensive processes. This research has modelled two electricity-intensive processes, namely the liquefaction of natural gas (LNG), and the aluminium smelting process. The models calculate the process variables for various power consumptions to obtain an envelope of feasible operation.

The results show that both processes have great potential for adjusting their electrical power consumption. The results show that the production rate needs to decrease to move towards to an operating point that is consistent with the available power. In the LNG case, electrical power consumption can be reduced to 65%, which corresponds to an operating point in which them LNG production rate is reduced to 59%. In the aluminium smelter case, in steady state operation, the electrical power consumption can be reduced to 74%, which corresponds to an operating point in which the aluminium production rate is reduced to 70%.

Results show that the reduction in production rate can be ameliorated by adjusting other secondary process variables. In the LNG process, increasing the LNG exit temperature and at the same time increasing the methane content in the LNG increases the LNG production rate to 104%. In the aluminium smelting process, increasing the alumina concentration and establishing the bath ratio to 1.25 can increase the aluminium production rate to 100.6%. Decreasing the temperature can increase the aluminium production rate to 112%.

This thesis has also studied how the PPM can exploit the energy storage in the aluminium smelter. The model simulated electrical power reductions of various durations and magnitudes to observe the transient behaviour of the process. The results showed that electrical power could be reduced below the 74% point found for the steady state operation. The process has to restore the electrical power consumption before the bath temperature exceeds any limit. During the power restoration, the temperature returns to its former value without the plant consuming more electrical power than the nominal electrical power consumption.

The comparison of both processes stated that the flexibility of an electricity-intensive process depends on how electrical power transforms throughout the operation. PPM can exploit factors

such as energy storage or the presence of chemical reactions to improve the flexibility of the process.

Flexible operation in electricity-intensive processes is crucial for achieving continued operation when an electrical contingency takes place, while minimising production losses. This thesis has studied the potential of flexible operation to have a better understanding of how electricity-intensive processes can exploit the available electrical power. This thesis has successfully shown that flexible operation is a better alternative to load shedding. Considering that a large number of electricity-intensive processes can benefit from flexible operation, the findings in this thesis open a wide field of future work in academic and industrial research.

Bibliography

ABB (2016). *ABB Process Power Manager. Ensure a reliable and stable energy supply*. Available from: https://library.e.abb.com/public/5c150d5dd42449d3895001870f2cfd17/3BNP101100_A-en_ABB_Process_Power_Manager_brochure.pdf. [Accessed: 15 September 2019].

Alemany, J. M., Arendarski, B., Lombardi, P., and Komarnicki, P. (2018). Accentuating the renewable energy exploitation: Evaluation of flexibility options. *International Journal of Electrical Power & Energy Systems*, 102:131 – 151.

Almada, J., Leão, R., Sampaio, R., and Barroso, G. (2016). A centralized and heuristic approach for energy management of an ac microgrid. *Renewable and Sustainable Energy Reviews*, 60:1396–1404.

Altenpohl, D. G. (1998). *Aluminum : Technology, Applications, and Environment, a Profile of a Modern Metal*. Wiley-TMS, Washington, D.C. : Warrendale, Pa., 6th edition.

AspenTech (2001a). *Aspen Physical Property System. Physical Property Data 11.1*. Available from: http://web.ist.utl.pt/ist11061/de/ASPEN/Physical_Property_Data_Aspen.pdf. [Accessed: 15 September 2019].

AspenTech (2001b). *Aspen Physical Property System. Physical Property Methods and Models 11.1*. Available from: http://web.ist.utl.pt/ ist11061/de/ASPEN/Physical_Property_Methods_and_Models.pdf. [Accessed: 15 September 2019].

AspenTech (2015). *AspenOne* (Version 8.8). [Software]. AspenTech. Available from: https://www.aspentech.com/en/products/engineering/engineering.

Biedler, P. (2003). *Modeling of an aluminum reduction cell for the development of a state estimator*. PhD thesis, West Virginia West Virginia University.

Blatch, G. I., Fyfe, M., and Taylor, M. P. (1996). *Process for controlling aluminium smelting cells*. European Patent EP0671488A2 (Patent).

Bogdanov, D. and Breyer, C. (2016). North-East Asian Super Grid for 100% renewable energy supply: Optimal mix of energy technologies for electricity, gas and heat supply options. *Energy Conversion and Management*, 112:176 – 190.

Bosma, P. and Nagelvoort, R. K. (2009). Liquefaction technology; developments through history. In *Proceedings of the 1st Annual Gas Processing Symposium*, pages 19–31. Elsevier.

BP p.l.c. (2019). *BP Statistical Review of World Energy 2018*. Available from: https://www.bp.com/en/global/corporate/energy-economics/statistical-review-of-world-energy.html. [Accessed: 15 September 2019].

Callaway, D. and Hiskens, I. (2011). Achieving controllability of electric loads. *Proceedings of the IEEE*, 99(1):184–199.

Caspari, A., Offermanns, C., Schäfer, P., Mhamdi, A., and Mitsos, A. (2019a). A flexible air separation process: 1. Design and steady-state optimizations. *AIChE Journal*. Available from: doi:10.1002/aic.16705.

Caspari, A., Offermanns, C., Schäfer, P., Mhamdi, A., and Mitsos, A. (2019b). A flexible air separation process: 2. Optimal operation using economic model predictive control. *AIChE Journal*. Available from: doi:10.1002/aic.16721.

Chalmers, H. and Gibbins, J. (2007). Initial evaluation of the impact of post-combustion capture of carbon dioxide on supercritical pulverised coal power plant part load performance. *Fuel*, 86(14):2109 – 2123.

Chalmers, H., Lucquiaud, M., Gibbins, J., and Leach, M. (2009). Flexible operation of coal fired power plants with postcombustion capture of carbon dioxide. *Journal of Environmental Engineering*, 135(6):449–458.

Chang-Chien, L., An, L. N., Lin, T., and Lee, W. (2012). Incorporating demand response with spinning reserve to realize an adaptive frequency restoration plan for system contingencies. *IEEE Transactions on Smart Grid*, 3(3):1145–1153.

Chase, M. W. (1998). *NIST-JANAF Thermochemical Tables 2 Volume-Set*. American Institute of Physics, Washington DC, 4th edition.

Child, M., Bogdanov, D., and Breyer, C. (2018). The role of storage technologies for the transition to a 100% renewable energy system in Europe. *Energy Procedia*, 155:44 – 60.

Child, M., Kemfert, C., Bogdanov, D., and Breyer, C. (2019). Flexible electricity generation, grid exchange and storage for the transition to a 100% renewable energy system in Europe. *Renewable Energy*, 139:80 – 101.

Chmielewski, D. J. (2014). Smart Grid: The basics - What? Why? Who? How? *Chemical Engineering Progress*, 110:28–34.

Cupertino, A. F., Xavier, L. S., Brito, E. M., Mendes, V. F., and Pereira, H. A. (2019). Benchmarking of power control strategies for photovoltaic systems under unbalanced conditions. *International Journal of Electrical Power & Energy Systems*, 106:335 – 345.

de Sisternes, F. J., Jenkins, J. D., and Botterud, A. (2016). The value of energy storage in decarbonizing the electricity sector. *Applied Energy*, 175:368 – 379.

Deign, J. (2017). *German firm turns aluminum smelter into a "virtual battery"*. Available from: https://www.greentechmedia.com/articles/read/german-firm-turns-aluminum-smelter-into-huge-battery. [Accessed: 15 September 2019].

Denholm, P., O'Connell, M., Brinkman, G., and Jorgenson, J. (2015). Overgeneration from solar energy in California. A field guide to the duck chart. Available from: https://www.nrel.gov/docs/fy16osti/65023.pdf. [Accessed: 15 September 2019].

Devold, H., Nestli, T., and Hunter, J. (2006). *All electric LNG Plants. Better, safer, more reliable - and profitable*. Available from https://library.e.abb.com/public/9e770a172afc8d7ec125779e004b9974/Paper%20LNG_Rev-20A_lowres.pdf. [Accessed: 15 September 2019].

Dickenson, T. C. (1997). *Valves, Piping and Pipelines Handbook*. Elsevier, Oxford, 3rd ed. edition.

Dorreen, M., Wright, L., Matthews, G., Patel, P., and Wong, D. S. (2017). Transforming the way electricity is consumed during the aluminium smelting process. In Zhang, L., Drelich, J. W., Neelameggham, N. R., Guillen, D. P., Haque, N., Zhu, J., Sun, Z., Wang, T., Howarter, J. A., Tesfaye, F., Ikhmayies, S., Olivetti, E., and Kennedy, M. W., editors, *Energy Technology 2017*, pages 15–25, Cham.Switzerland. Springer International Publishing.

Dotzauer, M., Pfeiffer, D., Lauer, M., Pohl, M., Mauky, E., Bär, K., Sonnleitner, M., Zörner, W., Hudde, J., Schwarz, B., Fabauer, B., Dahmen, M., Rieke, C., Herbert, J., and Thrän, D. (2019). How to measure flexibility - performance indicators for demand driven power generation from biogas plants. *Renewable Energy*, 134:135 – 146.

Drengstig, T., Kolås, S., and Støre, T. (2003). The impact of varying conductivity on the control of aluminium electrolysis cells. *Modeling, Identification and Control*, 24(4):205–216.

Eilers, H. and Schaub, G. (2016). Analysis of three-phase catalytic fuel synthesis reactors for flexible operation. *Chemical Engineering & Technology*, 39(11):2107–2116.

Enerdata (2018). *Global Energy Statistical Yearbook 2018*. Available from: https://yearbook.enerdata.net/total-energy/world-consumption-statistics.html. [Accessed: 15 September 2019].

European Commission (2018). *Communication from the Commission. A Clean Planet for all*. The European Commission.

Fazlollahi, F., Bown, A., Ebrahimzadeh, E., and Baxter, L. L. (2015). Design and analysis of the natural gas liquefaction optimization process - CCC-ES (Energy Storage of Cryogeni Carbon Capture). *Energy*, 90:244 – 257.

Floudas, C. A., Gümüş, Z. H., and Ierapetritou, M. (2001). Global optimization in design under uncertainty: Feasibility test and flexibility index problems. *Industrial & Engineering Chemistry Research*, 40(20):4267–4282.

Galasiu, I. and Galasiu, R. (2014). *Aluminium Electrolysis with Inert Anodes and Wettable Cathodes and with Low Energy Consumption*, chapter 1.4, pages 27–37. John Wiley & Sons, Ltd.

Gangale F. and Vasiljevska J. and Covrig F. and Mengolini A. and Fulli G. (2017). *Smart Grid Projects Outlook 2017: Facts, Figures and Trends in Europe*. Technical report, The European Commission.

Gheribi, A. E., Poncsak, S., Guérard, S., Bilodeau, J., Kiss, L., and Chartrand, P. (2017). Thermal conductivity of the sideledge in aluminium electrolysis cells: Experiments and numerical modelling. *The Journal of Chemical Physics*, 146:114701.

Ghosh, I., Sarangi, S. K., and Das, P. K. (2010). Synthesis of multistream heat exchangers by thermally linked two-stream modules. *International Journal of Heat and Mass Transfer*, 53(5):1070 – 1078.

Gils, H. C., Scholz, Y., Pregger, T., de Tena, D. L., and Heide, D. (2017). Integrated modelling of variable renewable energy-based power supply in Europe. *Energy*, 123:173 – 188.

Gloystein, H. (2016). *Australia's Gorgon LNG plant to restart within 30-60 days - Chevron*. Available from: https://www.reuters.com/article/chevron-lng-gorgon/australias-gorgon-lng-plant-to-restart-within-30-60-days-chevron-idUSL5N17905Q. [Accessed: 15 September 2019].

Golmohamadi, H., Keypour, R., Bak-Jensen, B., and Pillai, J. R. (2019). A multi-agent based optimization of residential and industrial demand response aggregators. *International Journal of Electrical Power & Energy Systems*, 107:472 – 485.

Gottwalt, S., Ketter, W., Block, C., Collins, J., and Weinhardt, C. (2011). Demand side management - A simulation of household behavior under variable prices. *Energy Policy*, 39(12):8163 – 8174.

Goyal, M., Chakravarty, A., and Atrey, M. (2014). Two dimensional model for multistream plate fin heat exchangers. *Cryogenics*, 61:70 – 78.

Grjotheim, K. and Welch, B. (1988). *Aluminium Smelter Technology: A Pure and Applied Approach*. Düsseldorf: Aluminium-Verlag, 2nd edition.

Guerrero, J., Chandorkar, M., Lee, T.-L., and Loh, P. (2013). Advanced control architectures for intelligent microgrids Part I: Decentralized and hierarchical control. *IEEE Transactions on Industrial Electronics*, 60(4):1254–1262.

Gutowski, T. G., Branham, M. S., Dahmus, J. B., Jones, A. J., Thiriez, A., and Sekulic, D. P. (2009). Thermodynamic analysis of resources used in manufacturing processes. *Environmental Science & Technology*, 43(5):1584–1590.

Hakim, L., Kubokawa, J., Yuan, Y., Mitani, T., Zoka, Y., Yorino, N., Niwa, Y., Shimomura, K., and Takeuchi, A. (2009). A study on the effect of generation shedding to total transfer capability by means of transient stability constrained optimal power flow. *IEEE Transactions on Power Systems*, 24(1):347–355.

Hanrahan, B. L., Lightbody, G., Staudt, L., and Leahy, P. G. (2014). A powerful visualization technique for electricity supply and demand at industrial sites with combined heat and power and wind generation. *Renewable and Sustainable Energy Reviews*, 31:860 – 869.

Harjunkoski, I., Maravelias, C., Bongers, P., Castro, P., Engell, S., Grossmann, I., Hooker, J., Méndez, C., Sand, G., and Wassick, J. (2014). Scope for industrial applications of production scheduling models and solution methods. *Computers and Chemical Engineering*, 62:161–193.

Haupin, W. (1995). Impact of bath composition on performance and economics of aluminum smelters. *Light Metal Age*, 53(11-12).

Haupin, W. (2001). Aluminum production and refining. In Buschow, K. J., Cahn, R. W., Flemings, M. C., Ilschner, B., Kramer, E. J., Mahajan, S., and Veyssière, P., editors, *Encyclopedia of Materials: Science and Technology*, pages 132 – 141. Elsevier, Oxford.

Haupin, W. (2016). *Interpreting the Components of Cell Voltage*, pages 153–159. Springer International Publishing, Cham. Switzerland.

He, T. and Ju, Y. (2016). Dynamic simulation of mixed refrigerant process for small-scale LNG plant in skid mount packages. *Energy*, 97:350 – 358.

He, T., Karimi, I. A., and Ju, Y. (2018). Review on the design and optimization of natural gas liquefaction processes for onshore and offshore applications. *Chemical Engineering Research and Design*, 132:89 – 114.

Hirsch, A., Parag, Y., and Guerrero, J. (2018). Microgrids: A review of technologies, key drivers, and outstanding issues. *Renewable and Sustainable Energy Reviews*, 90:402 – 411.

Hiveš, J., Thonstad, J., Sterten, Å., and Fellner, P. (1996). Electrical conductivity of molten cryolite-based mixtures obtained with a tube-type cell made of pyrolytic boron nitride. *Metallurgical and Materials Transactions B*, 27(2):255–261.

Holttinen, H., Tuohy, A., Milligan, M., Lannoye, E., Silva, V., Müller, S., and So, L. (2013). The flexibility workout: Managing variable resources and assessing the need for power system modification. *IEEE Power and Energy Magazine*, 11(6):53–62.

Ikeda, M. and Schaefer, L. (2011). Examining the effect of binary interaction parameters on VLE modelling using cubic equations of state. *Fluid Phase Equilibria*, 305(2):233 – 237.

Incropera, F. P., Dewitt, D., Bergman, T., and Lavine, A. (2011). *Principles of Heat and Mass Transfer*. John Wiley, Hoboken, N.J. : Chichester, 7th edition.

Iovine, A., Rigaut, T., Damm, G., Santis, E. D., and Benedetto, M. D. D. (2019). Power management for a dc microgrid integrating renewables and storages. *Control Engineering Practice*, 85:59 – 79.

Jenkins, J., Zhou, Z., Ponciroli, R., Vilim, R., Ganda, F., de Sisternes, F., and Botterud, A. (2018). The benefits of nuclear flexibility in power system operations with renewable energy. *Applied Energy*, 222:872 – 884.

Jeong, E. S. (2017). Optimization of power generating thermoelectric modules utilizing LNG cold energy. *Cryogenics*, 88:29 – 35.

Jessen, S. W. (2008). *Mathematical modeling of a Hall Héroult aluminium reduction Cell*. Master's thesis, Technical University of Denmark.

Jiang, H., Lin, J., Song, Y.-H., Li, X.-M., and Dong, J.-X. (2013). Frequency control by aluminum smelter load response in an isolated wind power system: A study for an industrial case. In *2013 IEEE Power Energy Society General Meeting*, pages 1–5.

Jin, Y., Chai, S., Duffy, J., Chin, C., and Bose, N. (2019). Hydrodynamics of a conceptual FLNG system in side-by-side offloading operation. *Ships and Offshore Structures*, 14(1):104–124.

Kamath, R. S., Grossmann, I. E., and Biegler, L. T. (2009). Modeling of multi-stream heat exchangers with phase changes for cryogenic applications. In de Brito Alves, R. M., do Nascimento, C. A. O., and Biscaia, E. C., editors, *10th International Symposium on Process Systems Engineering: Part A*, volume 27 of *Computer Aided Chemical Engineering*, pages 921 – 926. Elsevier.

Kanbur, B. B., Xiang, L., Dubey, S., Choo, F. H., and Duan, F. (2017). Cold utilization systems of LNG: A review. *Renewable and Sustainable Energy Reviews*, 79:1171 – 1188.

Kang, C., Ji, Z., and Chen, Q. (2012). Review and prospects of flexible operation of carbon capture power plants. *Dianli Xitong Zidonghua/Automation of Electric Power Systems*, 36(6):1–10.

Kirby, B. (2007). Ancillary services: Technical and commercial insights. *Retrieved October*, 4:2012.

Kolås, S. and Støre, T. (2009). Bath temperature and AlF_3 control of an aluminium electrolysis cell. *Control Engineering Practice*, 17(9):1035 – 1043.

Korenko, M., Vasková, Z., Priščák, J., Šimko, F., Ambrová, M., and Shi, Z. (2015). Density, viscosity and electrical conductivity of the molten cryolite electrolytes (Na_3AlF_6–SiO_2) for Solar Grade Silicon (Si–SoG) electrowinning. *Silicon*, 7(3):261–267.

Koytsoumpa, E. I., Bergins, C., and Kakaras, E. (2018). Flexible operation of thermal plants with integrated energy storage technologies. *Heat and Mass Transfer*, 54(8):2453–2460.

Kundur, P., Balu, N., and Lauby, M. (1994). *Power System Stability and Control*. McGraw-Hill, New York ; London.

Kuschel, G. I. and Welch, B. J. (2016). Further studies of alumina dissolution under conditions similar to cell operation. In Bearne, G., Dupuis, M., and Tarcy, G., editors, *Essential Readings in Light Metals: Volume 2 Aluminum Reduction Technology*, pages 112–118. Springer International Publishing, Cham.Switzerland.

Łaciak, M., Sztekler, K., Szurlej, A., and Włodek, T. (2019). Possibilities of Liquefied Natural Gas (LNG) use for power generation. *IOP Conference Series: Earth and Environmental Science*, 214.

Lambert, T., Hoadley, A., and Hooper, B. (2016). Flexible operation and economic incentives to reduce the cost of CO_2 capture. *International Journal of Greenhouse Gas Control*, 48:321–326.

Landry, J.-R., Fallah Fini, M., Soucy, G., Désilets, M., Pelletier, P., Rivoaland, L., and Lombard, D. (2018). Laboratory study of the impact of the cathode grade on the formation of deposits on the cathode surface in hall-héroult cells. In Martin, O., editor, *Light Metals 2018*, pages 1229–1233, Cham.Switzerland. Springer International Publishing.

Lannoye, E., Flynn, D., and O'Malley, M. (2012). Evaluation of power system flexibility. *IEEE Transactions on Power Systems*, 27(2):922–931.

Lee, D.-H., Ha, M.-K., Kim, S.-Y., and Shin, S.-C. (2014). Research of design challenges and new technologies for floating LNG. *International Journal of Naval Architecture and Ocean Engineering*, 6(2):307–322.

Lee, H., Byeon, G.-S., Jeon, J.-H., Hussain, A., Kim, H.-M., Rousis, A., and Strbac, G. (2019). An energy management system with optimum reserve power procurement function for microgrid resilience improvement. *IEEE Access*, 7:42577–42585.

Lee, I., Park, J., and Moon, I. (2018). Key issues and challenges on the liquefied natural gas value chain: A review from the process systems engineering point of view. *Industrial & Engineering Chemistry Research*, 57(17):5805–5818.

Li, N., Uçkun, C., Constantinescu, E. M., Birge, J. R., Hedman, K. W., and Botterud, A. (2016). Flexible operation of batteries in power system scheduling with renewable energy. *IEEE Transactions on Sustainable Energy*, 7(2):685–696.

Lin, Y.-J., Wong, D. S.-H., Jang, S.-S., and Ou, J.-J. (2012). Control strategies for flexible operation of power plant with CO_2 capture plant. *AIChE Journal*, 58(9):2697–2704.

Linde AG (2018). *LNG technology. Optimised solutions for small- to world-scale plants*. Available from: https://www.linde-engineering.com/en/images/LNG-Technology_tcm19-4577.pdf. [Accessed: 15 September 2019].

Linde AG (2019). *World-scale LNG plants*. Available from: https://www.linde-engineering.com/en/process_plants/lng-and-natural-gas-processing-plants/liquefied_natural_gas/world_scale_baseload_lng_production/index.html. [Accessed: 15 September 2019].

Liu, J., Fallah-Mehrjardi, A., Shishin, D., Jak, E., Dorreen, M., and Taylor, M. (2017). Investigation of the influence of heat balance shifts on the freeze microstructure and composition in aluminum smelting bath system: Cryolite-CaF_2-AlF_3-Al_2O_3. *Metallurgical and Materials Transactions B*, 48.

Liu, X., Wu, J., Jenkins, N., and Bagdanavicius, A. (2016). Combined analysis of electricity and heat networks. *Applied Energy*, 162:1238 – 1250.

Luo, X., Li, M., and Roetzel, W. (2002). A general solution for one-dimensional multistream heat exchangers and their networks. *International Journal of Heat and Mass Transfer*, 45(13):2695 – 2705.

Luo, X. and Wang, M. (2016). Optimal operation of MEA-based post-combustion carbon capture for natural gas combined cycle power plants under different market conditions. *International Journal of Greenhouse Gas Control*, 48:312–320.

Mamantov, G. and Marassi, R. (1987). *Molten Salt Chemistry : An Introduction and Selected Applications*. Springer Netherlands, 1st edition.

Martínez-Rodríguez, G., Fuentes-Silva, A. L., Lizárraga-Morazán, J. R., and Picón-Núñez, M. (2019). Incorporating the concept of flexible operation in the design of solar collector fields for industrial applications. *Energies*, 12(3):570.

Martínez-Velasco, J. and González-Molina, F. (2014). Calculation of power system overvoltages. In *Transient Analysis of Power Systems: Solution Techniques, Tools and Applications*, pages 100–194. Wiley.

Matlab (2010). *Matlab* (R2010a). [Software]. The MathWorks Inc. Available from: https://uk.mathworks.com/downloads/.

McFadden, F. J. S., Welch, B. J., and Austin, P. C. (2006). The multivariable model-based control of the non-alumina electrolyte variables in aluminum smelting cells. *JOM*, 58(2):42–47.

Mechleri, E., Fennell, P., and Dowell, N. (2017). Flexible operation strategies for coal- and gas-CCS power stations under the UK and USA markets. In *Energy Procedia*, volume 114, pages 6543–6551.

Mehrpooya, M. and Sharifzadeh, M. (2017). A novel integration of oxy-fuel cycle, high temperature solar cycle and LNG cold recovery - energy and exergy analysis. *Applied Thermal Engineering*, 114:1090 – 1104.

Michard, L. (2018). *Method for Controlling an Aluminium Reduction Cell*. WO2018202959A1 (Patent).

Miller, A. S. (2015). *Compressor conceptual design optimizatio*n. Master's thesis, Georgia Institute of Technology.

Mitra, S., Grossmann, I. E., Pinto, J. M., and Arora, N. (2012). Optimal production planning under time-sensitive electricity prices for continuous power-intensive processes. *Computers & Chemical Engineering*, 38:171 – 184.

Molenaar, D., Ding, K., and Kapoor, A. (2016). Development of industrial benchmark finite element analysis model to study energy efficient electrical connections for primary aluminium smelters. In Lindsay, S. J., editor, *Light Metals 2011*, pages 985–990. Springer International Publishing, Cham. Switzerland.

Molina-García, Á., Gabaldon, A., Faura, F., and Fuentes, J. A. (2001). New approaches to model electric demand in aluminium smelter industry. In *Conference Record of the 2001 IEEE Industry Applications Conference. 36th IAS Annual Meeting*, volume 2, pages 1426–1431 vol.2.

Molina-García, A., Kessler, M., Bueso, M. C., Fuentes, J. A., Gómez-Lázaro, E., and Faura, F. (2011). Modeling aluminum smelter plants using sliced inverse regression with a view towards load flexibility. *IEEE Transactions on Power Systems*, 26(1):282–293.

Mrabet, Z. E., Kaabouch, N., Ghazi, H. E., and Ghazi, H. E. (2018). Cyber-security in smart grid: Survey and challenges. *Computers & Electrical Engineering*, 67:469 – 482.

Mukherjee, S., Nateghi, R., and Hastak, M. (2018). A multi-hazard approach to assess severe weather-induced major power outage risks in the US. *Reliability Engineering and System Safety*, 175:283 – 305.

Naixiang, F., Jianping, P., Yaowu, W., Yuezhong, D., and Xian'an, L. (2016). Energy reduction technology for aluminum electrolysis: Choice of the cell voltage. In *Light Metals 2013*, pages 549–552. Springer International Publishing, Cham. Switzerland.

Nam, K., Chang, D., Chang, K., Rhee, T., and Lee, I.-B. (2011). Methodology of life cycle cost with risk expenditure for offshore process at conceptual design stage. *Energy*, 36(3):1554–1563.

Namboothiri, S., Lavoie, P., Cotton, D., and Taylor, M. (2009). Controlled cooling of aluminium smelting cell sidewalls using heat exchangers supplied with air. In *TMS Annual Meeting*, pages 317–322.

Nayyar, M. L. (1999). *Piping Handbook*. McGraw-Hill, London, 7th edition.

Nguyen, T.-V. and Elmegaard, B. (2016). Assessment of thermodynamic models for the design, analysis and optimisation of gas liquefaction systems. *Applied Energy*, 183:43 – 60.

Nicholls, M. G. (1997). Developing an integrated model of an aluminium smelter incorporating sub-models with different time bases and levels of aggregation. *European Journal of Operational Research*, 99(2):477 – 490.

Nieto, R. (2015). *Thermodynamics for Chemical Engineers [Termodinámica para Ingenieros Químicos]*. Universidad Politécnica de Madrid, Madrid, 2nd ed. edition.

Norðurál (2019). *Norðurál*. Available from: https://nordural.is/en/. [Accessed: 10 July 2019].

Nuytten, T., Claessens, B., Paredis, K., Bael, J. V., and Six, D. (2013). Flexibility of a combined heat and power system with thermal energy storage for district heating. *Applied Energy*, 104:583 – 591.

Pacheco, F., Refaat, H., and Pescosolido, D. (2012). Power management system in an industrial plant. In *2012 Petroleum and Chemical Industry Conference (PCIC)*, pages 1–7.

Papaefthymiou, G., Haesen, E., and Sach, T. (2018). Power system flexibility tracker: Indicators to track flexibility progress towards high-RES systems. *Renewable Energy*, 127:1026 – 1035.

Parizad, A., Khoshkhoo, H., Dehghan, S., and Moradtalab, R. (2017). An intelligent load and generation shedding procedure in an islanded network using a smart power management system. In *2017 Smart Grid Conference (SGC)*, pages 1–12.

Pavić, I., Capuder, T., and Kuzle, I. (2016). Low carbon technologies as providers of operational flexibility in future power systems. *Applied Energy*, 168:724 – 738.

Perry, R. H. and Green, D. W. (2008). *Perry's Chemical Engineers' Handbook*. McGraw-Hill, New York, 8th edition.

Peterson, R. D. and Wang, X. (2016). The influence of dissolved metals in cryolitic melts on hall cell current inefficiency. In *Essential Readings in Light Metals: Volume 2 Aluminum Reduction Technology*, pages 181–187. Springer International Publishing, Cham. Switzerland.

Peyneau, J.-M., Fiot, L., Mermet-Guyenet, S., and Rebouillat, O. (2016). *Low Power Operation at Aluminium Dunkerque Smelter*, pages 635–639. Springer International Publishing, Cham. Switzerland.

Phelan, M. (2018). Why grid resilience is moving behind the meter. Available from: https://www.decentralized-energy.com/articles/2018/07/why-grid-resilience-is-moving-behind-the-meter.html. [Accessed: 30 July 2019].

Pietrzyk, S. (2008). Anodic overvoltage on inert anodes in cryolite-alumina melts. *World of Metallurgy - ERZMETALL*, 61(5):308–313.

Poling, B. E. (2007). *The Properties of Gases and Liquids*. Boston: McGraw-Hill, 5th international edition.

Pospíšil, J., Charvát, P., Arsenyeva, O., Klimeš, L., Špiláček, M., and Klemeš, J. J. (2019). Energy demand of liquefaction and regasification of natural gas and the potential of LNG for operative thermal energy storage. *Renewable and Sustainable Energy Reviews*, 99:1 – 15.

Qadir, A., Sharma, M., Parvareh, F., Khalilpour, R., and Abbas, A. (2015). Flexible dynamic operation of solar-integrated power plant with solvent based Post-combustion Carbon Capture (PCC) process. *Energy Conversion and Management*, 97:7–19.

Qyyum, M. A., Long, N. V. D., Minh, L. Q., and Lee, M. (2018a). Design optimization of single mixed refrigerant lng process using a hybrid modified coordinate descent algorithm. *Cryogenics*, 89:131 – 140.

Qyyum, M. A., Qadeer, K., and Lee, M. (2018b). Comprehensive review of the design optimization of natural gas liquefaction processes: Current status and perspectives. *Industrial & Engineering Chemistry Research*, 57(17):5819–5844.

Raghami, A., Ameli, M. T., and Hamzeh, M. (2013). Primary and secondary frequency control in an autonomous microgrid supported by a load-shedding strategy. In *4th Annual International Power Electronics, Drive Systems and Technologies Conference*, pages 282–287.

Ravikumar, K. G., Alghamdi, T., Bugshan, J., Manson, S., and Raghupathula, S. K. (2015). Complete power management system for an industrial refinery. In *2015 IEEE Petroleum and Chemical Industry Committee Conference* (*PCIC*), pages 1–9.

Rye, K., Thonstad, J., and Liu, X. (2013). Heat transfer, thermal conductivity, and emissivity of Hall-Heroult top crust. *Essential Readings in Light Metals*, 2:630–638.

Saidur, R. (2010). A review on electrical motors energy use and energy savings. *Renewable and Sustainable Energy Reviews*, 14(3):877 – 898.

Schlafer, D., Mauss, M., Rauls, M., and Baumann, D. (2000). *Purification of caustic soda*. US 6113657 (Patent).

Sen, S. and Kumar, V. (2018). Microgrid control: A comprehensive survey. *Annual Reviews in Control*, 45:118 – 151.

Serth, R. W. and Lestina, T. G. (2014). Heat Exchangers. In Serth, R. W. and Lestina, T. G., editors, *Process Heat Transfer. Principles, Applications and Rules of Thumb*, chapter 3, pages 67 – 100. Academic Press, Boston, second edition.

Severo, D. S. and Gusberti, V. (2016). A modelling approach to estimate bath and metal heat transfer coefficients. In Bearne, G., Dupuis, M., and Tarcy, G., editors, *Essential Readings in Light Metals: Volume 2 Aluminum Reduction Technology*, pages 309–314, Cham. Switzerland. Springer International Publishing.

Shafie-Khah, M., Siano, P., Aghaei, J., Masoum, M. A. S., Li, F., and Catalão, J. P. S. (2019). Comprehensive review of the recent advances in industrial and commercial DR. *IEEE Transactions on Industrial Informatics*, 15(7):3757–3771.

Shi, J., Cui, P., Wen, F., Guo, L., and Xue, Y. (2017). Economic operation of industrial microgrids with multiple kinds of flexible loads. In *2017 IEEE Innovative Smart Grid Technologies - Asia* (*ISGT-Asia*), pages 1–6.

Shoreh, M. H., Siano, P., Shafie-Khah, M., Loia, V., and Catalão, J. P. (2016). A survey of industrial applications of demand response. *Electric Power Systems Research*, 141:31 – 49.

Short, J., Infield, D., and Freris, L. (2007). Stabilization of grid frequency through dynamic demand control. *IEEE Transactions on Power Systems*, 22(3):1284–1293.

Siano, P. (2014). Demand response and smart grids — A survey. *Renewable and Sustainable Energy Reviews*, 30:461 – 478.

Siemens AG (2018). SIMATIC Energy Management. Available from: https://www.automation.siemens.com/salesmaterial-as/ebook/simatic-energymanagement-en.pdf. [Accessed: 10 July 2019].

Skybakmoen, E., Solheim, A., and Sterten, Å. (1997). Alumina solubility in molten salt systems of interest for aluminum electrolysis and related phase diagram data. *Metallurgical and Materials Transactions B*, 28(1):81–86.

Stephenson, G. (2011). Integrate compressor performance maps into process simulation. *Chemical Engineering Progress*, 107(6):42–47.

Sterten, Å. and Solli, P. A. (1996). An electrochemical current efficiency model for aluminium electrolysis cells. *Journal of Applied Electrochemistry*, 26(2):187–193.

Stockmann, R., Forg, W., Bolt, M., Steinbauer, M., Pfeiffer, C., Paurola, P., Fredheim, A. O., and Sorensen, O. (2001). *Method for liquefying a stream rich in hydrocarbons*. US 6,253,574 B1 (Patent).

Strbac, G. (2008). Demand side management: Benefits and challenges. *Energy Policy*, 36(12):4419 – 4426.

Swaney, R. E. and Grossmann, I. E. (1985). An index for operational flexibility in chemical process design. Part I: Formulation and theory. *AIChE Journal*, 31(4):621–630.

Tingaev, P. (2013). The effect of calcium fluoride on alumina solubility in low temperature cryolite melts. *TMS Light Metals*, pages 685–688.

Todd, D., Caufield, M., Helms, B., Starke, M. R., Kirby, B. J., and Kueck, J. D. (2009). *Providing Reliability Services through Demand Response: A Preliminary Evaluation of the Demand Response Capabilities of Alcoa Inc.* Technical report, United States Department of Energy.

Ton, D. T. and Smith, M. A. (2012). The US department of energy's microgrid initiative. *The Electricity Journal*, 25(8):84–94.

Trianni, A., Cagno, E., and Accordini, D. (2019). A review of energy efficiency measures within electric motors systems. *Energy Procedia*, 158:3346 – 3351.

Trimet Aluminium SE (2019). *The aluminium smelter as "virtual battery"*. Available from: https://www.trimet.eu/en/ueber_trimet/energiewende/virtuelle-batterie. [Accessed: 15-September-2019].

UC Rusal (2016). How Aluminium Is Produced. Available from: https://www.aluminiumleader.com/production/how_aluminium_is_produced/. [Accessed: 15 July 2019].

van der Wal, O., Haugen, T., Holsten, P. E., and Lems, F. (2005). Not on my watch. How ABB's power management system prevents multi million dollar shutdowns. *ABB Review*. Issue 3/2005, pages 31-35.

van der Wijk, P. C., Brouwer, A. S., van den Broek, M., Slot, T., Stienstra, G., van der Veen, W., and Faaij, A. P. (2014). Benefits of coal-fired power generation with flexible CCS in a future northwest european power system with large scale wind power. *International Journal of Greenhouse Gas Control*, 28:216 – 233.

Vidal, J. A., Pheney, T. S., and McHugh, M. (2003). *Thermodynamics : Applications in Chemical Engineering and the Petroleum Industry*. Paris: Technip.

Wang, H., Yin, W., Abdollahi, E., Lahdelma, R., and Jiao, W. (2015). Modelling and optimization of CHP based district heating system with renewable energy production and energy storage. *Applied Energy*, 159:401 – 421.

Wang, W. and Lu, Z. (2013). Cyber security in the Smart Grid: Survey and challenges. *Computer Networks*, 57(5):1344–1371.

Watson, H. and Barton, P. (2016). Simulation and design methods for multiphase multistream heat exchangers. *IFAC - Papers OnLine*, 49:839–844.

Watson, H. A. and Barton, P. I. (2017). Modeling phase changes in multistream heat exchangers. *International Journal of Heat and Mass Transfer*, 105:207 – 219.

Watson, H. A., Vikse, M., Gundersen, T., and Barton, P. I. (2018). Optimization of single mixed-refrigerant natural gas liquefaction processes described by nondifferentiable models. *Energy*, 150:860 – 876.

Wetenhall, B., Race, J., Aghajani, H., Fernandez, E., Naylor, M., Lucquiaud, M., and Chalmers, H. (2017). Considerations in the development of flexible CCS networks. In *Energy Procedia*, volume 114, pages 6800–6812.

Wijayaratne, H., Hyland, M., McIntosh, G., Perander, L., and Metson, J. (2018). Balancing sodium impurities in alumina for improved properties. *Metallurgical and Materials Transactions.*, 49(5):2809–2820.

Wissner, M. (2011). The Smart Grid – A saucerful of secrets? *Applied Energy*, 88(7):2509 – 2518.

Xuan, Y. Y., Pretlove, J., and Thornhill, N. F. (2018). Assessment of flexible operation in an LNG plant. In *3rd IFAC Workshop on Automatic Control in Offshore Oil and Gas Production,* Esbjerg, Denmark, May 30 - June 01, 2018, volume 51(8), pages 158–163. Elsevier.

Yao, M., Hu, Z., Sifuentes, F., and Zhang, N. (2015a). Integrated power management of conventional units and industrial loads in China's ancillary services scheduling. *Energies.*, 8(5):3955–3977.

Yao, M., Hu, Z., Zhang, N., Duan, W., and Zhang, J. (2015b). Low-carbon benefits analysis of energy-intensive industrial demand response resources for ancillary services. *Journal of Modern Power Systems and Clean Energy*, 3(1):131–138.

Yu, M., Lu, R., and Hong, S. H. (2016). A real-time decision model for industrial load management in a smart grid. *Applied Energy*, 183:1488 – 1497.

Zhang, X. and Hug, G. (2014). Optimal regulation provision by aluminum smelters. In *2014 IEEE PES General Meeting Conference Exposition*, pages 1–5.

Zhao, H., Wu, Q., Hu, S., Xu, H., and Rasmussen, C. N. (2015). Review of energy storage system for wind power integration support. *Applied Energy*, 137:545 – 553.

Zhao, W., Yang, J., Hu, Z., and Wei, Y. (2011). Recent developments on the hydrodynamics of floating liquid natural gas (FLNG). *Ocean Engineering*, 38(14-15):1555–1567.

Zhou, L., Li, J., Li, F., Meng, Q., Li, J., and Xu, X. (2016). Energy consumption model and energy efficiency of machine tools: a comprehensive literature review. *Journal of Cleaner Production*, 112:3721 – 3734.

Zhu, S., Luo, P., Yang, Y., Lu, Q., and Chen, Q. (2017). Optimal dispatch for grid-connecting microgrid considering shiftable and adjustable loads. In *Proceedings IECON 2017 - 43rd Annual Conference of the IEEE Industrial Electronics Society*, volume 2017-January, pages 5575–5580.

Part V

Appendices

Appendix A

Thermodynamic Tables

The tables in this appendix give the thermodynamic parameters of the components present in the Liquefied Natural Gas (LNG) process. Tables A.3 and A.4 give the parameters for calculating the Wilson equations:

$$\ln(\Lambda_{ij}) = W_{ij}^{\mathrm{A}} + \frac{W_{ij}^{\mathrm{B}}}{T}$$

Tables A.5 and A.6 give the values for calculating the heat capacity as a function of the temperature:

$$c_{p,i}(T) = c_{p,i}^{\mathrm{A}} + c_{p,i}^{\mathrm{B}} T + c_{p,i}^{\mathrm{C}} \frac{T^2}{2} + c_{p,i}^{\mathrm{D}} \frac{T^3}{3} + c_{p,i}^{\mathrm{E}} \frac{T^4}{4} + c_{p,i}^{\mathrm{F}} \frac{T^5}{5}$$

$$\hat{c_p}(T) = \sum_{i}^{C} y_i c_{p,i}(T)$$

Table A.1: Critical temperature, critical pressure, and acentric factor for the components present in the LNG process

	Methane	Ethane	Propane	Butane	Pentane	Hexane	Heptane	Octane	Ethylene	Benzene	Nitrogen
T_c (K)	190.6	305.4	369.8	425.2	469.6	507.4	540.2	568.8	282.4	562.1	126.2
P_c (bar)	45.4	48.2	41.9	37.5	33.3	29.3	27	24.5	49.7	48.3	33.5
ω	0.008	0.098	0.152	0.193	0.251	0.296	0.351	0.394	0.085	0.212	0.04

Table A.2: Binary interaction parameters for the components present in the LNG process

$\times 10^{-3}$	Methane	Ethane	Propane	Butane	Pentane	Hexane	Heptane	Octane	Ethylene	Benzene	Nitrogen
Methane	0	0.422	24.151	22.644	15.811	22.073	-6.51	95.823	17.405	31.339	1912.042
Ethane	0.422	0	1.695	5.322	14.253	-43.36	18.005	-154.97	3.211	36.223	2626.211
Propane	24.151	1.695	0	-2.08	-4.33	3.052	36.109	5.3	-7.2	19.558	1544.264
Butane	22.644	5.322	-2.08	0	38.188	12.447	-6.9	41.64	144.538	9.9	1166.696
Pentane	15.811	14.253	-4.33	38.188	0	-0.97	15.871	-2.29	-74.38	22.415	1015.702
Hexane	22.073	-43.36	3.052	12.447	-0.97	0	2.107	7.492	-95.88	14.592	925.28
Heptane	-6.51	18.005	36.109	-6.9	15.871	2.107	0	-0.39	16.45	7.088	863.906
Octane	95.823	-154.97	5.3	4.164	-2.29	7.492	-0.39	0	-131.07	-2.85	820.549
Ethylene	17.405	3.211	-7.2	144.538	-74.38	-95.88	16.45	-131.07	0	28.355	2485.883
Benzene	31.339	36.223	19.558	9.9	22.415	14.592	7.088	-2.85	28.355	0	541.602
Nitrogen	1912.042	2626.211	1544.264	1166.696	1015.702	925.28	863.906	820.549	2485.883	541.602	0

Table A.3: $WA_{i,j}$ parameters for calculating the Wilson interaction parameter for the components present in the LNG process

	Methane	Ethane	Propane	Butane	Pentane	Hexane	Heptane	Octane	Ethylene	Benzene	Nitrogen
Methane	0	0	0	0	0	0	0	0	0	0	0
Ethane	0	0	0	0	0	0	0	0	0	0	0
Propane	0	0	0	0	0	0	0	0	0	0	0
Butane	0	0	0	0	0	0	0	0	0	0	0
Pentane	0	0	0	0	0	0	0	0	0	0	0
Hexane	0	0	0	0	0	0	0	1.0178	0	1.293	0
Heptane	0	0	0	0	0	0	0	0.5957	0	0	0
Octane	0	0	0	0	0	0.3288	0.2943	0	0	6.6159	0
Ethylene	0	0	0	0	0	0	0	0	0	0	0
Benzene	0	0	0	0	0	-0.1694	0	-2.0184	0	0	0
Nitrogen	0	0	0	0	0	0	0	0	0	0	0

Table A.4: $WB_{i,j}$ parameters for calculating the Wilson interaction parameter for the components present in the LNG process

	Methane	Ethane	Propane	Butane	Pentane	Hexane	Heptane	Octane	Ethylene	Benzene	Nitrogen
Methane	0	-328.516	-678.347	-1126.39	-1763.82	-2735.71	-4255.32	-6638.67	70.20263	214.4182	-42.726
Ethane	233.3427	0	-197.027	-399.174	-621.658	-879.731	-1192.84	-1587.79	-35.078	69.51568	332.8954
Propane	372.7099	158.0687	0	-147.555	-295.578	-450.943	-619.621	-808.038	-83.6681	-25.3408	477.0854
Butane	487.0566	267.3436	124.5198	0	-332.639	56.7867	-355.879	-482.531	176.9358	110.2054	610.7786
Pentane	595.9291	354.2429	216.1142	185.5863	0	157.0057	-195.908	-294.728	322.3934	-164.641	749.9415
Hexane	708.052	429.9996	290.0044	-52.1115	-177.524	0	54.7213	-165.574	419.7427	-648.209	897.0494
Heptane	825.6382	500.6356	353.5563	246.9737	157.3463	-48.226	0	-62.0158	504.0318	-339.785	1050.356
Octane	947.9277	569.8721	410.9342	303.02	215.6567	-255.819	-308.25	0	584.7198	-2677.55	1208.397
Ethylene	-138.23	-20.0714	49.78563	-231.5353	-538.735	-848.026	-1218.18	-1694.7	0	158.3332	-98.3335
Benzene	-352.708	-234.692	-147.654	-335.478	-40.2153	75.2621	132.7497	864.7643	-283.119	0	-126.388
Nitrogen	45.09756	-560.686	-1079.53	-1871.56	-3208.01	-5525.57	-9555.15	-16588.3	101.75	194.1133	0

Table A.5: c_p vapour for the components present in the LNG process

	A	B	C	D	E	F
Methane	32.454	0.016143	-6.1860E-05	-4.4229E-07	3.2418E-09	-4.2384E-12
Ethane	37.35	0.1812	-1.7006E-03	6.6188E-06	-8.8153E-09	2.8430E-12
Propane	46.89	0.3391	-3.3146E-03	1.3851E-05	-2.1974E-08	1.1395E-11
Butane	63.715	0.4442	-4.3568E-03	1.8314E-05	-2.9421E-08	1.5634E-11
Pentane	58.584	0.8648	-9.4218E-03	4.5762E-05	-9.3104E-08	6.9502E-11
Hexane	68.619	1.0361	-1.1117E-02	5.3053E-05	-1.0564E-07	7.6914E-11
Heptane	78.201	1.2205	-1.3167E-02	6.3241E-05	-1.2693E-07	9.3234E-11
Octane	87.862	1.4007	-1.5275E-02	7.4268E-05	-1.5122E-07	1.1288E-10
Ethylene	24.818	0.25319	-2.7803E-03	1.3615E-05	-2.7934E-08	2.1087E-11
Benzene	29.956	0.72987	-7.7953E-03	3.6924E-05	-7.2509E-08	5.1935E-11
Nitrogen	29.115	-2.5075E-04	2.1808E-06	-7.1478E-09	-3.7303E-14	3.4588E-14

Table A.6: c_p liquid parameters of the components present in the LNG process

	A	B	C	D	E	F
Methane	-7377.7	288.85	-4.4657	3.4329E-02	-1.3118E-04	1.9977E-07
Ethane	-1321.8	42.663	-5.0675E-01	2.9283E-03	-8.2435E-06	9.1071E-09
Propane	-275.73	10.846	-1.1925E-01	6.2514E-04	-1.5745E-06	1.5551E-09
Butane	23.4170	2.7538	-2.7527E-02	1.2738E-04	-2.7735E-07	2.4417E-10
Pentane	20.2550	3.2525	-3.1318E-02	1.3875E-04	-2.8373E-07	2.2764E-10
Hexane	57.3770	2.6073	-2.8273E-02	1.3985E-04	-3.0849E-07	2.5885E-10
Heptane	102.93	2.0224	-2.1573E-02	1.0425E-04	-2.2011E-07	1.7572E-10
Octane	235.15	-0.5947	4.1593E-03	-1.3744E-05	3.3047E-08	-3.0531E-11
Ethylene	-1701.1	56.486	-0.7031	4.2711E-03	-1.2688E-05	1.4838E-08
Benzene	101.43	0.2737	-3.3079E-03	1.6349E-05	-2.9215E-08	1.9585E-11
Nitrogen	-415400	19639	-371.44	351.40E-02	-1.6630E-02	3.1503E-05

Appendix B

Cleaner Energy Integration

As power system are moving towards a decarbonized future, its market is changing accordingly to this path. In Europe, the 20-20-20 directives set for 2020 are being accomplished, but there is still more goals to be achieved as mentioned in European Commission (2018). Thus, the amount of emerging Renewable Energy Sources (RES) is gradually increasing, while the fossil fuel sources share is decreasing. Whilst this sets the first steps towards the decarbonization, electrical power generation by RESs have the problem of not being as flexible as the power generation by fossil fuels. During this project, the term flexibility appears several times, and it refers to the capacity of a system to change its power or energy consumption without being put at risk. Thus, saying that the power generation by RESs is not that flexible, it means that the generation of electrical power by RESs is not as reliable as the one by fossil fuels. The reason for this is the availability of the resources generating the power. For instance, wind power generation might not be available when the power consumed by end-users is at its peak, whereas, a coal power generation has available fuel to be burnt.

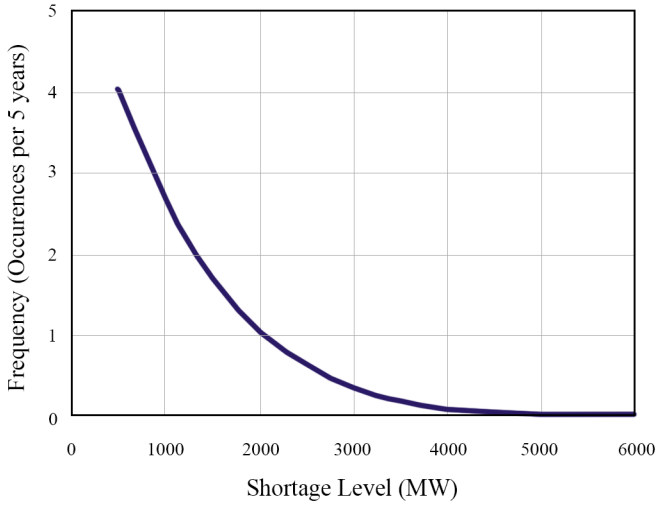


Figure B.1: Expected frequency and the respective magnitude of shortages in the UK during 1998 and 2003. The picture is extracted from Strbac (2008).

Due to the oscillating power generation caused by RESs, adopting a microgrid arrangement can help the power grid to handle the variation in the power generated. An example of this can be seen in the report by Denholm et al. (2015), where microgrids are used for the accommodation of a new photovoltaic plant. The study concluded that the flexibility provided by microgrids is a new concern to be addressed in order to alleviate the problems that the solar power could bring, but ultimately, microgrids and grid flexibility could accommodate the photovoltaic plant even if its implementation entailed an excess of 25% . Thus, inside-the-site arrangements also contributes to the integration of RESs. Additionally, Smart-Grid is an appropriate tool for dealing with these power fluctuation issues (Gangale F. and Vasiljevska J. and Covrig F. and Mengolini A. and Fulli G., 2017). With the information exchange is easier to alleviate the problems that can arise from the RES power generation, and furthermore, DSM also helps to balance the power grid as long as the power oscillations are predicted beforehand. This last sentence is a crucial element in this project; electrical failures are not usually predicted, but the average number of power failures is measured and the capacity of the plants is increased according to that number. For instance, a study made by Strbac (2008) estimated that, in the UK during the 5 years that the study took into account, the frequency of undergoing a shortage of 500MW was around 4 times. That tendency grows larger with curtailments of lower magnitudes, as seen in Figure B.1.

In this project, instead of installing a larger capacity on the generation plants, industrial plants are the ones dealing with the electrical contingencies, so that they both prevent the generation plants to increase their capacity, and deal with the fluctuations caused by the RES power generation.

The last two paragraphs have introduced two drivers for arranging an industrial plant with an inside-the-site structure, which are economic reasons and RES integration reasons. Nevertheless, the most important motive for this project, and in some cases for the process itself, is ensuring that the power is securely delivered from the power station to the process plant.

Appendix C

Flexible Operation in an LNG plant

This appendix shows additional information and calculations regarding the Liquefied Natural Gas process for a deeper understanding of the model.

C.1 Analysis of the Degrees of Freedom

The following tables shows the analysis of degrees of freedom. Each table shows the analysis for each equipment, and they do not include new variables introduced in previous tables. For instance, Table C.2 does not introduce the temperature at the inlet stream as a new variable, because it was already introduced in Table C.1.

Table C.1: Analysis of the Degrees of Freedom in the Precooling Heat Exchanger

Equation	Number	New Variables	Number	Notes
$F_{P1}h_{P1} - F_{P4}h_{P4} = F_{NG2}h_{NG2} - F_{NG1}h_{NG1} + F_{S2}h_{S2} - F_{S1}h_{S1} + F_{L2}h_{L2} - F_{L1}h_{L1}$	1	F_{P1} F_{P4} h_{P1} h_{P4} F_{L1} F_{L2} h_{L1} h_{L2} F_{S1} F_{S2} h_{S1} h_{S2} F_{NG1} F_{NG2} h_{NG1} h_{NG2}	16	
$h_i = h(T_i, P_i, z_i)$ $i = NG1, NG2, P1, P4, L1, L2, S1, S2$	8	T_i P_i z_i $i = NG1, NG2, P1, P4, L1, L2, S1, S2$	24	
$z_{NG1} = z_{NG2}$ $F_{NG1} = F_{NG2}$ $z_{P1} = z_{P2}$ $F_{P1} = F_{P2}$ $z_{P3} = z_{P4}$ $F_{P3} = F_{P4}$ $z_{L1} = z_{L2}$ $F_{L1} = F_{L2}$ $z_{S1} = z_{S2}$ $F_{S1} = F_{S2}$	10	z_{P2} F_{P2} z_{P3} F_{P3}	4	No mass exchange
$P_{NG1} = P_{NG2}$ $P_{P1} = P_{P2}$ $P_{P4} = P_{P3}$ $P_{L1} = P_{L2}$ $P_{S1} = P_{S2}$	5	P_{P2} P_{P3}	2	
Total	24		46	

Table C.2: Analysis of the Degrees of Freedom in the Natural Gas Flash Separator

Equation	Number	New Variables	Number	Notes
$F_{NG2} = F_{NG3} + F_{NG4}$	1	F_{NG3} F_{NG4}	2	
$F_{NG3} = \psi_{NG2} F_{NG2}$	1	ψ_{NG2}	1	
$\psi_{NG2} = f(T_{NG2}, P_{NG2}, z_{NG2})$	1	-	0	

Table C.2 Continued

$P_{NG2} = P_{NG3}$ $P_{NG2} = P_{NG4}$ $T_{NG2} = T_{NG3}$ $T_{NG2} = T_{NG4}$	4	P_{NG3} P_{NG4} T_{NG3} T_{NG4}	4
$z_{NG3} = f(T_{NG2}, P_{NG2})$ $z_{NG4} = f(T_{NG2}, P_{NG2})$	2	z_{NG3} z_{NG4}	2
$h_{NG3} = h(T_{NG3}, P_{NG3}, z_{NG3})$ $h_{NG4} = h(T_{NG4}, P_{NG4}, z_{NG4})$	2	h_{NG3} h_{NG4}	2
Total	11		11

Table C.3: Analysis of the Degrees of Freedom in the Liquefying Heat Exchanger

Equation	Number	New Variables	Number	Notes
$F_{L2}h_{L2} - F_{L5}h_{L5} = F_{NG5}h_{NG5} -$ $F_{NG3}h_{NG3} + F_{S3}h_{S3} - F_{S2}h_{S2}$	1	h_{NG5} F_{NG5} h_{S3} F_{S3} h_{L5} F_{L5}	6	
$h_{NG5} = h(T_{NG5}, P_{NG5}, z_{NG5})$ $h_{S3} = h(T_{S3}, P_{S3}, z_{S3})$ $h_{L5} = h(T_{L5}, P_{L5}, z_{L5})$	3	T_{NG5} P_{NG5} z_{NG5} T_{S3} P_{S3} z_{S3} T_{L5} P_{L5} z_{L5}	9	
$z_{NG3} = z_{NG5}$ $F_{NG3} = F_{NG5}$ $z_{S2} = z_{S3}$ $F_{S2} = F_{S3}$ $z_{L2} = z_{L3}$ $F_{L2} = F_{L3}$ $z_{L5} = z_{L4}$ $F_{L5} = F_{L4}$	8	z_{L3} z_{L4} F_{L3} F_{L4}	4	No mass exchange
$P_{NG3} = P_{NG5}$ $P_{S2} = P_{S3}$ $P_{L2} = P_{L3}$ $P_{L5} = P_{L4}$	4	P_{L3} P_{L4}	2	
Total	16		21	

Table C.4: Analysis of the Degrees of Freedom in the Subcooling Heat Exchanger

Equation	Number	New Variables	Number	Notes
$F_{S3}h_{S3} - F_{S6}h_{S6} = F_{NG6}h_{NG6} - F_{NG5}h_{NG5}$	1	h_{NG6} F_{NG6} h_{S6} F_{S6}	4	
$h_{NG6} = h(T_{NG6}, P_{NG6}, z_{NG6})$ $h_{S6} = h(T_{S6}, P_{S6}, z_{S6})$	2	T_{NG6} P_{NG6} z_{NG6} T_{S6} P_{S6} z_{S6}	6	
$z_{NG5} = z_{NG6}$ $F_{NG5} = F_{NG6}$ $z_{S3} = z_{S4}$ $F_{S3} = F_{S4}$ $z_{S6} = z_{S5}$ $F_{S6} = F_{S5}$	6	z_{S4} z_{S5} F_{S4} F_{S5}	4	No mass exchange
$P_{NG5} = P_{NG6}$ $P_{S3} = P_{S4}$ $P_{S6} = P_{S5}$	3	P_{S4} P_{S5}	2	
Total	12		16	

Table C.5: Analysis of the Degrees of Freedom of the Refrigerant Expansion Valves (V1, V2, and V3)

Equation	Number	New Variables	Number	Notes
$F_{P2} = F_{P3}$ $z_{P2} = z_{P3}$ $F_{L3} = F_{L4}$ $z_{L3} = z_{L4}$ $F_{S4} = F_{S5}$ $z_{S5} = z_{S4}$	6			No mass exchange
$h_{P2} = h_{P3}$ $h_{L3} = h_{L4}$ $h_{S4} = h_{S5}$	3	h_{P2} h_{P3} h_{L3} h_{L4} h_{S4} h_{S5}	6	Isenthalpic valves
$h_{P2} = h(T_{P2}, P_{P2}, z_{P2})$ $h_{L3} = h(T_{L3}, P_{L3}, z_{L3})$ $h_{S4} = h(T_{S4}, P_{S4}, z_{S4})$	3	T_{P2} T_{L3} T_{S4}	3	
$T_{P3} = f(h_{P3}, P_{P3}, z_{P3})$ $T_{L4} = f(h_{L4}, P_{L4}, z_{L4})$ $T_{S5} = f(h_{S5}, P_{S5}, z_{S5})$	3	T_{P3} T_{L4} T_{S5}	3	Calculated via iterations
Total	15		12	

Table C.6: Analysis of the Degrees of Freedom of the Precooling Compressor (Comp1)

Equation	Number	New Variables	Number	Notes
$F_{P4} = F_{P5}$	1	F_{P5}	1	Mass Balance
$z_{P4} = z_{P5}$ $z_{P5} = z_{P1}$	2	z_{P5}	1	Mass Balance
$P_{P5} = P_{P1}$	1	P_{P5}	1	
$h_{P5} = h(T_{P4}, P_{P4}, P_{P5}, z_{P4}, \eta_{Comp1})$	1	h_{P5} η_{Comp1}	2	
$T_{P5} = f(h_{P5}, P_{P5})$	1	T_{P5}	1	Temperatures are calculated via iterations
$W_{Comp1} = F_{P4}(h_{P5} - h_{P4})$	1	W_{Comp1}	1	
Total	7		7	

Table C.7: Analysis of the Degrees of Freedom of the Liquefying Compressor (Comp2)

Equation	Number	New Variables	Number	Notes
$F_{L5} = F_{L6}$	1	F_{L6}	1	Mass Balance
$z_{L5} = z_{L6}$ $z_{L6} = z_{L1}$	2	z_{L6}	1	Mass Balance
$P_{L6} = P_{L1}$	1	P_{L6}	1	
$h_{L6} = h(T_{L5}, P_{L5}, P_{L6}, z_{L5}, \eta_{Comp2})$	1	h_{L6} η_{Comp2}	2	
$T_{L6} = f(h_{L6}, P_{L6})$	1	T_{L6}	1	Temperatures are calculated via iterations
$W_{Comp2} = F_{L5}(h_{L6} - h_{L5})$	1	W_{Comp2}	1	
Total	7		7	

Table C.8: Analysis of the Degrees of Freedom of the Subcooling Compressor (Comp3)

Equation	Number	New Variables	Number	Notes
$F_{S6} = F_{S7}$	1	F_{S7}	1	Mass Balance
$z_{S6} = z_{S7}$ $z_{S7} = z_{S1}$	2	z_{S7}	1	Mass Balance
$P_{S7} = P_{S1}$	1	P_{S7}	1	
$h_{S7} = h(T_{S6}, P_{S6}, P_{S7}, z_{S6}, \eta_{Comp3})$	1	h_{S7} η_{Comp3}	2	
$T_{S7} = f(h_{S7}, P_{S7})$	1	T_{S7}	1	Temperatures are calculated via iterations
$W_{Comp3} = F_{S6}(h_{S7} - h_{S6})$	1	W_{Comp3}	1	
Total	7		7	

Table C.9: Analysis of the Degrees of Freedom of the Refrigerant Sea Coolers (C1, C2, and C3)

Equation	Number	New Variables	Number	Notes
$H_{Sea} = (F_{P5}h_{P5} - F_{P1}h_{P1}) + (F_{L6}h_{L6} - F_{L1}h_{L1}) + (F_{S7}h_{S7} - F_{S1}h_{S1})$	1	H_{Sea}	1	
Total	1		1	

Table C.10: Analysis of the Degrees of Freedom of the LNG Process

Equipment	Number of Equations	Number of Variables	Difference

Table C.10 Continued

Precooling Heat Exchanger	24	46	22
Liquefying Heat Exchanger	16	21	5
Subcooling Heat Exchanger	12	16	4
Natural Gas Flash Separator	11	11	0
Refrigerant Expansions Valves	15	12	-3
Precooling Compressor	8	8	0
Liquefying Compressor	8	8	0
Subcooling Compressor	8	8	0
Sea Water Cooler	1	1	0
Total	103	131	28

C.2 Discussion of the Assumptions Made in the LNG Process

This section discusses the reasons for making the assumptions in Section 5.6. The assumptions were:

1. Except for NG2 and NG6, all temperatures are fixed during the course of a single simulation. They are, however, changed for different simulations.
2. The heat exchangers are assumed to be large enough for reaching the established temperatures. This means that the piping system within the heat exchangers is long enough, so that the necessary heat is completely transferred from the hot streams to the cold streams.
3. There is no pressure drop due to the piping system.
4. The pressures after the Joule-Thomson valves in the refrigerant cycles are fixed (streams P3, L4, and S5 in Figure 5.1).

5. The natural gas at the beginning of the liquefaction (NG1 in Figure 5.1) comes from a precious unit in the natural gas plant, so the natural gas pressure is assumed constant at 30 bar.

6. The dynamic behaviour of the process is not considered, so the model calculates only the operating points when the process is at its steady state.

The first assumption is close to the behaviour of real industries. The temperature is constant for avoiding damaging the piping system due to thermal stress.

The model makes the second assumption to meet the assumption of the fixed temperature. This assumption simplifies all the dynamics involved in the heat exchangers. Nevertheless, this assumption is sensible, considering that heat exchangers are designed in order to have a larger constant time (τ, in s). That means that the tubes within the heat exchangers are longer than the minimum length needed for reaching the set temperature (Incropera et al., 2011; Serth and Lestina, 2014). Thus, assumption number two is sensible as long as the heats that are being exchanged are not too large.

Assumption number three can be considered reasonable since the pressure drop in the real industry is not significant. Moreover, a slight variation in the pressure will barely modify the saturation points, and, typically, in order to have a substantial consequence on the saturation points, the pressure needs to be varied around 0.5 bars. In the case of presenting pressure drop, the pressure drop will hardly reach the 0.1 bars (Dickenson, 1997; Nayyar, 1999).

The fourth assumption facilitate calculations regarding the expansion valve, so even when the refrigerant flow rate varies when a contingency takes place, the outlet pressure of the valve remains the same. This assumption makes sense considering that a valve follows the following equation:

$$F = C_v \sqrt{P_{disc} - P_{suction}} \tag{C.1}$$

where C_v is the valve coefficient, and it depends on the type of valve, the valve size, and the valve position (how open it is). The spectre of variation of C_v is quite extensive, so if the flow rate is changed, C_v can be changed for being adapted to the new flow rate.

Assumption 5 is an extension of assumption 3, but considering that the natural gas comes from upstream, and therefore, the pressure is already given.

Assumption 6 needs a deeper insight which is elaborated in the following section.

C.3 Assumption on the Dynamics of the LNG Process

There are three items of equipment in the LNG process that characterise the transient response of the process variables, the compressors, the valves, and the heat exchanger.

- **Rotatory machinery and valves:** When the electrical power consumption decreased, the compressors are slowed down, providing less energy to the refrigerant. The difference in energy also manifests when the refrigerant is expanded in the valves. The variation of energies is not instantaneous, but the stored energy in the refrigerants will make the rotatory equipment to slow down until reaching the new operating point gradually.
- **Heat exchangers:** In the heat exchangers, the refrigerants absorb heat from the natural gas. If the enthalpy of the refrigerants gradually decreases, the heat absorbed by them reduced gradually. If the absorbed heat is not enough, the natural gas will come out as vapour, and the process is jeopardized. In order to avoid the lack of heat absorption, the process has to reduce the natural gas flow rate.

The issue is to observe whether the change of heat absorbed by the refrigerants can be offset by the change of natural gas flow rate, so the difference of both heats (absorbed by the refrigerants and released by the natural gas) does not raise the natural gas temperature to its saturation point.

Figure C.1 shows a notional example of the transient behaviour of the subcooling stream and the natural gas stream at the exit of the process. In the graphs, the enthalpy of stream S6 decreases because the compressor is slowed down at time t_{C-1}. During a short period of time, the subcooling refrigerant is not able to absorb the same amount of heat from the natural gas, and consequently, the temperature of the natural gas rises, causing its enthalpy to rise. When the natural gas controlling the inflow of natural gas closes at time t_{V-1}, the enthalpy of natural gas decreases. However, the temperature of the natural gas is still higher than its former value since its enthalpy is higher than the refrigerant enthalpy. The enthalpy of the refrigerant is stable when its compressor reaches the new operating point at time t_{C-2}, and the natural gas flow rate keeps decreasing until it both enthalpies are equal.

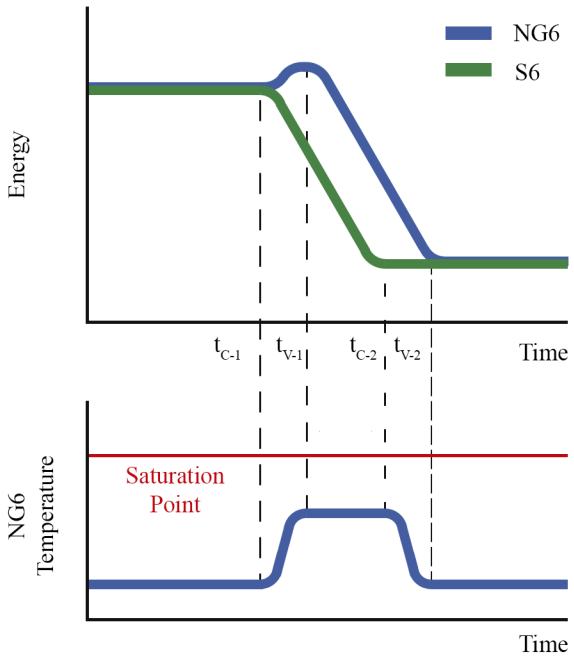


Figure C.1: Qualitative example of the natural gas valve controlling its flow rate and the subcooling compressor dynamic behaviour. In the upper graph the vertical axis is the total energy of the stream, and in the lower graph the vertical axis represents the temperature of NG6. In both cases, the horizontal axis represents the time. The red horizontal line in depicts the bubble point of the natural gas at a constant pressure. The stream names are referred to Figure 5.1

The issue is to know whether the rate of change of the natural gas flow rate can compensate for the decrease of heat absorption from the refrigerant. According to Fazlollahi et al. (2015) and He and Ju (2016), the stored energy in the refrigerants makes it possible that the LNG does not reach the saturation temperature. Another issue is to deal with the time response of the controllers. However, the PPM system can send the signals for reducing the consumption of the compressors and changing the set point simultaneously [1]. Thus, assumption number six is proved to be sensible.

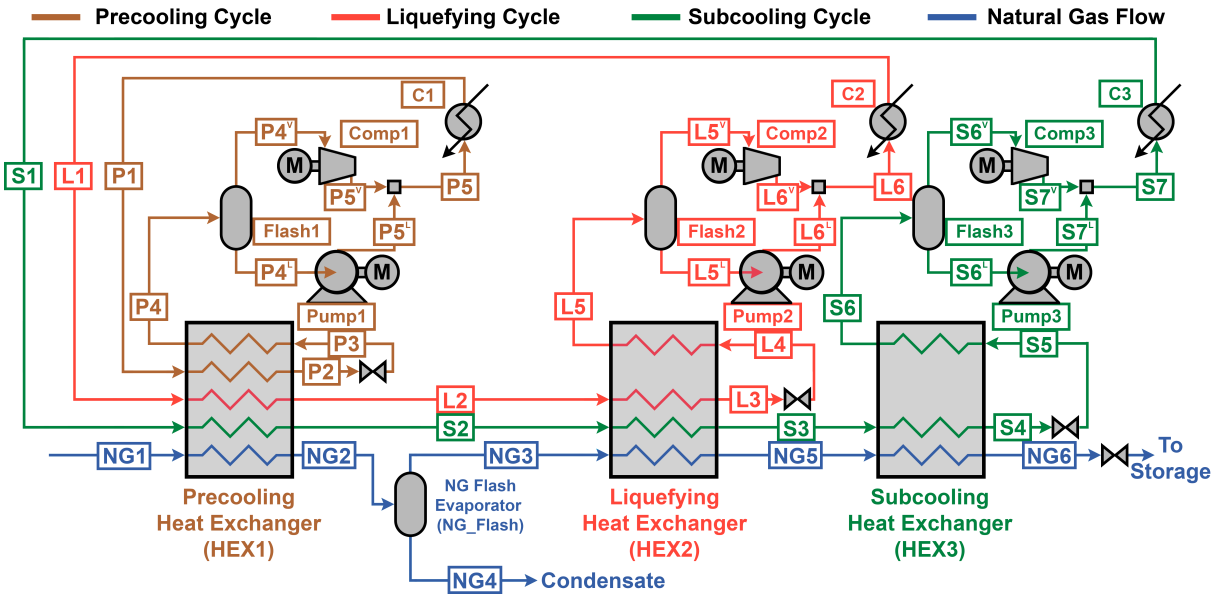


Figure C.2: Representation of the LNG process with flash drums and pumps after each heat exchanger.

C.4 Implementation of the Pumps

The LNG model included the Redlich-Kwong Soave (RKS) equations and the Rachford-Rice (RR) algorithm to calculate the thermodynamic properties in streams with one or two phases. The model assumes the temperatures at the exit of the heat exchangers to be constant. If the temperature of the refrigerants exiting their respective heat exchangers changes, their vapour fractions might change. The effects of changing these temperatures on the electrical power consumption can be observed using the RKS equations and the RR algorithm.

If these streams present a Vapour and Liquid Equilibrium (VLE), the model needs to implement a flash drum and a pump after each heat exchanger. Figure C.1 shows the LNG process with the pumps and flash drums.

This section analyses the effects of changing the temperatures of P4, L5, and S6 on the electrical power consumption. The analysis establishes the LNG production rate to 1 mol s^{-1}

C.4.1 Effects of the Temperature on the Flow Rate of the Refrigerant

Figure C.3 shows the effects on the precooling flow rate and the vapour fraction in P4 of varying the temperature of the precooling stream exiting HEX1 (P4). The results show that the flow rate steeply decreases when P4 has a VLE. The flow rate of the precooling refrigerant is calculated as:

$$F_{\text{Prec}} = \frac{F_{\text{NG1}}(h_{\text{NG2}} - h_{\text{NG1}}) + F_{\text{Sub}}(h_{\text{S2}} - h_{\text{S1}}) + F_{\text{Liq}}(h_{\text{L2}} - h_{\text{L1}})}{h_{\text{P1}} - h_{\text{P4}}} \tag{5.4}$$

Therefore, the precooling flow rate is inversely proportional to $h_{\text{P1}} - h_{\text{P4}}$. When P4 presents a VLE, the enthalpy is lower than when it is completely vapour. Therefore, the term $h_{\text{P1}} - h_{\text{P4}}$ increases when the temperature in P4 increases [2].

[1] Data provided by an engineer in ABB

[2] both terms h_{P1} and h_{P4} are negative

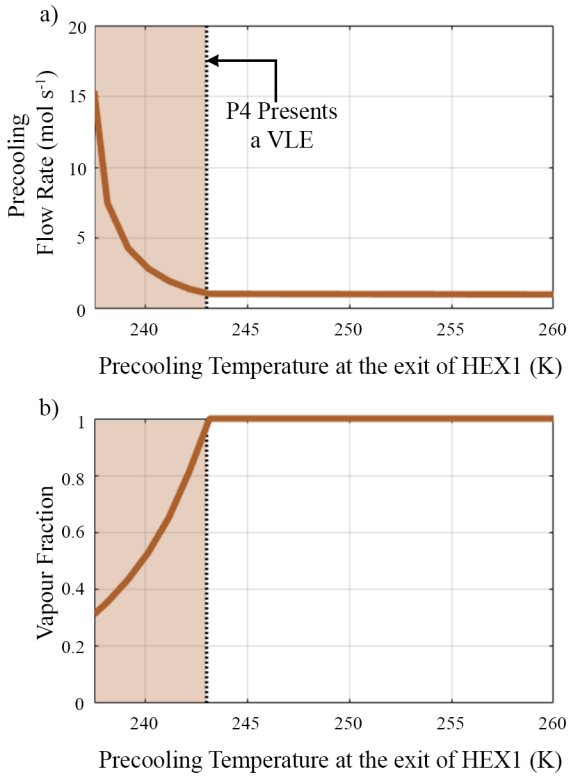


Figure C.3: Effects on the a) precooling flow rate (mol s^{-1}) and b) vapour fraction of varying the temperature of stream P4. The brown area represents the range in which P4 presents a VLE

Figure C.4 shows the effects on the liquefying flow rate and the vapour fraction in L5 of varying the temperature of the liquefying stream exiting HEX2 (L5). The liquefying flow rate is calculated as:

$$F_{\text{Liq}} = \frac{\psi_{\text{NG2}} F_{\text{NG1}} (h_{\text{NG5}} - h_{\text{NG3}}) + F_{\text{Sub}} (h_{\text{S3}} - h_{\text{S2}})}{h_{\text{L2}} - h_{\text{L5}}} \tag{5.5}$$

If the temperature in L5 increases, the term $h_{L2} - h_{L5}$ increases, and consequently, the flow rate decreases. Figure C.5 shows the effects on the subcooling flow rate and the vapour fraction in S6 of varying the temperature of the subcooling stream exiting HEX3 (S6). The subcooling flow rate is calculated as:

$$F_{Sub} = \frac{\psi_{NG2} F_{NG1} (h_{NG6} - h_{NG5})}{h_{S3} - h_{S6}} \tag{5.6}$$

If the temperature in S6 increases, the term $h_{S3} - h_{S6}$ increases, and consequently, the subcooling flow rate decreases.

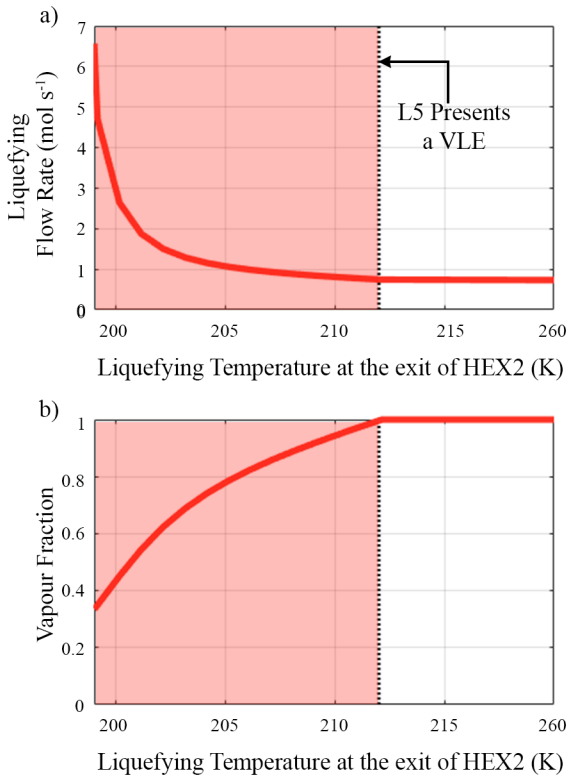


Figure C.4: Effects on the a) liquefying flow rate (mol s^{-1}) and b) vapour fraction of varying the temperature of stream L5. The red area represents the range in which L5 presents a VLE

C.4.2 Effects of the Temperature on the Electrical Power Consumption

When the refrigerants exiting their heat exchangers completely vaporise, their flow rates stop keep decreasing, but more slowly. Additionally, at that point, the pump does not work because there is no liquid in the stream.

Figure C.6.a) shows the specific consumptions of the compressor and the pump in the precooling cycle, and Figure C.6.b) shows the total consumptions of the compressor and the pump in the precooling cycle.

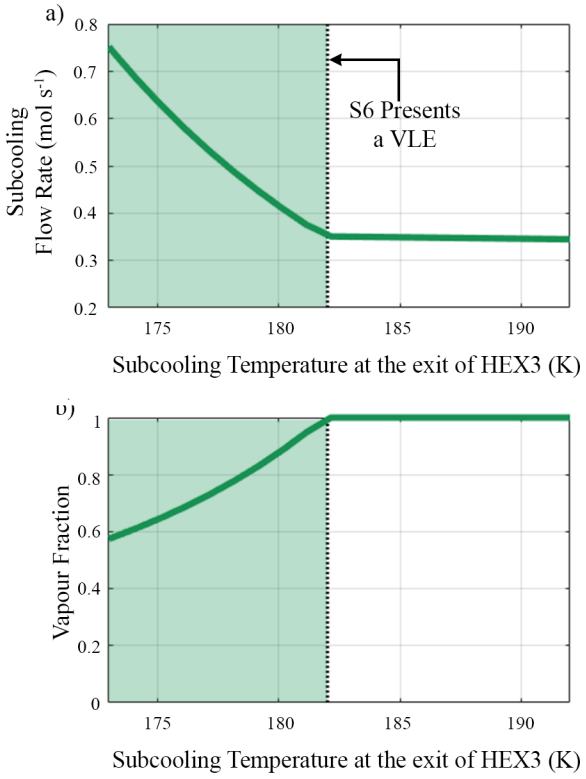


Figure C.5: Effects on the a) subcooling flow rate (mol s^{-1}) and b) vapour fraction of varying the temperature (K) of stream S6. The green area represents the range in which S6 presents a VLE.

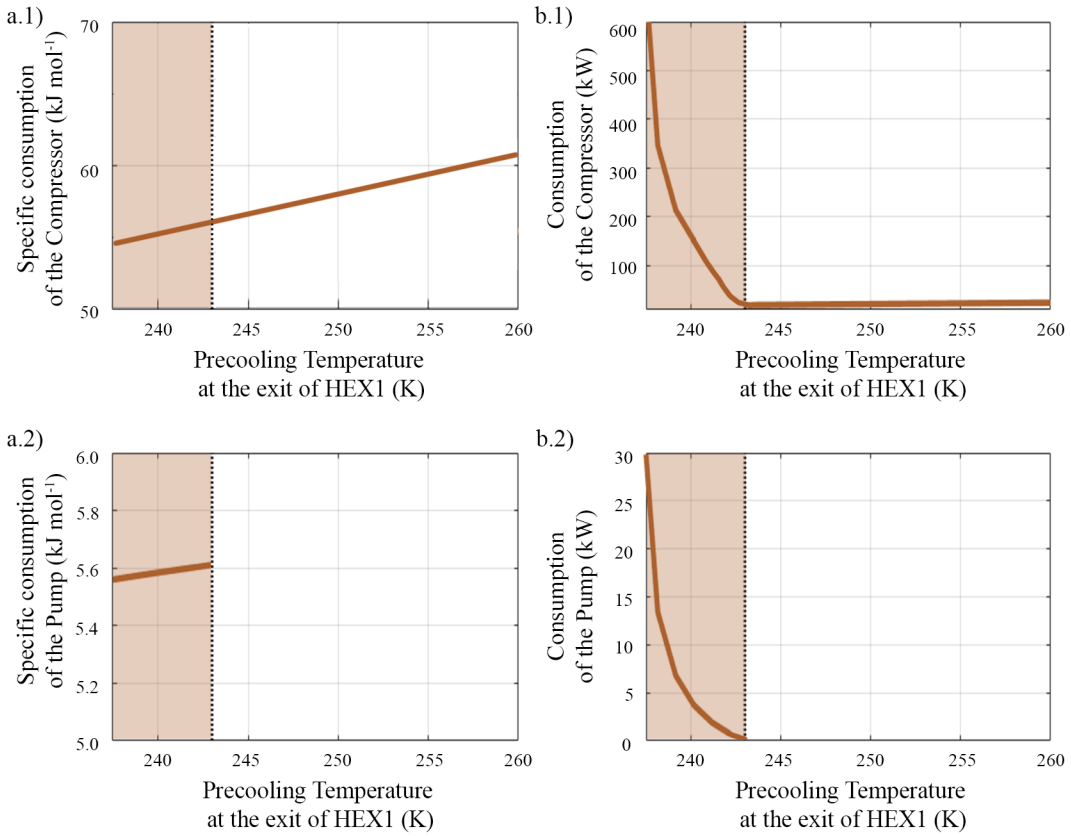


Figure C.6: Effects on the a.1) specific consumption of the compressor (kJ mol^{-1}), the a.2) specific consumption of the pump (kJ mol^{-1}), the b.1) total consumption of the compressor (kW), and the b.2) total consumption of the pump (kW) of the precooling cycle of varying the temperature (K) of the stream exiting HEX1. The brown area represents the range in which P4 presents a VLE.

Figure C.6.b) shows that the consumptions of the compressor and the pump are at their minimum when the P4 presents only a vapour phase.

Figure C.7.a) shows the specific consumptions of the compressor and the pump in the liquefying cycle, and Figure C.7.b) shows the total consumptions of the compressor and the pump in the liquefying cycle.

Figure C.8.a) shows the specific consumptions of the compressor and the pump in the subcooling cycle, and Figure C.8.b) shows the total consumptions of the compressor and the pump in the subcooling cycle.

Figure C.8.1) shows that the compressor exerts negative work when S6 presents a VLE. This is because at that point, the compressor falls within the choke zone, and the model calculates a work that is infeasible. Thus, the temperature of S6 has to be always above the saturation point.

Similar to the study of the discharge pressure of the compressors (Section 6), an optimum is found when the stream involving the heat exchanger are close to their saturation points. Figure C.9 shows the total consumption of the plant when the temperature in P4, L5, and S6 varies.

The electrical power consumption of the plant reaches a minimum when the temperatures of the refrigerants exiting their respective heat exchangers (P4, L5, and S6) are at their dew point.

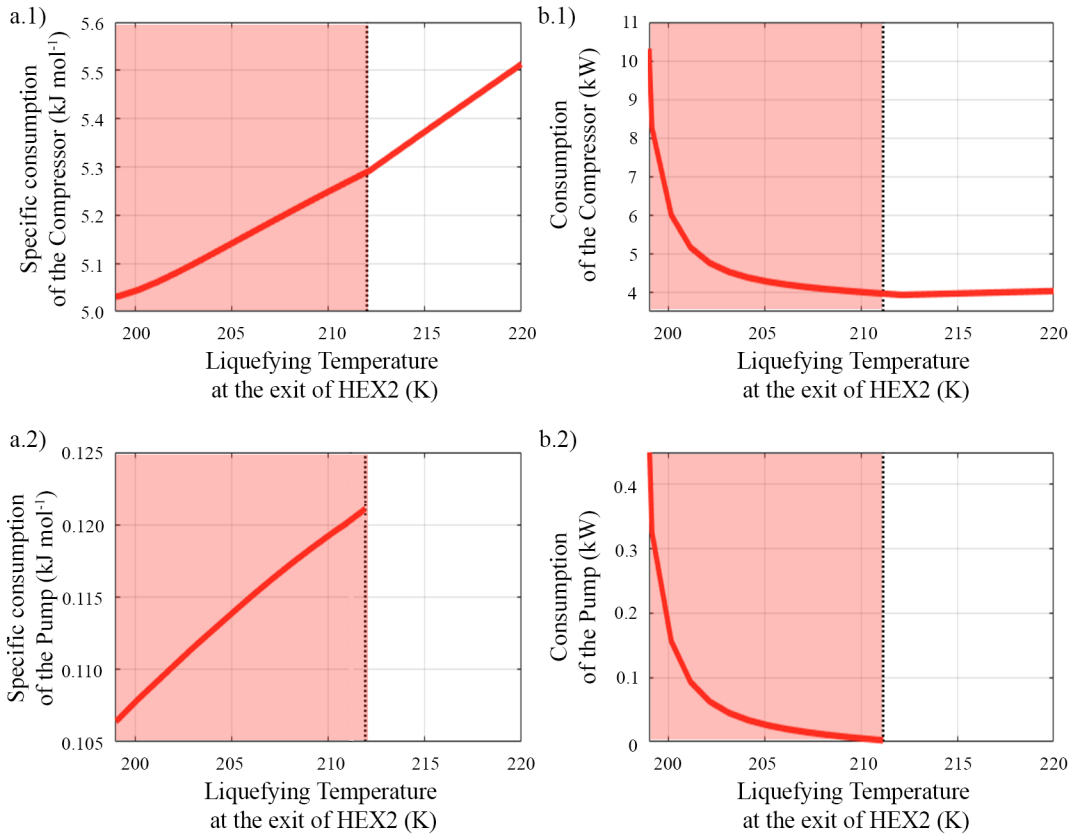


Figure C.7: Effects on the a.1) specific consumption of the compressor (kJ mol^{-1}), the a.2) specific consumption of the pump (kJ mol^{-1}), the b.1) total consumption of the compressor (kW), and the b.2) total consumption of the pump (kW) of the liquefying cycle of varying the temperature (K) of the stream exiting HEX2. The red area represents the range in which L5 presents a VLE.

The results show that the optimum set of temperatures is at 243 K for the precooling temperature, 212 K for the liquefying temperature, and 182 K for the subcooling temperature. The calculations for the nominal operation, however, established the temperatures at 260 K, 220 K, and 185 K. These results are very similar to the results obtained for the optimal set of pressures. Similar to that analysis, the temperature of stream P4, L5, and S6 are established above their optimum so that there is a margin of operability.

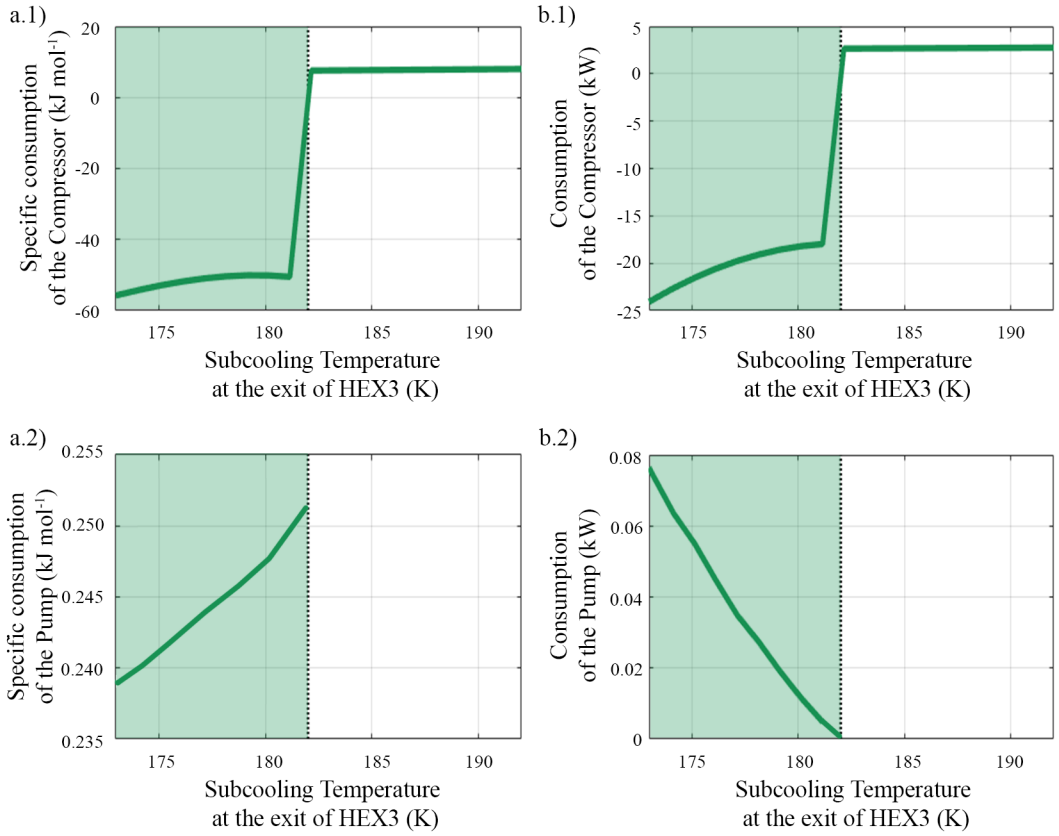


Figure C.8: Effects on the a.1) specific consumption of the compressor (kJ mol^{-1}), the a.2) specific consumption of the pump (kJ mol^{-1}), the b.1) total consumption of the compressor (kW), and the b.2) total consumption of the pump (kW) of the subcooling cycle of varying the temperature (K) of the stream exiting HEX3. The green area represents the range in which S6 presents a VLE.

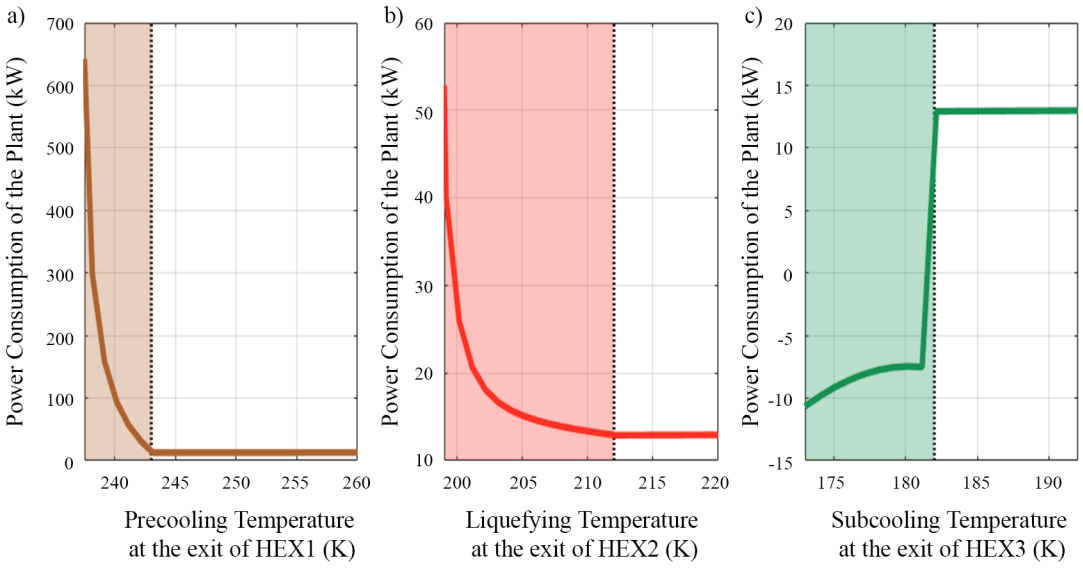


Figure C.9: Effects on the electrical power consumption of the plant (kW) of varying the a) temperature in P4 (K), the b) temperature in L5 (K), and the c) temperature in S6 (K). The shaded areas represent the range in which P4, L5, or S6 present a VLE.

C.5 Use of the Envelope of Feasible Operation

Figures 7.12-7.14 showed the behaviour of the electrical consumption when two variables are changed. However, the third variable is constant, and it is complicated to observe its influence on the consumption by having to observe another graph. Flexible operation aims to obtain an envelope of operation that the PPM can use.

Figure C.10 represents how the power consumption varies when the production rate and the flash temperature change for a family of LNG exit temperatures. There are three horizontal planes that cross the consumption planes. Each horizontal plane represents a given power consumption, the blue horizontal plane represents the nominal operation power consumption, the red horizontal plane represents a consumption 20% higher than the nominal power consumption, and the green horizontal plane represents a consumption 20% lower than the nominal consumption.

The intersections between each horizontal plane and the consumption planes will result in a family of curves. For this case, the family of curves is the family of LNG exit temperatures. Figure C.11 shows these curves for each horizontal plane.

Using the envelopes provides with the possible operating points consistent with the given power consumption. For example, if the power is reduced by 20%, the right-hand side graph in Figure C.11 will tell that the maximum production achievable is 81% of the nominal production rate. To do so, the flash temperature has to be reduced to 227 K, and the LNG exit temperature has to be increased to 111 K.

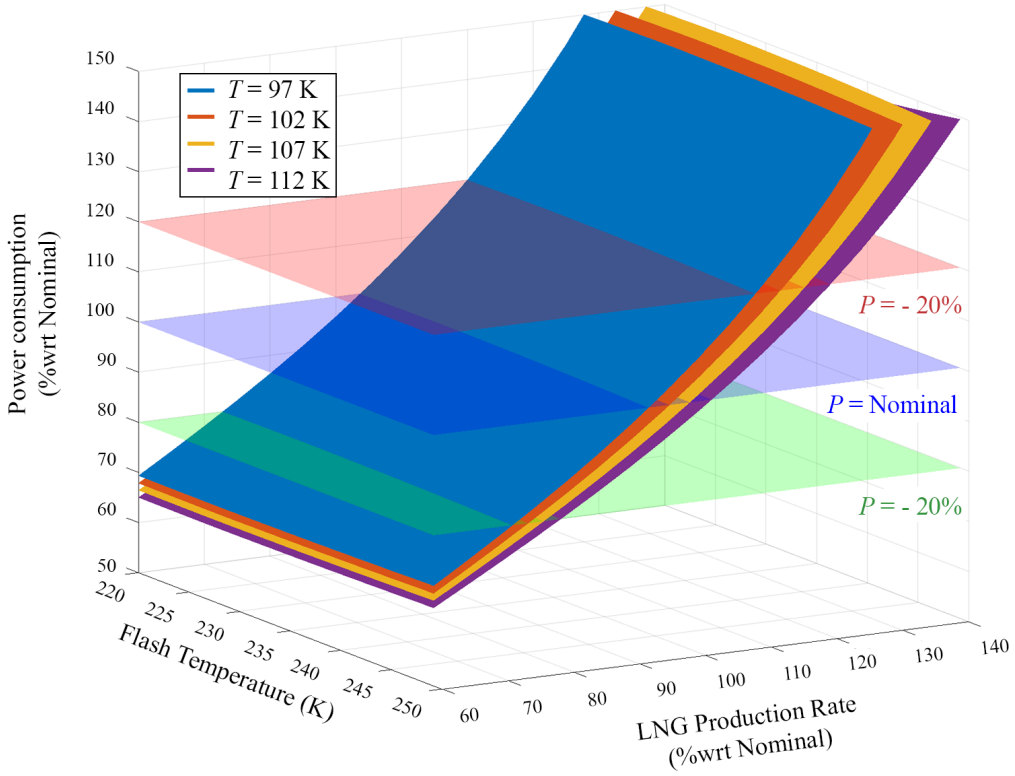


Figure C.10: Example of using the obtained graphs in Figure 7.12. Each curve represents a different natural gas temperature at the exit of the process, and each horizontal plane represents a different level of electrical power consumption. The intersections will give the values of the temperatures and production rate necessary to achieve the desired power consumption.

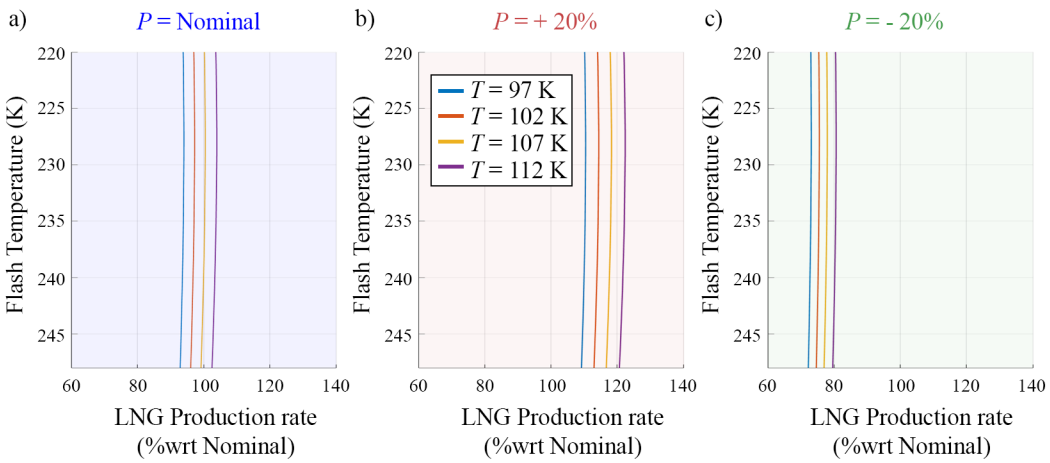


Figure C.11: Intersections between the curves and the horizontal planes in Figure C.10. The blue shaded graph represents the nominal consumption, the red shaded graph represents a power consumption 20% higher than its nominal value, and the green shaded area represents a power consumption 20% lower than its nominal value. Each line represents a different LNG temperature at the end of the process.

Figure C.10 shows, for a given electrical power consumption, the possible LNG production rates, the possible LNG exit temperature, and the possible flash drum temperatures for adapting the process to the new power consumption. The horizontal planes shown in Figure C.10 can be adjusted to any height, so the variables at any the power reduction can be observed. These envelopes of feasible operation are a manner to illustrate how flexible operation can work with different variables.